POLITECNICO
MILANO 1863

SCUOLA DI INGEGNERIA INDUSTRIALE
E DELL'INFORMAZIONE

Structure and properties of the polaron in doped poly(3-alkyl thiophenes): DFT modeling of the vibrational spectra.

TESI DI LAUREA MAGISTRALE IN
MATERIALS ENGINEERING AND NANOTECHNOLOGY
INGEGNERIA DEI MATERIALI E DELLE NANOTECNOLOGIE

Author: **Carlo Saporiti**

Student ID: 10576998
Advisor: Prof. Chiara Castiglioni
Co-advisor: Prof. Daniele Fazzi
Academic Year: 2022-23

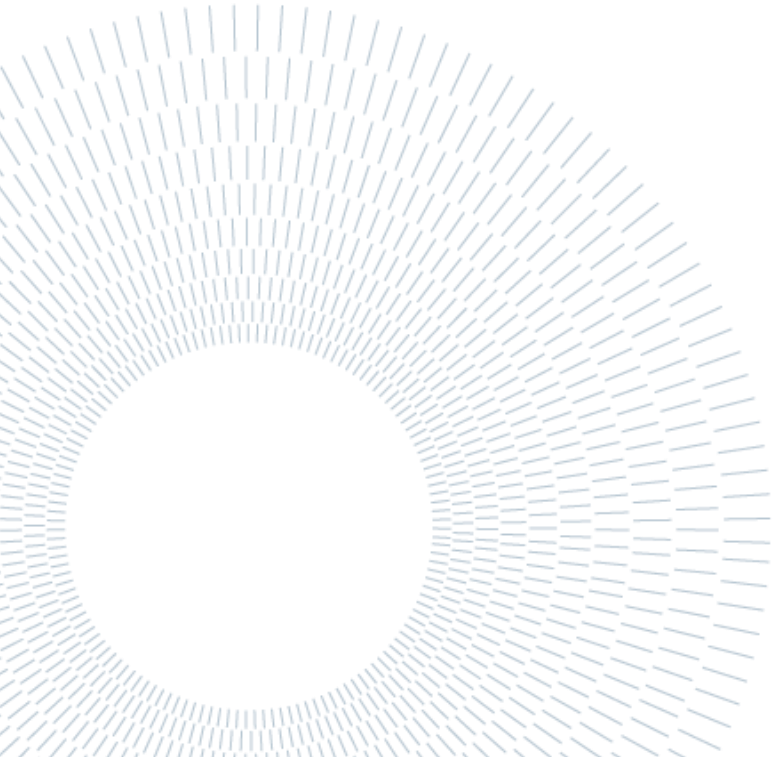

Abstract

π-conjugated polymers, and in particular poly(3-hexyl thiophene) (P3HT), are materials of great interest for their peculiar chemical-physical properties, which deserved fundamental researches and applied studies toward technological applications for organic photovoltaics, light emitting diodes (OLEDs) and field effect transistors (OFETs). Some interesting applications require an enhancement of the electrical conductivity, which can be obtained if the polymer is properly doped. The doping procedure consists in oxidizing/reducing the polymer via chemical or electrochemical processes.

The doping process induces changes in the electronic structure of organic conjugated materials, thus determining variations of their molecular structure and vibrational dynamics, since they large π electrons-phonon coupling. For this reason, the vibrational spectroscopy, namely IR and Raman spectroscopy, is a powerful characterization technique for the investigation of both structural and electronic properties.

The main purpose of this Thesis is the application of quantum-chemical methods, such as Density Functional Theory (DFT), for the simulation of the spectroscopic response of P3HT and its oligomers in their neutral (pristine) and charged (doped) species. DFT simulations allow to get insights, at the molecular level, about the structural and vibrational properties of the doping induced charge defect, i.e. the so-called polaron.

Firstly, quantum-chemical calculations are applied to molecular models of isolated unsubstituted neutral and singly charged oligothiophenes, with an increasing number of thiophene rings (from six – T6, to fourteen – T14). Passing from the neutral to the charged/doped state, the IR and Raman spectra of oligothiophenes exhibit new intense bands in the wavenumber region between 1000 and 1600 cm^{-1}. These bands are silent or barely silent in the IR and at Raman spectra respectively, when the oligomers are in their neutral/pristine state. For this reason, the bands are called IRAVs (Infrared Activated Vibrations) and RAVs (Raman Activated Vibrations) and constitute the spectroscopic fingerprints of the polaronic species.

DFT simulations correctly predict the vibrational spectra of the neutral species and of the charged forms, namely the IRAVs. On the contrary, the RAVs are not well predicted by the current DFT calculations. The full rationalization of the vibrational

spectra of pristine and doped oligothiophene is achieved by the study of the local IR and Raman intensity parameters, that are the derivatives of the dipole moment and polarizability with respect to the individual carbon/carbon (CC) stretching coordinates, and by the analysis of the vibrational eigenvectors of the ECC-like (Effective Conjugation Coordinate) normal modes. Moreover, the study of the structural relaxation occurring upon charging allows the evaluation of the so called polaron delocalization length.

As a second step, to better simulate the experimental spectra of P3HT, we have considered more realistic molecular models for the neutral and charged species, by including the alkyl-side chains. The DFT simulations show that their vibrational spectra show remarkable analogies with those of the corresponding unsubstituted oligothiophenes and confirmed that the IRAVs and RAVs activation mechanisms do not depend by the molecular model, namely by the inclusion of the lateral chains.

Finally, a comparison between the DFT calculated IR and Raman spectra and the experimental ones of doped P3HT is presented. The simulated IR spectra are in good agreement with the experimental result: they can be used to interpret and corroborate the analysis of the IR spectrum of doped P3HT. On the contrary, the simulated Raman spectra of the doped species are dominated by a very strong RAV peak, characterized by a low vibrational frequency, which cannot find correspondence with a similar experimental feature.

The last result suggests that both a qualitative and a quantitative DFT calculation of the Raman spectra of charged species is quite delicate and it can be very complicated to achieved. Furthermore, for a quantitative structural and vibrational analysis, DFT calculations should go beyond the single-molecule limit and consider model systems able to take into account, for instance, the intermolecular interactions of the oligothiophenes with the dopant counterions (in the case of chemical doping) and, possibly, able to simulate the Raman resonance effect, by paving the way to new approaches for quantum-chemical calculations as applied to vibrational spectroscopy of π-conjugated materials. This represents a tremendous future challenge for the theoretical and computational modelling of functional organic materials.

Key-words: vibrational spectroscopy, Density Functional theory, IRAVs and RAVs, polaron.

Abstract in italiano

I polimeri π-coniugati, ed in particolare il poli(3-esil tiofene) (P3HT), sono materiali di grande interesse sia dal punto di vista della ricerca fondamentale sia per le applicazioni tecnologiche, che riguardano settori come il fotovoltaico organico, lo sviluppo di diodi emettitori di luce (OLED) e di transistor ad effetto di campo (OFET). Per alcune applicazioni che richiedono elevata conducibilità elettrica, è possibile incrementarne le prestazioni mediante la tecnica di drogaggio (ad esempio drogaggio chimico o elettrochimico).
I cambiamenti indotti dal drogaggio chimico nella struttura elettronica di questi materiali determinano variazioni della struttura molecolare e della dinamica vibrazionale, a causa dell'elevato accoppiamento elettrone- fonone. Per questo motivo, la spettroscopia vibrazionale, cioè la spettroscopia IR e Raman, è una potente tecnica di caratterizzazione per lo studio delle proprietà sia strutturali sia elettroniche di tali materiali.

Lo scopo principale di questa tesi è l'applicazione della teoria del funzionale di densità (DFT) per la simulazione della risposta spettroscopica di P3HT drogato e dei suoi oligomeri. Questo studio permette di ottenere informazioni sulla struttura molecolare ed elettronica del difetto di carica indotto dal drogaggio, denominato polarone, attraverso l'interpretazione della sua risposta vibrazionale.

In primo luogo, i calcoli quanto-chimici sono stati applicati a modelli di molecole isolate rappresentati da oligotiofeni di diversa lunghezza, non sostituiti (ovvero senza catena alchiliche laterali). Nelle simulazioni sono state cambiate la lunghezza di catena degli oligotiofeni (da sei anelli tiofenici – T6, a quattordici -T14) e lo stato elettronico, neutro (specie pristina) e singolarmente carico (radical catione, specie drogata carica). Passando dallo stato neutro a quello drogato, gli spettri IR e Raman degli oligotiofeni mostrano nuove bande intense nella regione compresa tra 1000 e 1600 cm^{-1}, che sono silenti o quasi silenti rispettivamente nell'IR e nel Raman, quando gli oligomeri sono nello stato neutro. Per questo motivo sono chiamate IRAVs (Infrared Activated Vibrations) e RAVs (Raman Activated Vibrations) e costituiscono le impronte spettroscopiche del polarone. Le simulazioni DFT predicono correttamente le IRAV e le RAV degli oligotiofeni, permettendo la loro completa razionalizzazione mediante l'analisi dei parametri locali di intensità IR e Raman (derivate del dipolo e della polarizzabilità rispetto alle coordinate di CC stretching) e mediante l'analisi degli autovettori dei modi normali del tipo ECC (Effective Conjugation Coordinate). Inoltre, lo studio del rilassamento strutturale che si verifica a seguito del drogaggio permette di stimare la lunghezza di delocalizzazione del polarone.

Successivamente, al fine di simulare con maggiore accuratezza gli spettri sperimentali disponibili per P3HT, sono stati considerati modelli molecolari di oligotiofeni neutri e carichi con catene laterali alchiliche. Le simulazioni DFT mostrano che i loro spettri vibrazionali presentano molte analogie con quelli dei corrispondenti oligotiofeni non sostituiti, e confermano che i meccanismi di attivazione delle IRAV e delle RAV non dipendono dal modello molecolare (con o senza catene alchiliche) adottato.

Infine, viene presentato un confronto tra gli spettri IR e Raman calcolati con metodo DFT e quelli sperimentali di P3HT drogato. Gli spettri IR simulati sono in buon accordo con il risultato sperimentale e possono quindi essere utilizzati per interpretare e guidare l'analisi dello spettro IR di P3HT drogato. Al contrario, gli spettri Raman simulati delle specie cariche sono dominati da un intensissimo picco RAV, caratterizzato da bassa frequenza, che non trova corrispondenza con i dati sperimentali.

Quest'ultimo risultato chiarisce che ottenere una buona predizione DFT degli spettri Raman delle specie cariche è molto difficile. Per superare questa difficoltà sarebbe necessario, ad esempio, utilizzare modelli in grado di tener conto dell'interazione intermolecolare degli oligotiofeni con il controione della specie drogante e, possibilmente, in grado di simulare l'effetto di risonanza Raman, aprendo la strada a nuovi approcci per la simulazione, con metodi quanto-chimici, della risposta spettroscopica di materiali π -coniugati. Ciò costituisce una rilevante sfida futura per la modellistica teorica dei materiali organici funzionali.

Parole chiave: spettroscopia vibrazionale, teoria del funzionale della densità, IRAV e RAV, polarone.

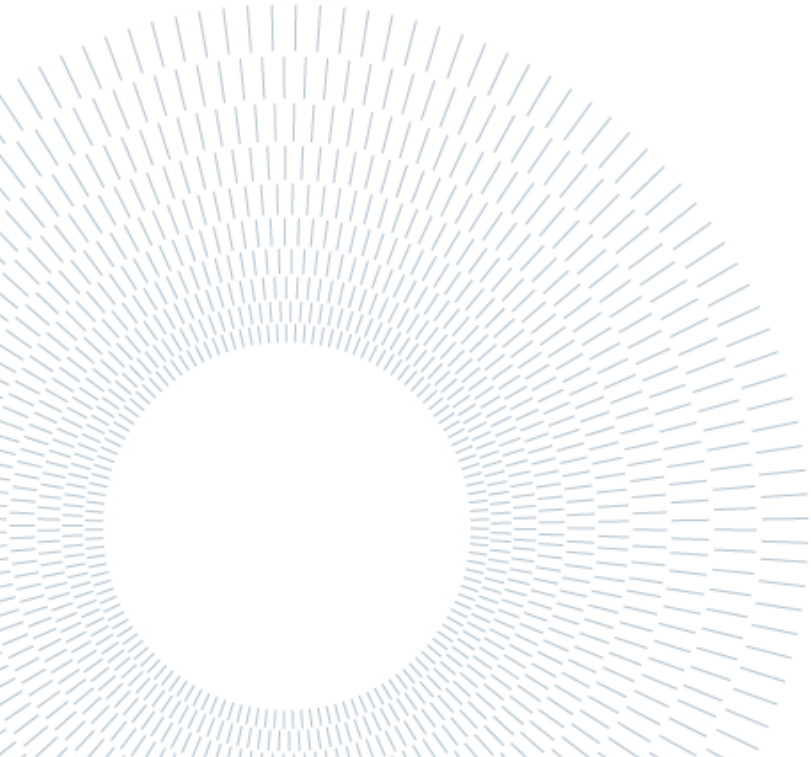

Contents

1 Introduction

1.1. The scientific relevance of π-conjugated polymers and the importance of vibrational spectroscopy.

Since the discover of conductive polyacetylene (PA) in 1977, semiconductive and conductive polymers gained a lot of interest among the scientific community because of their peculiar chemical-physical properties, which required the development of new theoretical models for their understanding **[1-2]**. Moreover, it was immediately foreseen that these materials were promising candidates to realize innovative organic-based opto-electronic devices **[3]**. Today, π-conjugated polymers are applied in organic solar cells (OSCs), light emitting diodes (OLEDs) and field effect transistors (OFETs).

One of the main advantages of organic molecular semiconductors over traditional inorganic ones is their processability: thin films of these materials can be produced by vacuum deposition techniques for oligomers and small molecules or printing and coating techniques for polymers. In this way, organic semiconductors can in principle be deposited onto almost any substrate, paving the way to the so called molecular and flexible electronics. Among all the possible classes of organic molecular semiconductors, this thesis deals with π-conjugated polymers and in particular with poly (3-hexyl thiophene) (P3HT).

π-conjugated polymers exhibit semiconductive properties thank to the π electrons delocalization, arising from the overlapping of the p-orbitals of adjacent carbon atoms: this results in the formation of π-bonding and π*-antibonding orbitals, which give rise to quasi-continuous energy bands (like the valence and conduction bands in inorganic semiconductors) as the number of conjugated units, therefore the effective conjugation length (ECL), increases (see Figure 1.1).

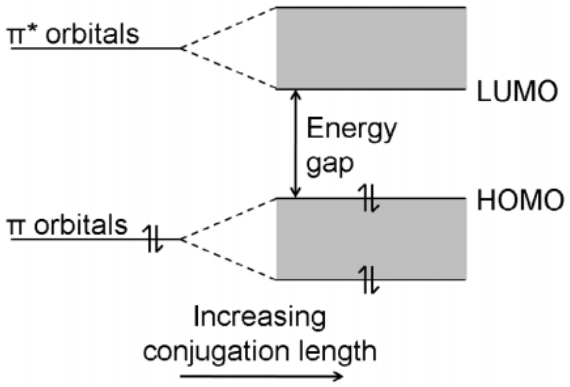

Figure 1.1: sketch of the π- orbital energy levels in a conjugated polymer.

The most relevant energy levels for opto-electronic applications are the frontier levels, namely the highest occupied molecular orbital (HOMO) and the lowest unoccupied molecular orbital (LUMO), which are separated by an energy gap in the range 1,5-3,0 eV **[4]**. The energy gap between the HOMO and the LUMO can be properly tuned by chemical substitution of the monomeric units with electron-rich or electron-poor substituents, making π-conjugated polymers suitable for light-emitting and light-harvesting applications.

The conductivity of π-conjugated polymers can be increased from semiconductive up to conductive levels by p- or n-type doping, namely by oxidizing or reducing the system via chemical or electrochemical techniques. When properly doped, such materials can be employed as artificial muscles, chemical and bio sensors and for the development of flexible and wearable thermoelectric generators and coolers **[5-7]**.

The doping process induces the formation of charged defects, known as polarons or bipolarons if one or two charges are injected into the π-conjugated polymer respectively: they are bound charged states with a specific spatial extension and are accompanied by distorted geometry, often referred as "lattice relaxation", with respect to the neutral states.

In this thesis we will focus only on singly charged radical ions and so only polaron states will be analyzed. For the sake of simplicity, to better understand the impact of doping on the electronic structure, we mention here the simple case of unrelaxed molecular orbitals. In such frame, the electronic structure of a polaron can be defined as a singly occupied molecular orbitals (SOMO) whose energy level is between the HOMO and LUMO of the neutral species. For a p-doping process, the one considered in our study, the SOMO is located near the LUMO of the pristine polymer, causing two possible electronic transitions (i.e. absorption bands), one generally in the visible and one usually in the near-infrared regions, the SOMO-to-LUMO and HOMO-to-SOMO transitions respectively, as depicted in Figure 1.2. In the same figure is reported also the case for n-doping **[8]**.

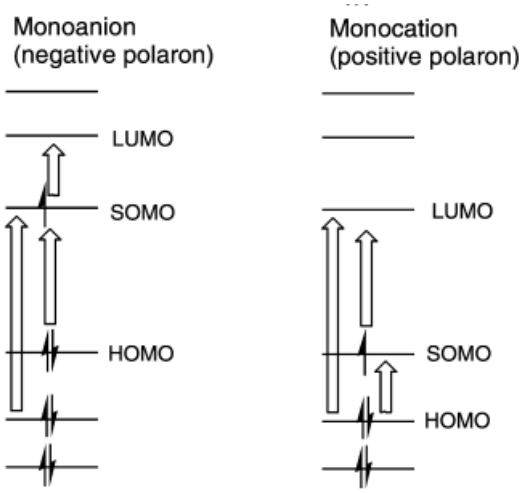

Figure 1.2: sketch of the frontier π- orbital energy levels in a conjugated polymer upon reduction (left panel) and oxidation (right panel) processes.

High chemical purity and structural homogeneity of the π-conjugated polymer, thus meaning a low number of conjugation-breaking defects, are fundamental parameters to have a high electrical conductivity. Also, regioregularity of the lateral substituents is determinant for the electrical conductivity of the polymer: it is well-known that regiorandom materials exhibit lower values of conductivity, since the π-conjugation along the chain is partially hindered by conformational distortions and the π-π stacking is less effective **[9]**.

Among all π-conjugated polymers, poly(alkyl-thiophenes) and in particular P3HT, show great interest in both academic and industrial research fields because of their unique features **[10-12]**:

1) solubility in various solvents, due to their lateral alkyl chains,
2) capability of retaining they relevant electronic characteristics upon ring substitution,
3) interesting optical properties, like strong electroluminescence in the neutral state.

Moreover, P3HT can be processed into micro and nanofibers in order to exploit the advantages of anisotropy in terms of molecular, mechanical and electrical properties. Last, quantum confinement effects can be employed to develop novel nanoscaled organic devices, such as single-fibres organic field effect transistors.

Vibrational spectroscopy, namely IR and Raman spectroscopy, plays an important role in unveiling the structure of polyconjugated materials: in scientific literature there exists a lot of works aiming at studying the phases, degree of molecular order, conformation and other relevant structural parameters of P3HT **[13-19]**. IR and Raman

spectroscopy allowed to determine that in the solid state P3HT is a semicrystalline polymer, consisting in amorphous and crystalline domains. The amorphous phase is characterized by a disordered morphology where polymer chains can adopt different conformations: typically, both the conjugated backbone and the lateral alkyl chains are conformationally distorted.

Moreover, the crystalline domains can show different morphologies, characterized by a different degree of order. It is possible to distinguish at least three different phases **[15]**:

(i) Fully crystalline phase, called Phase II: it has been clearly detected in single crystals of P3HT oligomers, like 3HT8. In this phase the thiophene backbone chain adopts a regular, planar conformation, with the thiophene rings lying in a plane, and the lateral alkyl chains are in all-trans conformation. The packing between chains is effective, thanks to the interactions between the ordered inter-digitated alkyl chains. In a few cases, this structure has been observed for the P3HT polymer.

(ii) Crystalline, called Hairy A phase (Phase II): the thiophene rings of the backbone are coplanar with randomly oriented hexyl side chains, with random conformation. This phase is typical of microcrystalline samples of the oligomers and of the P3HT polymer.

(iii) Hairy B phase: the backbone of the polymer can accommodate some conformational disorder and the trans-planar hexyl chains have a random conformation. The 3-D order is partially lost, so that a possible model is that of a bundle of quasi-straight chains oriented along a common direction, without a translational order in the direction orthogonal to the chain axis.

All the above morphologies can be simultaneously present in the same sample and their spectroscopic features are the result of the convolution of the contribution from different phases, with weights proportional to their relative amount.

Beside the structural properties, vibrational spectroscopy can be exploited also to investigate the electronic properties, thanks to the intrinsic relationship between molecular structure and optoelectronic properties. In π- conjugated materials, since the large electron-phonon coupling, changes in the electronic structure due for instance to chemical doping induce variations in the nuclear structure and dynamics, which can indeed be detected by IR and Raman spectroscopy.

The Raman spectrum of π-conjugated polymers is dominated by peaks whose associated normal modes involves the collective simultaneous stretching and shrinking of the quasi-single and quasi-double carbon-carbon (CC) bonds of the molecular backbone: this kind of vibrations are named ECC (Effective Conjugation Coordinate) **[20-22]** oscillations, they are Raman active however silent or almost silent in the IR. The charge injection upon the doping process of a breaks the translational

symmetry of the polymer chain and polarizes the CC bonds in a domain (of a few thiophene rings) of the backbone. From the spectroscopic point of view, the main effect of this phenomenon is that the charge transfer allows the activation in the IR spectrum of vibrational transitions associated to ECC normal modes with absorption intensity that is similar to that of electronic transitions: these new bands induced by the doping are called IRAVs, thus meaning Infra-Red Activated Vibrations **[22-28]**.

Since IRAVs are substantially IR-silent when π-conjugated materials are in the pristine state and become IR-active upon doping, they are considered as the most specific empirical optical probe of the formed charged defect in the polymeric chains: this means that IR spectroscopy, and in particular the appearance of the strong IRAVs, allows the detection of polarons and bipolarons.

Since IR spectroscopy is a relatively simple characterization technique, and because of its specificity and sensitivity, IRAVs are considered the vibrational signature of polaron defects. The analysis and interpretation of the IRAV features provide unvaluable information about the polarons density, dynamics and spatial extent, as well as the structure relaxation-charging relationships.

The study of the origin and of the modulation of IRAV according to the level of doping and of the sample morphology can highlight the charge transfer processes and can give insights also about the possible potential new applications of the doped polymers, even exploiting their peculiar electronic structure, e.g. though coupling of polarons and surface plasmons to develop IR antennas **[29].**

The diagnosis of the charge transfer from the dopant to the π-conjugated polymer induces variations also in their Raman spectrum, with the appearance of new features, named RAVs (Raman Activated Vibrations), not present when the polymer is in the pristine state. Since Raman spectroscopy is more versatile than IR for in situ measurements, a deepening in the vibrational assignment and interpretation of the RAVs could improve the use of the Raman, not only for the recognition of the doping but also for a thorough description of the molecular and electronic structure of charge defects.

1.2. Outline and aims of the Thesis.

The appearance of IRAVs and RAVs in vibrational spectra of π-conjugated materials is rationalized by the ECC theory, as proposed by Zerbi, Castiglioni et al. originally dealing with the mechanism of activation of the IRAVs of polyacetylene (PA) and its oligomers, the so-called oligoenes **[22-28, 30]**. The scientific community published also studies regarding the dynamics and IRAVs of polythiophenes **[31-35]**, but since the advent of quantum-chemical simulations very few works dealing with the rationalization of IRAVs, dynamics and vibrational spectra of P3HT and polythiophenes were presented.

The aim of this Thesis is to apply DFT calculations in order to:

1) explain and rationalize the empirical evidence of the appearance of strong IRAVs and RAVs when pristine P3HT undergoes a chemical doping process, thus meaning the interpretation of IR and Raman spectra of doped P3HT with the help of molecular models;
2) illustrate the activation mechanisms of IRAVs by means of the study of the local IR and Raman parameters and by means of the analysis of the eigenvectors of the activated normal modes;
3) characterize from the molecular perspective the doping induced charged defect, i.e. the so called polaron, through the analysis of its peculiar vibrational structure;
4) study the relaxation of the geometry of the polymeric chain, as induced by the charge transfer from the dopant to the polymer. Among the other structural characteristics, it is interesting the study of the delocalization length of the polaron in terms of number of thiophene units affected by perturbation induced by the electronic charge.

In order to achieve the listed purposes, we analyze various molecular models of P3HT and of its oligomers, by means of quantum-chemical calculations. All the simulations we are going to present in this Thesis are affected by some intrinsic limitations either related to the DFT method or to the structural models we adopted, namely:

1) the calculations are carried out *in vacuo*, thus meaning that they do not take into account any kind of intermolecular interactions. In particular, all our molecular models do not consider the dopant counterion and they refer to isolated molecules, without dealing with the crystalline structure of the polymer, so the interaction with the surrounding polymeric chains is not exploited.
2) the intrinsic Self Interaction Error (SIE) and the missing of static electron correlation (i.e., single-determinant approach), proper of the DFT method, thus leading to over-delocalization effects.

This Thesis is constituted by the current introduction and five principal chapters:

- Chapter 2 reports the molecular vibrational problem, focusing on the methods used to calculate the vibrational frequencies and IR and Raman intensities, which are the experimental variables obtainable from the spectra. Density Functional Theory (DFT) is shortly presented as an approximated method to solve the electronic Schrödinger equation, and the ECC theory is summarized, focusing on its extension to polythiophenes. Finally, the main computational details used to carry out the calculations on the molecular models are presented.

- Chapter 3 is dedicated to the calculated results regarding unsubstituted oligothiophenes: we will focus on the effect of the chain length of the oligomer backbone both for neutral and charged oligothiophenes; we will then underline the variations in terms of geometry and vibrational spectra for each oligomer, from the hexamer to that featuring fourteen thiophene units, upon hole injection, that is simulating the p-doping. We will analyze the effect of different functionals in the quantum-chemical calculations on geometrical and spectroscopic features, exploiting the hybrid B3LYP and the range-separated CAM-B3LYP.
- Chapter 4 is dedicated to the results regarding the molecular models of alkyl-substituted oligothiophenes: we will firstly compare the predicted IR and Raman spectra and their relative local parameters of alkyl-substituted oligothiophenes with those of unsubstituted oligothiophenes. We will analyze the effect of the chain length of the alkyl substituents, by comparing the vibrational spectra and the geometry parameters of an octamer of (3-hexyl thiophene) and of (3-ethyl thiophene).
- Chapter 5 reports the comparison of the DFT calculated IR and Raman spectra of charged alkyl-substituted oligothiophenes with the experimental spectra of doped P3HT, recorded by the researchers of the FunMat Laboratory[1]. We will also present a preliminary DFT calculation on a structural model which includes the dopant counterion, suggesting a possible way to solve - or at least reduce - some problems concerning the quantum-chemical simulation of the Raman spectrum of charged species.
- Chapter 6 summarizes the results obtained in the current work, presenting future perspectives concerning the DFT quantum-chemical calculations as applied to vibrational spectroscopy of doped π-conjugated materials.

[1] Dipartimento di Chimica, Materiali e Ingegneria Chimica “G. Natta”, Politecnico di Milano

2 Theory and methods

2.1. The vibrational spectra: physical phenomena, observables and modelling of the spectroscopic response.

2.1.1. Infrared and Raman spectra: the experimental observables.

Figure 2.1 shows the experimental IR spectrum of the P3HT polymer in its pristine state. This spectrum is an example of the typical pattern of an absorption IR spectrum: it presents several bands, which are ascribed to the excitation of different vibrational modes of P3HT, by means of the absorption of photons at characteristic frequencies in the region of the mid-IR. Each k-th absorption band corresponds to a transition between two adjacent vibrational levels of a given vibrational normal mode Q_k of P3HT, which requires the exchange of one quantum of vibrational energy from the radiation field and the matter. The separation of the adjacent vibrational levels of the quantum harmonic oscillator (e.g., between levels with $n_k = 0$ and $n_k = 1$) is $\Delta E = h\nu_k^{vib}$, so the appearance of an absorption peaks means that the matter has absorbed photons with frequency matching the vibrational one: $h\nu^{photon} = h\nu_k^{vib}$ and the k-th oscillator has changed its state (e.g. from $|n_k >= |0 >$ to $|n_k >= |1 >$).

Usually, instead of frequencies (in s^{-1}) the horizontal axis of the IR spectrum reports wavenumbers (in units of cm^{-1}), namely $\tilde{\nu} = \frac{\nu}{c}$, where c is the speed of the light.

In a similar way, the Raman spectrum (see in Figure 2.2 the Raman spectrum of P3HT) is plotted versus the so-called Raman shifts, namely the position of the k-th Raman scattering peak is:

$$\Delta\nu_k = h\nu^{laser} - h\nu_k^{scattered} = h\nu_k^{vib}$$

Also in this case the physical process corresponds to the excitation of normal vibrations with characteristic frequency ν_k^{vib} , but the phenomenon is completely different from the IR absorption. Indeed, the Raman spectroscopy deals with the inelastic scattering of the photons of a (monochromatic) laser. As for the IR absorption, there is an exchange of energy between the radiation field and the matter, which "absorbs" a photon with energy $h\nu^{laser}$ and instantaneously re-emit a photon with a lower energy, namely $h\nu_k^{scattered} = h\nu^{laser} - h\nu_k^{vib}$, with a net energy transfer to the matter: $\Delta E = h\nu_k^{vib}$.

The process illustrated above explains the Stokes Raman Spectrum, which is accompanied by another inelastic scattering phenomenon (anti-Stokes Raman) where the exchanged energy is provided by the matter and $h\nu_k^{scattered} = h\nu^{laser} + h\nu_k^{vib}$. Since the anti-Stokes

process corresponds to the de-excitation of a vibrational level different from the fundamental one, the anti-Stokes Raman spectrum is weak, because of the low population of the excited vibrational levels at room temperature. For this reason, usually the only one Stokes Raman spectrum is recorded. The Raman shifts are often measured using the wavenumber scale in cm^{-1}.

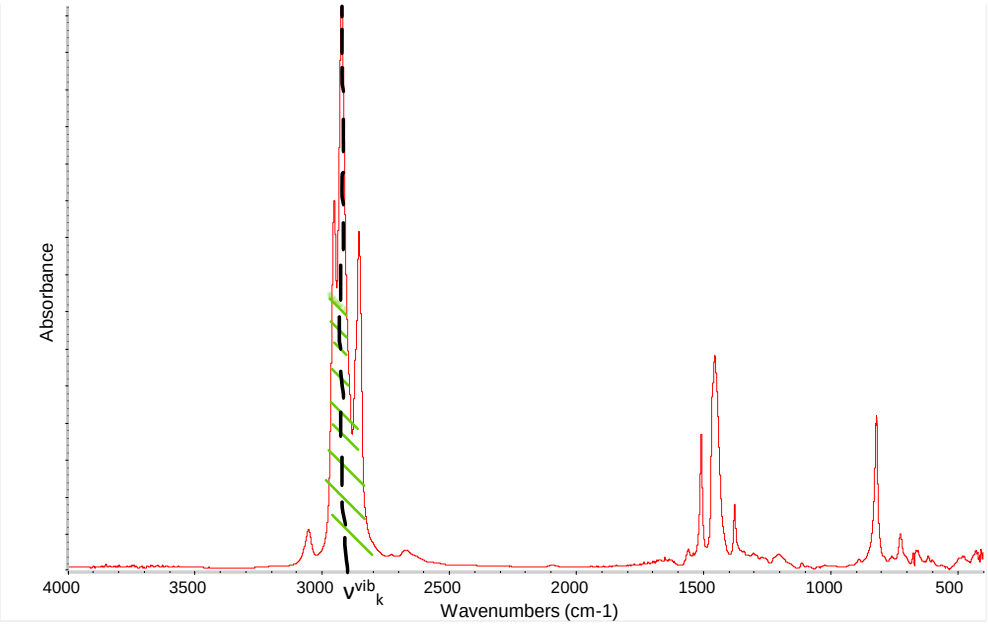

Figure 2.1: IR spectrum of P3HT

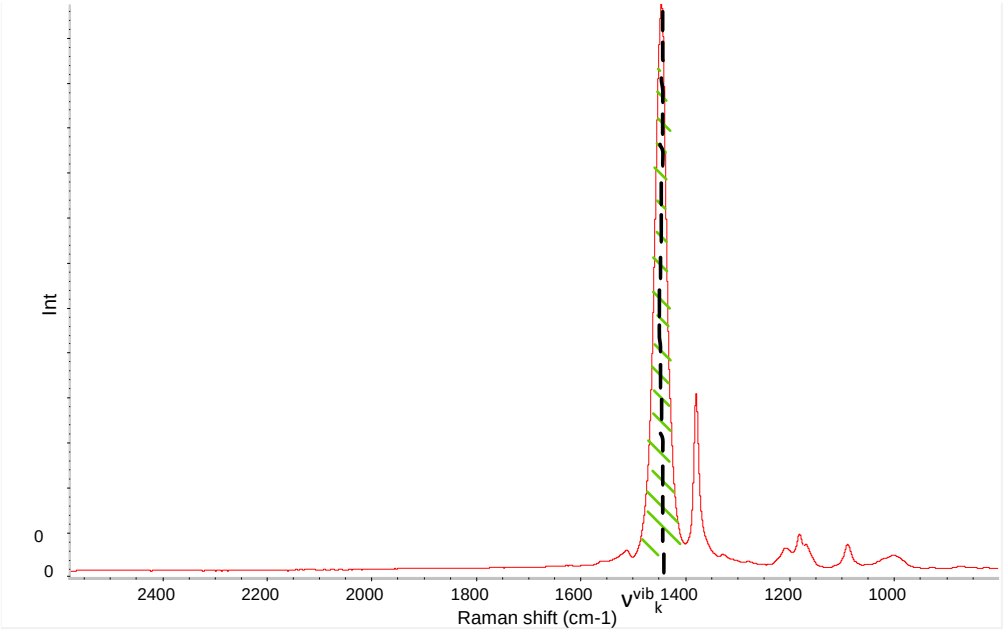

Figure 2.2: Raman spectrum of P3HT.

Vibrational spectra (IR and Raman) provide the following observables:

- The collection of vibrational frequencies, which correspond to the position of the maxima of the absorption (or scattering) IR (or Raman) bands, indicated in Figures 2.1 and 2.2 by ν_k^{vib}.
- IR (or Raman) intensities, namely the area under the bands associated to a given ν_k^{vib}, indicated in Figures 2.1 and 2.2 by the dashed green lines.

Figures 2.1 and 2.2 show that each band has a characteristic width (usually measured as Full Width at Half Maximum - FWHM). The broadening of the vibrational peaks is due to the intrinsic nature of quantum vibrational levels (i.e. their finite life-time) and also to the so-called inhomogeneous broadening, due to the disordered environment. Moreover, it is quite frequent that two or more bands show a partial overlap: in this case, large and structured absorption (or scattering) features are observed. For this reason, it may happen that the characteristic vibrational frequency of a weak band partially overlapping to a stronger one should be deduced by the position of a shoulder of the main band. Deconvolution procedures are sometimes exploited aiming at the "separation" of the different overlapped bands.

The frequencies are properties characteristic of the molecules (or crystals) and do not depend on the amount of material. For instance, they are independent from the concentration of the species in a solution, if we are in a concentration range which does not cause the formation of aggregates, where the intermolecular interactions can affect the molecular structure and thus vibrational frequencies. Instead, the IR absorption intensities, according to the Lambert-Beer law, increase linearly with the concentration c and with the IR beam path L in the sample. For a sample in solution, the so-called absolute band intensity of the k-th band is the measured intensity (area of the absorption band) normalized by the factor $c \times L$.

Absolute IR intensities of a solid sample (for instance a film) are more difficult to be obtained, because they require an accurate determination of the sample thickness and of its density. This is the reason why often the experimental spectra give us the information on "relative" intensities, but not their absolute values.

In the case of the Raman spectra, the intensity of a band is referred as Raman Cross Section of the transition. Also the Raman bands intensities depend on the number of molecules probed during the experiments, which in turns depend on the scattering volume (volume probed by the laser photons); moreover, they depend on the laser power and wavelength and on the geometry adopted for the detection of the scattered photons. All these variables imply that the absolute Raman intensity - the Raman response by one individual molecule – can be hardly obtained.

In conclusion, the comparison between the predicted and experimental Raman spectra focuses in most of the cases on the so-called intensity pattern (i.e. relative intensities). For this reason, the label of the vertical axis in the plots of experimental spectra often is "Raman

intensity (arbitrary units)" and the same is usual in the case of IR spectra of solid samples or solutions of unknown concentration.

On the other hand, both for the IR and the Raman spectra, a nice prediction of the intensity pattern justifies a confident use of the calculated absolute intensities.

2.1.2. Calculation of the vibrational frequencies: the dynamic problem in harmonic approximation.

The interpretation of the vibrational spectra in terms of molecular structure and of physical properties of the molecule, requires the knowledge of all the "ingredients" which determine the spectral observables. This is important for an empirical analysis of the spectra, mainly based on the comparison among different samples and on the so-called spectroscopic correlations and spectroscopic markers and is mandatory if the theoretical modelling of the spectra is the strategy adopted to support the interpretation.

In this Section, we report the fundamental equations, which allow obtaining the set of frequencies associated to the 3N-6 vibrational normal modes of a molecule with N atoms. The relevant point is that the vibrational frequencies come from the intramolecular potential energy $V(\boldsymbol{\xi})$, which can be approximated as a quadratic function of nuclear displacements coordinates (harmonic approximation):

$$V(\boldsymbol{\xi}) = V_0 + \sum_i \left.\frac{\partial V}{\partial \xi_i}\right|_0 \xi_i + \frac{1}{2}\sum_{ij} \left.\frac{\partial^2 V}{\partial \xi_i \partial \xi_j}\right|_0 \xi_i\, \xi_j = \frac{1}{2}\sum_{ij} f_{ij}\, \xi_i\, \xi_j = \frac{1}{2}\tilde{\boldsymbol{\xi}}\, \boldsymbol{F}\boldsymbol{\xi} \qquad \text{(eq. 2.1)}$$

In eq. 2.1 $\boldsymbol{\xi}$ and $\tilde{\boldsymbol{\xi}}$ are respectively the 3Nx1 column vector and the 1x3N row vector of the cartesian displacement coordinates of the nuclei, $f_{ij} = \left.\frac{\partial^2 V}{\partial \xi_i \partial \xi_j}\right|_0$ is the force constant which describes the dynamical coupling between the coordinates ξ_i and ξ_j. In eq. 2.1 the subscript 0 indicate that the quantity is evaluated at the equilibrium geometry. The second equality of eq. 2.1 is obtained in the assumption $V_0 = 0$ and taking into account that, at the equilibrium, the first derivatives of the intramolecular potential energy are 0 according to the requirement: $-\overrightarrow{\nabla_{\boldsymbol{\xi}}} V = \mathbf{0}$ (vanishing forces on the nuclei).

The kinetic energy of the nuclei is a quadratic form of the velocities, collected in the vector $\dot{\boldsymbol{\xi}}$:

$$T(\dot{\boldsymbol{\xi}}) = \frac{1}{2}\sum_i m_i \dot{\xi}_i^2 = \frac{1}{2}\tilde{\dot{\boldsymbol{\xi}}}\, \boldsymbol{M}\dot{\boldsymbol{\xi}} \qquad \text{(eq. 2.2)}$$

$\boldsymbol{M}$ is the diagonal matrix 3Nx3N collecting the masses of the atoms (each atomic mass appears three times, in correspondence of the three Cartesian coordinates of each atom). The knowledge of $V(\boldsymbol{\xi})$ and $T(\dot{\boldsymbol{\xi}})$ allows writing the classical equations of the motion, namely the system of differential equations:

$$\frac{d}{dt}\left(\frac{\partial T}{\partial \dot{\xi}_k}\right) + \frac{\partial V}{\partial \xi_k} = m_k \ddot{\xi}_k + \sum_j f_{kj}\xi_j = 0 \qquad k = 1,2,\ldots 3N \qquad \text{(eq. 2.3)}$$

Eq. 2.3 describes 3N coupled harmonic oscillators. The particular solutions – in the vibrational space - are in the form:

$$\xi_j(t) = A_j^s q_s^0 \cos(2\pi\nu_s t + \varphi_s) \qquad \text{(eq. 2.4)}$$

while the general solution is:

$$\xi_j(t) = \sum_s A_j^s q_s^0 \cos(2\pi\nu_s t + \varphi_s) \qquad \text{(eq. 2.5)}$$

The values of the vibrational frequencies $\{\nu_s\}$ can be obtained solving the set of algebraic homogeneous linear equation obtained from the set of differential equations (eq. 2.3), after the substitution of the particular solution (eq. 2.4):

$$(\boldsymbol{M}^{-1}\boldsymbol{F} - \lambda_s \mathbf{1})\boldsymbol{A}^s = \mathbf{0}, \qquad \lambda_s = (2\pi\nu_s)^2 \qquad \text{(eq. 2.6)}$$

If we ask for non-trivial solutions of eq. 2.6 ($\boldsymbol{A}^s \neq \mathbf{0}$), this requires:

$$\det(\boldsymbol{M}^{-1}\boldsymbol{F} - \lambda_s \mathbf{1}) = 0 \qquad \text{(eq. 2.7)}$$

Equation 2.7 is the so-called secular equation; in the secular equation the unknown λ_s, called frequency parameter, appears with a maximum power of 3N, so we expect finding 3N solutions, namely 3N values for λ_s. However, six roots of eq. 2.7 are null: they correspond to the non-vibrational degrees of freedom of the molecule, namely to the three translations and to the three rigid rotations of the molecule, which do not modify the intra-molecular potential energy V. Because the Hessian of V (i.e., the $\boldsymbol{F}$ matrix) evaluated in the equilibrium geometry of the molecule is positive definite, this guarantees that the 3N-6 non-zero values λ_s are positive and the set of 3N-6 vibrational frequencies can be obtained as $\nu_s = \frac{1}{2\pi}\sqrt{\lambda_s}$.

Once the values of the vibrational frequencies are determined, eq. 2.6 allows the determination of a set of vectors $\boldsymbol{A}^s$. Each $\boldsymbol{A}^s$ is called "vibrational eigenvector" of the normal mode Q_s. The matrix $\boldsymbol{A}$ formed by the collection of the $\boldsymbol{A}^s$ vectors can be regarded as the transformation which relates the cartesian coordinates of the atoms ($\boldsymbol{\xi}$) and the set of "normal coordinates" Q_s, which evolve with the time following the harmonic law: $Q_s = q_s^0 \cos(2\pi\nu_s t + \varphi_s)$, e.g. which are simple harmonic oscillator. Indeed, the following expression is the compact form of eq. 2.5:

$$\boldsymbol{\xi} = \boldsymbol{A}\,\boldsymbol{Q} \qquad \text{(eq. 2.8)}$$

Interestingly, when one only normal mode Q_w is excited ($q_w^0 \neq 0$ *and* $q_s^0 = 0$ *for* $s \neq w$) eq. 2.8 becomes:

$$\boldsymbol{\xi} = \boldsymbol{A}^{\boldsymbol{w}} Q_w = \boldsymbol{A}^w q_w^0 \cos(2\pi\nu_w t + \varphi_w) \quad \text{(eq. 2.9)}$$

Eq. 2.9 tell us that, when a normal mode is excited, all the atoms of the molecule oscillate *in phase at the same frequency* following the time evolution of a simple harmonic oscillator. The individual components of $\boldsymbol{A}^s$ describe the amplitude and direction of the oscillation for each atom of the molecule. Typically, localized normal modes show $\boldsymbol{A}^s$ eigenvectors with few large components. Collective modes present $\boldsymbol{A}^s$ eigenvectors with many components of similar values, which implies that a large number of atoms participate to the normal mode, oscillating with similar amplitudes.

As it will be clear in the following Chapters, the analysis of the computed vibrational eigenvectors allows the assignment of the vibrational bands, i.e. the description of the kind of vibration associated to each vibrational frequency, which is mandatory for the

rationalization of the spectral features. For instance, looking to eigenvectors we are able to recognize "stretching modes", which mainly involve changes of bonds length during the vibration, "bending" or "torsional" modes, which involve changes of the valence angles or of the torsional ones, etc. However, very often, normal vibrations are a rather complex mixing of vibrational displacements and can involve simultaneously stretching, bending and torsion of different chemical groups. Also in these cases, the eigenvectors analysis allows to rationalize changes of the spectra occurring in a set of molecules showing structural analogies, as for instance the polythiophene oligomers of increasing length, which are the object of this thesis.

As an example, in Figure 2.3 the sketch of the vibrational eigenvector of the stronger Raman line of T6 (unsubstituted oligothiophene constituted by six thiophene rings) is illustrated: the green segments indicate that the bond stretches, while the blue segments indicate that the bond shrinks. This mode can be classified as a collective CC stretching, with a contribution by CH in-plane bending (red arrows on H atoms).

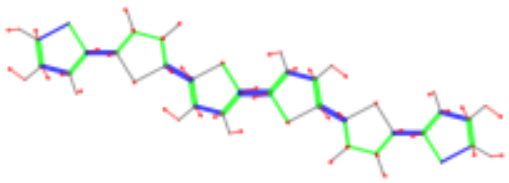

Figure 2.3: example of sketch of the eigenvector of a vibrational normal mode.

2.1.3. Calculation of the IR and Raman intensities.

The band intensities are obtained experimentally in the following way:

- IR spectrum: The intensity of the k-th band, A_k^{IR} , is the integral of the absorbance, namely the area of a whole band. As already mentioned, only the knowledge of the number of molecules responsible of the absorption allows the determination of the absolute intensity, I_k^{IR}.
- Raman spectrum: the band Cross-Section (σ_k^{Raman}) is the integral (area) of a Raman band. It is affected by the geometry of the experiment, by the polarization of the incident and scattered light and by several other factors. Absolute Raman intensities are rarely determined.

The derivation of the expressions describing the vibrational intensities require the Quantum Mechanical treatment of the vibrational transitions under the effect of the radiation field. In particular, the first order perturbation theory allows obtaining formulas for the probability of the vibrational transition associated to the absorption of a photon, giving rise to an IR

absorption band, while the description of the Raman scattering requires the use of the second order perturbation theory. Very roughly, the last observation explains why the Raman scattering is usually described as a weak phenomenon and why the development of the Raman spectroscopy has been driven by the availability of efficient sources (the lasers) and effective photons detectors.

Refs **[36-39]** provide a detailed description of the theory of the vibrational intensities. Here below we report the relationships that can be obtained in "double harmonic" approximation, namely under the assumption of harmonic intramolecular potential energy (eq. 2.1, Section 2.1.2), also referred as "mechanical harmonicity", and in the hypothesis of "electrical harmonicity", which implies that both the molecular dipole moment and the molecular polarizability are linear function of the normal coordinates Q_s.

In this framework, we can obtain IR and Raman selection rules. The first selection rule states that only vibrational transitions between adjacent vibrational levels can be induced by events such as IR absorption and Raman scattering. This explains why, both in the infrared and in the Raman spectra, the strongest bands usually correspond to the so-called fundamental transitions, which require the absorption by the matter of one only quantum of vibrational energy ($\Delta E = h\nu_k^{vib}$), corresponding to the energy distance between adjacent vibrational levels.

Importantly, the above-mentioned selection rule is the consequence of the double harmonic approximation, while weaker bands – which are often observed and ascribed to multiple quanta transitions cannot be described at this level of approximation. In this regard, while discussing the theoretical prediction of a spectrum, it is important to remember that the calculations are usually made in the hypothesis of double harmonic approximation, so they cannot reproduce experimental features different from the fundamental transitions. The spectra modelling reported in this thesis exploits the double harmonic approximation, so it deals with fundamental transitions.

In the framework illustrated above, the following remarkable relationships are obtained:

$$I_k^{IR} = K\left|\frac{\partial \vec{M}}{\partial Q_k}\right|^2 \qquad \text{(eq. 2.10)}$$

$$\sigma_k^{Raman} \div \left|\frac{\partial \boldsymbol{\alpha}}{\partial Q_k}\right|^2 \qquad \text{(eq. 2.11)}$$

where $\vec{M}$ is the molecular electric dipole moment and $\boldsymbol{\alpha}$ the molecular polarizability tensor and the derivatives are evaluated at the equilibrium geometry.

Eq. 2.10 tell us that the fluctuation of the molecular dipole moment during the vibration along the normal coordinate $Q_k$is the physical quantity which determines if Q_k is "IR active" (the IR selection rule is indeed: $\frac{\partial \vec{M}}{\partial Q_k} \neq \mathbf{0}$); moreover, the value of $\frac{\partial \vec{M}}{\partial Q_k}$ determines if an allowed transition (and the IR band associated to it) is strong or weak.

The absolute IR intensity is calculated according to eq. 2.10, where the constant K is a factor which depends on the units adopted. Usually, the values of $\frac{\partial \vec{M}}{\partial Q_k}$ are expressed in units of Debye Å^{-1} amu$^{-1/2}$ or e amu$^{-1/2}$and the absolute IR intensities are measured in km mol^{-1}.

Eq. 2.11 describes the simplest relationship between the Raman cross section of the k-th normal mode and the derivative of the molecular polarizability with respect to Q_k, and refers to an experiment where all the scattered photons are collected. Usually, the experimental set-up allows the collection of the scattered photons which propagate in a selected direction - typically parallel to the incident laser beam, in the so-called back-scattering geometry, or at 90° with respect to the incident beam.

According to the experimental set-up, it results that the cross section depends on combinations of the proper spatial averages of the elements of the Raman polarizability tensor, and usually it is re-written as a combination of the invariants of the $\frac{\partial \boldsymbol{\alpha}}{\partial Q_k}$ tensor.

For a Raman experiment conducted on an isotropic sample, where the incident laser light is polarized, but the scattered photons are collected (e. g. in backscattering) without selecting any polarization direction (no polarizer in the path of the scattered beam), we have:

$$\sigma_k^{Raman} = C_k \times \frac{1}{45}\left(45\,{\alpha'_k}^2 + 7\,{\gamma'_k}^2\right) \qquad \text{(eq. 2.12)}$$

In eq. 2.12 $\alpha'_k = \frac{1}{3}\,trace\left(\frac{\partial \boldsymbol{\alpha}}{\partial Q_k}\right)$ and γ'_k is the so-called "anisotropy" of the $\frac{\partial \boldsymbol{\alpha}}{\partial Q_k}$ tensor.

The quantity $I_k = \frac{1}{45}\left(45\,{\alpha'_k}^2 + 7\,{\gamma_k}^2\right)$ is called "Raman activity". The constant C_k is a rather complex factor, which depends on the experimental set-up. However, if we are interested to the theoretical prediction of the relative cross-sections of the Raman bands, $C'_k = \left(\frac{1}{\nu_k}\right)$ is the only factor needed for a comparison between theory and experiment. Indeed, making some reasonable approximation, we can show that C'_k is the only one term in the expression of C which affects in different way the cross section of the different k-bands the Raman spectrum.

In conclusion, when we plot a theoretically predicted Raman spectrum, we must use Raman intensities obtained from the computed Raman activities according to the relationship:

$$\mathcal{I}_k^{Raman} = \frac{1}{\nu_k}\left\{\frac{1}{45}\left(45\,{\alpha'_k}^2 + 7\,{\gamma'_k}^2\right)\right\} \qquad \text{(eq. 2.13)}$$

The Raman activity is usually expressed in units of Å^4 amu^{-1}, the $\frac{\partial \boldsymbol{\alpha}}{\partial Q_k}$ tensor in units of Å^2 amu$^{-1/2}$ or bohr^2 amu$^{1/2}$.

As for the IR, we can deduct from eq. 2.13 a Raman selection rule: it tells us that Raman active normal modes are such that there is at least one element of the Raman polarizability tensor is different from zero, $\frac{\partial \alpha_{uv}}{\partial Q_k} \neq 0$.

Raman and IR activities are ruled by the symmetry of the molecules, which allows determining, without any calculation, if a given normal mode is infrared active and if it is

Raman active. In other words, the symmetry analysis tells us if $\frac{\partial \vec{M}}{\partial Q_k} \neq \mathbf{0}$ and if $\frac{\partial \boldsymbol{\alpha}}{\partial Q_k} \neq \mathbf{0}$. In some cases, the effect of symmetry is immediately evident if one compares the IR and the Raman spectrum: for instance, for a molecule characterized by an inversion centre we observe the so-called "mutual exclusion", namely IR active normal modes are inactive in the Raman spectrum and vice-versa. This happens for instance for the oligomers of unsubstituted polythiophene with even number of rings and with planar conformation.

2.2. The electronic problems and the Density Functional Theory (DFT).

2.2.1. Theoretical foundation and concepts of the DFT.

The calculation of the vibrational spectra requires the determination of the physical quantities which are the "ingredients" determining the values of the experimental observables. These quantities ultimately depend on the molecular and on the electronic structure, which in turns is described by the molecular wavefunction (ψ_{mol}, including the electronic and nuclear wavefunction), which should be determined by solving the time-independent Schrödinger equation:

$$H_{mol}\psi_{mol} = E_{mol}\psi_{mol} \qquad \text{(eq. 2.14)}$$

The Born-Oppenheimer approximation **[40]** exploits the large difference between electronic and nuclear masses to separate the Quantum Physical problem for a molecule into an electronic problem and a problem for the nuclei. Referring to the discussion of the vibrational problem (Section 2.1), it is important to stress that we need to solve the electronic problem, ruled by the electronic Hamiltonian (parametrized by the nuclear coordinates $\boldsymbol{X}$), to obtain:

- The intramolecular potential energy surface $V(\boldsymbol{X})$.
- The equilibrium geometry of the molecule ($\boldsymbol{X}_0$) and then the force constants matrix.
- The molecular dipole moment and polarizability and their derivatives with respect to nuclear displacements.

The analytic solution of the electronic problem can be obtained only for the ion-molecule H_2^+; the case of many-electrons polyatomic molecules, must be faced by means of approximated methods which allow the calculation of the electronic wavefunctions, of the electronic energies and of the related quantities, which allow to predict the molecular properties.

A very effective approach, largely employed for the Quantum Mechanical study of molecular systems, is the Density Functional Theory, that will be abbreviated here as DFT **[41-43]**.

The theoretical foundation of DFT is the fact that the wavefunction and the one-particle electron density of a system constituted by N electrons are related through:

$$\rho(\boldsymbol{r}) = \rho(\boldsymbol{r}_1) = N \int \dots \int |\psi(x_1, x_2, \dots, x_N)|^2 d\sigma_1 \dots d\sigma_N dx_2 \dots dx_N \qquad \text{(eq. 2.15)}$$

where x_i and σ_i are the electronic spatial and spin coordinates respectively.

From $\rho(\boldsymbol{r})$ it is possible to calculate the total number N of the electrons of the considered system with:

$$N = \int \rho(\boldsymbol{r}) d\boldsymbol{r} \qquad \text{(eq. 2.16)}$$

The DFT is based on the Hohenberg-Kohn theorems, that refer to a system in which the electrons move under the effect of an external potential *V(**r**)*.

1) The first Hohenberg-Kohn theorem states that a ground-state system is fully and uniquely described by the electron density ρ. In other words, the external potential and so the total energy of the system is a functional of the electron density. Thanks to this theorem ρ can be used in eq. 2.15 to determine the ground-state wave function ψ and all other electronic properties of the system.
2) The second Hohenberg-Kohn theorem states that the electron density of the ground state minimizes its energy, and that the variational principle is applicable to functional of the energy, here labelled as $E_{DFT}(\rho)$, according to which the energy of a system calculated by DFT is always grater or equal to the real energy of system.

The energy functional $E_{DFT}(\rho)$ is given by the sum of three contributions:

$$E_{DFT}(\rho) = T(\rho) + V_{ne}(\rho) + V_{ee}(\rho) \qquad \text{(eq. 2.17)}$$

where $T(\rho)$ is the kinetic energy, $V_{ne}(\rho)$ is the nuclei- electron interaction and $V_{ee}(\rho)$ is the electron-electron interaction.

$V_{ee}(\rho)$ can be written as the sum of coulombic interaction term, $J(\rho)$, and the exchange interaction term, $K(\rho)$, according to

$$V_{ee}(\rho) = J(\rho) + K(\rho) \qquad \text{(eq. 2.18)}$$

In order to further expand the expression of $E_{DFT}(\rho)$, it is possible to use the Kohn-Sham approach, in which the electrons wavefunction is built based on molecular orbitals Φ_i forming a Slater determinant and $T(\rho)$ is split up into two contributions, such that:

1. $T(\rho) = T_0(\rho) + T_c(\rho)$ (eq. 2.19)

2. $\rho(\boldsymbol{r}) = \sum_i^N |\Phi_i(\boldsymbol{r})|^2$ (eq. 2.20)

where $T_0(\rho)$ is the non-interacting term and $T_c(\rho)$ is the correlation term.

Now, the complete expression of the energy functional $E_{DFT}(\rho)$ is:

$$E_{DFT}(\rho) = T_0(\rho) + T_c(\rho) + V_{ne}(\rho) + J(\rho) + K(\rho) \qquad \text{(eq. 2.21a)}$$

which can be re-written as:

$$E_{DFT}(\rho) = T_0(\rho) + V_{ne}(\rho) + J(\rho) + E_{xc}(\rho) \qquad \text{(eq. 2.21b)}$$

where $E_{xc}(\rho) = T_c(\rho) + K(\rho)$ is the exchange correlation functional.

While there exist analytical expressions for $T_0(\rho)$, $V_{ne}(\rho)$ and $J(\rho)$, the exchange correlation functional contains all the unknown terms of the energy functional and so approximations of $E_{xc}(\rho)$ at various levels of theory have to be introduced. Indeed, while performing a DFT calculation we must select the kind of exchange-correlation functional which we consider to be the most suitable for our simulation.

The time-independent Schrödinger equation in the Kohn-Sham form

$$\left(-\frac{1}{2}\Delta_1 - \sum_{I01}^{N}\frac{Z_I}{r_{I_1}} + \int\frac{\rho(r_2)}{r_{12}}d\,r_2 + V_{xc}(r_1)\right)\Phi_i(r_1) = \varepsilon_i\Phi_i(r_1) \qquad \text{(eq. 2.22)}$$

with

$$V_{xc}(\rho) = \frac{\partial E_{xc}(\rho)}{\partial\rho} \qquad \text{(eq. 2.23)}$$

must be solved to obtain the Kohn-Sham orbitals, expressed as a basis, leading to the eigenvalue problem.

In this study we will exploit the Hybrid B3LYP functional **[44-46]** and the range-separated CAM-B3LYP functional **[47-48]** as approximated expression of the exchange correlation functional and the polarized 6-31G** (or 6-31G(d,p)) basis set **[41]**.

2.2.2. Closed and open shell systems: the restricted and the unrestricted configuration.

In this thesis we will treat oligothiophenes in the neutral and charged state.

Neutral molecules are usually described as *closed shell* systems, thus meaning that each molecular orbital (MO) is occupied by two electrons with opposite spin, while *open shell* systems are characterized by unpaired electrons, belonging to different spin-orbitals, namely with a different "spatial" description. In order to understand the differences between these systems, the total spin $\hat{S}$ and the spin *multiplicity* of the system have to be defined:

$$\hat{S} = \sum_{i=1}^{N} s_i(i) \qquad \text{(eq. 2.24)}$$

$$multiplicity = 2S + 1 \qquad \text{(eq. 2.25)}$$

where the total spin of a system with N electrons is the vector sum of all electrons spins $s_i(i)$, the multiplicity is the number of possible orientations of the total spin and S is the spin quantum number, which can assume half-integer or integer values. The total spin angular momentum can assume the values:

$$\hat{S}^2 = S(S+1). \qquad \text{(eq. 2.26)}$$

Closed shell systems, i.e. those characterized by an electronic configuration with paired spin in each occupied molecular orbital, present spin quantum number S=0 and so multiplicity equals to 1: for this reason, they are defined as singlet. For what concerns open shell systems, as the charged radical cations which are object of our study, they are described as systems with only one unpaired electron: this kind of open shell systems present S=½ and can assume s_z values ½, -½ . For this reason, its spin multiplicity equals to 2. Of course, there exist other kinds of open shell systems with increasing spin quantum number, multiplicity and total spin: a summary of the most important possibilities is reported in Table 2.1. As an example, a system with an even number of electrons, could adopt an open shell configuration. This is the case of a molecule with the two highest occupied orbitals forming a pair with the same energy (degenerate orbitals), which, according to the Hund rule should be both occupied by one electron. The two electrons have parallel spins, thus resulting in a triplet state, S= 1.

Table 2.1: spin quantum number, multiplicity and total spin of closed and open shell systems.

Spin quantum number S	**Multiplicity 2S+1**	**Total spin S^2=S(S+1)**
0	1 → singlet	0
1/2	2 → doublet	0,75
1	3 → triplet	2
3/2	4 → quartet	3,75
2	5 → quintet	6

Moreover, also systems characterized by an even number of electrons, and which do not show degenerate molecular orbitals, can adopt an open shell configuration of the ground state (this phenomenon is typical of the so called biradicaloid molecules). Their electronic configuration can be described in two different ways:

1. *Restricted configuration*: spins α and β are restricted to occupy the same spatial orbital.
2. *Unrestricted configuration*: each spin (α and β) is allowed to have different spatial orbitals.

A schematic representation of the two possible configurations is reported in Figure 2.4:

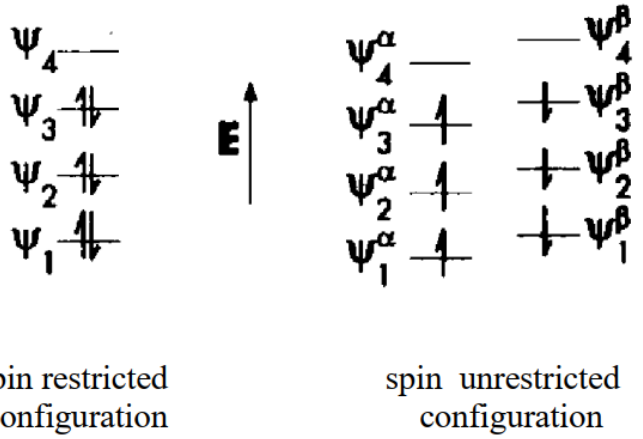

Figure 2.4: schematic representation of the spin restricted and unrestricted configurations.

In table 2.2 we summarize the main advantages and drawbacks concerning the use of restricted and unrestricted configurations.

Table 2.2: main advantages and drawbacks of spin restricted and unrestricted configurations.

	ADVANTAGES	DRAWBACKS
RESTRICTED CONFIGURATION	Restricted closed shell ψ have correct and well-defined value of the total spin, according to the values reported in Table2.1. In other words, they are eigenfunctions of the total spin operator $\hat{S}^2$.	• A ψ with proper spin and antisymmetry cannot be described as a single Slater determinant. • Restricted open shell ψ do not consider spin polarization.
UNRESTRICTED CONFIGURATION	Unrestricted open shell ψ do describe spin polarization because they allow α and β spin electrons to occupy different spatial orbitals.	• Unrestricted open shell ψ are not eigenfunctions of $\hat{S}^2$. • They suffer from the spin contamination by states with higher spin.

2.3. The ECC theory

ECC (Effective Conjugation Coordinate) theory was developed in order to rationalize the peculiar characteristics of the Raman spectra of many polyconjugated organic materials, and in particular of the polymers known as conducting polymers and their oligomers.

The idea behind the ECC model is that for these systems it is possible to define a collective vibrational coordinate of the nuclei, called ECC or Я coordinates, which represents a particular trajectory of the nuclei in the vibrational space, characterized by the maximum coupling with the π electrons (electron-phonon coupling). For a generic oligoene constituted by N CC bonds, the ECC is analytically defined as **[20, 21, 30]**:

$$R_{ECC} = \frac{1}{\sqrt{N}} \sum_{j=1}^{N} (-1)^j R_j \qquad \text{(eq. 2.27)}$$

where R_j is the internal stretching coordinate of the j-th CC bond and the j index labels the CC bonds from one to the other end of the molecule.

Considering the polyacetylene (PA), which is treated as an oligoene of infinite length, thus meaning a 1D crystal with translational unit constituted by one single and one double CC bond, the ECC defined in Equation 2.24 becomes:

$$R_{ECC} = \frac{1}{\sqrt{2}} (R_1 - R_2) \qquad \text{(eq. 2.28)}$$

and so is the valence **q=0** phonon coordinate defined as the out-of-phase stretching of the single (R_1) and of the double (R_2) CC bond belonging to the unit cell of the 1-D crystal **[22]**.

The equilibrium position of the ECC coordinate defines the "degree of alternation" of the sequence of conjugated CC bonds that form the skeleton of conducting polymers and their oligomers. This parameter, known as BLA (Bond Length Alternation), depends on the degree of delocalization of the π electrons and is the structural parameter most sensitive to confinement phenomena due to distortion of the conformation, defects, finite size of the molecule, intermolecular interactions.

Moreover, the ECC coordinate allows to describe the distortion of the equilibrium molecular geometry passing from the ground state to the first excited state. The typical effect is a significant change in BLA, for example from a quasi-single/near-double alternating bond structure to a structure with almost equalized bonds. The BLA variation from the neutral to the excited state is responsible for the Stokes shift typically observed by comparing absorption and fluorescence spectra of polyconjugated molecules.

The introduction of the collective ECC coordinate in the study of the vibrational dynamics of polyacetylene and other polyconjugated polymers has made it possible to rationalize the characteristics of Raman spectra and their variations within families of parent molecules, such as polyenes of increasing length.

The ECC coordinate does not coincide with a single normal mode. However, the normal modes described by eigenvectors with an important projection on the ECC turn out to be

the most interesting, because they determine the most evident spectroscopic characteristics (they are responsible for the most intense bands) and carry information related to the electronic structure (conjugation of π electrons and their mobility).

It has also been shown that the ECC coordinate plays an important role in explaining the appearance at IR of strong transitions, associated with vibrational modes of charge defects (polarons) that are formed when conducting polymers are doped, i.e. the so-called Infra-Red Activated Vibrations (IRAVs).

The ECC theory can be applied also to polyconjugated polymers more complex than polyenes, like polythiophenes (PT) studied in this thesis.

Considering a generic polythiophene, it can be treated as an infinite 1D crystal with its translational unit constituted by two thiophene units in trans-planar conformation, as represented in Figure 2.5.

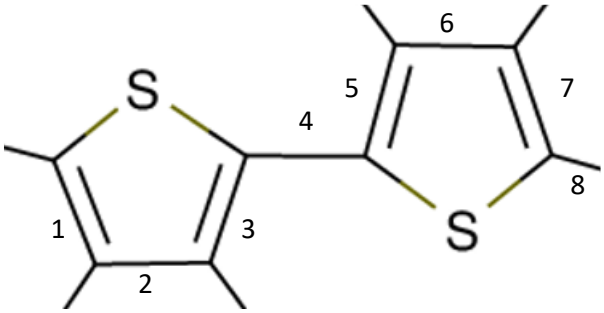

Figure 2.5: schematic representation of the translational unit of a generic polythiophene.

According to the numeration of the CC bonds presented in Figure 2.4, the analytical expression of the ECC for a polythiophene, derived from equation 2.24, becomes **[20]**:

$$R_{ECC} = \frac{1}{\sqrt{8}}(R_2 - R_1 + R_4 - R_3 + R_6 - R_5 + R_8 - R_7) \qquad \text{(eq. 2.29)}$$

From the spectroscopic point of view, the ECC theory allows rationalizing the strong Raman transitions and the onset of IRAVs of the polythiophene and of its oligomers, also in the case of oligothiophenes with lateral alkyl chains, as it will be demonstrated in this thesis. The main difference with respect to the simple case of polyenes regards the fact that the number of degrees of freedom in the vibrational space is increased: the coupling of the ECC with them induces the formation of several IRAVs upon the doping process instead of only two, as it happens in the IR spectrum of PA. An analogous consideration is valid also for the Raman spectrum of neutral PT and P3HT, which is dominated by transitions associated to normal modes involving the ECC oscillation **[49]**.

2.4. Computational details

In this Section we collect all the technical-computational details regarding the DFT simulations presented in the following Chapters of this thesis.

Guess geometry and molecular editor. The guess geometry of all the molecular models that will be optimized by the DFT calculation to obtain the minimal energy of the system are realized with the Avogadro and IQmol molecular editors.

Quantum-chemical simulation: the input file. All the DFT simulations are performed with the GAUSSIAN G09 software **[50]**.

From the operative point of view, performing a quantum-chemical simulation means three consequential steps:

1) Development of the *input* file *(.inp)*
2) Run of the computation by the GAUSSIAN G09 software.
3) Checking of the correct termination of the calculation (the output file must end with *normal termination)* and analysis of the produced data with the *post-processing* operations.

Four files are generated at the end of a quantum-chemical simulation:

1) The *input file* (*.inp*)
2) The *output file* (*.out*), which contains all the results of the calculation.
3) The *checkpoint file* (*.chk*)
4) The *formatted checkpoint file* (*.fchk*), obtained with the command *gformo09d* to the checkpoint file.

The fundamental step to perform a quantum-chemical calculation is the production of the so-called *input* file *(.inp)*, which is constituted as follow:

```
%chk=3PT8.chk
#P B3LYP/6-31G(d,p) opt freq(Raman)

3ET8

0 1
  H   17.1774990   -1.8395470    0.0286330
  C   16.1845640   -1.4364130    0.1722690
  C   15.8239980   -0.2752300    0.7965420
  C   14.4176290   -0.0378890    0.8196270
  C   13.7081290   -1.0574030    0.1846390
  C   12.2951570   -1.2602320   -0.0262530
  C   11.6941190   -2.3432590   -0.6564040
  C   10.2870530   -2.3096230   -0.7247150
  C    9.7575680   -1.1593370   -0.1229180
  C    8.4147480   -0.6908550    0.0290360
  C    8.0118800    0.5113640    0.6150020
  C    6.6307770    0.7544550    0.6273710
  C    5.9016020   -0.2942180    0.0340920
  C    4.5032450   -0.4947000   -0.1468330
  C    3.8851310   -1.6121090   -0.7214860
```

Figure 2.6: example of the starting lines of an input file for quantum-chemical simulations.

The first line expresses the name of the checkpoint file.

The second line contains the following information:

- #P to have an output file in the extended version.
- B3LYP describes the level of theory used to perform the calculation, by the indication of the functional adopted. In our study we exploited the B3LYP and the CAM-B3LYP functionals. For the charged species a *U* before the functional is added, so B3LYP and CAM-B3LYP become UB3LYP and UCAM-B3LYP respectively, in order to adopt the unrestricted configuration (see Section 2.2).
- 6-31G(d,p) or 6-31G** indicates the atomic orbitals (AO) basis set which is adopted to express the molecular orbitals (MOs)
- After the previous needed indications, the operations the computation has to perform must be indicated. In particular, our DFT simulations aim at performing the geometry optimization, with the keyword *opt*, and the IR and Raman spectroscopic features, with the keyword *freq(Raman)*.

The third line is left blank.

The fourth line contains the title of the quantum-chemical calculation.

The fifth line is left blank.

The sixth line contains the charge and the multiplicity of the system. In our study we dealt with neutral and singly charged oligothiophenes, for which line six is written as *0 1* and *1 2* respectively.

Then, the molecular geometry of the considered molecule is reported: it can be expressed in cartesian coordinates or in internal coordinates as Z-matrix.

The last line of the input file must be left blank, otherwise the calculation gives error.

Constrained geometry optimization. All the neutral model molecules considered in this thesis, both the unsubstituted oligothiophenes and the oligothiophenes with lateral alkyl chains, are characterized by a planar geometry, which is not the most energetically stable structure for the isolated molecules: if full geometry optimization of the oligothiophenes is performed, the backbone assumes a non-planar conformation **[15]**. Similar considerations regard the oligothiophenes in the charged state: the self-localization of the charged defect introduced by the doping process, i.e. the polaron, modifies the conformation of the considered oligomers. Since we would like to describe the properties of a solid-state material, which is characterized by a sequence of co-planar rings, we had to constrain the geometry during the optimization procedure to obtain a model molecule with planar structure. The procedure is different for unsubstituted oligothiophenes and for oligothiophenes with lateral alkyl chains:

1. **Unsubstituted models.** In order to obtain a planar structure of neutral and charged oligomers, it was sufficient to impose that DFT simulation recognizes the C_{2h} symmetry of the considered molecules: the standard keyword IOp(2/17=4) in the GAUSSIAN G09 software was modified into IOp(2/17=2) to change the tolerance for

distance comparisons in symmetry determination. This procedure was adopted for all the unsubstituted oligothiophenes in the neutral and charged state.

2. **Models with lateral alkyl chains.** In this case, symmetry considerations do not provide any help since oligothiophenes with lateral alkyl chains do not belong to any point symmetry group, due to the presence of lateral substituents. In order to obtain a planar structure of the backbone, we had to perform a constrained geometry optimization: the keyword changes from *opt* to *opt(modredundant)* to impose all the dihedral angles to be fixed at 180°. With reference to Figure 2.7, the dihedral angle is defined as (S-C2-C5′-S′). In the input file after the molecular geometry of the oligothiophene a series of lines with indication like *D S-C2-C5′-S′ F* id added, where S, C2, C5′ and S′ are labelled according to the specific numeration of the atoms in order to define all the dihedral angles present in the backbone.

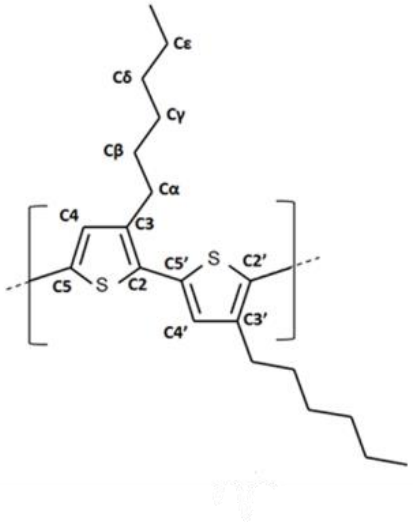

Figure 2.7: chemical structure and atom numbering of the repeating unit of P3HT and its oligomers.

Post-processing and data analysis. The command *gauarchive* file.fchk file.out reorganizes all the results of the DFT simulation contained in the output file. This command generates a series of folders containing all the geometrical and spectroscopic parameters of the molecule, either directly calculated during the Gaussian run or obtained after a postprocessing of its output data (collected in the chk file). Among the other data we obtain the optimized geometry, the force constants, the sketch of the eigenvectors associated to every normal mode the IR and Raman spectra and the associated local parameters, and many other data. The program was developed by Prof. M.[2]Tommasini.

The analysis of the collected data we carried out in this thesis work regards not only the simulated vibrational spectra of neutral and charged oligothiophenes but also the IR and

[2] Dipartimento di Chimica, Materiali e Ingegneria Chimica “G. Natta”, Politecnico di Milano.

Raman local parameters and the equilibrium bond length values referred to the CC bonds of the backbone of the oligomers: the numeration of the CC bonds, present on the x-axis of the plots containing these parameters, is obtained by assigning the a numerical code to each C(j)-C(k) bond of the backbone (running along the molecular backbone from one end to the other, and matching it with the corresponding pair of atoms (j,k) in the Gaussian input data relative to the molecular geometry). To better clarify the procedure, we report in Figure 2.8 the complete atomic numbering of the backbone of the octamer of (3-ethyl thiophene), according to the molecular geometry specified in the input file of the computation for this molecule and also the numeration of the CC bonds.

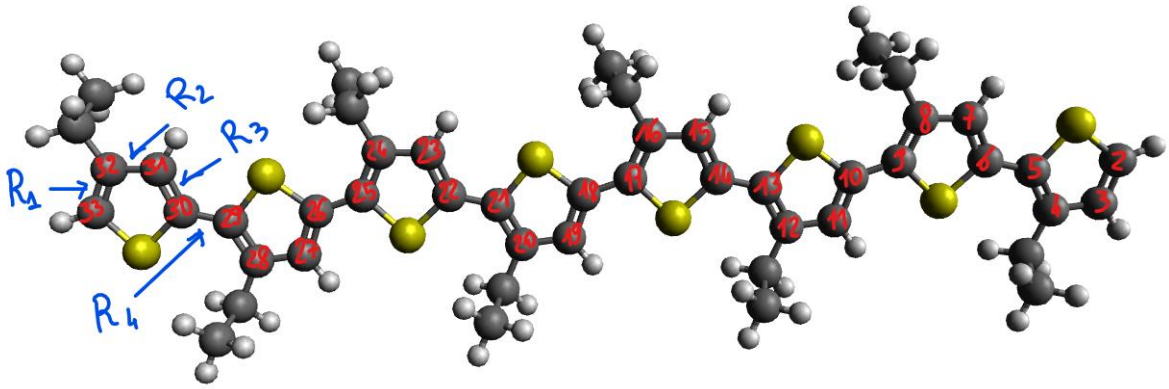

Figure 2.8: numeration of the C atoms and CC bonds for 3ET8 according to the Gaussian input.

The comparison between the simulated IR and Raman spectra with the experimental results is performed visualising the spectra in the Omnic software. An empirical scaling factor of 0,9742 has been applied to the computed frequencies in order to fit experimental data: this value is obtained such that the second most intense peak of the Raman spectrum of neutral 3HT8, that is the model of the octamer of (3-hexyl thiophene), coincides in frequency with the one of the experimental spectrum of P3HT.

3 Molecular models of unsubstituted oligothiophenes.

3.1. The effect of the chain length on the geometry and on the vibrational spectra of neutral and charged oligothiophenes.

In this Section, we will present the computed IR and Raman spectra of the neutral and charged unsubstituted oligothiophenes of increasing chain length, from six to fourteen rings constituting the backbone of the molecule. The aim of this Section is to understand the effect of the chain length on the spectroscopic properties of the considered oligomers in both the pristine (undoped) and charged (doped) states. In particular, after presenting the computed IR and Raman spectra of the oligothiophenes, we will focus our attention on the results regarding the most intense IR and Raman ECC normal mode. Indeed, this ECC normal mode represents the most relevant spectroscopic feature of these materials and in general for any sp-2 carbon based conjugated material, especially when considering the molecules in the charged (doped) states: we will show its vibrational eigenvector, pointing out the collective oscillation of the atoms, and how its frequency and intensity change by increasing the chain length. In order to understand the above spectroscopic features, it is useful to analyse the IR and Raman intensity local $\left(\frac{\partial M}{\partial R}\right)$ and the polarizability derivative$\left(\frac{\partial \alpha}{\partial R}\right)$ both with respect to the CC stretching internal coordinate. We will mainly focus on the stretching of the CC bonds over the other internal coordinates because, according to the definition given in Chapter 2 of the Я coordinate, the ECC-like normal modes involve the out-of-phase stretching of the quasi-single and quasi-double CC bonds and they are the spectroscopic fingerprints of polyconjugated materials. These parameters are affected by the number of thiophenes constituting the oligomeric chain and by the charge transferred in the doped state.

We will finally focus our attention on the geometrical properties of oligothiophenes in both pristine and charged (doped) state, especially by considering the computed equilibrium bond lengths of single and double bonds. These parameters are mostly affected by the doping procedure resulting in a change of the Bond Length Alternation (BLA) parameter, that is the length difference between two adjacent carbon bonds, according to the following equation:

$$BLA_k = R_{k\,C-C} - R_{(k-1)C=C} \qquad \text{(eq. 3.1)}$$

where $R_{k\,C\text{-}C}$ is the equilibrium bond length of the k-th quasi-single CC bond and $R_{(k\text{-}1)\,C=C}$ is the equilibrium bond length of the (k-1)-th quasi-double CC bond.

All parameters were obtained by DFT calculations considering the hybrid B3LYP functional and the Pople double split valence basis set with diffuse and polarization functions (6-31G**). Neutral species (0) were computed in the restricted (closed-shell) configuration, while charged species (i.e., radical cation, +1) were treated in the unrestricted configuration (as doublet).

We use the label T*n*, with *n* the number of thiophene rings, for indicating a neutral oligothiophene chain (e.g., T6: six thiophene rings in the neutral/pristine state), and the label T*n*(+1) for the oligothiophene in the charged (doped state) (e.g., T6(+1): six thiophene rings in the doped/charged state). Globally we considered the following chain lengths: T6, T8, T12, T14 and T6(+1), T8(+1), T12(+1), T14(+1).

It is important to specify that all the results related to the charged species refer to a singly charged radical-cation, meaning that a single electron is withdrawn from the highest occupied molecular orbital (HOMO) of the neutral (pristine) oligomer: this situation describes the formation of the so-called polaron, that is a charge defect (namely an hole trapped by the potential created by the structural relaxations of the nuclei upon charging) induced within the oligomer chain after the doping.

Such model is quite far from the real doping process, where the polymer chains and the dopants interact one another. Indeed, within this frame, the inter-molecular interactions between the charged oligomer and the counter-ion (dopant) are not taken into account. Here, we focus only on the oligomer side, at the end of a charge transfer of 1 electron from the polymer to the dopant. Despite the limits of such description, for the above reason, it should be suitable for the description of the doped phases where the anions are rather distant from the doped polymer, as it happens in the crystalline phase.

All the oligothiophenes are assumed to be in the *trans-planar* conformation **[15]**, as it is represented in Figure 3.1. Moreover, all the model oligomers do not bear any lateral alkyl chain, instead present in P3HT, which are substituted with hydrogen atoms.

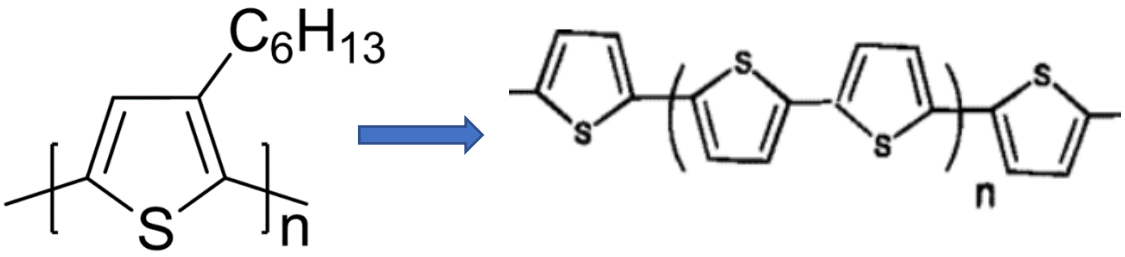

Figure 3.1: Chemical structure of P3HT and unsubstituted oligothiophenes. In our study n is such that the total number of thiophene units ranges from 6 to 14.

3.1.1. Neutral oligothiophenes

We will start the discussion presenting the spectroscopic and geometrical features of the oligothiophenes in the pristine state, focusing on their change with the increasing number of thiophenes constituting the molecular backbone.

In all the simulations, the optimized geometry of all the molecules is planar, since we imposed the calculation to recognize the C_{2h} symmetry of unsubstituted oligothiophenes, which otherwise would tend to distort when isolated.

IR spectra and dipole derivative parameters. In Figure 3.2 we report the calculated Infra-Red (IR) spectrum of neutral oligothiophenes with increasing length, from T6 to T14; the wavenumber of the spectra ranges from 500 to 4000 cm^{-1}.

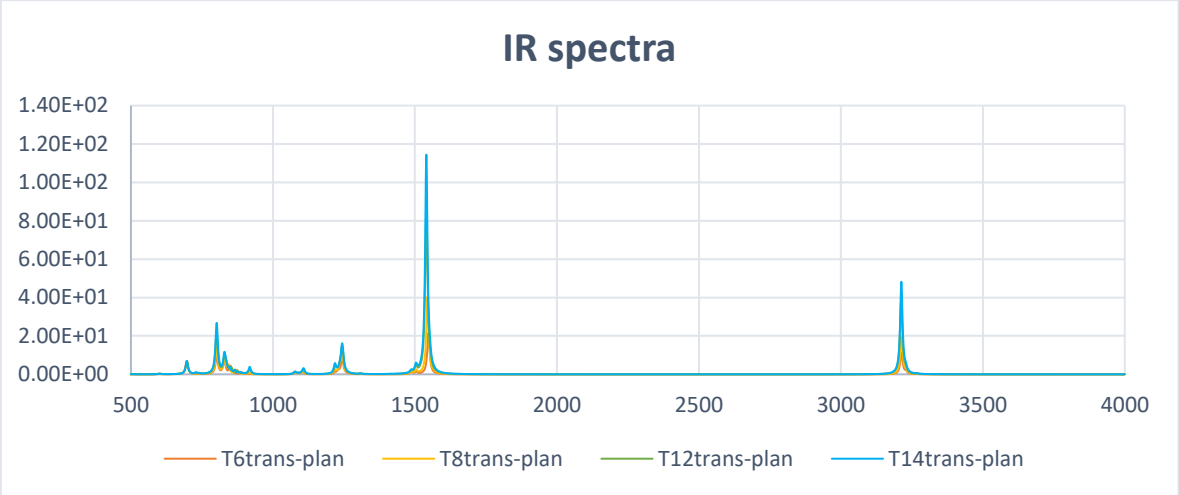

Figure 3.2: IR spectra of neutral Tn. In orange the IR spectrum of T6, in yellow the IR spectrum of T8, in green the IR spectrum of T12 and in light blue the IR spectrum of T14. The vertical axis report IR intensities (km mol^{-1}/cm^{-1})

Figure 3.3 shows the same IR spectra of Figure 3.2 in specific spectral regions, in order to better underline the differences between spectra.

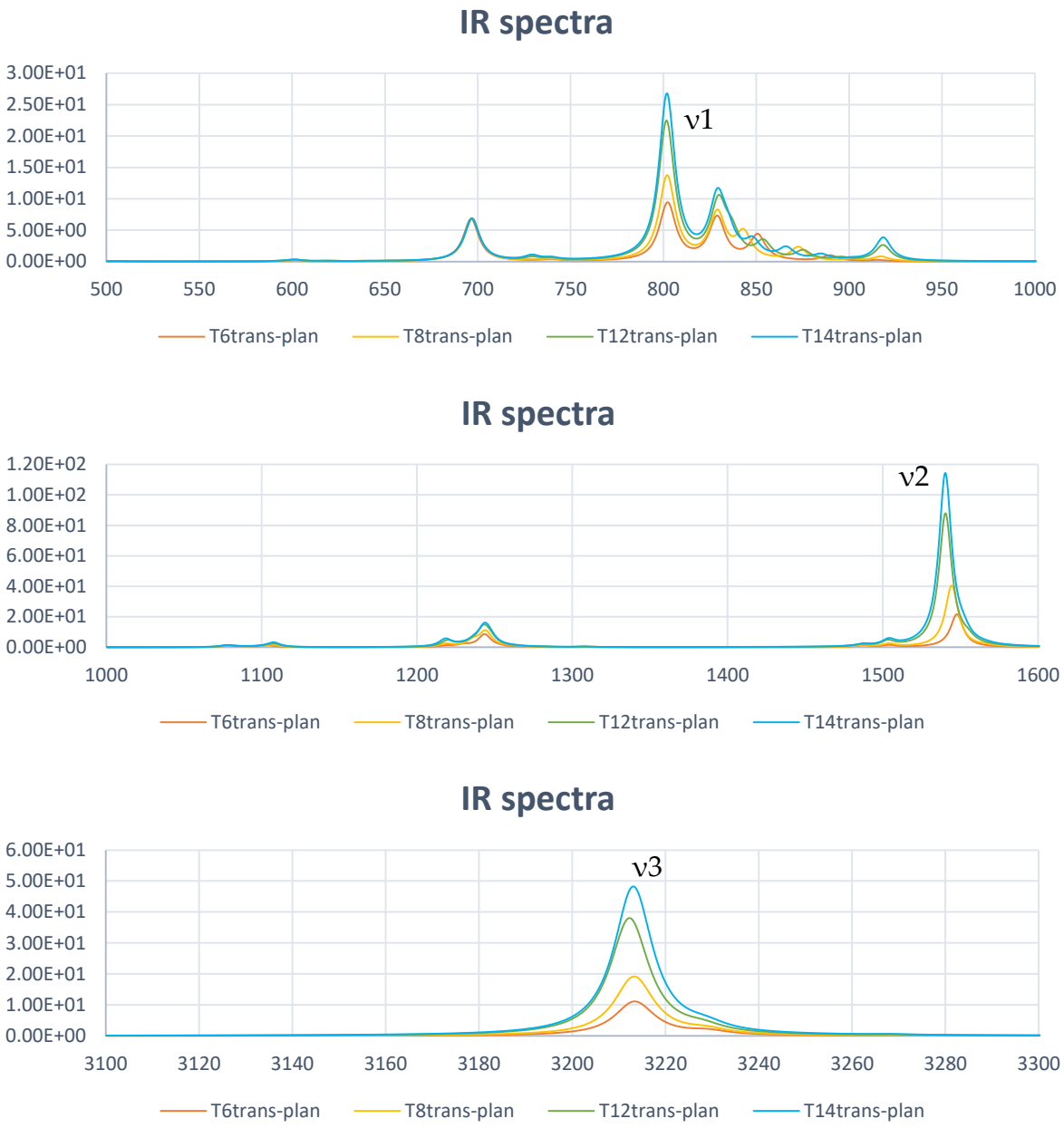

Figure 3.3: zoomed IR spectra of neutral Oligothiophenes. IR spectra from 500 to 1000 cm^{-1}; IR spectra from 1000 to 1600 cm^{-1}; IR spectra from 3100 to 3300 cm^{-1}.

From the previous spectra, it is evident that the IR spectrum of Tn presents three main bands:

1) The first, labelled ν1, is a doublet in the wavenumber region from 800 and 850 cm^{-1}, whose associated normal modes are represented by C-H out-of-plane deformation modes, in the thiophene units of the central part of the molecule, while the peak at 700 cm^{-1} is determined by C-H out-of-plane deformation mode in the peripheric rings of the chain.
2) the most intense peak, labelled ν2, has frequency around 1550 cm^{-1}, whose associated normal mode is represented by the anti-symmetric stretching of the *quasi*-double C=C bonds of each thiophene ring. It cannot be ascribed to the ECC (Effective Conjugation coordinate) mode, namely to the typical, strongly Raman active, vibration of polyconjugated molecules. A smaller contribute to this normal mode is given by the antisymmetric stretching of the C-S bonds of the thiophene rings and by the in-phase stretching of the inter-ring C-C bonds on half molecule; the node in the centre of the oligomer induces the phase inversion of the normal mode (for a sketch of the eigenvector see Section 3.1.3).
3) The third important peak, labelled ν3, has frequency around 3210 cm^{-1}, whose associated normal mode is represented by the in-phase antisymmetric stretching of the C-H bonds of each thiophene unit.

It is important to underline the fact the most relevant band in the IR spectra of Tn oligothiophenes is the one indicated as ν2; in fact, considering for example the T12 case, the ratio between the intensity of ν2 with the other two peaks (ν3 and ν1) read as:

$$\frac{I_{\nu 2}}{I_{\nu 3}} = \frac{1375[\frac{km}{mol}]}{327[\frac{km}{mol}]} \approx 4{,}2 \qquad \frac{I_{\nu 2}}{I_{\nu 1}} = \frac{1375\left[\frac{km}{mol}\right]}{207\left[\frac{km}{mol}\right]} \approx 6{,}6$$

The analysis of the IR spectra of neutral oligothiophenes allows to make some general considerations about the effect of the chain length on the IR properties:

a. Considering the most relevant bands of the IR spectra, it is possible to notice how their frequency slightly changes by moving from short (T6) to long (T14) oligomers, thus suggesting that the chain length has a very modest influence on the frequency of the IR bands.

b. The whole IR spectrum is subjected to an increase of the intensity.

It is important to underline the fact that the overall increasing intensity of the IR spectrum passing from short to long oligomers is modest, especially if compared with what happens for the charged molecules, as it will be shown later in the chapter. For

neutral Tn oligomers, the IR intensity increase with chain length is mainly due to the additivity of the contribution to IR intensity by each thiophene units; it is possible to demonstrate it by summing up all the IR intensities associated to every normal mode and dividing the result by the number of the thiophene rings, according to the following equation:

$$I_n = \frac{[\sum_{k=1}^{s} I_k]}{n} \qquad \text{(eq. 3.2)}$$

where I_n [km/mol] is the normalized IR intensity with respect to the number (n) of thiophene units constituting the Tn oligothiophene; I_k [km/mol] is the IR intensity of every normal mode; s is the total number of IR active normal modes and n is the number of the thiophene rings present in the considered molecule.

The results of eq.3.2 are reported in table 3.1:

Table 3.1: normalized total IR intensity with respect to the number of thiophene units for neutral oligothiophenes with increasing chain length.

Oligothiophene	Normalized IR intensity in (km/mol)
T6	213
T8	242
T12	283
T14	298

The computed IR intensity is rather constant by increasing Tn, thus confirming the additivity of IR intensity with n, as reported in Figure 3.4.

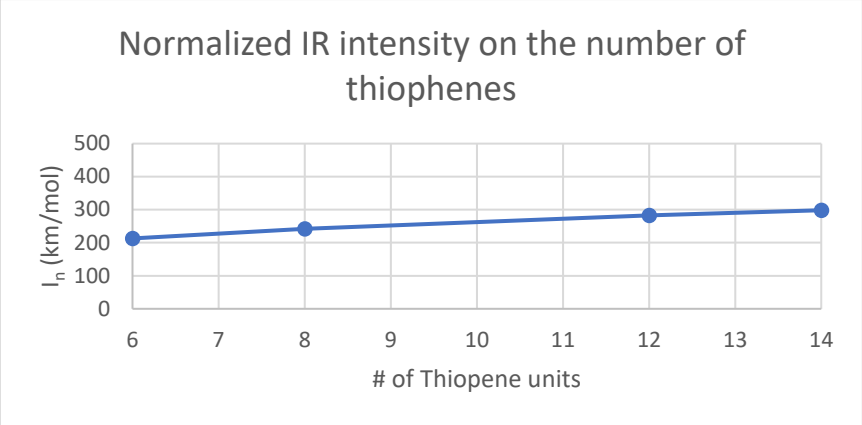

Figure 3.4: Total IR intensity normalized on the number of thiophene units.

It is interesting to notice that the general IR intensity increasing with the number of thiophenes doesn't occur for the peak at 700 cm^{-1} because, involving the final rings, is not additive with the number of thiophene units.

It is possible to rationalize the slight increasing trend of the normalized IR intensity on the number of thiophene rings, as it can be appreciated in Figure 3.4, by means of the dipole derivative parameters, because they directly affect the infra-red intensities, according to the equations presented in Chapter 2. Figure 3.5, in which the central CC bond is indicated by a yellow dot, reports the y-component of the derivative of the dipole moment with respect the internal coordinate of CC stretching, indicated as ∂My/∂R. We choose to report only ∂My/∂R and not the x- and z- components, because ∂Mz/∂R is null due to the perfect planarity of the models and since y represents the long axis of the molecule, which is the direction along which a large charge flux takes place during the vibrations, namely the dipole derivative component along this direction become the relevant one in charged oligothiophenes.

Similar considerations could be done also for the other internal coordinates that define the normal modes associated to the relevant IR peaks. We decide to report the ∂M/∂R parameter because the CC stretching normal mode is the responsible for the most intense peak in the IR spectrum of oligothiophenes.

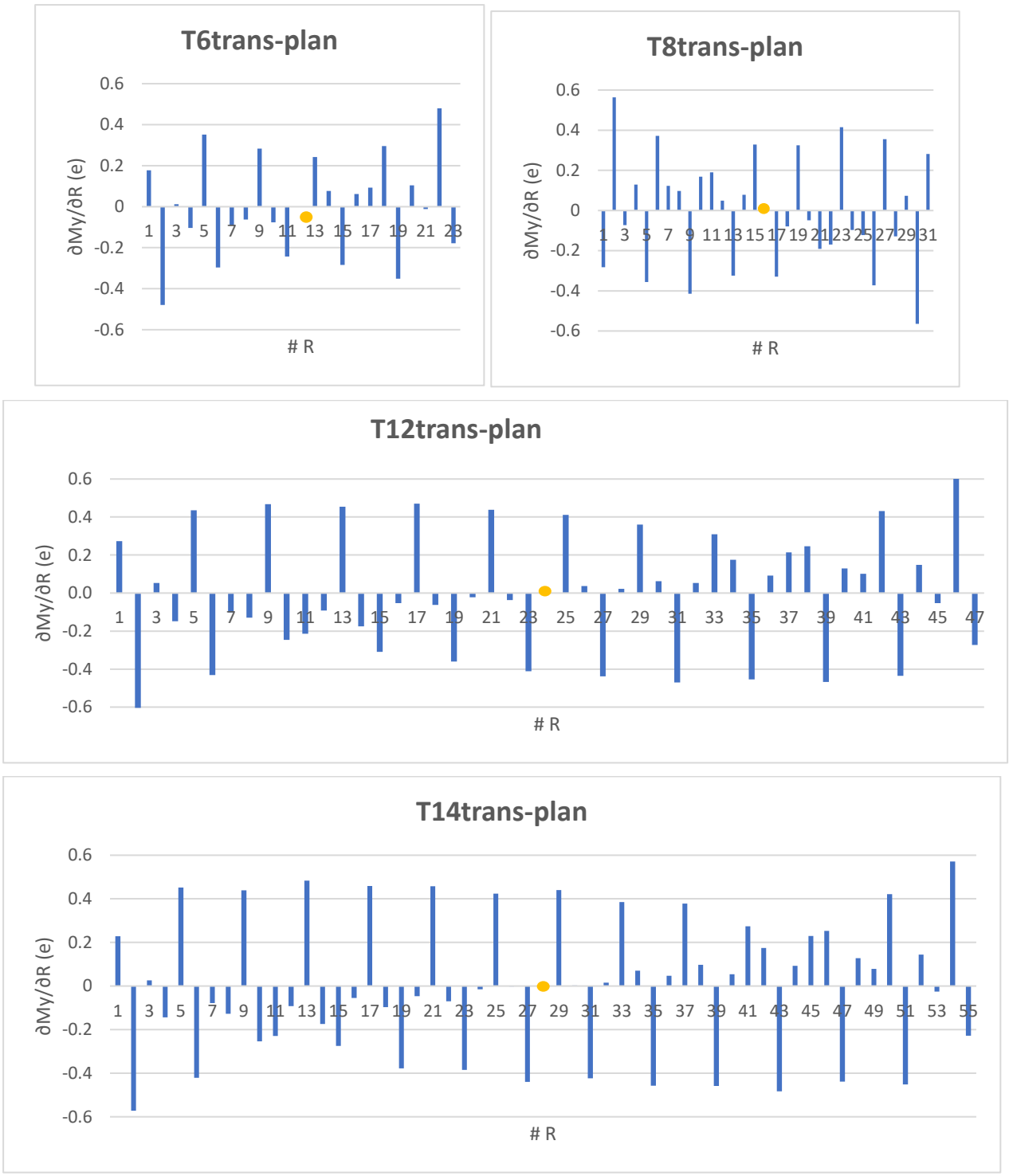

Figure 3.5: from the top to the bottom: y-component of dipole derivative with respect C-C stretching internal coordinate of neutral T6, T8, T12, T14. On the horizontal axis # R indicates the label of C-C single or double bond constituting the backbone of the oligothiophene (the bonds are numbered sequentially from the left to the right end of the molecule).

From Figure 3.5 it is possible to notice how the dipole derivative with respect to the stretching internal coordinate of the central bond, that is the centre of inversion, is null. It is also interesting to notice that the pattern of the ∂M/∂R parameter is symmetric with respect to the central C-C bond due the C_{2h} symmetry of the various Tn, but with opposite sign due to the presence of the centre of inversion. Finally, from the plots in Figure 3.5 it is clear that the modulus of the dipole derivative with respect the C-C bonds stretching slightly increases with the increasing chain length of the oligothiophene, thus explaining the reason why the intensity of the peaks in the IR spectrum increases slightly more than linearly by increasing number of the thiophene units.

Raman spectra and polarizability parameters. Figure 3.6 shows the Raman spectrum in the 900-1600 cm-1 region (where the most intense peaks of the spectrum are concentrated) of neutral oligothiophenes with increasing chain length, from T6 to T14.

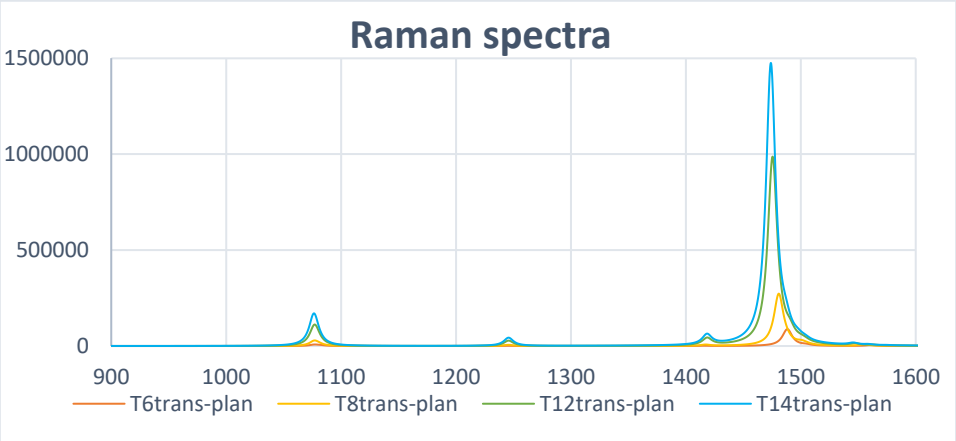

Figure 3.6: Raman spectrum of neutral Tn. In orange the Raman spectrum of T6, in yellow the Raman spectrum of T8, in green the Raman spectrum of T12 and in light blue the Raman spectrum of T14. The vertical axis report Raman Intensities ($Å^4$ amu^{-1}/cm^{-2})

The Raman spectrum of neutral Tn is constituted by a single very intense band, that dominates all the Raman features, whose frequency is in the wavenumber range from 1470 and 1490 cm^{-1}. The associated normal mode is represented by the collective out of phase stretching of the single and double CC bonds, which means that all the single bonds (C-C), both the one within each thiophene unit and the inter-ring bonds, shrink (or stretch), while the double bonds (C=C) stretch (or shrink). For this reason, the presented normal mode is ascribed to a collective ECC mode or Я mode.

For what concerns the effect of the chain length on the Raman properties of neutral oligothiophenes, from Figure 3.6 it is possible to notice that the red-shift (i.e., lower

wavenumbers) of the frequency of the Raman peak passing from short to long oligomers is surely more significant with respect to the case of IR spectra, in fact:

$$\Delta\nu_{Raman} = \nu_{T6} - \nu_{T14} = 15\ cm^{-1}$$

$$\Delta\nu_{IR} = \nu_{T6} - \nu_{T14} = 8\ cm^{-1}.$$

This will be further analysed in Section 3.3.1 dedicated to the insight about the most intense Raman mode.

It is important to underline the fact that the predicted frequency dispersion of the ECC peak in the simulated Raman spectrum for oligothiophenes with increasing chain length is not observed experimentally **[13]** : this effect is a further evidence of the fact that B3LYP overestimates the delocalization of π electrons (the so-called delocalization error) and so its conjugation length, that is the main parameter affecting the position (frequency) of the Raman peak. Also in the case of Raman spectra, the increasing chain length has an influence on the intensity of the band, causing its increasing. However, at difference from IR intensity, the trend of the Raman intensity of the ECC mode is more than linear with n. Such trend is expected because of the strong coupling of the ECC mode with π electrons, which in turns makes the Raman polarizability tensor very sensitive to electrons delocalization.

Indeed, the analysis of the local Raman parameters, namely the polarizability derivative with respect to the internal coordinate of CC stretching, indicated in the following as $\partial\alpha/\partial R$, allows the rationalization of this phenomenon, because it directly affects the Raman intensity of the ECC mode, according to the equations presented in chapter 2. In Figure 3.7 we report the trace of the $\partial\alpha/\partial R$ parameter of every carbon bond constituting the backbone of the molecule for the four considered oligomers, we indicate the central CC bond with a red dot. The analysis of this parameter is appropriate, because in oligothiophenes the tensor $\partial\alpha/\partial R$ exhibits a dominant diagonal element in the direction of the molecular axis, while the out-of-diagonal elements of the tensor provide a small contribute to the tensor. For this reason, the behaviour of $\partial\alpha/\partial R$ is captured just by one of the tensor invariants, namely the sum of the diagonal elements of the tensor (trace). It is useful to specify that from now on the symbol $\partial\alpha/\partial R$ indicates the trace of the polarizability tensor, indicated in the whole work with the symbol $\boldsymbol{\alpha}$.

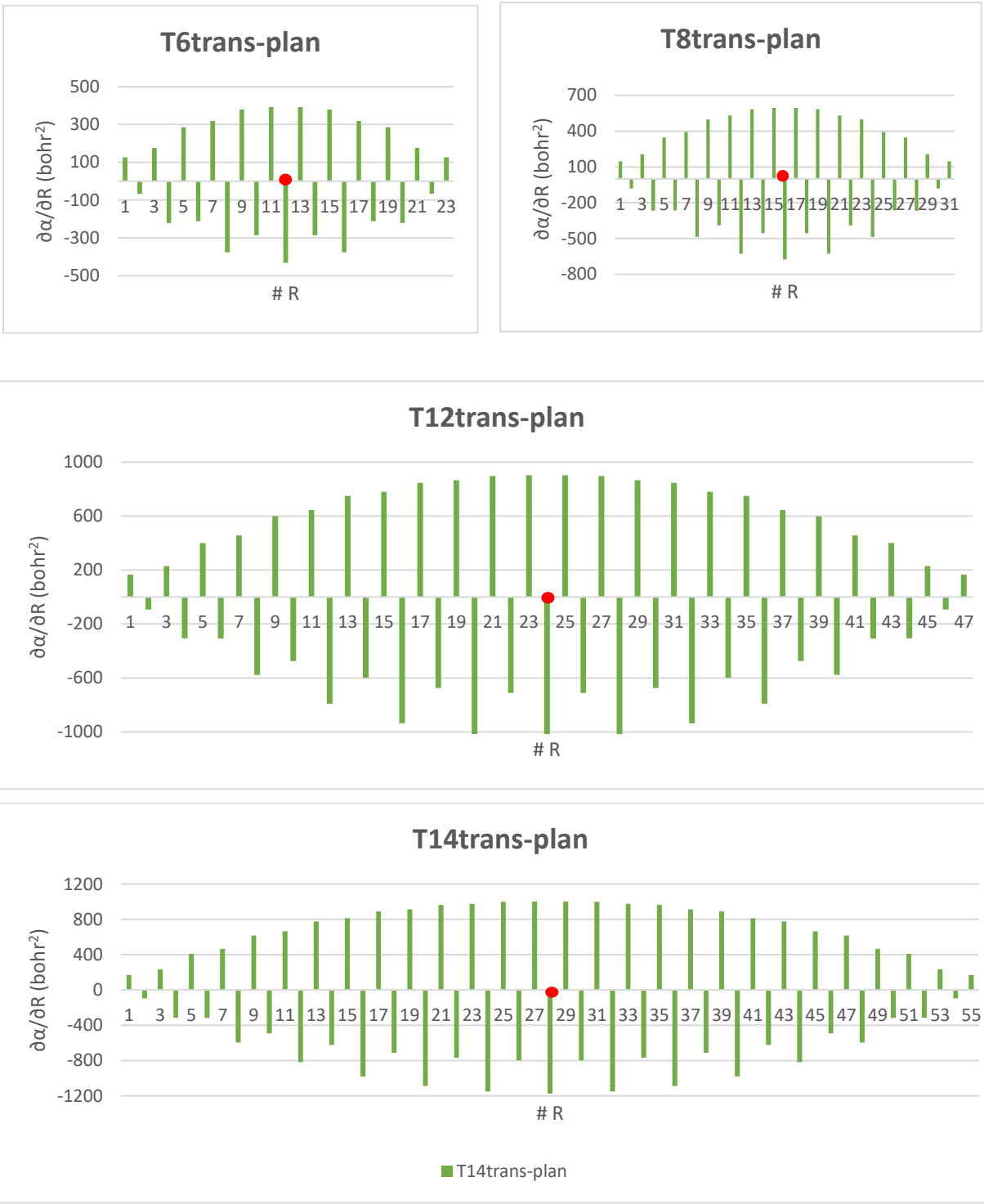

Figure 3.7: from the top to the bottom polarizability derivative with respect C-C stretching internal coordinate of neutral T6, T8, T12, T14. On the horizontal axis # R indicates the number of C-C single or double bond constituting the backbone of the oligothiophenes.

From Figure 3.7, it is clear how the ∂α/∂R parameter assumes larger absolute values with the increasing chain length of the oligothiophene (passing from a maximum value

of 400 bohr² to a maximum value of 1000 bohr²), thus explaining the more than linear increasing intensity of the Raman peak with n. More precisely, if we do the normalization procedure of the Raman activity on the number of thiophene units, already presented in the IR case, we find out that the normalized Raman activity exhibits a linear trend with the chain length. The formula is:

$$I_n = \frac{[\sum_{k=1}^{s} I_k]}{n} \qquad \text{(eq. 3.3)}$$

where I_n [Å⁴/amu] is the normalized total Raman activity with respect to the number of thiophene units constituting the oligothiophene; I_k [Å⁴/amu] is the Raman activity of every normal mode; s is the total number of normal modes and n is the number of the thiophene units present in the considered molecule. The results are reported in Figure 3.8 and Table 3.2.

Table 3.2: normalized total Raman activity with respect to the number of thiophene for oligothiophenes with increasing chain length.

Oligothiophene	Normalized Raman activity in (A⁴/amu)
T6	83857
T8	192504
T12	457152
T14	580114

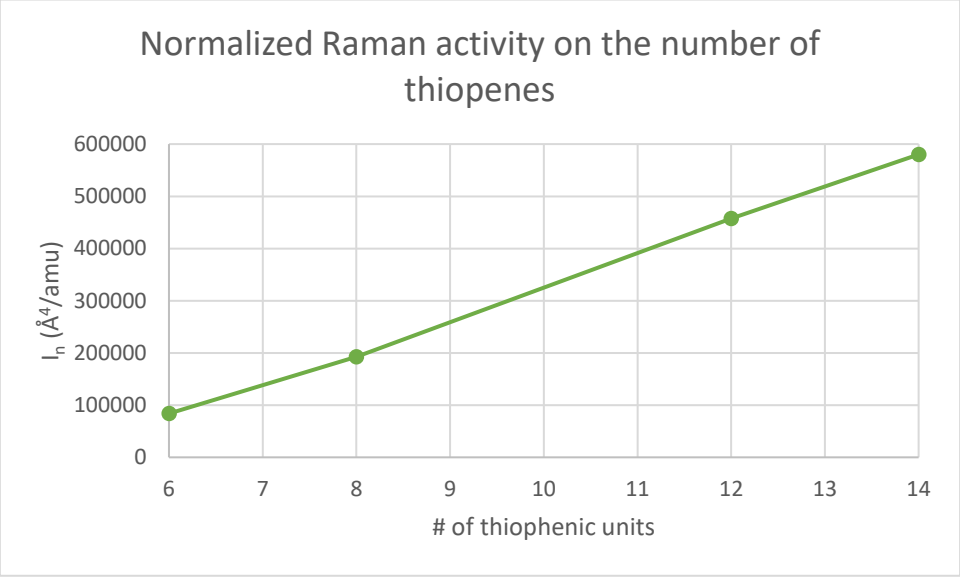

Figure 3.8: Total Raman activity normalized on the number of thiophene unit.

Moreover, the ∂α/∂R parameter allows to obtain another important information about the structure of the neutral oligothiophene: in all four considered molecules the pattern of the Raman parameter presents a rigorous alternation of positive (relative to the stretching of quasi-double CC bonds) and negative values (relative to the stretching of quasi-single CC bonds). The sign change follows the pattern of the bond length along with the molecular backbone of all the neutral oligomers, which is characterized by the alternation of quasi-double and quasi-single carbon bonds. This characteristic can be appreciated by the analysis of the geometrical parameters, namely the equilibrium bond length of the single and double C-C bonds, that will be presented in the following Section.

Geometrical parameters. Figure 3.9 shows the pattern of the bond length of every single and double C-C bond constituting the backbone of the oligothiophenes; the central CC bond is indicated by a blue dot.

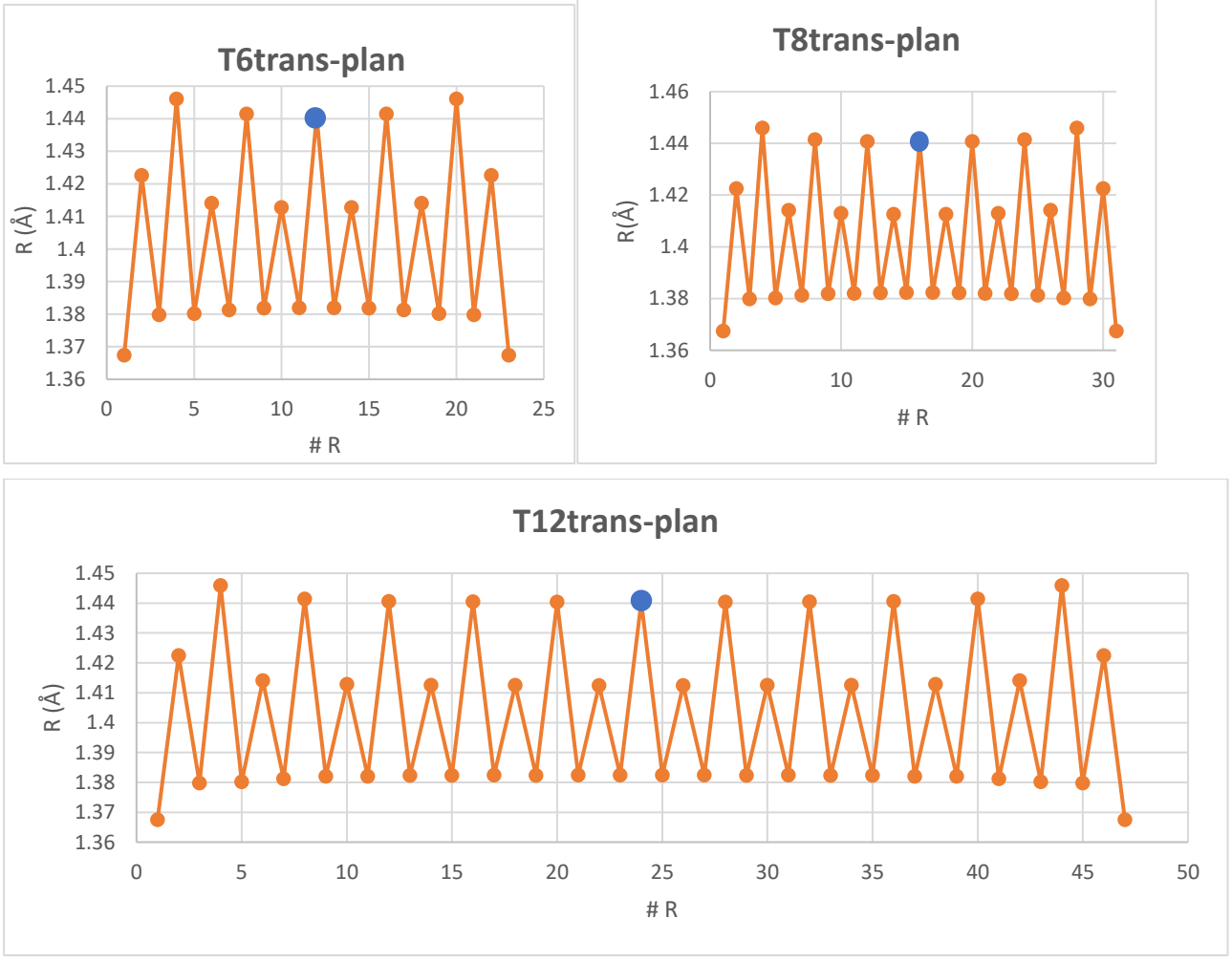

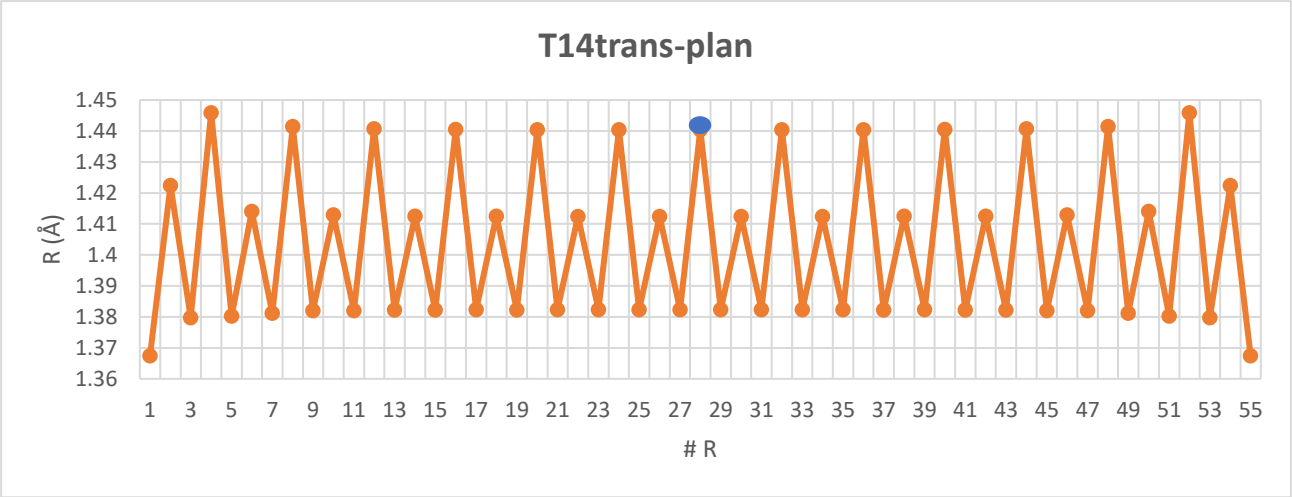

Figure 3.9: bond length of neutral T6, T8, T12, T14. On the horizontal axis # R indicates the number of C-C single or double bond constituting the backbone of the oligothiophene.

The data shown in Figure 3.9 go on par with the result obtained analysing the $\partial\alpha/\partial R$ parameter: all the odd C-C bonds exhibit a length near 1,37 Å and so they can be considered as quasi-double C-C bonds, while all even bonds show a quasi-single bond character. Indeed, they are characterized by a length between 1,41 Å and 1,43 Å for the quasi-single bond belonging to the thiophene rings (its shortness indicates the high aromaticity of each thiophene) and a length near 1,45 Å for what concerns the inter-ring bond. The alternation of quasi-single and quasi-double bonds predicted by looking at the sign of the polarizability derivative parameters is further confirmed by the analysis of the bond lengths.

In order to evaluate the effect of the chain length onto the geometrical properties, it is convenient to calculate the average of the Bond Length Alternation, indicated as <BLA>, according to the following equation:

$$< BLA > = < R_{C-C} > - < R_{C=C} > = \frac{\sum_{k=1}^{N} R_{2k}}{N_{C-C}} - \frac{\sum_{k=1}^{N} R_{(2k-1)}}{N_{C=C}} \qquad \text{(eq. 3.4)}$$

where BLA is the Bond Length Alternation [Å]; N is the total number of C-C bonds, R_{2k} are the length of the even CC bonds, that are single C-C bonds, $R_{(2k-1)}$are the length of the odd CC bonds, that are C=C double bonds, $N_{C\text{-}C}$ is the total number of single C-C bonds and $N_{C\text{-}C}$ bonds is the total number of C-C double bonds.

For the four considered oligothiophenes the following results hold, reported in table 3.3:

Table 3.3: average BLA for oligothiophenes with increasing chain length.

Oligothiophene	<BLA> (Å)
T6	0,049879
T8	0,048430
T12	0,046903
T14	0,046490

From these results, it is evident that the average BLA is small, as expected for highly conjugated systems like oligothiophenes. It is anyway significant to underline the decreasing trend of the BLA parameter with the increasing chain length, thus indicating the increasing π electrons delocalization length passing from short to long oligomers.

3.1.2. Charged oligothiophenes.

In this Section we will analyse the effect of the chain length on the geometry and on the IR and Raman vibrational spectra of oligothiophenes with an increasing number of thiophene rings when they undergo a doping process. These models aim to simulate the formation of a singly charged cation and the so-called polaron charge defect within the oligomer chain, because of the extraction of a single electron from the highest occupied molecular orbital of pristine (neutral) oligothiophene to the dopant.

We will follow the same scheme adopted in Section 3.1.1: we will firstly present the IR spectrum of charged oligothiophenes and its correlation with the IR intensity local parameters, then we will show the Raman spectrum and the Raman intensity local parameters. Finally, we will focus our attention on the geometrical parameters, mainly the equilibrium CC bond lengths and Bond Length Alternation (BLA).

IR spectra and dipole derivative parameters. Figure 3.10 reports the IR spectrum of charged oligothiophenes with increasing chain length, from T6 to T14, in the wavenumber region between 1000 and 1600 cm^{-1}, where the most intense IR peaks appear, namely the so-called IRAV. The spectroscopic features of the corresponding neutral oligothiophenes in the pristine states, like the -CH out-of-plane deformations at 700 and 800 cm^{-1} or the -CH stretching at 3200 cm^{-1}, are still present in the case of charged molecules, but their IR intensity with respect to the IRAV peaks is weaker, in such way those IR characteristics can be considered negligible.

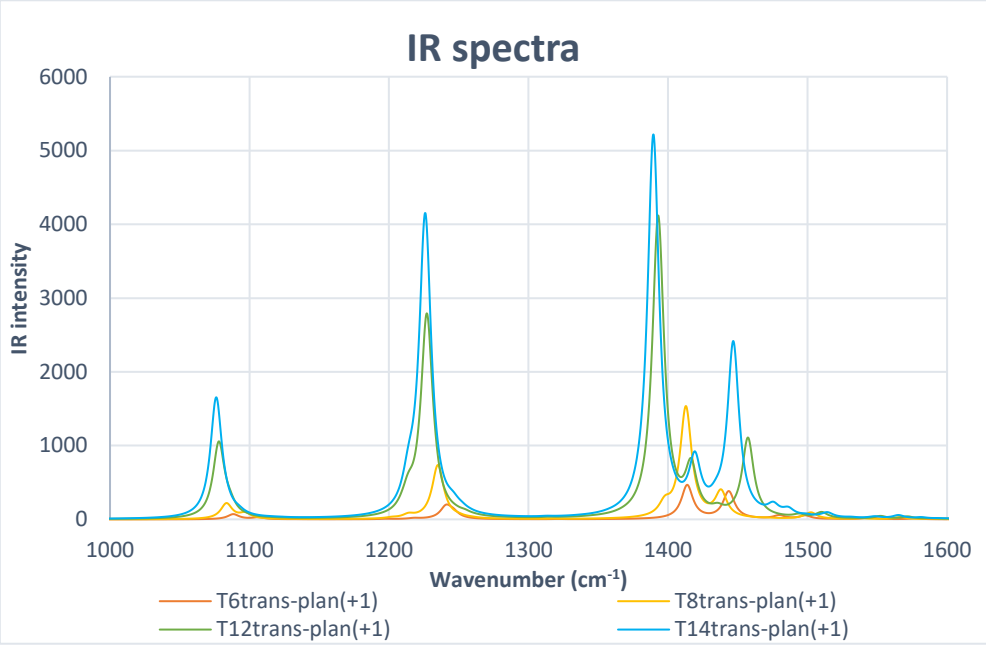

Figure 3.10: IR spectrum of charged Tn(+1). In orange the IR spectrum of T6(+1), in yellow the IR spectrum of T8(+1), in green the IR spectrum of T12(+1) and in light blue the IR spectrum of T14(+1).

From Figure 3.10 it is possible to notice that the IR spectrum of charged oligothiophenes is characterised by four main peaks:

1) The first relevant peak has frequency between 1070 and 1090 cm^{-1}, whose associated normal mode is represented by the collective in-phase stretching of the single C-C bonds, both those within each thiophene unit and the inter-ring ones, while the quasi-double C=C bonds are essentially not involved; a contribute to the normal mode is also given by the in-phase stretching of the two C-S bonds of each thiophene, which vibrate out-of-phase with respect to the single C-C bonds. Because of the inversion symmetry, the IR active modes have ungerade character, so that if the single C-C bonds on half molecule stretch (shrink), the C-S bonds shrink (stretch) and the vibration inverts the phase due to the presence of a node in the centre of the oligomer.
2) The second important peak has frequency around 1230 cm^{-1}, whose associated normal mode is determined by the out-of-phase stretching of the single C-C bonds within each thiophene and the single C-C inter-ring bonds, by the in-phase stretching of the double C=C bonds and by the in-phase stretching of the C-S bonds (except for the first thiophene ring and the last one of half molecule),

that vibrate in-phase with the single C-C bond within the ring. This normal mode presents a node in the centre of the molecule.

3) The most intense IR band has frequency around 1400 cm^{-1} and the normal mode is the Я-like normal mode, thus the collective out-of-phase stretching of the single C-C bonds and the double C=C bonds, resembling the Raman ECC mode of the neutral oligothiophenes: all the single C-C bonds shrink (or stretch), while all the double C=C bonds stretch (or shrink) and a smaller contribute arises from the in-phase stretching of the C-S bonds in each thiophene unit. The collective vibration inverts its phase through the central node.
4) The fourth relevant peak has frequency around 1450 cm^{-1}, whose associated normal mode is a Я-like mode, very similar with respect to the previous one, with three nodes and so the collective vibration changes its phase four times.

The appearance of collective modes – characterized by one or more nodes located along the chain - is typical of oligomers and reveals the close correlation between their vibrational normal modes and the phonons of the parent polymer (described as an ideally infinite 1-D crystal) **[50]**.

Even if a systematic comparison between neutral and charged oligothiophenes for what concerns both vibrational spectra and geometry will be presented in Section 3.2, from Figure 3.10 it is possible to make some general considerations about the differences between the IR spectrum of oligothiophenes in the doped state and in the pristine state:

a. The IR intensity of the most important peaks is extremely high with respect to the one of the IR spectra of neutral corresponding oligomer: to take consciousness of this fact, it is sufficient to look at the scale of the IR intensity, comparing Figure 3.10 and Figure 3.2,whose maximum value is about 6000 km mol^{-1}/cm^{-1} for the IR spectrum of charged Tn(+1) and about 120 km mol^{-1}/cm^{-1} for the one of neutral Tn and so their ratio equals about 50. This aspect can be easily rationalized by means of the dipole derivative parameter with respect to the internal CC stretching coordinate, as it will be shown later in this Section.
b. Vibrational modes showing a similar pattern as those described above at points from 1 to 4 are pretty silent in the IR when the oligothiophenes are in the pristine state: they become IR active upon the doping process, taking the name of Infra-Red Activated Vibrations (IRAVs). A detailed explanation about IRAVs and the mechanisms they arise from will be given in Section 3.2; so far, it is important to notice that all the strong IR transitions described at points 1-4 shows some ECC-like character.

We will now focus our attention on the effect of chain length on the IR spectrum of charged oligothiophenes with increasing number of thiophene rings and from Figure 3.10 we can notice that:

a. The red-shift of the frequency of the IR peaks when the number of thiophenes increases is more pronounced than in the case of neutral oligothiophenes, especially if we consider the most intense IRAV at 1400 cm^{-1}, thus confirming the fact that the ECC-like normal modes are very sensitive to the conjunction length, arising from the π electrons delocalization on the molecular backbone: the longer the conjugation length, the lower the force constant associated with the Effective Conjugation Coordinate (ECC) and its vibrational frequency, thus explaining the important red-shift of the frequency passing from short to long oligomers;

b. The intensity of the IR peaks increases with the increasing number of thiophenes constituting the molecular skeleton.

By adopting the same procedure presented in Section 3.1, it is possible to demonstrate that the increasing of the IR intensity for what concerns charged oligothiophenes cannot be ascribed only to the additivity of IR intensity with the number of thiophenes, as it occurs in the case of neutral oligothiophenes. We calculate I_n [km/mol], the normalized IR intensity with respect to the number of Thiophene units constituting the oligothiophene, according to the following equation:

$$I_n = \frac{[\sum_{k=1}^{s} I_k]}{n} \qquad \text{(eq. 3.5)}$$

where I_k [km/mol] is the IR intensity of every normal mode; s is the total number of IR active normal modes and n is the number of the thiophene rings present in the considered molecule. The results are reported in Table 3.4 and Figure 3.11:

Table 3.4: normalized IR intensity with respect to the number of thiophene units for charged oligothiophenes with increasing chain length.

Oligothiophene	Normalized IR intensity in (km/mol)
T6(+1)	3765
T8(+1)	6888
T12(+1)	14405
T14(+1)	17905

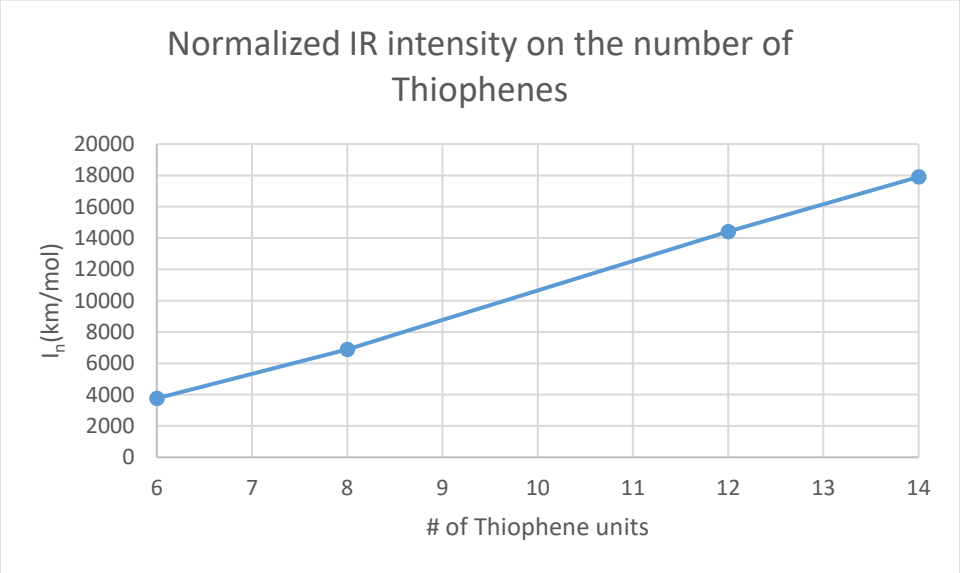

Figure 3.11: Total normalized IR intensity on the number of thiophene units for charged oligothiophenes with increasing chain length.

From Figure 3.11 it is evident that the normalized IR intensity on the number of the thiophene units in the molecular backbone exhibits a linear trend with the chain length and so the IR intensity increases more than linearly passing from short to long oligomers. For this reason, at difference of the case of neutral oligothiophenes, the increasing of IR intensity with increasing chain length cannot be explained simply by considering the additivity of this property with the number of thiophene rings. The more then linear increment of the IR intensity with the chain length is another important proof of the peculiarity of the IRAVs, which show analogies with the parent strongly active Raman modes of the neutral molecules (showing a more than linear increase of their intensity) and justify their description as "IR activated" Raman vibrations, when polyconjugated molecules are subjected to a doping process.

Also in the case of charged oligothiophenes, the IR intensity increasing with the chain length of the oligomer can be fully rationalized by taking into account the local IR intensity parameters, mainly the dipole derivative with respect to the C-C stretching internal coordinate, $\partial M/\partial R$, whose its y-component in the direction of the molecular axis (which is the largely dominant one) is represented in Figure 3.12 for oligothiophenes of increasing chain length.

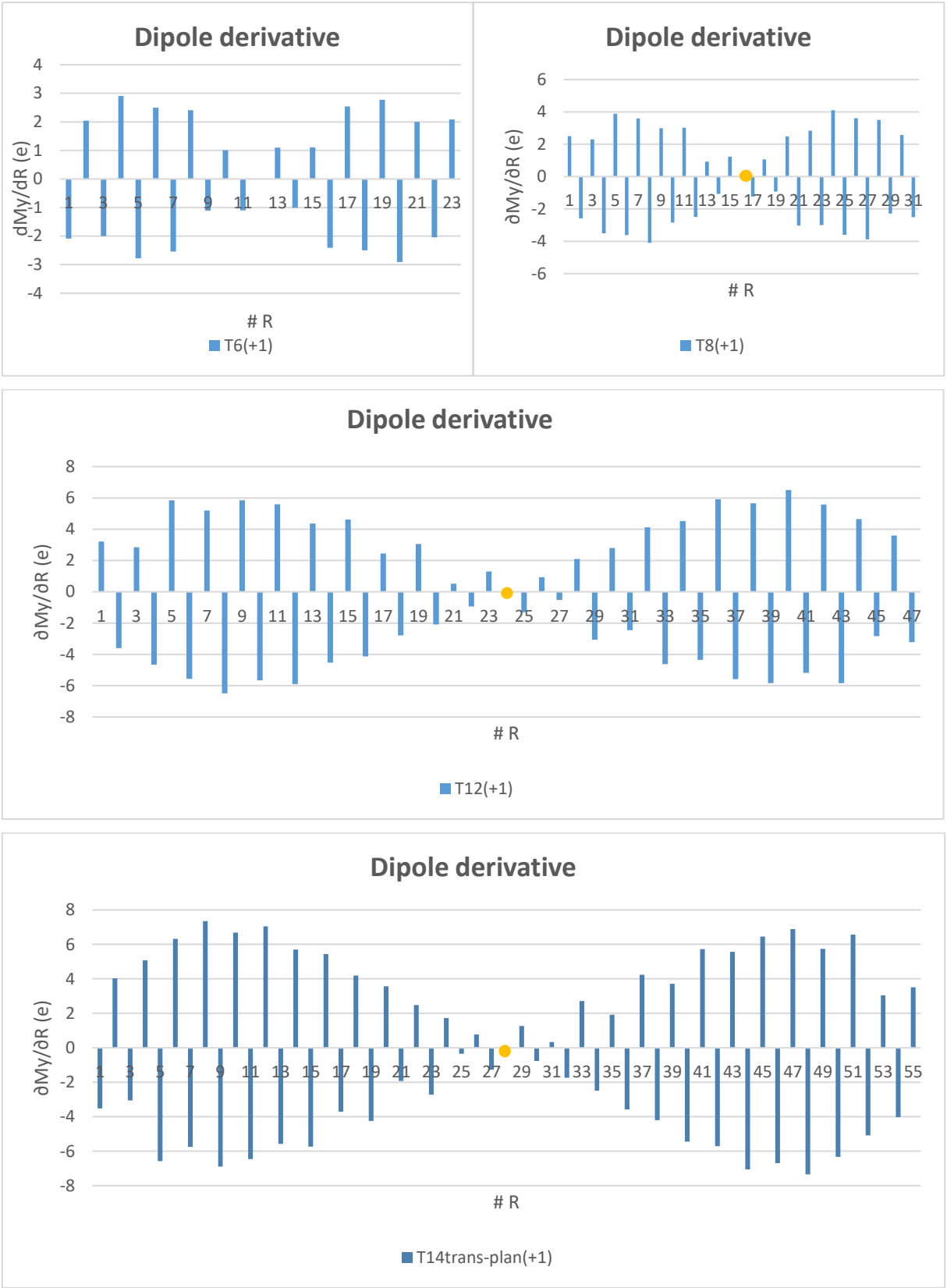

Figure 3.12: from the top to the bottom: y-component of dipole derivative with respect C-C stretching internal coordinate of charged T6(+1), T8(+1), T12(+1), T14(+1). On the horizontal axis # R indicates the number of C-C single or double bond constituting the back

Looking at the scale of the ∂My/∂R parameter on the vertical axis of the graphs in Figure 3.12 it is possible to realize that the local IR intensity parameter is indicatively one order of magnitude higher if compared with the corresponding values of the oligothiophenes in the pristine state (considering for example the T12 model, for the charged oligomer the maximum value of ∂My/∂R is slightly above 6e, while for the neutral specie it approaches 0,6e) , thus explaining the enormous difference between the intensity of the IR spectrum of neutral oligomers and of the charged ones upon the doping process.

For what concerns the effect of the chain length, from Figure 3.12 it is clear how the values of $\partial M^y/\partial R$ parameter increase with the number of thiophenes of the backbone and their difference passing from short to long oligothiophenes is significant, thus explaining why the IR intensity becomes higher in long oligomers.

The local IR intensity parameters allows to rationalize the activation of the IRAVs, once the pristine oligothiophene is doped: their high values not only explain the high intensity of the IR peaks but also represent a proof of the polarization of the CC bonds after the electron charge transfer from the oligothiophene to the dopant. The perfect alternation of positive and negative values that $\partial M^y/\partial R$ parameters assume when the oligothiophenes are charged, as it can be easily appreciated from Figure 3.12, constitutes another important feature. We will focus our attention on these fundamental aspects in Section 3.2, when a detailed explanations about the IRAVs activation and a comparison between neutral and doped oligothiophene with the same number of thiophene units will be provided.

Raman spectra and polarizability derivative parameters. We now present in Figure 3.13 the Raman spectrum of charged oligothiophenes with increasing chain length. We choose to report only the 1000-1600 cm^{-1} wavenumber region, where the most intense Raman peaks take place.

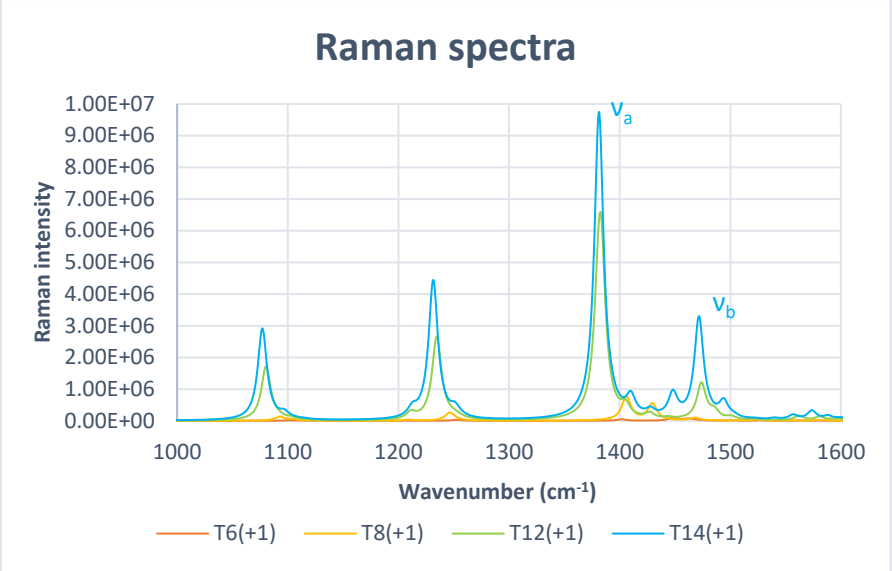

Figure 3.13: Raman spectrum of charged T(n). In orange the Raman spectrum of T6(+1), in yellow the Raman spectrum of T8(+1), in green the Raman spectrum of T12(+1) and in light blue the Raman spectrum of T14(+1).

First of all from Figure 3.13 it is possible to notice that the Raman spectrum of oligothiophenes in the doped state presents a more structured pattern with respect to the one of the corresponding neutral oligomers and precisely the four peaks structure of the Raman spectrum is very similar, even for what concerns the frequency of the normal modes, to the IR spectrum of charged oligothiophenes, as presented in the previous Section. In particular:

1) The first important peak has frequency around 1080 cm^{-1} and the associated normal mode presents the same features of the one of the IR spectrum, thus showing some ECC-like character, with the difference that in the Raman case two nodes exist, thus meaning the vibration changes its phase three times;
2) The normal mode associated to the 1250 cm^{-1} peak has similar characteristics of the corresponding one in IR spectrum, but also in this case the number of nodes increases from one to two;
3) The most intense Raman peak, labelled ν_a, has frequency slightly between 1380 and 1450 cm^{-1} and the associated normal mode is a Я-like mode, mainly localized in the central part of the oligomer (this occurs especially for long oligomers), with two nodes;
4) The last relevant peak, labelled ν_b, has frequency around 1450 cm^{-1} and the normal mode is a Я-like mode with four nodes, it is well localized in the end thiophene rings of the molecule for what concerns long oligomers, while for the short ones the vibration is more collective.

The fact that the normal modes generating the IR and Raman peaks in the spectra of charged oligothiophenes present similar features with a different number of nodes can be ascribed to the C_{2h} symmetry of the considered molecules: the normal modes with an odd number of nodes allow the presence of the centre of inversion and so they are IR active and silent in the Raman, while the ones with an even number of nodes are Raman active and IR silent, according to the mutual exclusion of IR and Raman activity for what concerns symmetric molecules.

It is interesting to notice that the two Я modes, indicated in points 3 and 4 in the previous list, become more collective, basically involving the whole oligothiophene, in short oligomers and especially in T6(+1) model, while the rather localized character of the two normal modes is extremely clear when considering long species. This aspect can be ascribed to the excessive shortness of the model, which does not allow seeing any further effect of localization of the charge defect, different from the mere confinement due to the finite size of the model molecule. In other words, when the molecule size is comparable to the typical size of the polaron (i. e. its typical size when embedded in a polymer chain) the degree of self-localization of the charge defect cannot be investigated.

In the following Figures, we report on the left panel the sketches of the vibrational eigenvectors of the two Я-like Raman active normal modes, indicated as ν_a (Figure 3.14) and ν_b (Figure 3.15). The eigenvectors underline the differences between them and the less localized character passing from long to short oligothiophenes.

On the right panel of the same Figures 3.14 and 3.15 we report the eigenvectors of the IR active normal modes, which we can correlate to the two Я-like Raman active normal modes sketched on the left, because they have similar frequency and they are very intense in the respective spectra In every image of the eigenvectors, the frequency, the IR intensity in km/mol and the Raman activity in A^4/amu are specified; moreover, the green segments mean that the considered bonds stretch, while the blue ones shrink and the thickness of the coloured segment indicates the extent of the bond stretching/shrinking involved during the vibration. The yellow and red circles indicate the molecular region characterized by the same phase of the ECC vibration and so they highlight the presence of nodes.

1449 cm^{-1}; 0 km/mol; 406561 A^4/amu

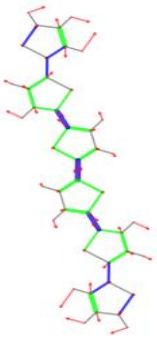

T6(+1)

1414 cm^{-1}; 7183 km/mol; 0 A^4/amu

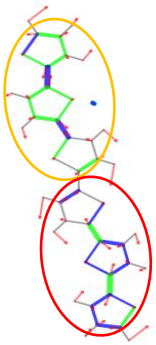

1406 cm^{-1}; 0 km/mol; 3234998 A^4/amu

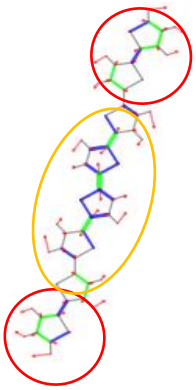

T8(+1)

1413 cm^{-1}; 23654 km/mol; 0 A^4/amu

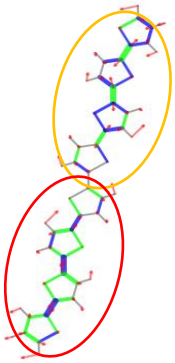

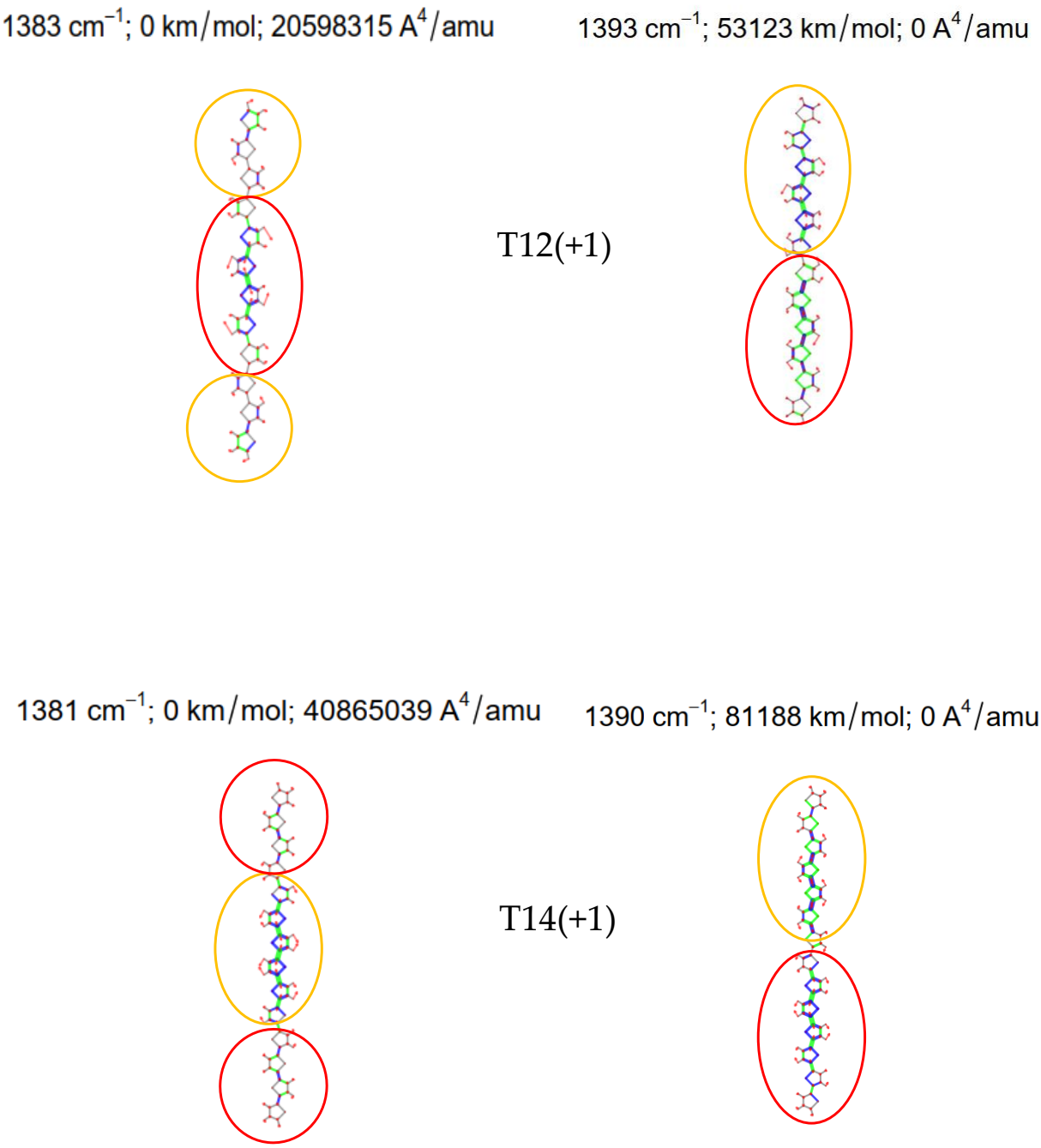

Figure 3.14: left panel: schematic representation of the ECC-like normal mode indicated as ν_a for charged oligothiophenes with increasing chain length; right panel: corresponding IR ECC-like mode.

1462 cm^{-1}; 0 km/mol; 241121 A^4/amu

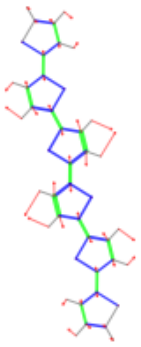

T6(+1)

1444 cm^{-1}; 5808 km/mol; 0 A^4/amu

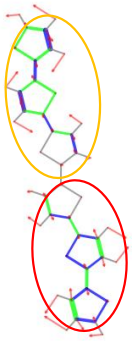

1430 cm^{-1}; 0 km/mol; 2283161 A^4/amu

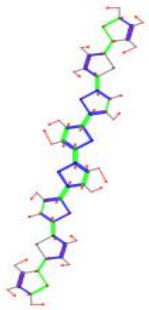

T8(+1)

1438 cm^{-1}; 5444 km/mol; 0 A^4/amu

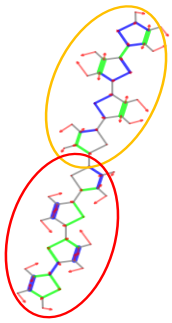

1474 cm^{-1}; 0 km/mol; 5160506 A^4/amu

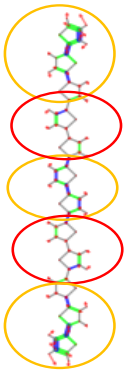

T12(+1)

1457 cm^{-1}; 16789 km/mol; 0 A^4/amu

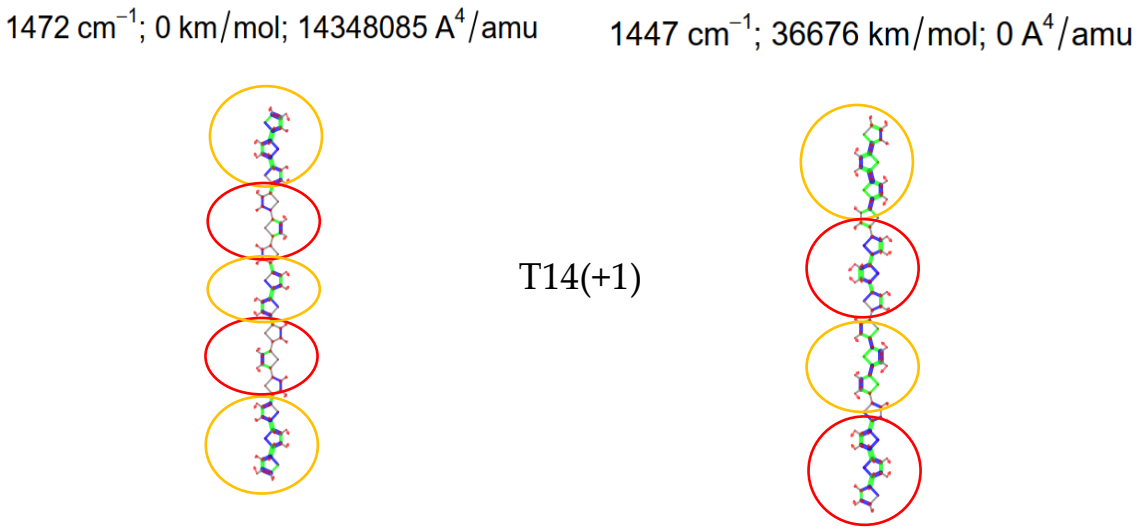

Figure 3.15: schematic representation of the ECC-like normal mode indicated as νb for charged oligothiophenes with increasing chain length; right panel: corresponding IR ECC-like mode.

This phenomenon of course has relevant effects on the Raman spectrum: in fact, if we calculate the frequency difference between ν_a and ν_b and the ratio between the intensity of the two peaks for the four oligothiophenes, we notice that the frequency difference and the Raman activity ratio of the two considered peaks increase passing from short to long oligomers; the results are reported below, in Table 3.5:

Table 3.5: frequency difference and Raman active ratio of the two Raman most intense peaks, labelled as νa and νb.

Oligothiophene	**ν_a - ν_b**	**$I_{\nu a}/I_{\nu b}$**
T6(+1)	1462-1449 = 13 cm^{-1}	406561/241121= 1,69
T8(+1)	1430-1406 = 24 cm^{-1}	3234998/2283161= 1,42
T12(+1)	1474-1383 = 91 cm^{-1}	20598315/5160506= 3,99
T14(+1)	1472-1381 = 91 cm^{-1}	40865039/14348085= 2,85

To rationalize such phenomenon, it is useful to report in Figure 3.16 the Raman spectrum of the four considered oligothiophenes normalized with respect to the most intense Raman peak.

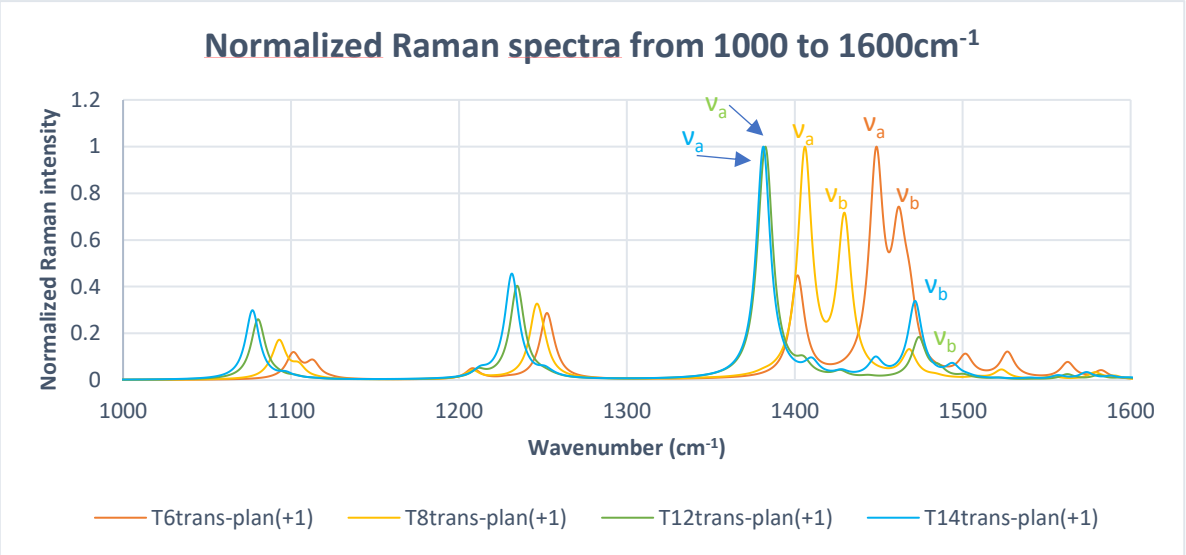

Figure 3.16: Normalized Raman spectrum on the most intense Raman peak. In orange the normalized Raman spectrum of T6(+1), in yellow the normalized Raman spectrum of T8(+1), in green the normalized Raman spectrum of T12(+1) and in light blue the normalized Raman spectrum of T14(+1).

Figure 3.16 is useful also to discuss the effect of the chain length on the frequency of the Raman peaks. The spectrum of T6(+1) and T8(+1) are basically not appreciable if compared with the one of T12(+1) and T14(+1) due to the extremely high intensity of the latter , as it is evident from Figure 3.13: also in the case of Raman spectra of charged oligothiophenes, we can notice a remarkable red-shift of the frequency passing from short to long oligomers, especially for what concerns the most intense Raman ECC mode. This phenomenon is rationalized as follow: the longer the oligomer, the higher is the conjugation length, the more pronounced is the softening of the vibration and so the lower is the frequency of the Raman peaks. Notably the Я mode labelled ν_b does not follow this trend and in fact $(\nu_b)_{T12} < (\nu_b)_{T14} < (\nu_b)_{T6} < (\nu_b)_{T8}$: this can be ascribed to the more localized character of the ECC-like normal mode with respect to ν_a and so it is less sensitive to the delocalization effects deriving from the chain length.

We now focus our attention on the effect of the chain length on the intensity of the Raman spectrum: from Figure 3.13 it is evident that the Raman intensity is subjected to a so dramatic increasing passing from short to long oligomers that Normalized Raman spectra were needed to underline the differences between the spectra of the different molecules. We adopted the normalization procedure of the Raman intensity on the number of thiophene units, as presented in the previous Sections, according to the following equation:

$$I_n = \frac{[\sum_{k=1}^{s} I_k]}{n} \qquad \text{(eq. 3.6)}$$

where I_n [Å^4/amu] is the normalized total Raman activity with respect to the number of thiophene units constituting the oligothiophene; I_k [Å^4/amu] is the Raman intensity of every normal mode; s is the total number of normal modes and n is the number of the thiophene units present in the considered molecule. Considering I_n values allows to understand the more than linear trend of the Raman intensity with the chain length of the oligomers. The results are reported in Table 3.6 and Figure 3.17:

Table 3.6: normalized Raman activity with respect to the number of thiophene units for charged oligothiophenes with increasing chain length.

Oligothiophene	**Normalized Raman activity In (Å^4/amu)**
T6(+1)	219925
T8(+1)	1045453
T12(+1)	5024289
T14(+1)	7346286

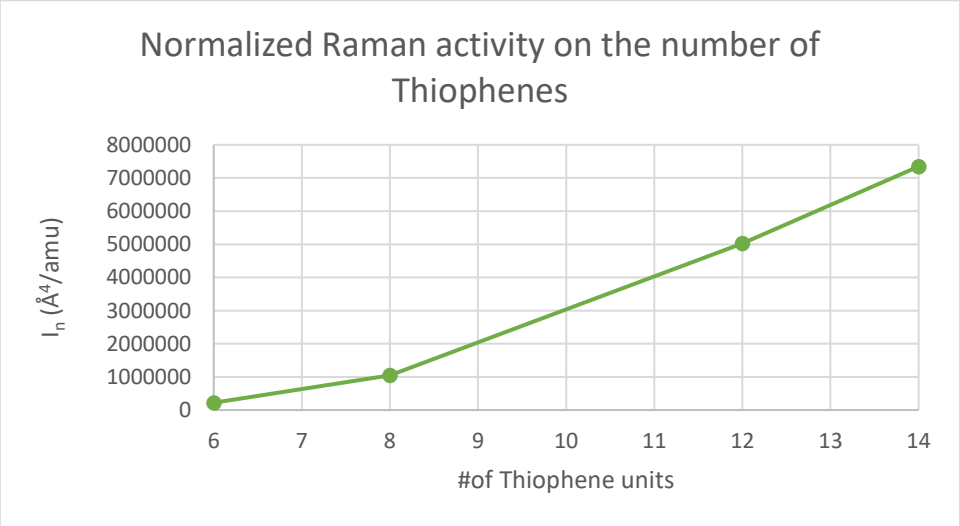

Figure 3.17: Total Raman activity normalized on the number of thiophene units.

The intensity of the Raman spectrum of charged oligothiophenes is much higher with respect to the one of the corresponding neutral oligomers; to appreciate this aspect it is sufficient to look at the scale of Figure 3.6 (Raman spectrum of pristine oligothiophenes), whose maximum value is $1{,}5 \cdot 10^5$ Å^4 amu^{-1}/cm^{-2} and Figure 3.13

(Raman spectrum of doped oligothiophenes),whose maximum value is 10^7 Å^4 amu^{-1}/cm^{-2}. It is interesting to underline how the dramatic increasing of the computed Raman intensity for charged species seems to be peculiar for thiophene-based polymers. Such phenomenon doesn't occur in simpler classes of polyconjugated materials, like polyenes: in a generic polyene constituted by 15 CC bonds, the Raman activity of the most intense Raman peak passes form $6{,}5\times10^6$ A^4/amu for the neutral oligomer to 1.1×10^6 A^4/amu for the corresponding charged species **[30]**. Moreover, from the experimental point of view the enormous difference between the Raman intensity of doped and pristine P3HT does not occur.

It is possible to rationalize the dramatic intensity increase with the number of thiophene units by means of the local Raman parameters, mainly the polarizability derivative with respect to the internal CC stretching coordinate, $\partial\alpha/\partial R$, which assume extremely high values passing from short to long oligomers, as depicted in Figure 3.18.

The $\partial\alpha/\partial R$ local parameters allow not only the rationalization of the trend of the Raman intensities, but also give important information on the structural relaxation of the oligothiophenes when fully charged. In all the graphs of Figure 3.18 we can notice that the local Raman parameters values invert their sign starting from a certain CC bond, thus meaning that in the central region of the molecule, perturbed by the charge defect, the quasi-single C-C bonds behaves as a quasi-double C=C bonds and viceversa; in other words, according to the description offered by the $\partial\alpha/\partial R$ local parameters, the charged oligothiophenes present a quinoid structure in the perturbed region, while the peripheral thiophene units are not involved. This explains why the most intense ECC-like normal modes has two nodes: the $\partial\alpha/\partial R$ parameters approach null value in correspondence of the CC bond separating the peripheral rings to the perturbed region of the molecule; that CC bond does not stretch or shrink, causing the nodes in the normal modes.

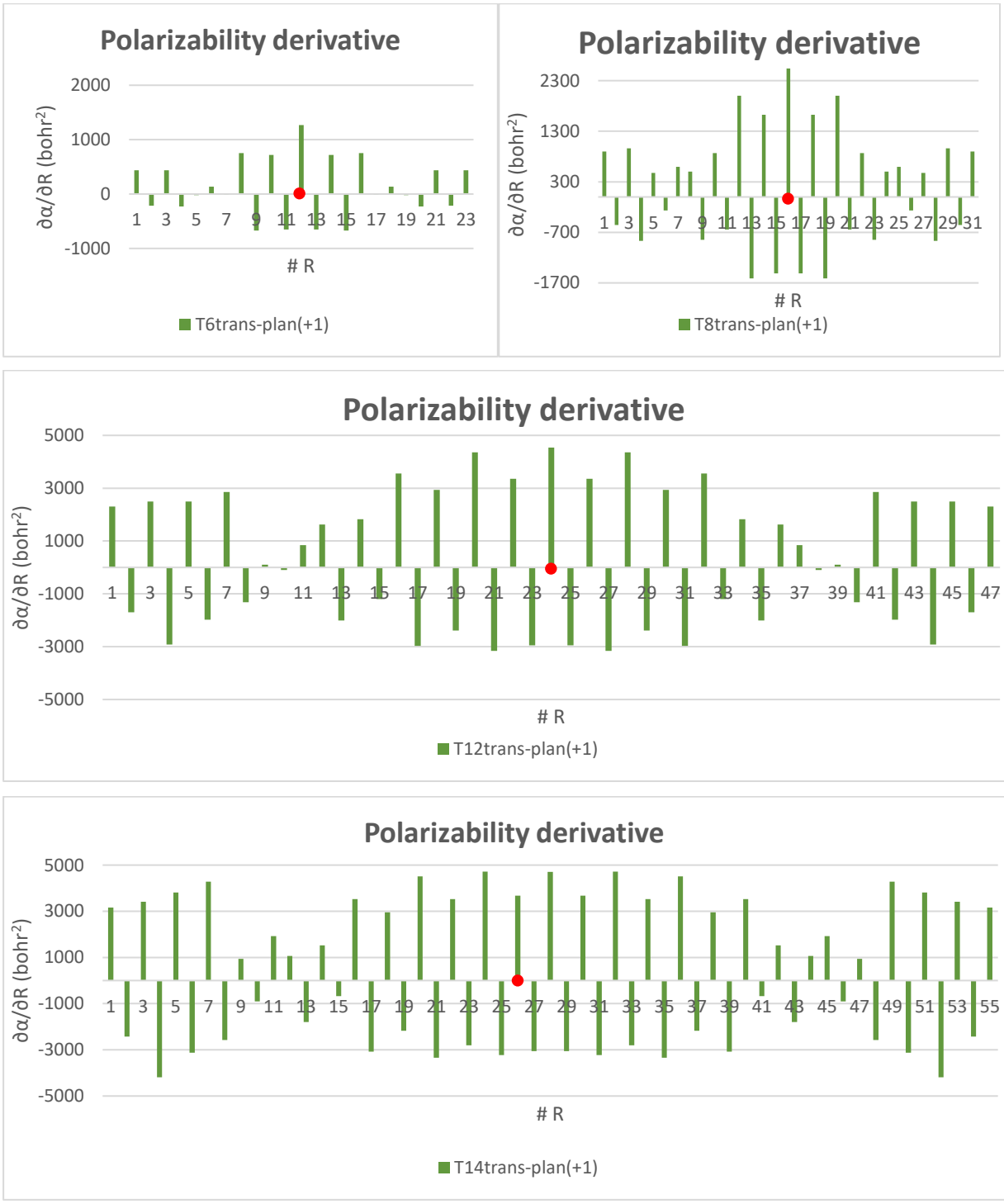

Figure 3.18: polarizability derivative with respect C-C stretching internal coordinate of charged T6(+1), T8(+1), T12(+1), T14(+1). On the horizontal axis # R indicates the number of C-C single or double bond constituting the backbone of the oligothiophene.

Geometrical parameters. In Figure 3.19 we report the values of the equilibrium bond length for every CC bond constituting the oligothiophene backbone.

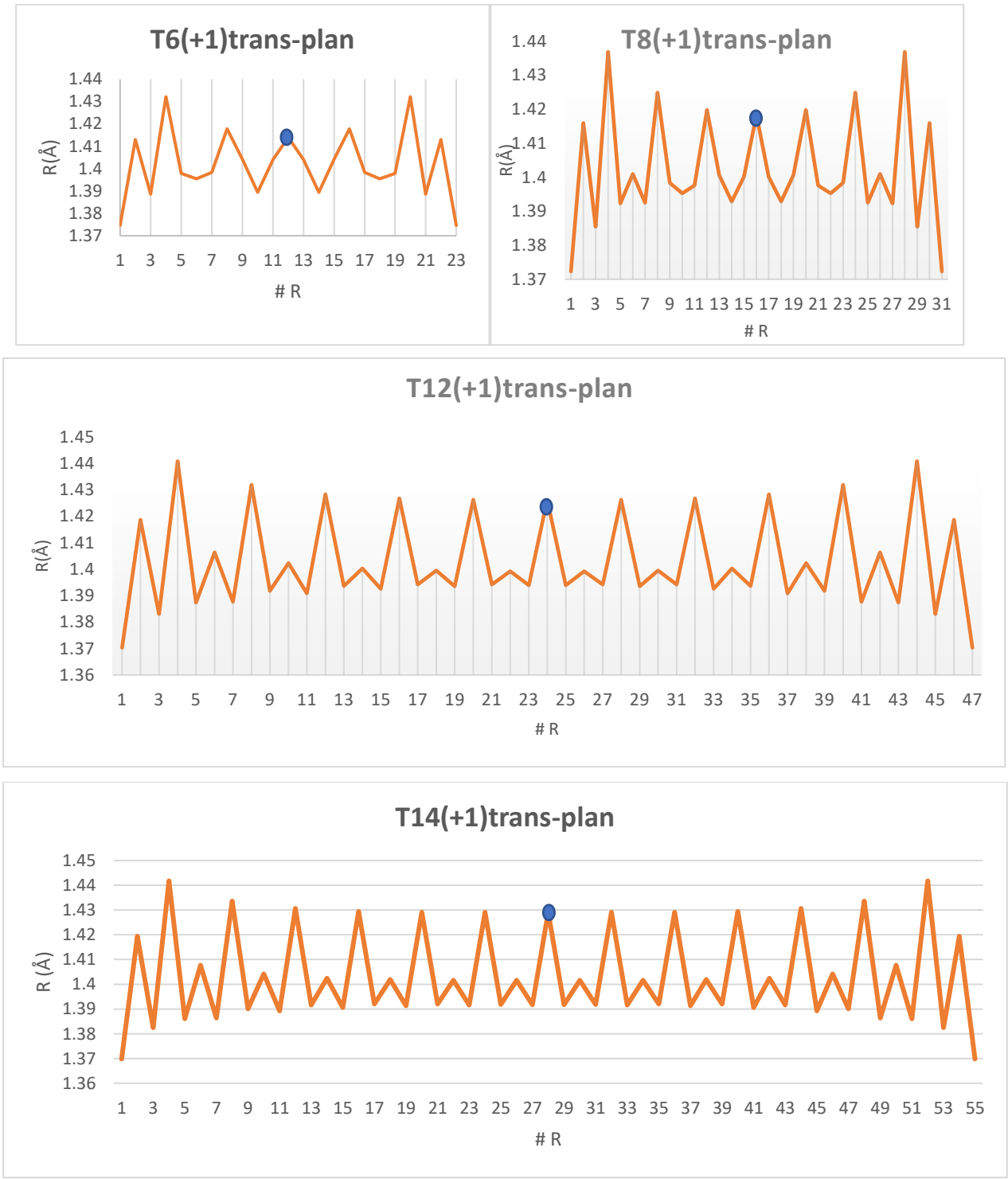

Figure 3.19: bond length of charged T6(+1), T8(+1), T12(+1), T14(+1). On the horizontal axis # R indicates the number of C-C single or double bond constituting the backbone of the oligothiophene.

Even if a systematic comparison between charged and neutral oligothiophenes for what concerns the geometry of the molecules will be presented in Section 3.2, some general consideration about the geometry of fully charged oligothiophenes and how it changes passing from short to long oligomers can be presented. First of all, by comparing Figure 3.19 and Figure 3.9, it can be noticed that only the single and double CC bonds of the peripheral thiophene units maintain practically unaltered their equilibrium length values, paralleling the results of the $\partial\alpha/\partial R$ local parameters, while the CC bonds within the central region of the molecule where is mainly located the excess of positive charge, i.e. the so-called polaron, undergo an important relaxation mechanism, in particular the quasi-single C-C bonds shorten and the quasi-double C=C bonds become longer.

The equilibrium bond length values of T6(+1) model are the only ones among the four considered oligomers that parallel the results predicted by the local Raman parameters, presented in the previous Section, even in the perturbed central region of the molecule: the quasi-single and quasi-double CC bonds invert, forming a quinoid structure. The quinoidization phenomenon is attenuated passing from short to long oligothiophenes, contrasting the geometry which could be inferred considering the $\partial\alpha/\partial R$ local parameters: especially in T12(+1) and T14(+1) models, the charge transfer from the oligomer to the dopant induces the equalization of the length of the quasi-single and quasi-double CC bonds within each thiophene unit of the defected region. A detailed analysis of the above features will be presented in Section 3.2.

It is useful to specify that from now on the quasi single and quasi double bond notation is referred to the geometry of the neutral molecule, in fact they correspond to even and odd positions respectively, along the backbone, irrespective to geometry changes upon doping.

3.1.3. The most intense IR and Raman transitions of neutral and charged oligothiophenes: analysis of the associated normal modes and their chain length dependence.

In this Section we will focus our attention on a comparative analysis – also from a quantitative point of view - of the IR and Raman normal mode which presents the strongest IR or Raman intensity. We will consider the whole set of oligothiophenes, both in the pristine and doped (fully charged) state, which have been already presented in Sections 3.1.1 and 3.1.2. We will analyse the frequency dispersion in IR and Raman and the bands intensity variation with the increasing number of thiophene units constituting the backbone of the oligomers, in order to highlight the effects of chain length on these spectroscopic features and different behaviour of neutral and charged oligothiophenes. We will also provide a detailed description of the

eigenvectors associated to the considered normal modes, underlining the differences between the IR and Raman active one.

We decide to concentrate on the most intense IR and Raman normal modes because they represent the most important spectroscopic fingerprints for polyconjugated materials, even if their IR and Raman spectra exhibit other relevant peaks, as we presented in the previous Sections. Moreover, analysing the frequency dispersion and the intensity variation with the number of thiophene units of the most intense IR and Raman peak allows to obtain important information on the minimum chain length and so the shortest oligomer able to properly model P3HT.

The IR most intense normal mode. Figure 3.20 reports on the left panel the eigenvector of the most intense IR normal mode of neutral oligothiophenes (T6-T14) and in the right panel those of charged species. In every image of the eigenvectors, the frequency, the IR intensity in km/mol and the Raman activity in A^4/amu are specified; moreover, the green segments mean that the considered bonds stretch, while the blue ones shrink; the thickness of the coloured segment indicates the extent of the bond stretching/shrinking involved during the vibration. The yellow and red circles indicate the molecular region characterized by the same phase of the vibration in the subsequent structural units (one thiophene ring + one interring CC bond) and so they allow detecting the presence of nodes.

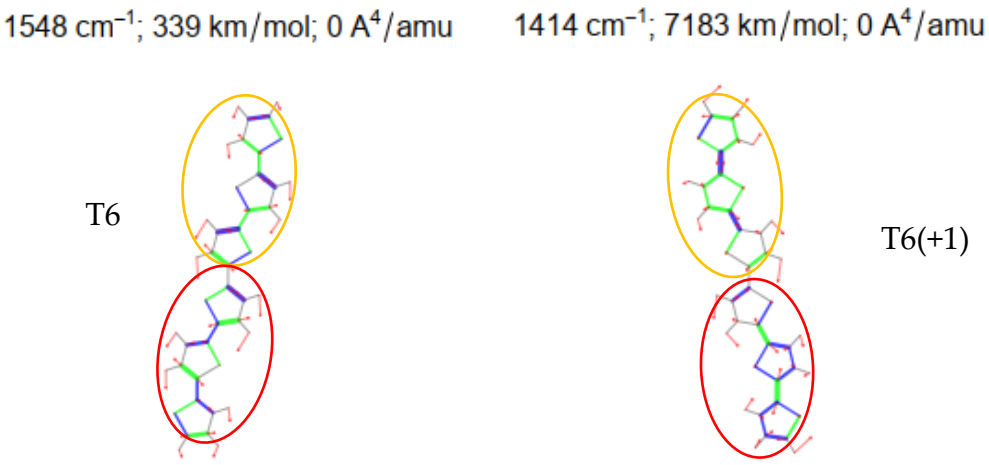

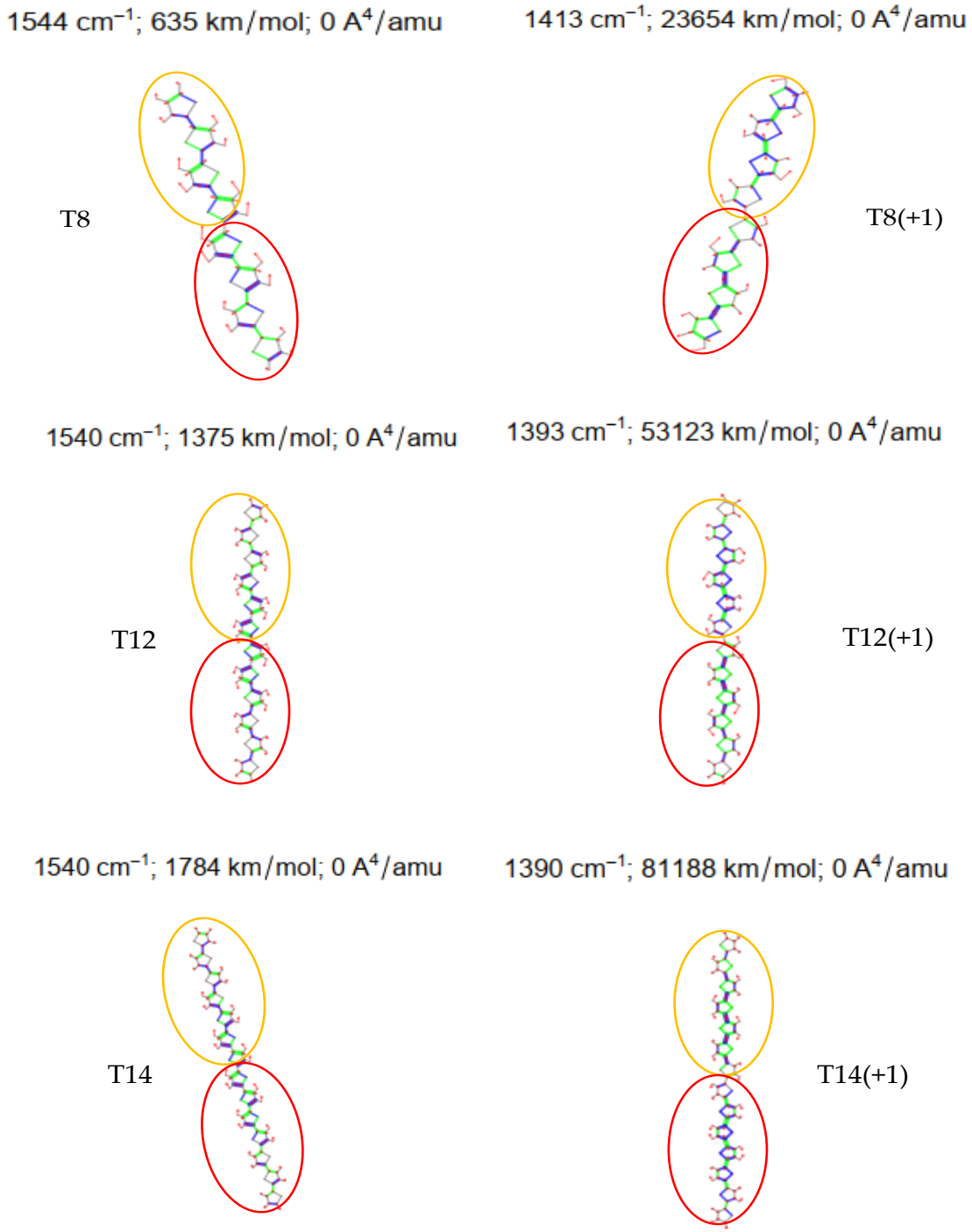

Figure 3.20: Eigenvector of the most intense IR normal mode of neutral oligothiophenes in the left panel and of charged oligothiophenes on the right panel for oligomers with increasing chain length, presented in the order T6, T8, T12 and T14 from the top to the bottom.

From Figure 3.20 it is evident that the most intense IR normal mode presents only one node in the centre of the oligomer for both pristine and doped oligothiophenes: in fact,

only one yellow and one red circle are needed, thus meaning that the vibration changes its phase once. The main difference between the most intense IR mode of neutral and charged oligothiophenes is the nature of the vibration inside each structural unit.

In the neutral case, the vibration is the out-of-phase stretching of the double C=C bonds of each thiophene unit (one double CC bond stretches and the other one shrinks simultaneously), which is accompanied by the in-phase stretching of the single interring C-C bonds (in one half of the molecule they stretch and in the other one they shrink), thus meaning that this vibration cannot be classified as ECC-like normal mode.

In the charged case the vibration is an ECC-like mode, thus meaning that all the quasi-single CC bonds shrink, and all the quasi-double CC bonds stretch in one half of the molecule and the opposite behaviour occurs in the second half. Notably, considering the T6(+1) model the ECC-like character is only partial because the single interring CC bonds and the single CC bonds of the rings mostly vibrate out-of-phase, while it is well defined in longer charged oligomers. The presence of a node located on the central CC bond guarantee that these modes have ungerade symmetry, and thus they are IR active.

We now focus our attention on the effect of chain length on the frequency of the most intense IR normal mode in Figure 3.21 and on its IR intensity and its IR intensity normalized on the number of thiophene units in Figure 3.22; the numerical values are reported in table 3.7.

Table 3.7: frequency and IR intensity of the most intense IR normal mode for neutral and charged oligothiophenes.

Oligothiophene	**Frequency (cm^{-1})**	**IR intensity (km/mol)**	**Normalized IR intensity on the number of thiophene units (km/mol)**
T6	1548	339	57
T8	1544	635	79
T12	1540	1375	115
T14	1540	1784	127
T6(+1)	1414	7183	1197
T8(+1)	1413	23654	2957
T12(+1)	1393	53123	4426
T14(+1)	1390	81188	5799

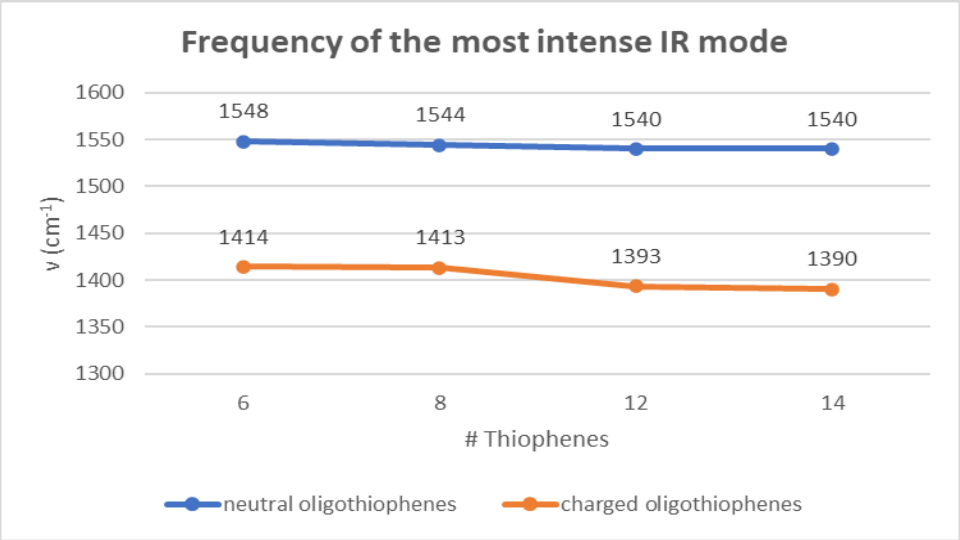

Figure 3.21: frequency of the most intense IR normal mode for neutral and charged oligothiophenes with increasing chain length.

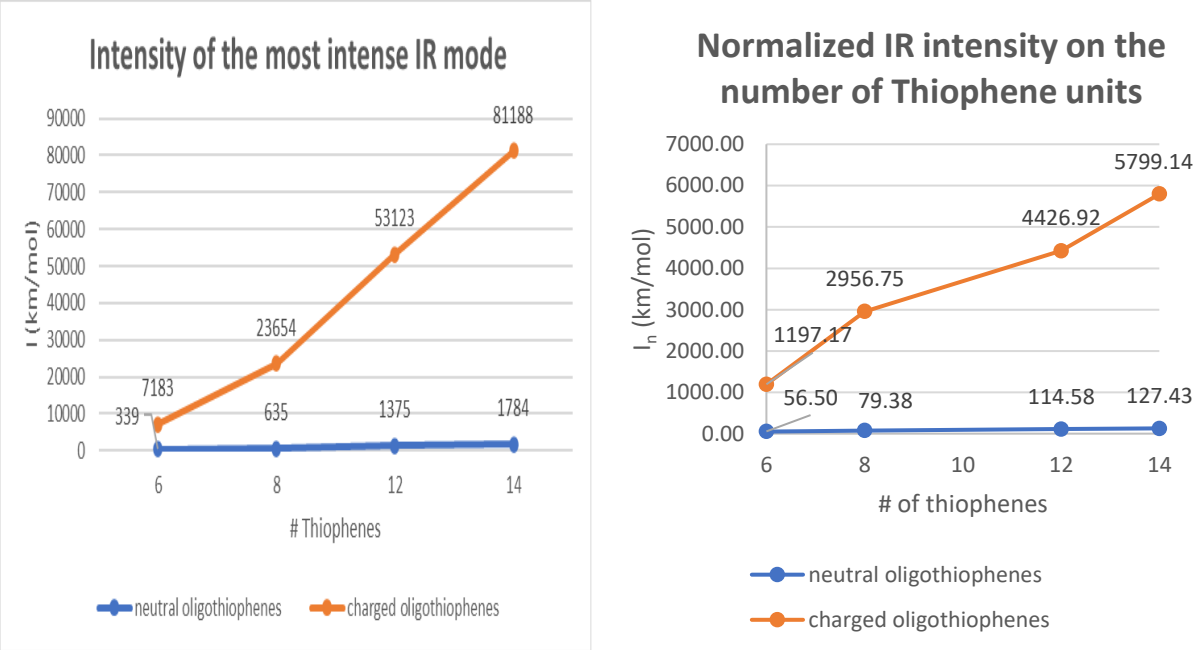

Figure 3.22: Intensity and normalized intensity on the number of thiophene units of the most intense IR normal mode for neutral and charged oligothiophenes with increasing chain length.

From the reported data, the following results hold:

1) Even if for both pristine and doped oligothiophenes the frequency undergoes a red-shift passing from short to long oligomers, the frequency dispersion

with the increasing number of thiophene units is more important in the case of charged oligothiophenes with respect to the case of neutral oligomers, in particular:

- For neutral oligothiophenes $\Delta\nu_{max} = \nu_{T6} - \nu_{T14} = 1548 - 1540 = 8\ cm^{-1}$
- For charged oligothiophenes $\Delta\nu_{max} = \nu_{T6(+1)} - \nu_{T14(+1)} = 1414 - 1390 = 24\ cm^{-1}$

2) The increasing of the intensity of the considered peak with the number of thiophene units occurs for both neutral and charged oligothiophenes, with anyway important differences:
   - For pristine oligomers $\frac{I_{T14}}{I_{T6}} = \frac{1784\ km/mol}{339\ km/mol} = 5{,}3$
   - For doped oligomers $\frac{I_{T14(+1)}}{I_{T6(+1)}} = \frac{81188\frac{km}{mol}}{7183\frac{km}{mol}} = 11{,}3$

3) The intensity of the most relevant IR normal mode increases when the doping of the oligothiophenes in pristine state occurs (the factor is about 40, starting from T8) in fact:
   - For T6 model, $\frac{I_{T6(+1)}}{I_{T6}} = \frac{7183\frac{km}{mol}}{339\frac{km}{mol}} = 21{,}2$
   - For T8 model, $\frac{I_{T8(+1)}}{I_{T8}} = \frac{23654\frac{km}{mol}}{635\frac{km}{mol}} = 37{,}2$
   - For T12 model, $\frac{I_{T12(+1)}}{I_{T12}} = \frac{53123\frac{km}{mol}}{1375\frac{km}{mol}} = 38{,}6$
   - For T14 model, $\frac{I_{T14(+1)}}{I_{T14}} = \frac{81188\frac{km}{mol}}{1784\frac{km}{mol}} = 45{,}5$

From the previous results some important considerations can be obtained:

1) The frequency dispersion of the most intense IR normal mode with the increasing number of thiophene rings is strictly related to the kind of vibration: for neutral oligothiophenes, since the IR mode is not an ECC mode, its frequency is practically insensitive to the chain length, while in the case of charged oligomers the strongest IR activated vibration (IRAV) is a Я-like normal mode. Indeed, the frequency of the Я vibration decreases with the increasing number of thiophene units because the conjugation length increases, provoking the decrease of the associated force constant, thus explaining the relevant red-shift of the frequency of the most intense ECC-like IRAV **[20, 30]**.

2) Also the intensity of the most relevant IR normal mode of neutral oligothiophenes appears almost insensitive to the chain length, in fact its normalized intensity on the number of thiophene rings is almost constant with the chain length, especially considering the results concerning T12 and T14 models. For what concerns the intensity of the IR ECC-like mode of charged oligothiophenes, it is significant to underline the fairly linear trend of this parameter with the number of thiophene units; this result is particularly evident starting from the intensity of the ECC-like IRAV of the T8(+1) model, as it clearly appears from Figure 3.22.
3) The extremely high intensity of the most intense IR normal mode of charged oligothiophenes with respect to the intensity of the one of neutral oligomers explicitly proves that the doping has a dramatic effect. Namely, we observe the rise in the IR spectrum of Infra-Red activated vibrations (IRAVs), silent in the pristine case, when the charge is transferred from the oligothiophene to the dopant upon the doping process.

The most intense Raman normal mode. Figure 3.23 shows the eigenvector of the most intense Raman mode for neutral and charged oligothiophenes with increasing number of thiophene units, from T6 to T14. Also in this case the coloured circles indicate the molecular regions in which the collective vibration of the oligomers units has the same phase and so it is easy to individuate the presence of nodes where the normal mode changes its phase.

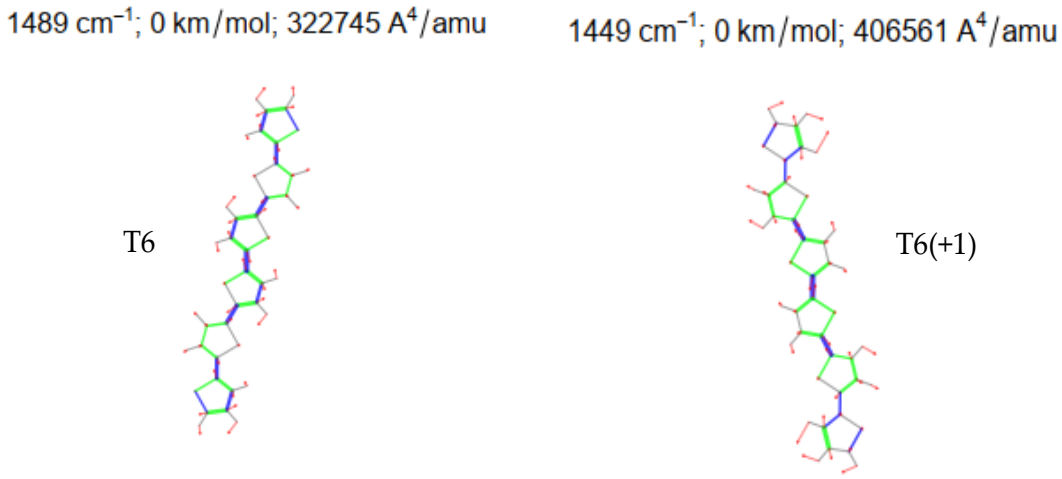

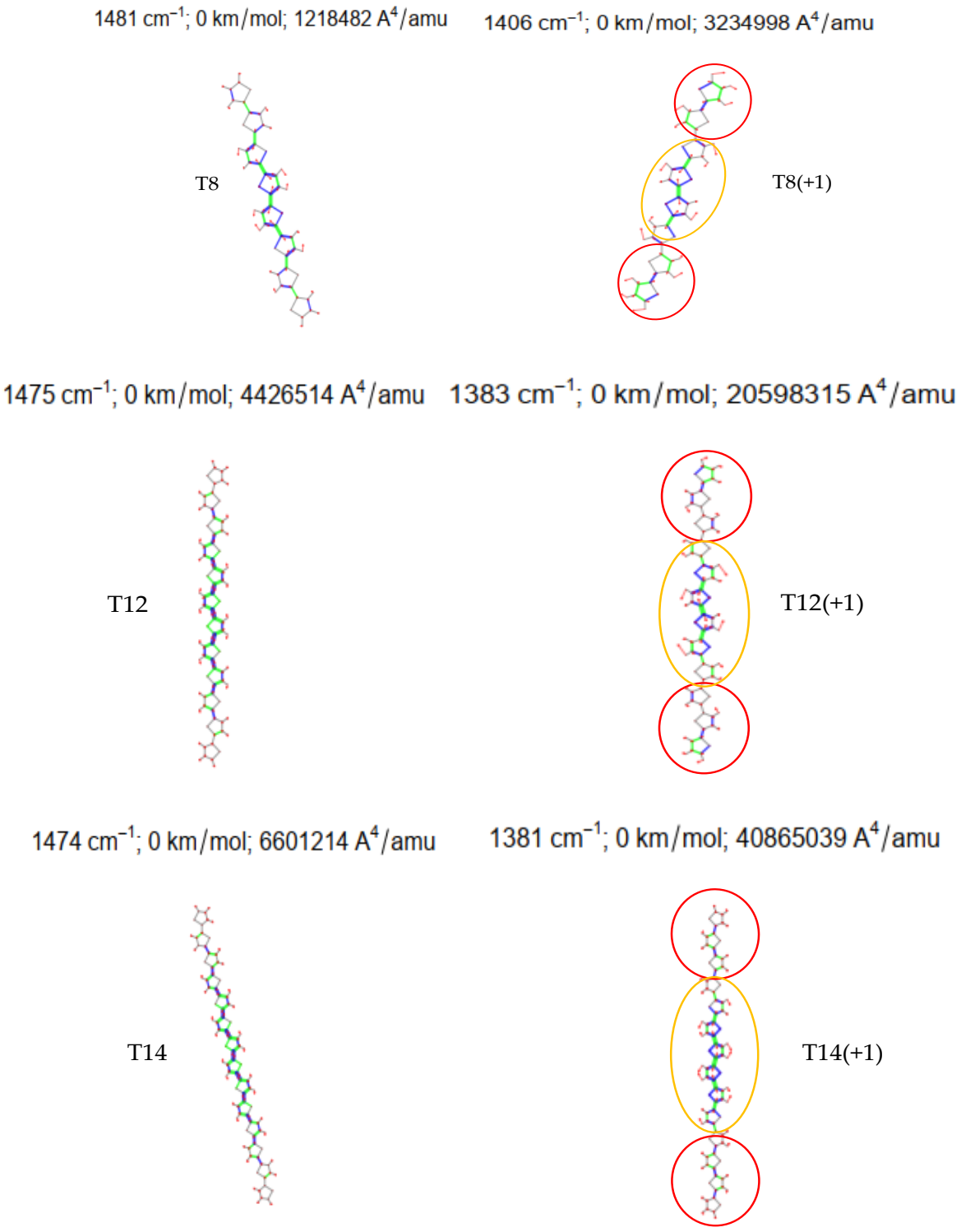

Figure 3.23: Eigenvector of the most intense Raman normal mode of neutral oligothiophenes in the left panel and of charged oligothiophenes on the right panel for oligomers with increasing chain length presented in the order T6, T8, T12 and T14 from the top to the bottom.

From Figure 3.23 it is evident that the eigenvector of neutral and charged oligothiophenes present some similar features. In particular the vibration determining the most intense Raman peak of the neutral chains is a pure Я mode, thus meaning it is determined by the collective alternate stretching/shrinking of all CC bonds. According to the ECC pattern, all the single bond within each thiophene unit and the inter-ring ones vibrate in phase, and all the quasi-double C=C bonds stretch or (shrink) with opposite phase with respect to the single bonds: in other words, if the single CC bonds shrink (stretch), the double CC bonds simultaneously stretch (shrink). It is important to underline the fact that the pure ECC Raman mode of neutral oligothiophenes mainly involves the central region of the oligomeric backbone, while the peripheral CC bonds practically do not participate to the collective vibration: this phenomenon is particularly relevant for long oligomers, while in the T6 model the Я mode basically involves the whole molecule. However, even if their contribution is small, the peripheral rings always vibrate in phase with the inner units.

For what concerns the most intense Raman normal mode of charged oligothiophenes, the vibration is still an ECC-like mode but in this case is characterized by the presence of two nodes, located two or three ring apart from the ends, thus meaning that the ECC-like vibration changes its phase twice. This is evident in long oligomers: in T6(+1) model in fact the ECC-like character is not well defined in the peripheral thiophene rings, where the single CC bond within each thiophene and the single inter-ring one vibrate out-of-phase (look at the red circles). Moreover, in T6(+1) and T8(+1) models the contribution to the vibration of the single CC bonds within each thiophene unit of the central region (yellow circle) is very small, at difference of what occurs in longer models, where the ECC-like character is clear. Also in the case of doped oligothiophenes, the localization of the stretching and shrinking of the CC bonds in the central region of the molecular backbone is confirmed, while the contribution of the peripheral thiophene units is negligible, especially in T8(+1), T12(+1) and T14(+1) models.

We now report in Figure 3.24 and 3.25 respectively how the frequency and the Raman activity, also normalized on the number of thiophene units, of the most intense Raman mode change with the increasing chain length of the oligomer; the numerical values are summarised in Table 3.8.

Table 3.8: frequency and Raman activity of the most intense Raman normal mode for neutral and charged oligothiophenes.

oligothiophene	frequency (cm^{-1})	Raman activity (A^4/amu)	Normalized Raman activity on the number of thiophene units (A^4/amu)
T6	1489	$3{,}23 \cdot 10^5$	$5{,}38 \cdot 10^4$
T8	1481	$1{,}22 \cdot 10^6$	$1{,}52 \cdot 10^5$
T12	1475	$4{,}43 \cdot 10^6$	$3{,}69 \cdot 10^5$
T14	1474	$6{,}60 \cdot 10^6$	$4{,}72 \cdot 10^5$
T6(+1)	1449	$4{,}07 \cdot 10^5$	$6{,}78 \cdot 10^4$
T8(+1)	1406	$3{,}23 \cdot 10^6$	$4{,}04 \cdot 10^5$
T12(+1)	1383	$2{,}06 \cdot 10^7$	$1{,}72 \cdot 10^6$
T14(+1)	1381	$4{,}09 \cdot 10^7$	$2{,}92 \cdot 10^6$

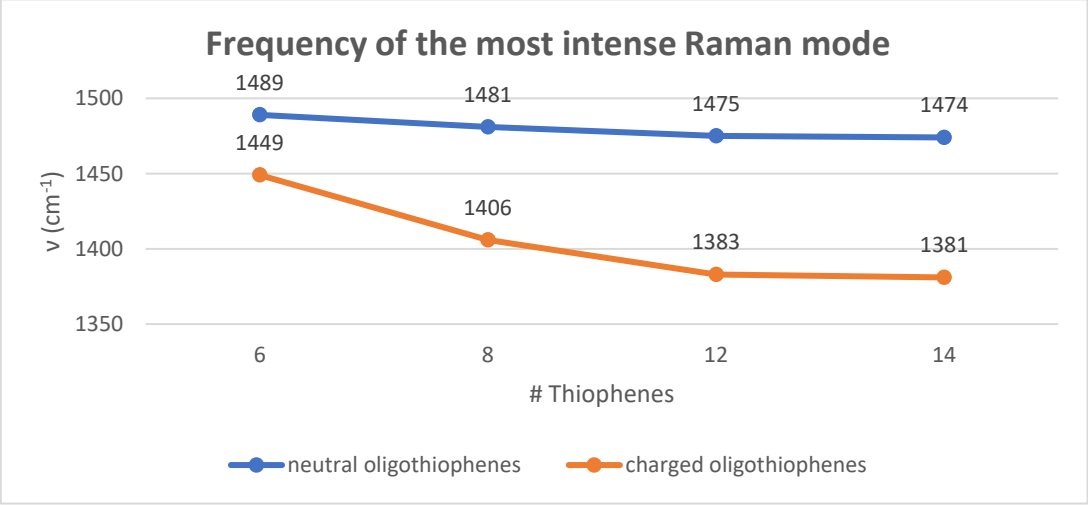

Figure 3.24: frequency of the most intense Raman normal mode for neutral and charged oligothiophenes with increasing chain length.

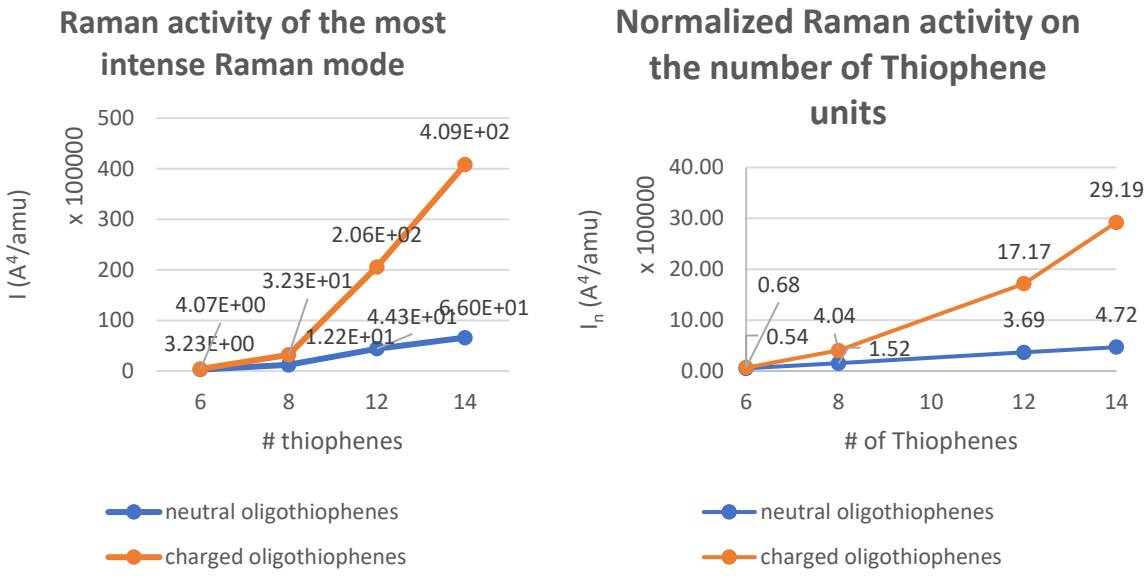

Figure 3.25: Raman Activity and normalized Raman activity on the number of thiophene units of the most intense Raman normal mode for neutral and charged oligothiophenes with increasing chain length.

The results concerning the most intense Raman normal mode are:

1) The frequency undergoes a red-shift with the increasing number of thiophenes constituting the backbone of the oligomer for both pristine and doped oligothiophenes and the frequency decreasing is more pronounced for the charged species, in fact:

   - For neutral oligothiophenes $\Delta\nu_{max} = \nu_{T6} - \nu_{T14} = 1489 - 1474 = 15\ cm^{-1}$
   - For charged oligothiophenes $\Delta\nu_{max} = \nu_{T6(+1)} - \nu_{T14(+1)} = 1449 - 1381 = 68\ cm^{-1}$

2) The Raman activity increases passing from short to long oligothiophenes and this phenomenon is particularly intensified in the charged species:
   - For pristine oligomers $\frac{I_{T14}}{I_{T6}} = \frac{6601214\ A^4/amu}{322745\ A^4/amu} = 20{,}5$
   - For doped oligomers $\frac{I_{T14(+1)}}{I_{T6(+1)}} = \frac{40865039\frac{A^4}{amu}}{406561\frac{A^4}{amu}} = 100{,}5$

3) The Raman activity increases upon the doping process of the oligothiophenes in pristine state, in particular:
   - For T6 model, $\frac{I_{T6(+1)}}{I_{T6}} = \frac{406561\ A^4/amu}{322745\ A^4/amu} = 1{,}3$
   - For T8 model, $\frac{I_{T8(+1)}}{I_{T8}} = \frac{3234998\ A^4/amu}{1218482\ A^4/amu} = 2{,}7$

- For T12 model, $\frac{I_{T12(+1)}}{I_{T12}} = \frac{20598315\ A^4/amu}{4426514\ A^4/amu} = 4{,}7$
- For T14 model, $\frac{I_{T14(+1)}}{I_{T14}} = \frac{40865039\ A^4/amu}{6601214\ A^4/amu} = 6{,}2$

Some considerations can be obtained from the previous results:

1) The frequency red-shift of the most intense ECC Raman mode, both for neutral and charged oligothiophenes, is explained by the fact that the vibration is a Я mode with no or two nodes, in the case of pristine and doped oligomers respectively. Increasing the number of thiophene units constituting the molecular backbone corresponds to a conjugation length increasing: the higher the conjugation length, the lower the force constant associated with the Effective Conjugation Coordinate (ECC) and so the lower the frequency of the normal mode.
   We anticipate here that the predicted 68 cm^{-1} shift of the frequency of the Я-like normal mode of charged oligothiophenes is very large if compared with the frequency shifts observed experimentally considering the Raman spectrum of doped P3HT samples. The obtained results can be interpreted as a proof of the delocalization error induced by the choice of the DFT functional, namely B3LYP, in conjunction with an overestimation of the Raman intensity of the ECC-like vibration localized on the charge defect, see also point 3 below. This issue will be carefully analysed in Chapter 5, were predicted and experimental spectra will be compared.
2) Focusing on the effect of the oligomeric chain length on the Raman activity, we can notice the super-linear trend of this parameter with the number of thiophene units. Moreover, at difference from the IR intensity of the most intense IR normal mode, the Raman activity, especially considering doped oligothiophenes, does not reach a saturation value, as it clearly appears from Figure 3.25, but it seems to continue to increase when the number of thiophene units of the backbone increases as well: to take consciousness of this fact it is sufficient to look at the value of the Raman activity of the T14(+1) model, that is more than hundred times higher with respect to the one of the T6(+1) model and also at the normalized Raman activity on the number of thiophene values, which does not approach any plateau limit.
3) Another important consideration regarding the Raman activity of the most intense ECC-like normal mode is the fact that it undergoes a remarkable increasing when the oligothiophene is subjected to the doping process: this phenomenon is not observed either experimentally in the case of P3HT and in other polyconjugated systems, like polyenes and polyacetylene **[30]**; actually, in models mimicking polyenes, the Raman activity of the ECC-like normal mode

does not increase when the charge is extracted from the oligomers in pristine state (see Section 3.1.2).

The final relevant result obtained from the collected data regarding the most intense IR and Raman normal mode is that the T12 model seems to approach plateau values for what concerns both the IR and Raman frequency dispersion with the number of thiophene units of the molecule and also for what concerns the IR intensity. This fact suggests that we can reasonably assume that the oligomer with twelve thiophene units as rather good model - with minimum chain length - in order to properly mimic P3HT.

We conclude this Section presenting on the same plot in Figure 3.26 the region of the IR and Raman normalized spectra, where the most intense IR and Raman peak are located, for neutral and charged oligothiophenes.

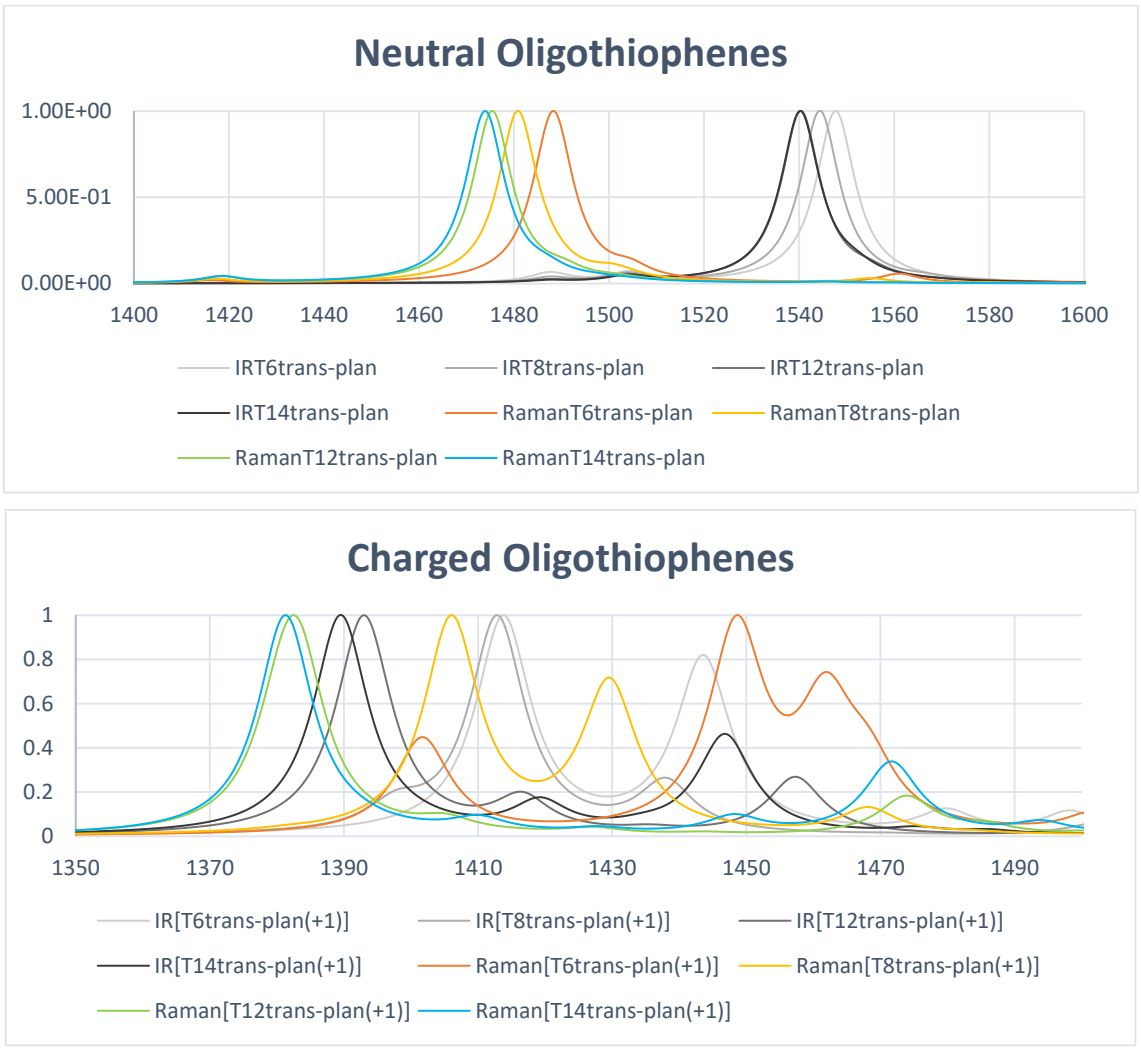

Figure 3.26: the IR and Raman most intense peak in the respective spectra for neutral and charged oligothiophenes.

Figure 3.26 is useful to notice that for neutral oligothiophenes the IR and Raman most intense peak present a net difference in frequency, while experimentally this phenomenon is less pronounced; for charged oligothiophenes the frequency differences between the IR and Raman peak are smaller. The numerical data are reported below:

- for T6 model: $\Delta\nu = \nu_{IR} - \nu_{Raman} = 1548 - 1489 = 59$ cm^{-1}
- for T8 model: $\Delta\nu = \nu_{IR} - \nu_{Raman} = 1544 - 1481 = 63$ cm^{-1}
- for T12 model: $\Delta\nu = \nu_{IR} - \nu_{Raman} = 1540 - 1475 = 65$ cm^{-1}
- for T14 model: $\Delta\nu = \nu_{IR} - \nu_{Raman} = 1540 - 1474 = 66$ cm^{-1}
- for T6(+1) model: $\Delta\nu = \nu_{IR} - \nu_{Raman} = 1414 - 1449 = -35$ cm^{-1}
- for T8(+1) model: $\Delta\nu = \nu_{IR} - \nu_{Raman} = 1413 - 1406 = 7$ cm^{-1}
- for T12(+1) model: $\Delta\nu = \nu_{IR} - \nu_{Raman} = 1393 - 1383 = 10$ cm^{-1}
- for T14(+1) model: $\Delta\nu = \nu_{IR} - \nu_{Raman} = 1390 - 1381 = 9$ cm^{-1}

3.2. Spectroscopic and geometrical properties of neutral and charged oligothiophenes with the same number of thiophene units.

In this Section we will focus our attention on the spectroscopic and geometrical properties of oligothiophenes, by comparing molecules with the same chain length in the neutral and charged state. The aim of this Section is to understand how the IR and Raman spectrum of a neutral oligothiophene with a fixed number of Thiophene units change when it undergoes the doping process. In particular, we will rationalize the appearance of Infra-Red Activated Vibrations (so called IRAVs), in the IR spectrum of oligothiophenes in the charged state.

Because IRAVs are silent when conjugated materials are in the pristine state, they basically constitute the IR spectroscopic fingerprint of the charge defect as induced by the doping process. The explanation of the IRAVs activation mechanism and of their extremely high IR intensity can be obtained by looking to the local IR intensity parameters, mainly the dipole derivative with respect to the internal CC stretching coordinate, $\partial\mathbf{M}/\partial R$.

For what concerns the Raman spectrum of oligothiophenes when they pass from the pristine to the doped state, we will analyse in detail the relevant Raman local parameters, namely the polarizability derivative with respect to the internal CC stretching coordinate, $\partial\boldsymbol{\alpha}/\partial R$; it will be shown that these parameters are related to the structural variations of the geometry induced by the charge transfer from the oligomer to the dopant.

We eventually will underline similarities and differences between the geometry of the charged oligothiophenes as they can be inferred by looking to the $\partial\alpha/\partial R$ parameters and the ones predicted by the analysis of the equilibrium bond length value of the CC bonds. From these results it is possible to understand where the most perturbed region of the oligomer is located and the number of CC bonds that relax to a different geometry with respect the equilibrium one of the neutral oligothiophenes; it is also possible to infer the spatial extent of the polaron, that is the charge defect induced by the doping process.

All DFT calculations reported in the current section refers to the B3LYP functional and the 6-31G(d,p) basis set. The unrestricted configuration is considered for the charged species (q = +1), which are indeed open-shell radical-cation.

It is important to underline that all DFT calculations, for both neutral and charged states, exhibit C2h symmetry, because the geometry of the molecular backbone was constrained as planar.

The notation used to indicate the various oligothiophenes is the same adopted in Section 3.1: Tn for the neutral oligomers and Tn(+1) for the charged species.

3.2.1. IR spectrum and dipole derivative parameters of neutral and charged oligothiophenes.

We start the discussion with a comparison between the computed IR spectra of pristine and doped oligomers, from T6 to T14.

Neutral T6 and charged T6(+1). In Figure 3.27 are reported the IR spectrum of T6 and T6(+1) (left panel) in the wavenumber region between 500 and 1700 cm^{-1}, where the most relevant IR peaks are concentrated. On the right panel are reported the normalized IR spectra (normalized on the most intense IR band).

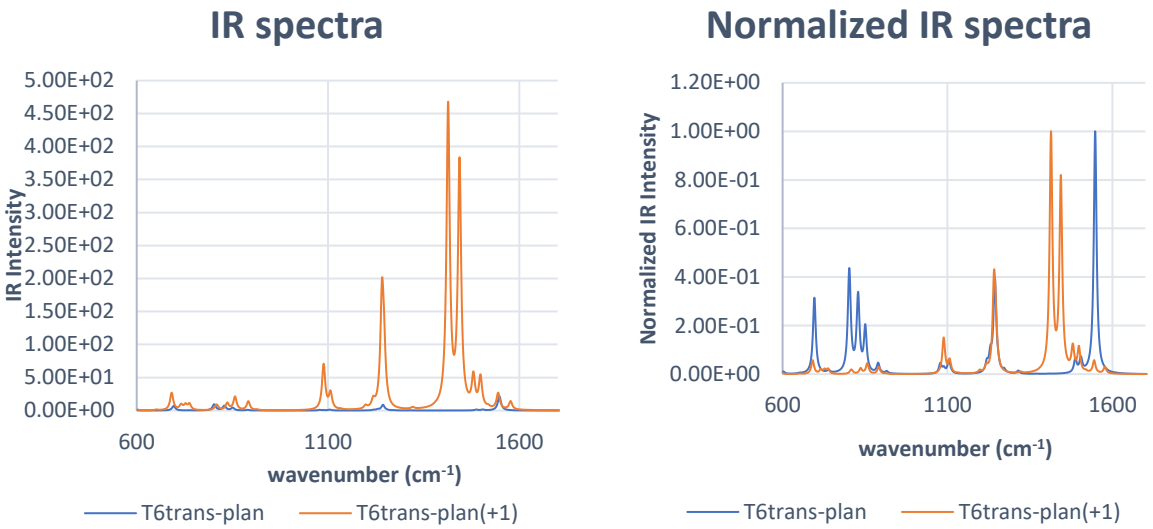

Figure 3.27: IR spectrum (left panel) and normalized IR spectrum on the most intense IR peak (right panel) of neutral T6 and charged T6(+1).

The detailed analysis of the IR spectrum of T6 and T6(+1) is already presented in Section 3.1; we now underline the differences between the pristine and the doped oligomer.
The most important evidence from the left panel of Figure 3.27 is the fact that the IR spectrum of T6(+1) exhibits in the wavenumber region between 1000 and 1600 cm^{-1} four so intense peaks that the IR spectrum of neutral T6 appears negligible. In particular, the peaks at 1088 and 1241 cm^{-1} are present also in the IR spectrum of the neutral oligomer, showing very similar frequencies and eigenvectors, but they undergo a magnification of the intensity upon the doping process ; instead, the two intense peaks at 1414 (it corresponds to the most intense IR transition) and 1444 cm^{-1} respectively are peculiar only of the IR spectrum of T6(+1), as it clearly appears from the right panel of Figure 3.27.

The very high intensity of the 1414 cm^{-1} band of the IR spectrum of T6(+1) is further highlighted by the right panel of Figure 3.27 which compare the spectra of the neutral and charged molecule after normalization to the most intense band. It is clear that in the IR spectrum of the pristine oligomer the C-H out-of-plane deformation normal modes in the wavenumber region around 700-800 cm^{-1} show appreciable IR intensity with respect to the most intense peak, while in the case of the doped oligomer their normalized intensity is very weak.

We now want to focus our attention on the two most intense bands of the IR spectrum of T6(+1), whose associated normal modes are ECC-like modes. The sketch of the vibrational eigenvectors is reported in Figure 3.28 and allows visualizing the nuclear trajectories. To be precise, the analogy with the Я-vibration of the mode responsible

of the most intense peak (1414 cm^{-1}) is not so stringent: while the inter-ring bonds and the quasi-double CC bonds vibrate with the right, opposite, phase according to the ECC pattern, all the quasi-single CC bond of each thiophene unit doesn't show the correct phase or are at rest. The ECC-like character is much clearer considering the eigenvector associated to the (less strong) 1444 cm^{-1} peak: in this vibration, which presents a node in the centre of the oligomer as required by the IR selection rules, all the CC bonds belonging to each half-molecule stretch or shrink according to the ECC pattern.

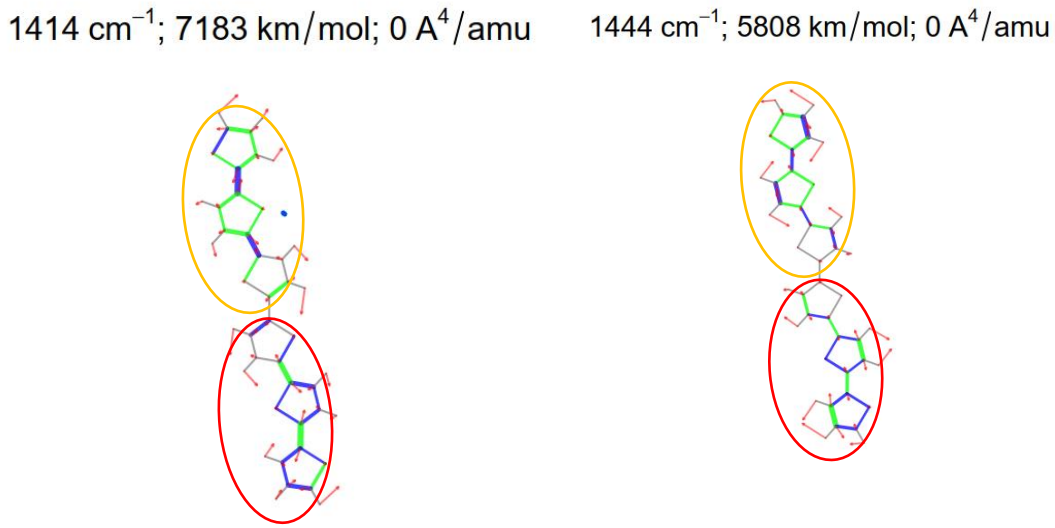

Figure 3.28: sketch of the eigenvector of the two intense IR normal modes for T6(+1): left mode at 1414 cm-1, right mode at 1444 cm-1.

For what concerns the two strong peaks at 1088 and 1241 cm^{-1}, the associated normal modes show some ECC-like character:

- The normal mode associated to the 1088 cm^{-1} peak show that all the quasi-single CC bonds stretch or shrink with the correct phase according to the ECC pattern, but the quasi-double CC bonds basically do not participate.
- In the normal mode associated to the 1241 cm^{-1} quasi-single and quasi-double CC bonds of each thiophene unit vibrate as prescribed by the ECC pattern, while the inter-ring CC bonds do not.

Their eigenvectors are reported in Figure 3.29, and they correspond to the intense transitions in the charged case; interestingly, modes close in frequency and with similar eigenvectors exist in the IR spectrum if the oligomer is in the neutral/pristine state, but they show a very modest intensity (for example for the peak around 1100 cm^{-1} the IR intensity in the neutral case is 14 km/mol, while in the charged case it is 1078 km/mol).

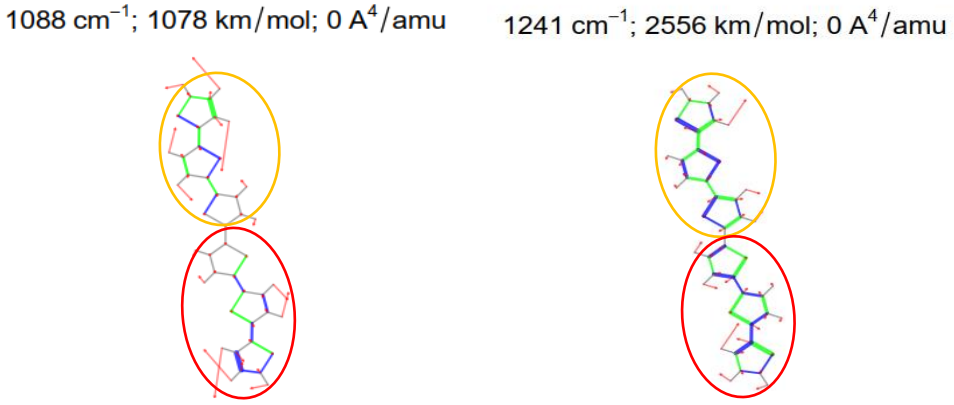

Figure 3.29: sketch of the eigenvectors of the two intense IR normal modes of T6(+1), whose IR peaks have frequency 1088 cm^{-1} (left) and 1241 cm^{-1} (right) respectively.

Neutral T8 and charged T8(+1). Figure 3.30 reports the IR spectrum (left panel) and the normalized IR spectrum on the most intense IR peak (right panel), both in the wavenumber region between 500 and 1700 cm^{-1}, of pristine T8 and doped T8(+1).

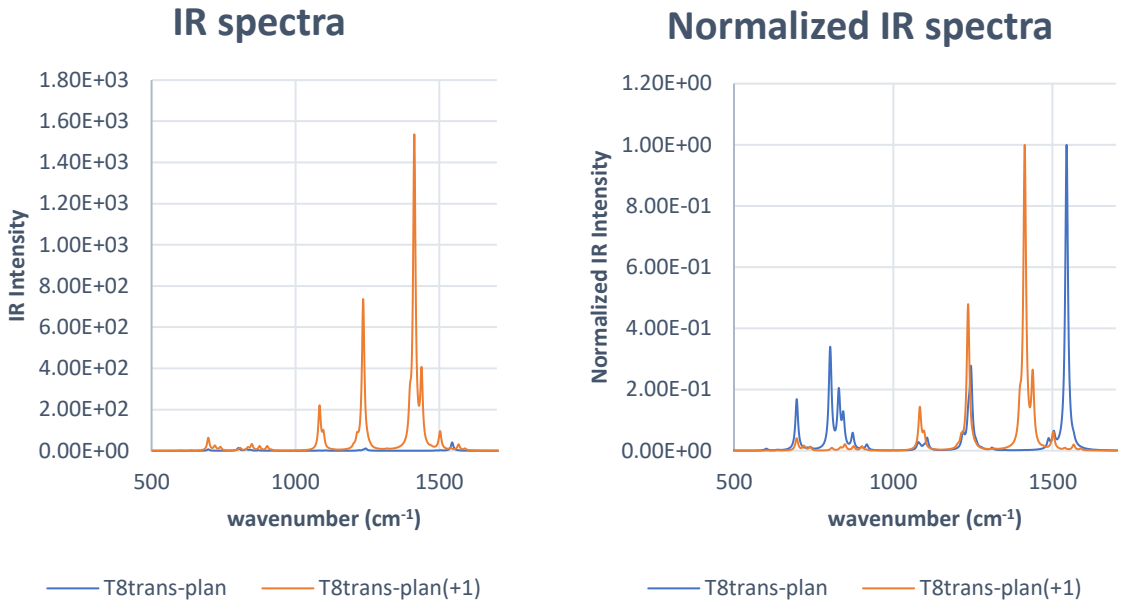

Figure 3.30: IR spectrum (left panel) and normalized IR spectrum on the most intense IR peak (right panel) of neutral T8 and charged T8(+1).

The four peaks structure of the IR spectrum of the charged oligomer, already presented in the case of T6 model, appears also in the case of T8 model: the peaks have frequency 1084, 1235, 1413 and 1438 cm^{-1} respectively and they have an extremely high intensity with respect the IR spectrum of neutral T8. The first two peaks already exist in the IR

spectrum of T8, while the latter ones are peculiar of the IR spectrum of the charged oligothiophene; the sketch of the eigenvector of the normal mode associated to the four peaks is reported in Figure 3.31.

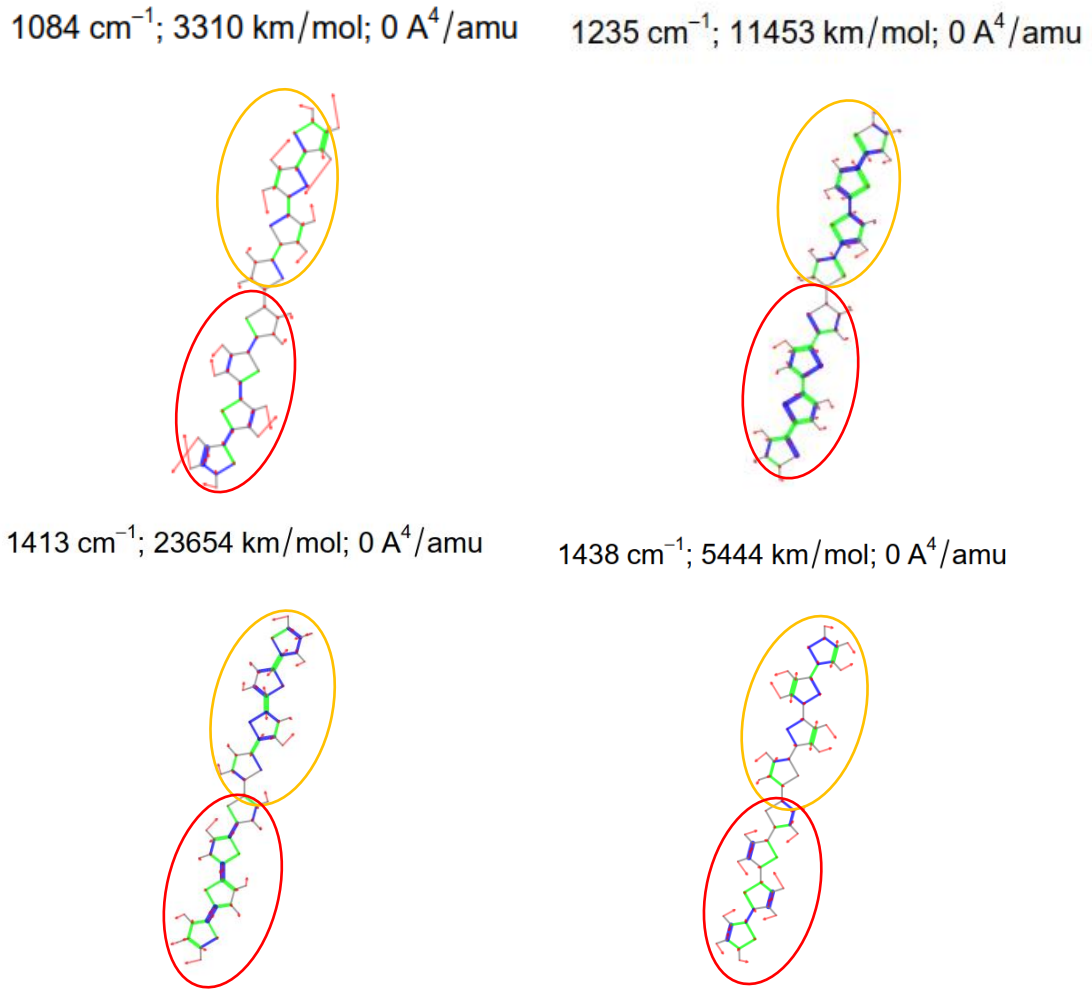

Figure 3.31: sketch of the eigenvector of the four intense IR normal modes of charged T8(+1), whose IR peaks have frequency 1084, 1235, 1413 and 1438 cm^{-1} respectively.

For the description of the ECC-like character of the normal modes, it recalls the one presented for the T6(+1) model. It is interesting to notice that the ECC-like character of the normal mode associated to the 1413 cm^{-1} peak is much more clear in the T8(+1) model, especially focusing on the inner rings, with respect to the T6(+1) model (the corresponding peak is at 1444 cm^{-1}), while the opposite consideration holds for the second peculiar peak of IR spectrum of the charged specie (1438 cm^{-1} for T8(+1) and 1444 cm^{-1} for T6(+1)).

T12 and T14: neutral vs. charged species. We decided to discuss together the T12 and T14 models because they present very similar features, especially for what concerns the description of the eigenvector of the normal modes. Figures 3.32 and 3.33 show the IR spectra (left panel) and the IR spectra normalized on the most intense peak (right panel), both in the wavenumber region between 500 and 1700 cm^{-1}, of neutral T12 and charged T12(+1) and neutral T14 and charged T14(+1) respectively.

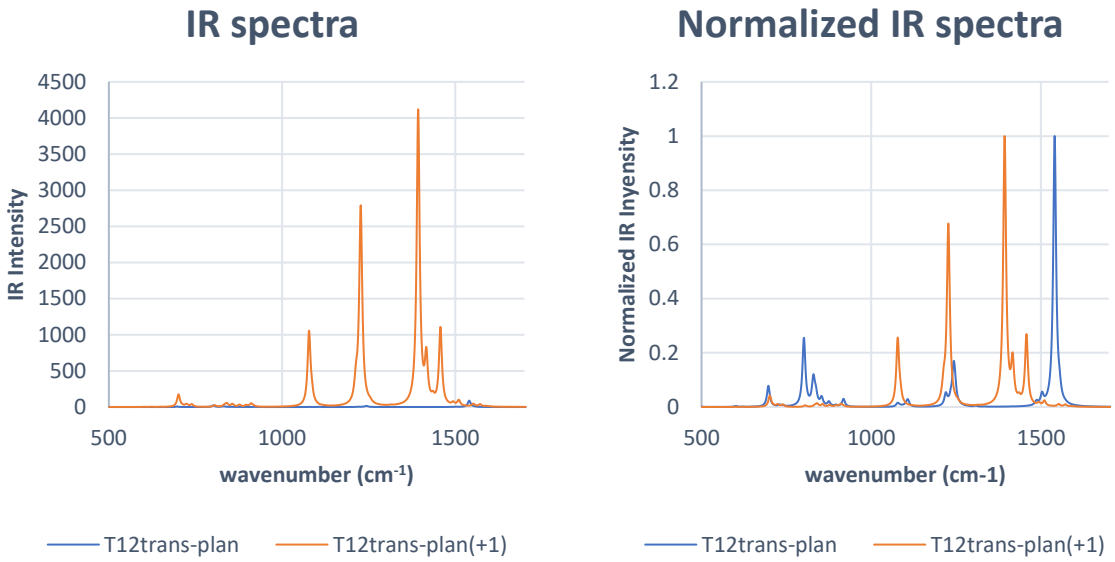

Figure 3.32: IR spectrum (left panel) and normalized IR spectrum on the most intense IR peak (right panel) of neutral T12 and charged T12(+1).

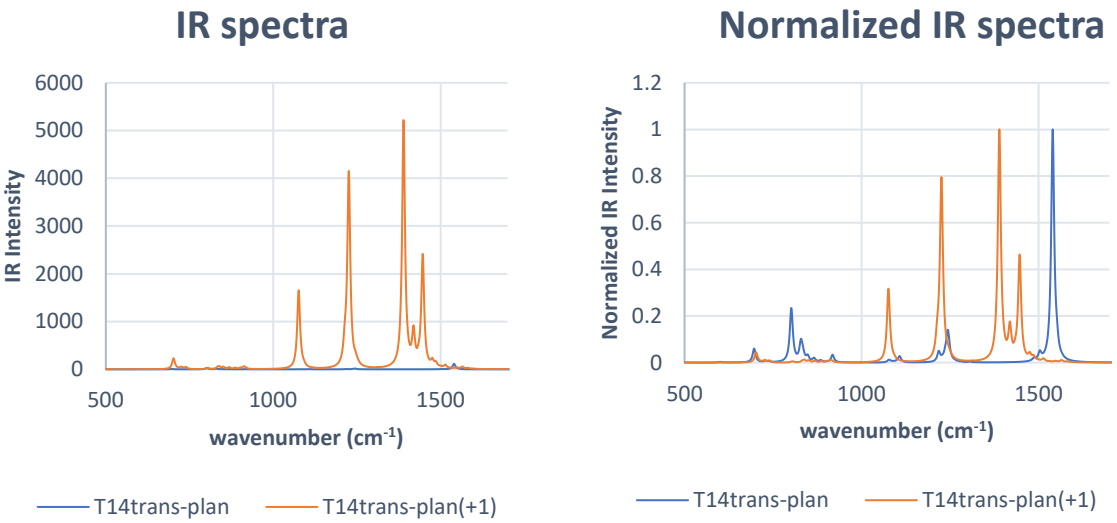

Figure 3.33: IR spectrum (left panel) and normalized IR spectrum on the most intense IR peak (right panel) of neutral T14 and charged T14(+1).

Figures 3.32 and 3.33 confirm that also for long oligomers the IR spectrum of charged oligothiophenes is constituted by four very intense peaks, that are silent or almost silent in the IR spectrum of neutral oligothiophenes. The frequency of the four peaks are 1078, 1227, 1393 (the most intense IR peak) and 1457 cm^{-1} for T12(+1), 1076, 1226, 1390 (the most intense IR peak) and 1447 cm^{-1} for T14(+1) respectively; the sketch of the eigenvector of the associated normal mode to each peak listed above is reported in Figure 3.34, on the left panel for T12(+1) model and on the right panel for T14(+1) model.

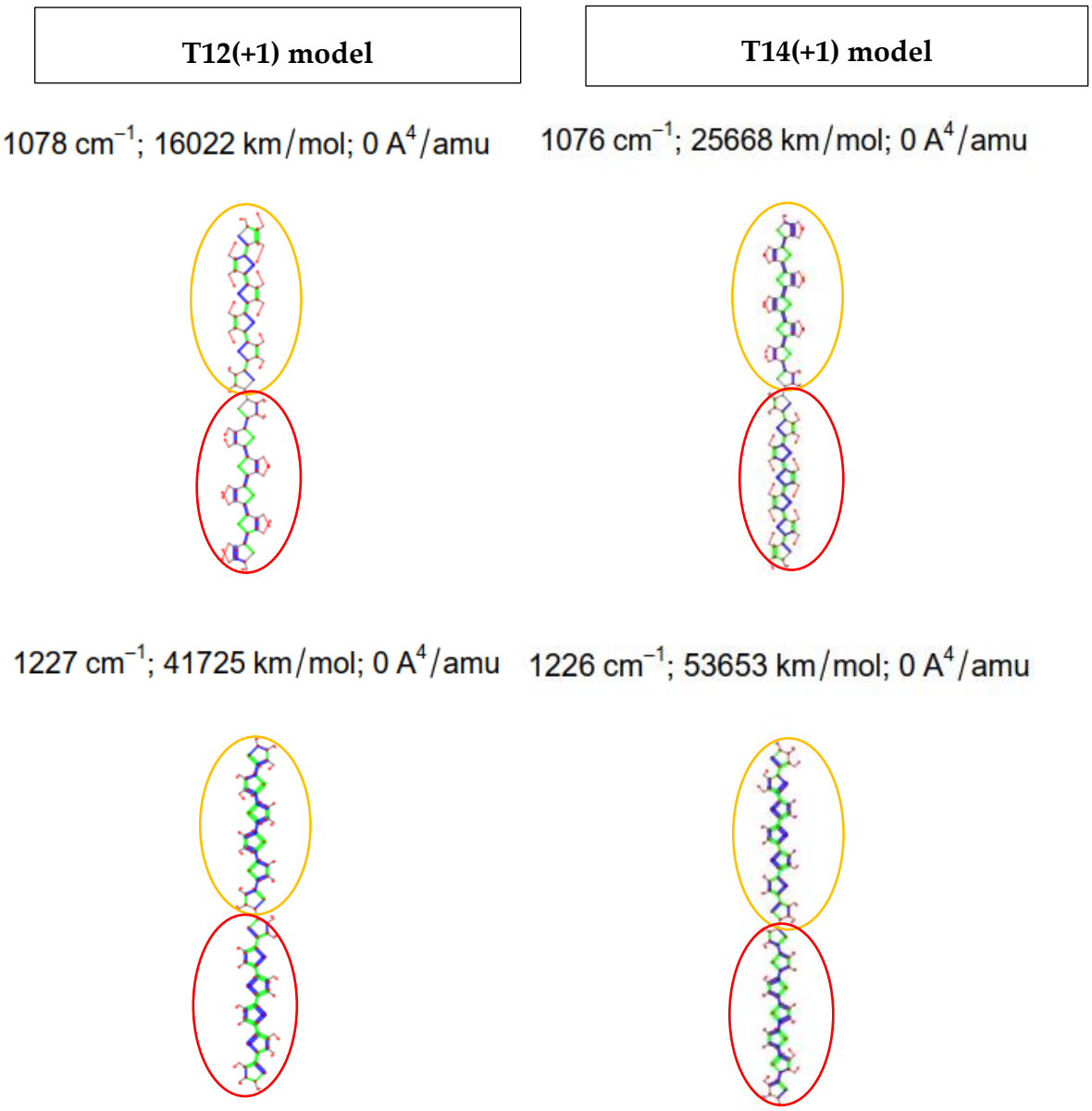

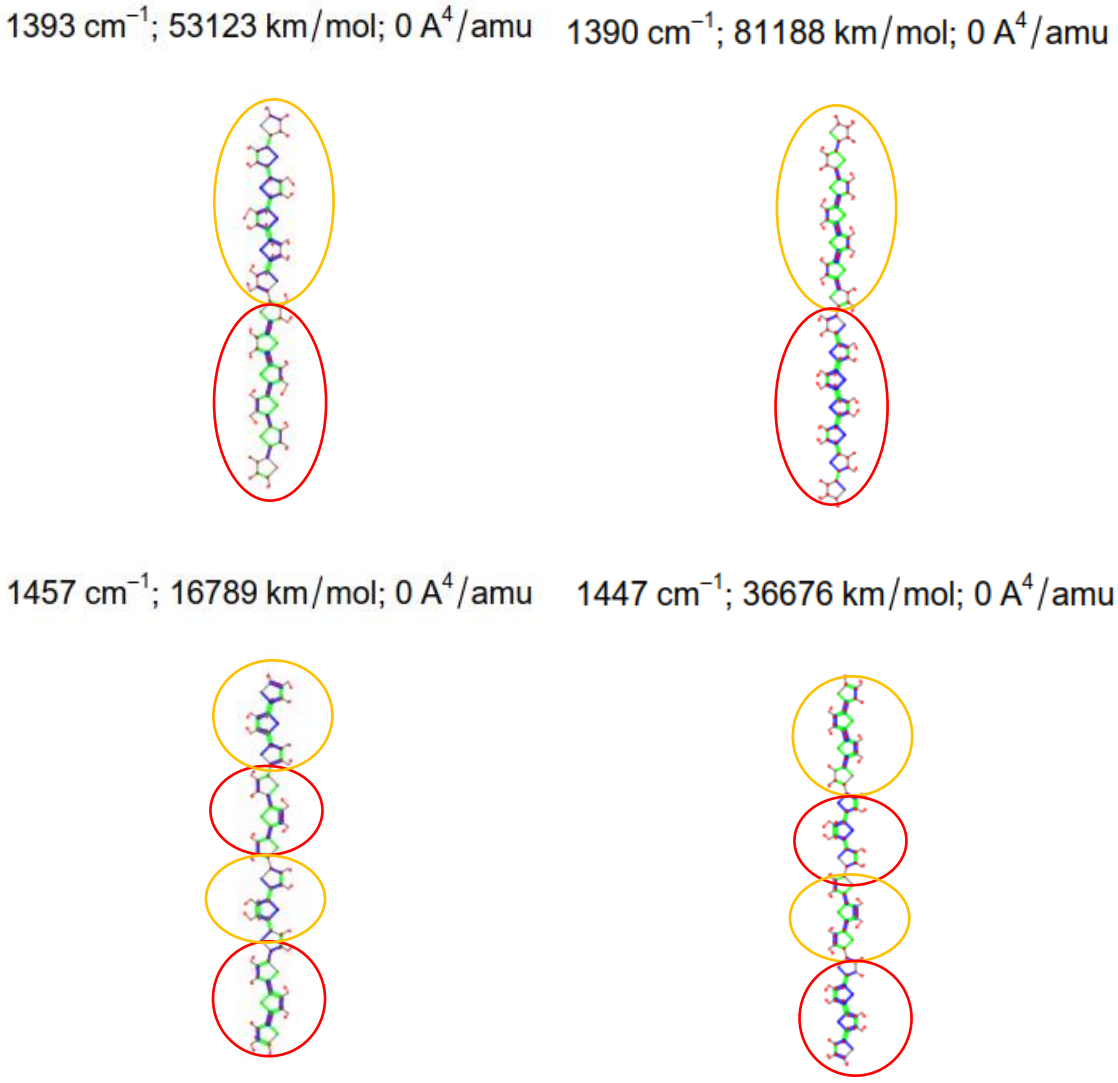

Figure 3.34: sketch of the eigenvector associated to the four intense peaks of the IR spectrum of charged T12(+1) and T14(+1).

For what concerns the ECC-like character of the normal modes, there are analogies with the features presented for T6(+1) and T8(+1) models. It is interesting to observe that in long oligomers, the eigenvectors associated to the strong peaks in the IR spectrum of charged species both exhibit a clear ECC-like character. The most intense IR active vibration presents a single node in the centre of the molecule, while the second one exhibits three nodes, one in the centre of the molecule and two located after three or four thiophene units from the end of the oligomer, in T12(+1) model, and in T14(+1) model respectively. This underlines the fact that in long oligothiophene also the less collective ECC-like vibrations are strongly IR active, thus suggesting that the geometrical and electrical perturbations upon charging are especially effective in the more central rings where the charge and the structural relaxation is mostly localized.

The onset of IRAVs. The four previously described intense normal modes, associated to the strong bands of the IR spectrum of charged oligothiophenes, are classified as IRAVs: these vibrations are silent or almost silent in the IR when the oligomer is in the neutral state and become active when the oligomer is in the charged state. Because the four extremely intense peaks in the IR spectrum of charged/doped oligothiophenes are negligible or absent in the IR spectrum of neutral/pristine corresponding oligomer, they constitute the corresponding IR spectroscopic fingerprints of the polaron. Such vibrations become active in the IR (with generally high IR intensity) after the doping process, because the charge self-localizes inside the oligomeric chain, modifying the bond length alternation **[29]**.

The full rationalization of the onset of the IRAVs can be obtained by means of the local IR intensity parameters, namely the dipole derivative with respect to the internal C-C stretching coordinate, ∂My/∂R. We report in Figure 3.35 the y-component, the one along the molecular axis, because large charge fluxes (and thus a large dipole fluctuation) are expected to occur in this direction. Indeed, it is by far the largest component of ∂**M**/∂R in the case of the charged oligothiophenes.

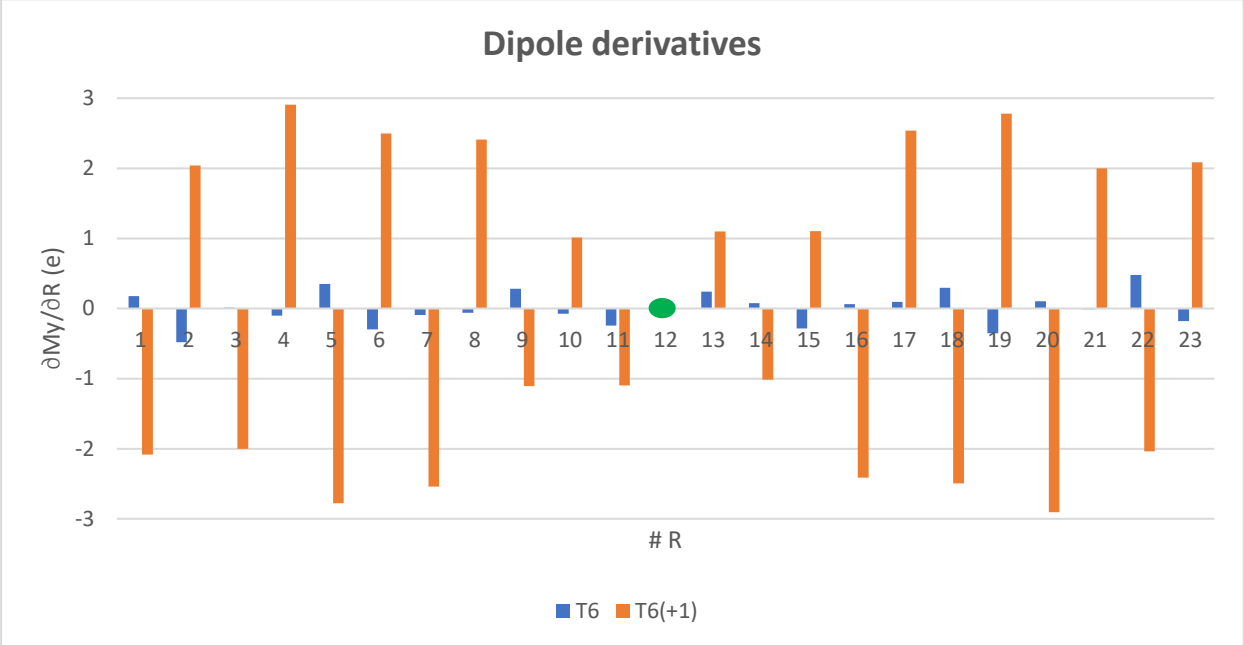

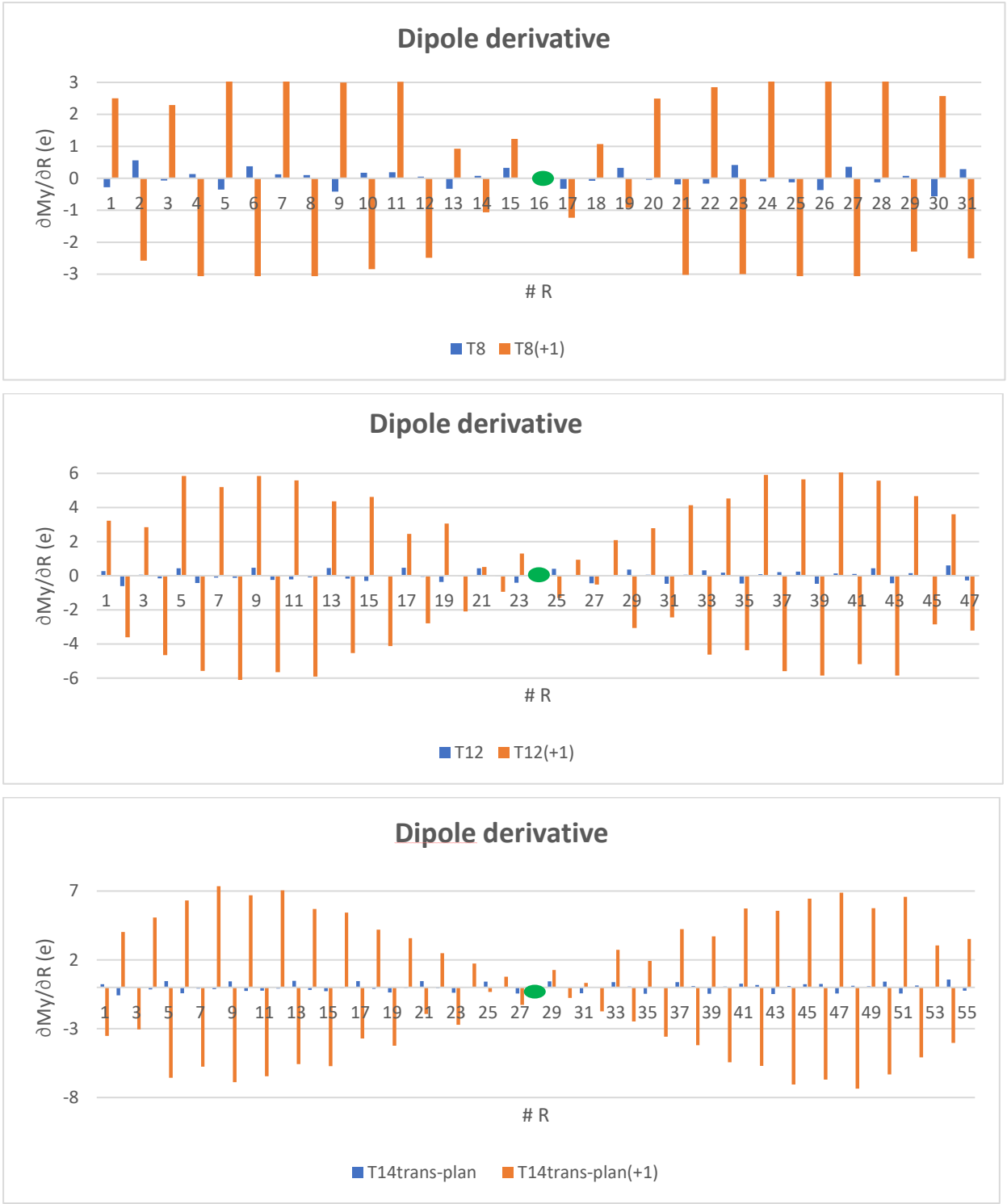

Figure 3.35: y-component of dipole derivative with respect C-C stretching internal coordinate of neutral and charged oligothiophenes. On the horizontal axis # R indicates the number of C-C single or double bond constituting the backbone of the oligothiophene.

The analysis of the ∂My/∂R parameters allows to obtain some important results:

1. In both neutral and charged case, the dipole derivative with respect to the stretching internal coordinate of the central bond (indicated by the green dot in Figure 3.35), that is the centre of inversion, is null.
2. The modulus of ∂My/∂R shows very large values in the case of charged Tn(+1) if compared with the ones of the neutral Tn, thus meaning that the doping induced charge onto the oligomer backbone promotes the polarization of the quasi-single and quasi-double C-C bonds, which are instead substantially non-polar in neutral Tn (small values of ∂My/∂R parameters)
3. The ∂My/∂R of the Tn(+1) species shows a perfect alternation of sign, that doesn't occur in the Tn species, in particular, considering the left half portion of the molecule, ∂My/∂R shows positive values for even CC bonds and negative values for odd CC bonds if we consider the T6(+1) and T14(+1) models and viceversa for the T8(+1) and T12(+1) models: the different signs depends only on the different orientation of the chain axis y, while the sign inversion from even to odd sites is the relevant characteristic. This phenomenon is particularly important because it means that the doping induces large IR activity for the alternating stretching and shrinking of the C-C bonds (e.g., for any ECC-like vibration). Notice that also the C-C bonds located in the peripheral thiophene units of the oligomer present large values of ∂My/∂R (in the Tn(+1) model) and they concur to the intensification of collective ECC-like modes.

The large IR intensity of the ECC-like IRAVs can be better rationalized through a more explicit definition of the Effective Conjugation Coordinate (ECC) for a general oligothiophene **[20, 30]**; we will refer to Figure 3.36 for the numeration of the CC bonds, needed to properly define the Я coordinate for the T2 structural unit.

$$Я = \frac{1}{\sqrt{8}}(R_2 - R_1 + R_4 - R_3 + R_6 - R_5 + R_8 - R_7) \qquad \text{(eq. 3.7)}$$

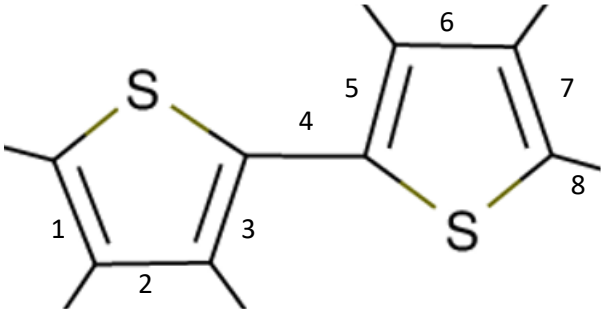

Figure 3.36: numeration of C-C bonds in a schematic representation of the Bithiophene molecule.

Eq. 3.7 describes the ECC, **q=0** phonon coordinate of the polymer, described as a 1-D crystal, but can be easily extended to any oligomer formed by an even number of thiophene units. Let us consider the expression of the dipole derivative with respect a normal mode Q_k:

$$\frac{\partial M_y}{\partial Q_k} = \sum_t \frac{\partial M_y}{\partial r_t} L_{tk} \cong \sum_i \frac{\partial M_y}{\partial R_i} L_{ik} \qquad \text{(eq. 3.8)}$$

where Q_k is the k-th normal coordinate, $\{r_t\}$ is the set of the internal valence coordinates, L_{tk} is the element of the vibrational eigenvector expressed on the basis set of the internal coordinates, $\{R_i\}$ is the sub-set of the C-C stretching internal coordinates. The approximated equality holds for normal modes like ECC-like modes of the doped molecules, because the dipole derivatives with respect to the CC stretching internal coordinates have remarkably high values compared to the other dipole derivatives.

In the case of charged oligothiophenes $\frac{\partial M_y}{\partial R_i}$ presents opposite sign for the stretching of adjacent CC bonds and also L_{ik} associated to an ECC-like mode have opposite sign when the label i indicates a quasi-single or a quasi-double CC bond, because in ECC-like normal modes single and double CC bonds stretch out-of-phase according to the given definition of the Я coordinate: for these reasons the contributions from the individual CC bonds to $\frac{\partial M_y}{\partial Q_k}$ sum up, thus explaining the very high IR intensity of the ECC-like normal mode **[30]**. It is important to underline the fact that both $\frac{\partial M_y}{\partial R_i}$ and L_{ik} systematically change the sign through the inversion centre located on the central bond of the molecule. The above observation comes from a look to Figure 3.35, focusing on the pattern of the dipole derivatives on left side and on the right one with respect to the green dot, and considering the L_{ik} of the IR active modes, which have always a central node, through which the vibration inverts its phase, namely they are ungerade modes.)

3.2.2. Raman spectrum and polarizability derivative parameters of neutral and charged oligothiophenes.

We now focus on the Raman spectrum and local parameters of neutral and charged oligothiophenes, from T6 to T14 model. As in the IR case, the detailed analysis of the Raman spectrum of neutral and charged oligothiophenes is already presented in Sections 3.1.2 and 3.1.3, so here we limit to underline how the Raman spectrum of the considered oligomers changes passing from the pristine to the doped state.

Neutral T6 and charged T6(+1). We report in Figure 3.37 the Raman spectrum of T6 and T6(+1) in the wavenumber region from 1000 to 1700 cm^{-1}, where the most intense peaks appear.

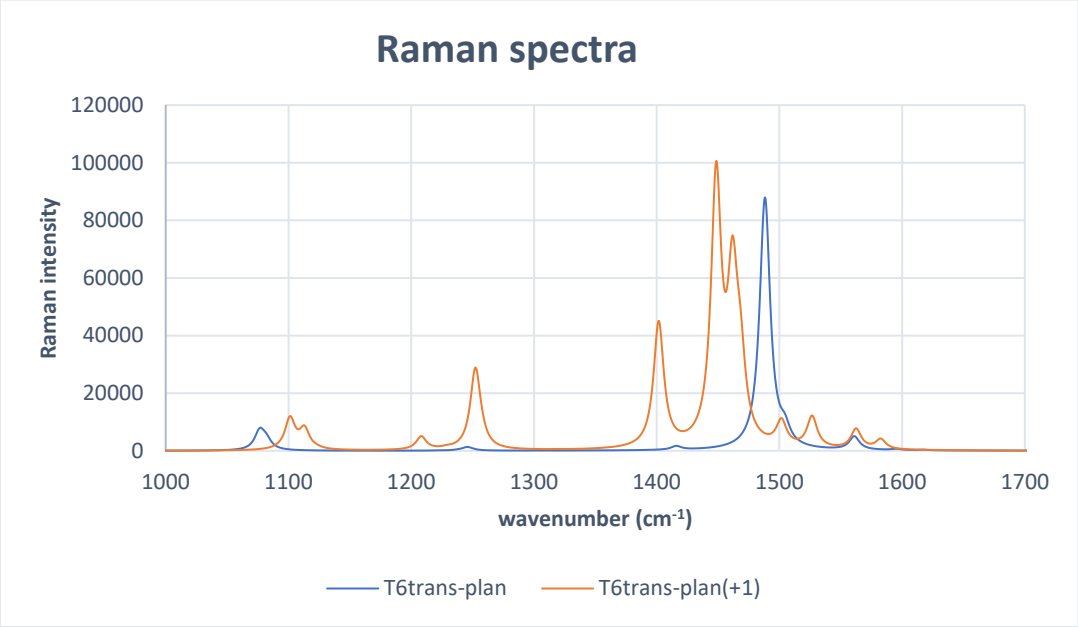

Figure 3.37: Raman spectrum of neutral T6 and charged T6(+1).

While the Raman spectrum of the neutral T6 is dominated by one single very intense peak at 1489 cm^{-1}, whose associated normal mode is the collective ECC vibration, the Raman spectrum of charged T6(+1) is more structured, presenting six relevant peaks with frequency at 1101, 1252, 1402, 1449 (the most intense Raman peak), 1462 and 1468 cm^{-1}. The sketch of the eigenvector of the associated normal modes is reported in Figure 3.38.

1101 cm^{-1}; 0 km/mol; 36512 A^4/amu

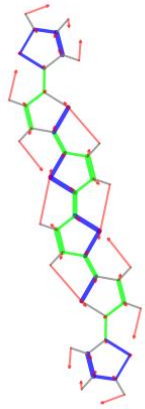

1252 cm^{-1}; 0 km/mol; 105660 A^4/amu

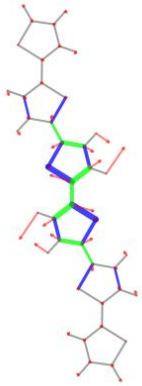

1402 cm^{-1}; 0 km/mol; 186291 A^4/amu

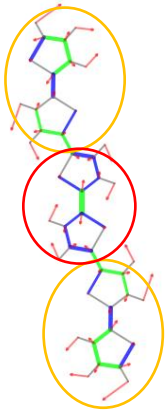

1449 cm^{-1}; 0 km/mol; 406561 A^4/amu

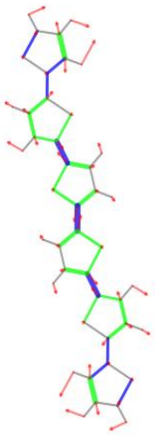

1462 cm^{-1}; 0 km/mol; 241121 A^4/amu

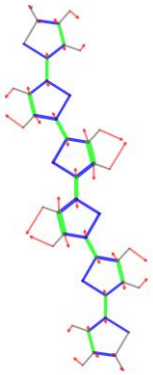

1468 cm^{-1}; 0 km/mol; 104741 A^4/amu

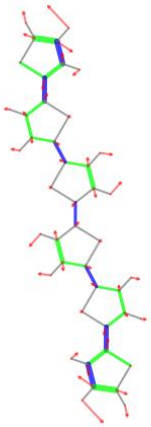

Figure 3.38: sketch of the eigenvectors of the normal modes associated to the six intense peaks of the Raman spectrum of T6(+1).

Because the normal modes associated to 1402 and 1468 cm^{-1} peaks of the Raman spectrum of T6(+1) were not considered in Section 3.1.2, their eigenvectors will be described here below.

The normal mode associated to the 1402 cm^{-1} Raman peak presents two nodes located after two thiophene rings from the end of the oligomer and it shows some ECC-like character because the quasi-double CC bonds stretch out-of-phase with respect to the single inter-ring CC bonds, but the quasi-single CC bond within each thiophene unit vibrates with the wrong sign with respect to the ECC pattern.

For what concerns the normal mode associated to the 1468 cm^{-1} Raman peak, it is a Я-like vibration at the peripheral thiophene units, while the ECC-like character is lower in the central region of the molecule: in particular all inter-ring CC bonds vibrate in phase, and they are out-of-phase with respect to the quasi-double CC bonds, but the single CC bonds within the thiophene rings stretch with the wrong sign.

Also all the other normal modes associated to the intense peaks of the Raman spectrum of T6(+1) exhibit some ECC-like character:

- The normal mode associated to the 1101 cm^{-1} peak because all the quasi-single CC bonds, except for the single bond within the last thiophene unit, stretch in-phase, but the quasi-double CC bonds vibrate with the wrong sign or do not participate.
- The normal mode associated to the 1252 cm^{-1} peak, extremely localized on the central thiophene units, because the CC bonds of the thiophenes stretch or shrink with the correct phase according to the ECC pattern, while the inter-ring bonds do not.
- The normal mode associated to the 1449 cm^{-1} peak because all the quasi-double CC bonds and the inter-ring ones stretch or shrink with the correct phase, but the quasi-single CC bond of each thiophene ring vibrates with the wrong sign.

The normal mode associated to the 1462 cm^{-1} is very similar to the pure ECC vibration. Notice that the eigenvector phase is the opposite with respect to the usual definition of ECC: indeed, all the quasi-single CC bonds stretch (the segments are coloured in green), while all the quasi-double CC bonds shrink (the segments are coloured in blue); however, the phase of the eigenvector is irrelevant at all for our discussion: the sketch of the eigenvector can be regarded as a snapshot of the nuclei trajectory at one of the two turning points of the vibrational mode. In this case it simply describes the "maximum compression" along the ECC coordinate, which is usually sketched according to the nuclei displacement at the "maximum elongation".

Neutral T8 and charged T8(+1). In Figure 3.39 we report the Raman spectrum in the wavenumber region between 1000 and 1700 cm^{-1} of the neutral T8 and charged T8(+1).

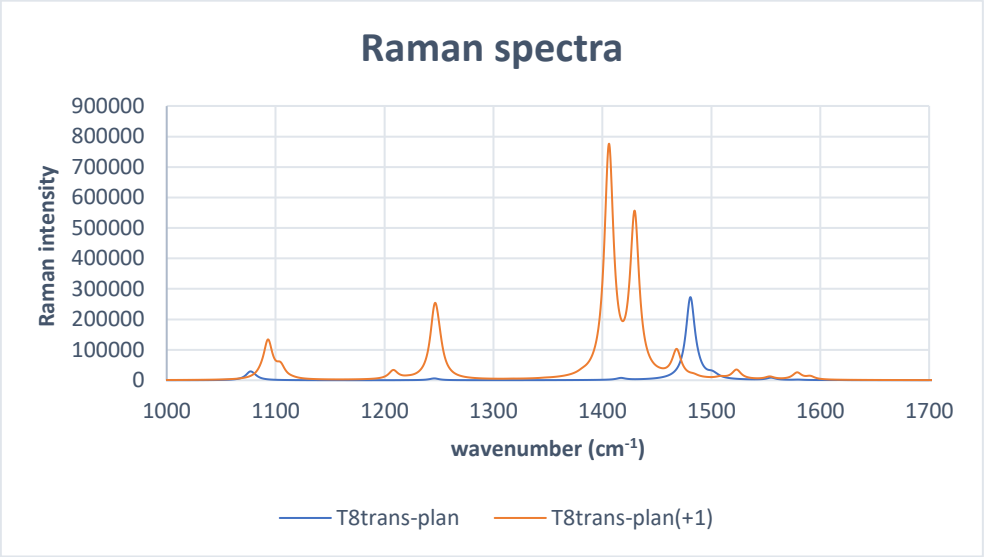

Figure 3.39: Raman spectrum of neutral T8 and charged T8(+1).

The Raman spectrum of charged T8(+1) presents five intense peaks, whose frequencies are 1093, 1246, 1406 (the most intense peak), 1430 and 1468 cm^{-1}, whose eigenvectors are sketched in Figure 3.40.

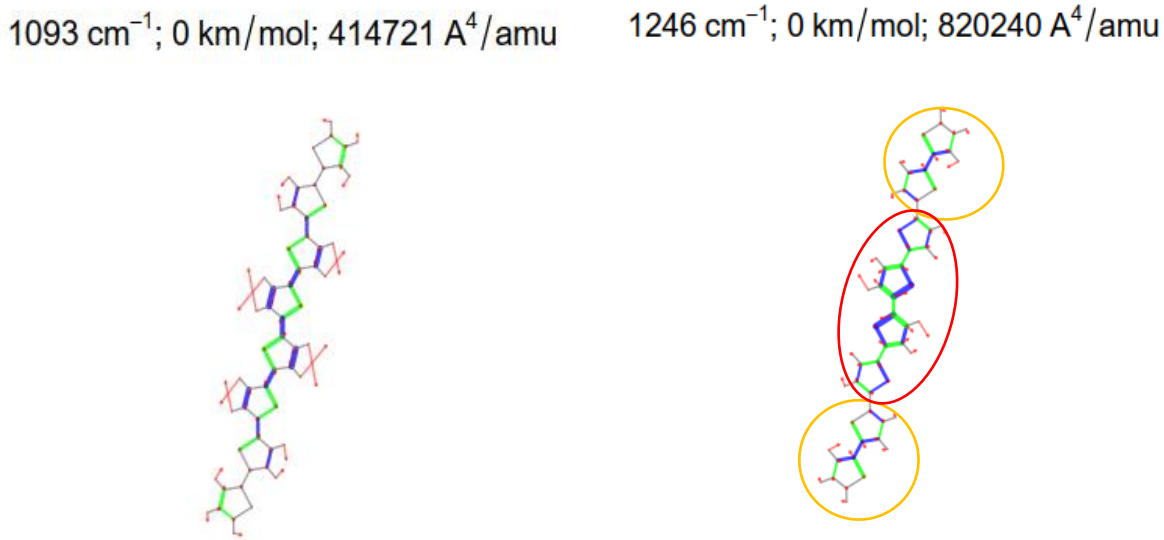

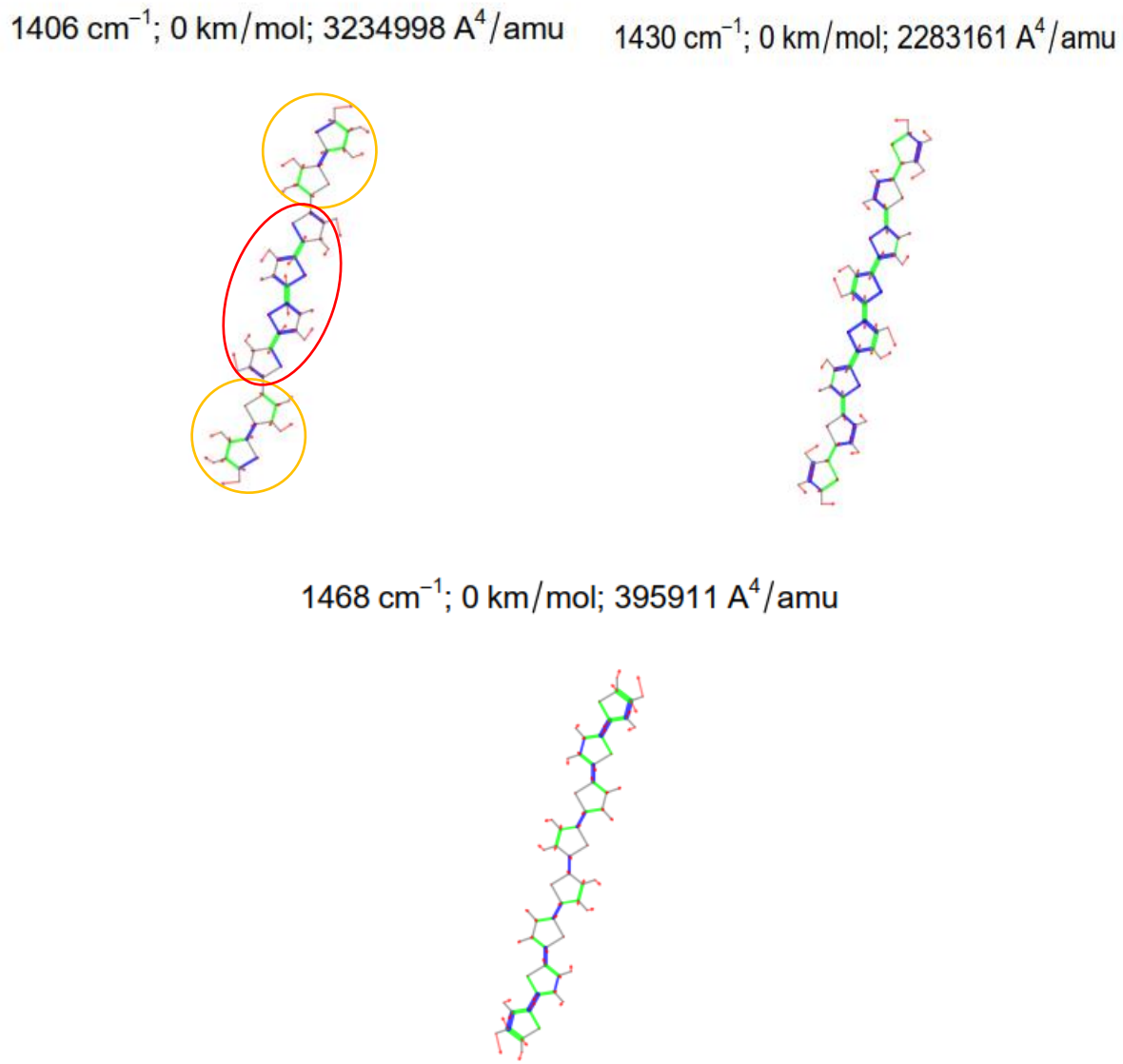

Figure 3.40: sketch of the eigenvector of the normal modes associated to the five intense peaks of the Raman spectrum of T8(+1).

The description of the ECC-like character of the normal modes parallels the one presented for the T6(+1) model.

Neutral T12 and charged T12(+1); neutral T14 and charged T14(+1). In Figures 3.41 we report the Raman spectrum, in the wavenumber region between 1000 and 1600 cm^{-1}, of T12 and charged T12(+1) on panel above and of neutral T14 and charged T14(+1) on panel below respectively.

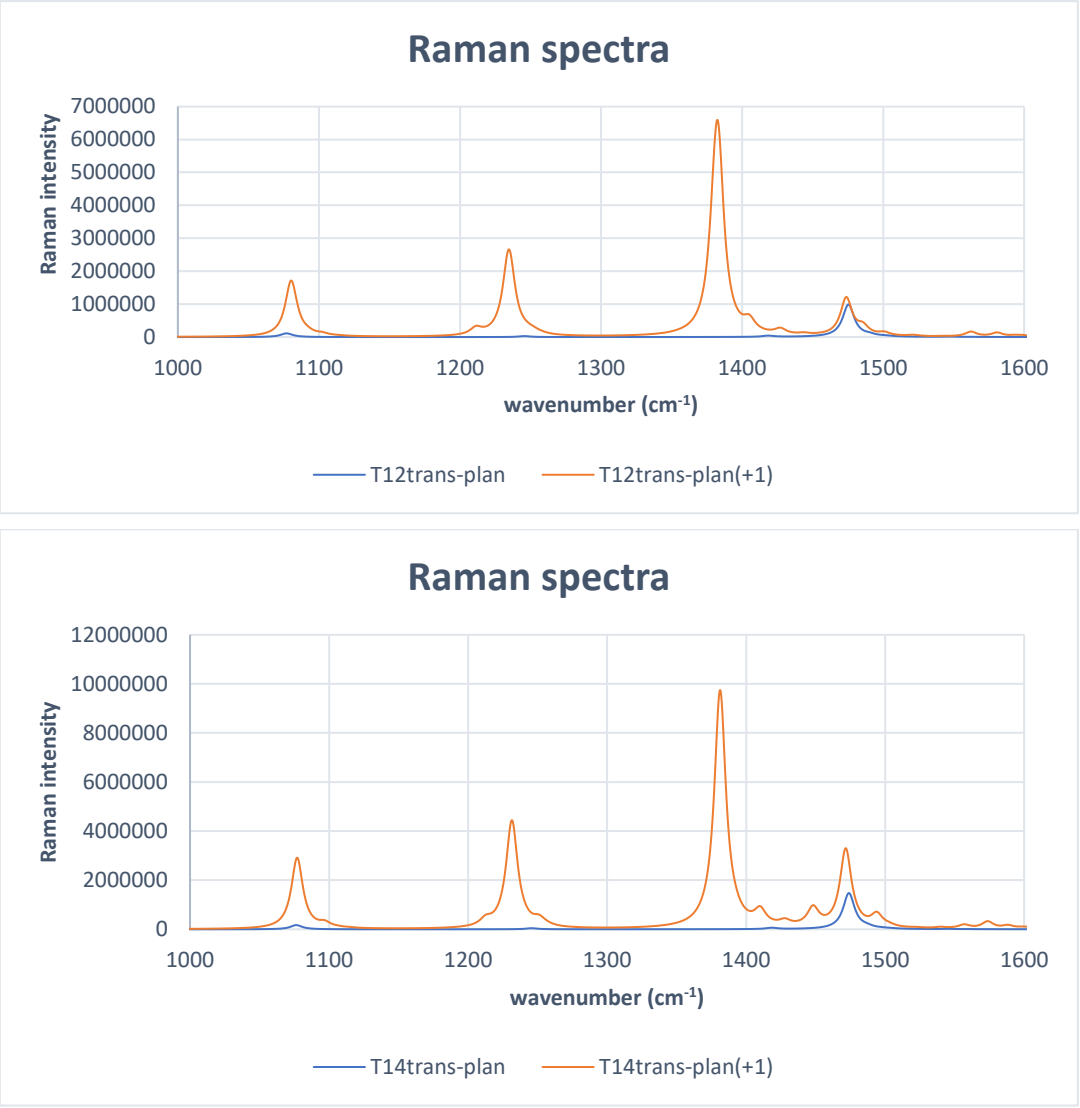

Figure 3.41: top panel: Raman spectrum of neutral T12 and charged T12(+1); bottom panel: Raman spectrum of neutral T14 and charged T14(+1).

The Raman spectrum of T12(+1) and T14(+1) is characterised by four very intense peaks. The frequencies of the four peaks are 1084, 1234, 1383 (the most intense peak) and 1474 $cm^{-1}$for T12(+1), 1077, 1232, 1381 (the most intense peak) and 1472 cm^{-1} for T14(+1); the sketch of the associated eigenvector is reported in Figure 3.42, in the left panel the ones of T12(+1) and in the right panel the ones of T14(+1).

T12(+1) model	T14(+1) model
1080 cm^{-1}; 0 km/mol; 5415847 A^4/amu	1077 cm^{-1}; 0 km/mol; 9521003 A^4/amu
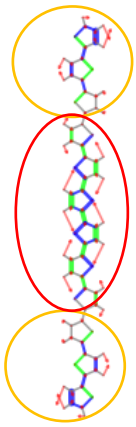	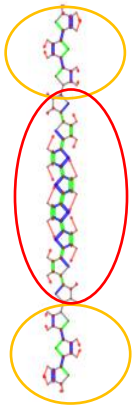
1234 cm^{-1}; 0 km/mol; 8657456 A^4/amu	1232 cm^{-1}; 0 km/mol; 13110618 A^4/amu
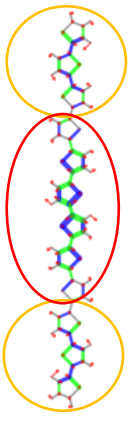	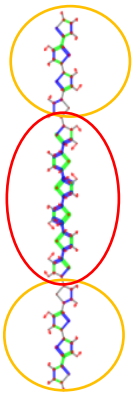

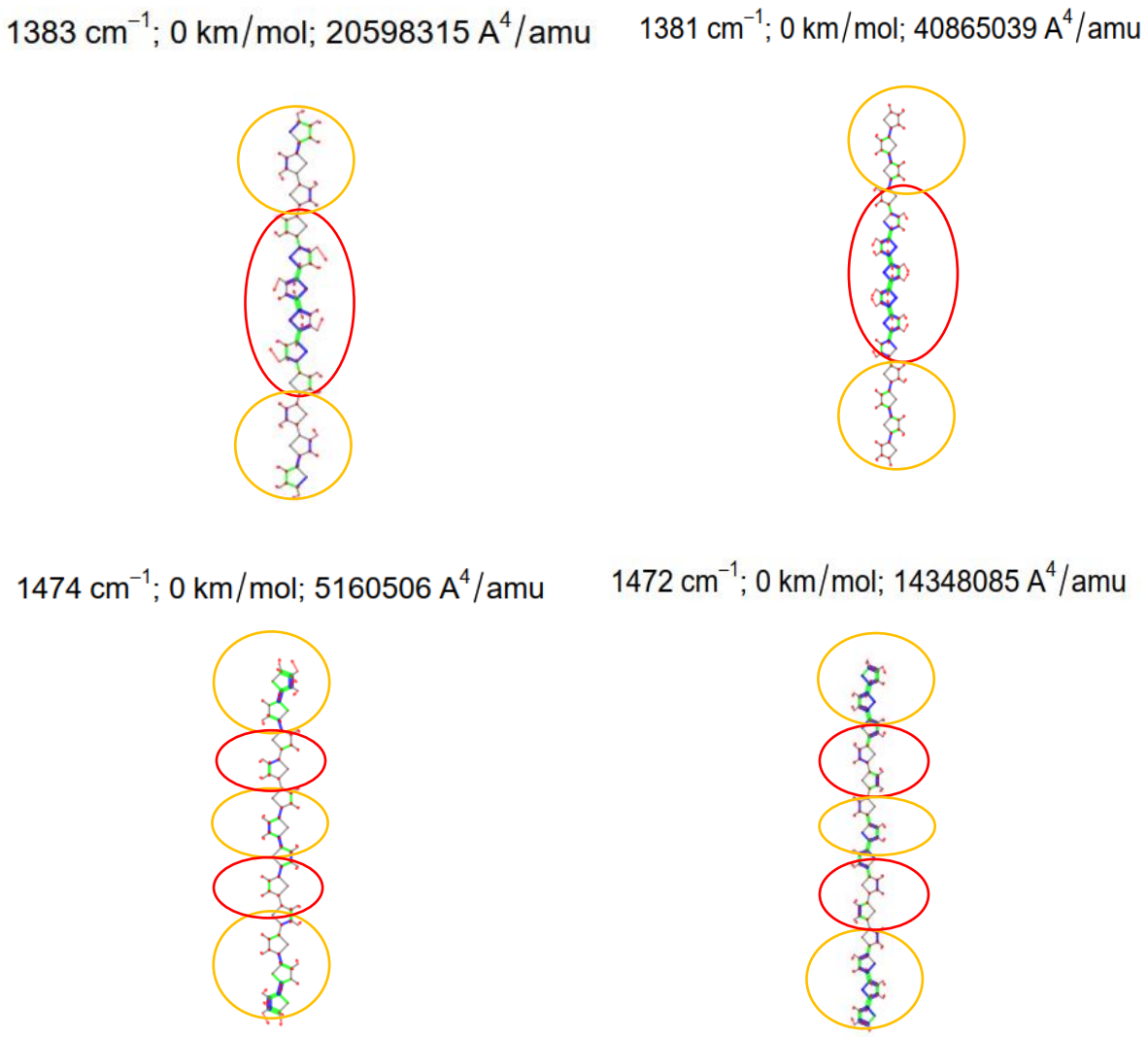

Figure 3.42: sketch of the eigenvector associated to the four intense peaks of the Raman spectrum of charged T12(+1) and T14(+1).

For the description of the ECC-like character of the normal modes, recall the one presented for the T6(+1) model. It is interesting to notice that in both the T12(+1) and T14(+1) models, all the ECC-like Raman active normal modes present two or four nodes, and a more localized character of the Я-like vibration: in particular, focusing on the two most intense Raman transitions, the normal modes associated to the most intense peak is localized in the central region of the oligothiophene, while the vibration associated to the second most intense peak is more localized at the peripheral thiophene units.

The onset of RAVs. The four previously described intense normal modes, associated to the strong peaks of the Raman spectrum of the charged oligothiophenes, are

classified as RAVs (Raman Active Vibrations): they are silent or almost silent in the Raman spectrum when the oligomer is in the neutral state and become active when the oligomer is in the charged state. Because the four extremely intense peaks in the Raman spectrum of charged/doped oligothiophenes are negligible or absent in the Raman spectrum of neutral/pristine corresponding oligomer, they should constitute the spectroscopic fingerprints of the polaron, when the material is investigated through Raman spectroscopy.

The full rationalization of the onset of the RAVs can be obtained by means of the local Raman intensity parameters, namely the polarizability derivative with respect to the internal C-C stretching coordinate, labelled as $\partial\alpha/\partial R$, whose trace values for the neutral and the charged oligothiophenes are reported in Figure 3.43.

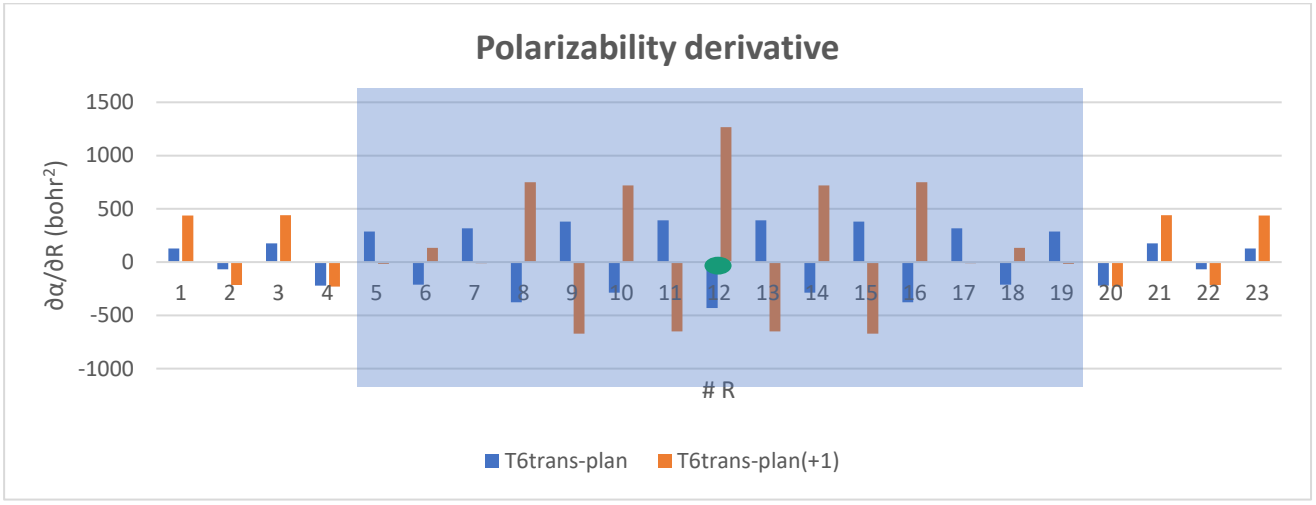

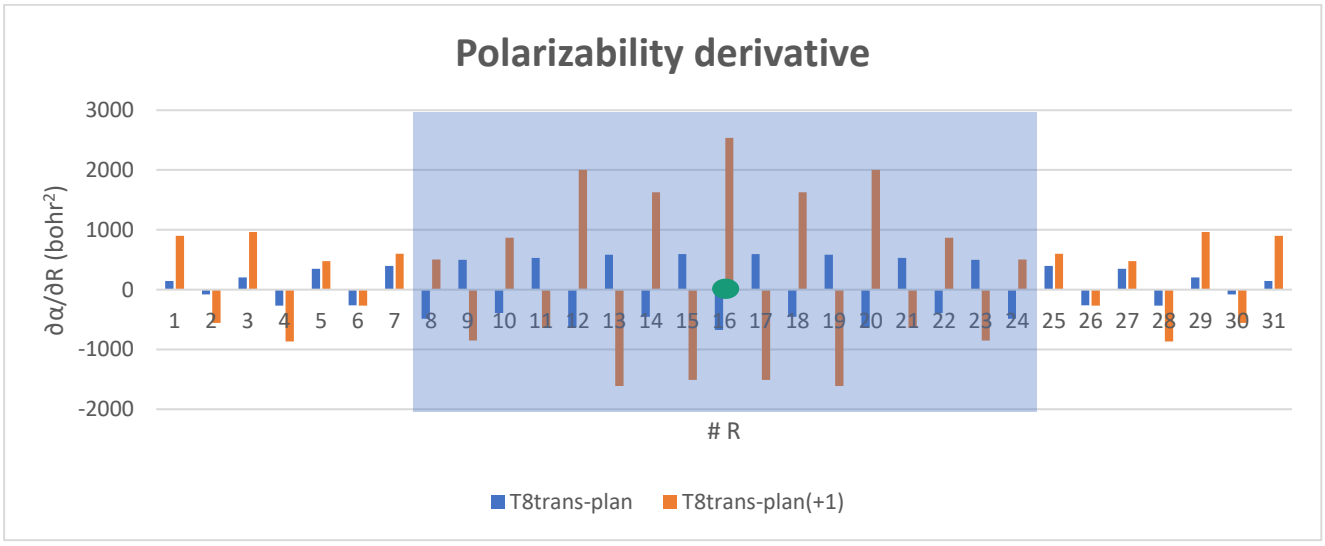

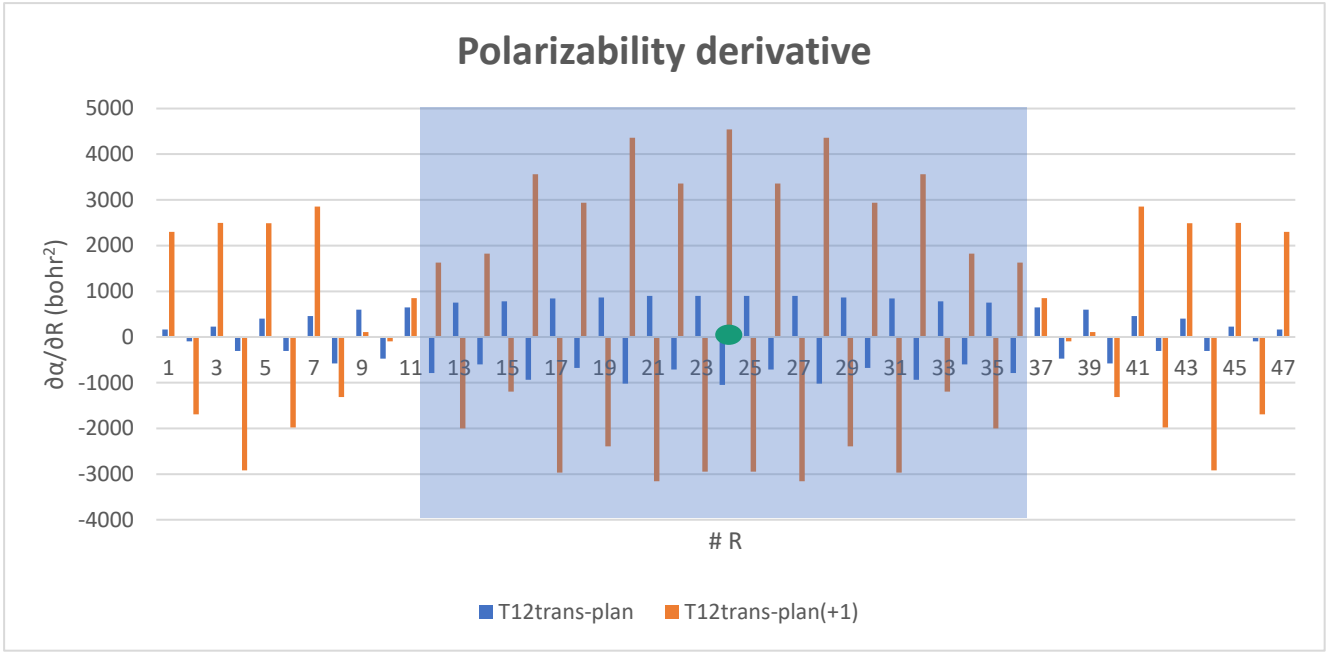

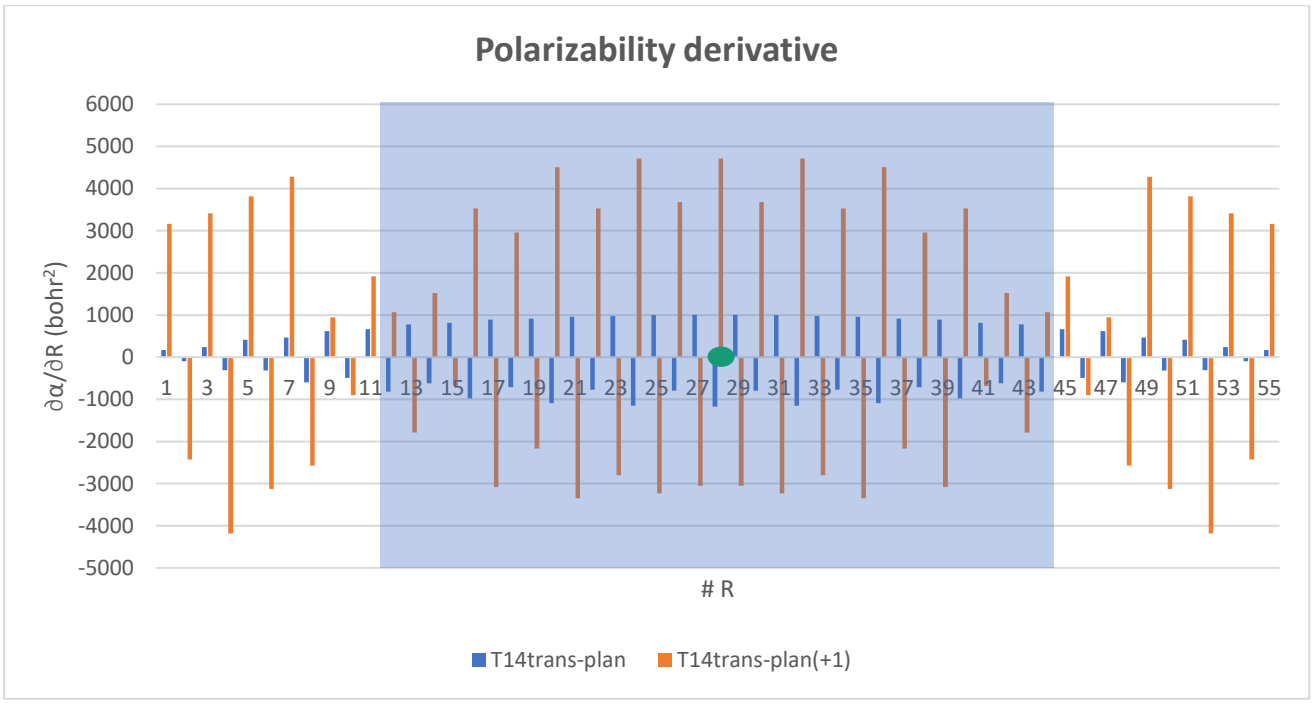

Figure 3.43: polarizability derivative with respect C-C stretching internal coordinate of neutral and charged oligothiophenes. On the horizontal axis # R indicates the number of C-C single or double bond constituting the backbone of the oligothiophene.

The analysis of the ∂$\boldsymbol{\alpha}$/∂R parameters allows to obtain valuable results:

1. The absolute values of ∂$\boldsymbol{\alpha}$/∂R parameters of charged oligothiophenes are much larger with respect to the ones showed by the corresponding neutral oligomer, thus explaining the dramatic increasing of the intensity of the Raman spectrum and in particular of the extremely high Raman activity of the normal modes showing ECC-like character. The rationalization of this aspect can be obtained through the definition of the polarizability derivative with respect to the C-C stretching internal coordinate, according to the following equation:

$$\frac{\partial \boldsymbol{\alpha}}{\partial Q_k} = \sum_t \frac{\partial \boldsymbol{\alpha}}{\partial r_t} L_{tk} \cong \sum_i \frac{\partial \boldsymbol{\alpha}}{\partial R_i} L_{ik} \qquad \text{(eq. 3.9)}$$

   where Q_k is the k-th normal coordinate, $\{r_t\}$ is the set of the internal valence coordinates, L_{tk} is the matrix element of the vibrational eigenvector, $\{R_i\}$ is the sub-set of the C-C stretching internal coordinates.
   Because of the way the Я coordinate is defined, the quasi-single and quasi-double CC bonds stretch out-of-phase in ECC-like normal modes and so L_{tk} presents values with opposite sign; also $\frac{\partial \alpha}{\partial R_i}$ shows positive and negative values for double and single CC bond stretching respectively and so the contributions from the individual CC bonds to $\frac{\partial \alpha}{\partial Q_k}$ sum up, implying very large Raman activity of the ECC-like normal modes.
2. It is important to underline a significant difference in the ∂α/∂R parameters between short and long oligothiophenes. In T6(+1) and T8(+1) models the largest value of the ∂α/∂R parameters is the one respect to the central bond (indicated in Figure 3.43 with a green dot); in fact the most intense Raman normal mode shows a high contribution by the stretching of the central CC bond (see the eigenvector of the vibration associated to 1449 and 1406 cm^{-1} peaks for T6(+1) and T8(+1) respectively). On the other hand, in T12(+1) and T14(+1) models the largest values of the ∂α/∂R parameters involve the stretching of several CC bonds in the central region of the oligomer, thus explaining why the most intense Raman normal mode is an ECC-like vibration mostly localized in the central region of the molecule (see the eigenvector of the vibration associated to 1383 and 1381 cm^{-1} peaks for T12(+1) and T14(+1) respectively).
3. Another interesting aspect is the fact that in all the considered models of the oligothiophenes, the ∂α/∂R parameters show large values also in the peripheral regions of the oligomer, thus explaining why (at least) one intense RAV is an ECC-like vibration mostly localized in the outer thiophene rings of the oligomer.

4. The $\partial\alpha/\partial R$ parameters do not change sign in the peripheral thiophene units when the oligomer passes from the neutral to the charged state, while in central region of the oligomer sign inversion occurs, a phenomenon that is highlighted in Figure 3.43 by the light-blue panel. From this, it is possible to compute the spatial extent of the charge defect, i.e. the so-called polaron. Indeed, it can be associated to the region of the molecule characterized by a systematic inversion of the sign of the local Raman parameters; the results are reported in Table 3.9. Recalling the fact that in neutral oligomers the quasi-single C-C bonds show negative values for $\partial\alpha/\partial R$, while quasi-double C-C bonds show positive values for $\partial\alpha/\partial R$, it is possible to observe that the $\partial\alpha/\partial R$ parameters indicates that the structure in the central region has a quinoid character, namely it is strongly perturbed by the injected charge by the doping process, while the peripheral thiophene units remain substantially unaffected by the charge defect; the transition from the unperturbed region to the perturbed one occurs through the equalization of the CC bonds, this because the transition CC bonds exhibit small values of the $\partial\alpha/\partial R$ parameters.

Table 3.9: frequency and Raman activity of the most intense Raman normal mode for neutral and charged oligothiophenes.

Oligothiophene	Number of CC bonds from which $\partial\alpha/\partial R$ sign inversion occurs	Corresponding thiophene unit from which $\partial\alpha/\partial R$ sign inversion occurs	Polaron spatial extent
T6-T6(+1)	5	2	4 thiophene units
T8-T8(+1)	8	3	4 thiophene units + the external inter-ring bonds
T12-T12(+1)	12	4	6 thiophene units + the external inter-ring bonds
T14-T14(+1)	12	4	8 thiophene units + the external inter-ring bonds

3.2.3. The geometry relaxation when the oligothiophenes pass from the neutral to the charged state.

In this Section we analyse which are the effects of the doping process on the equilibrium geometry of the considered oligothiophenes and in particular on the equilibrium length of the quasi-single and quasi-double CC bonds. In figure 3.44 we compare on the same plot the equilibrium bond length of each oligomer in the pristine and doped state, from T6 to T14.

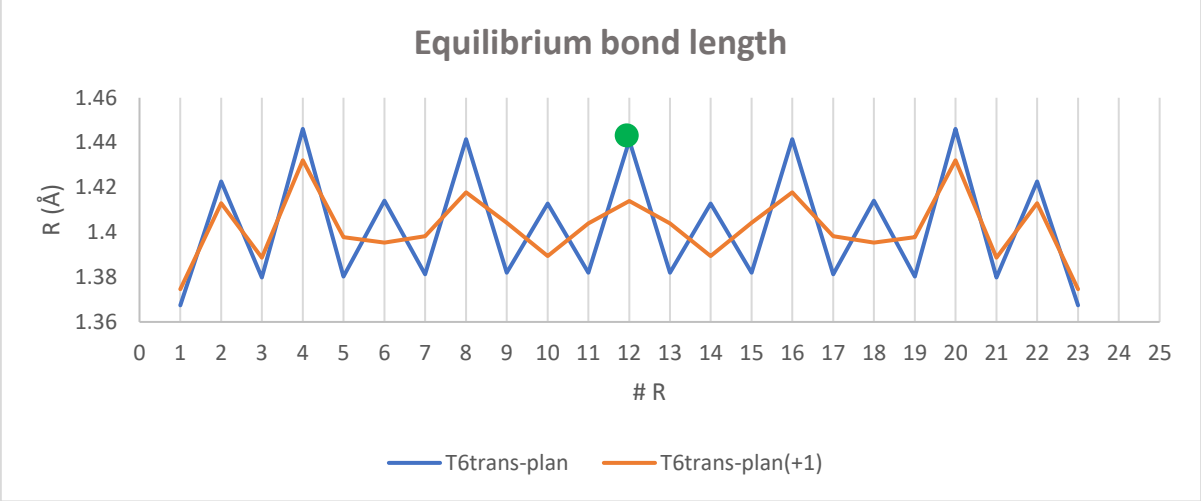

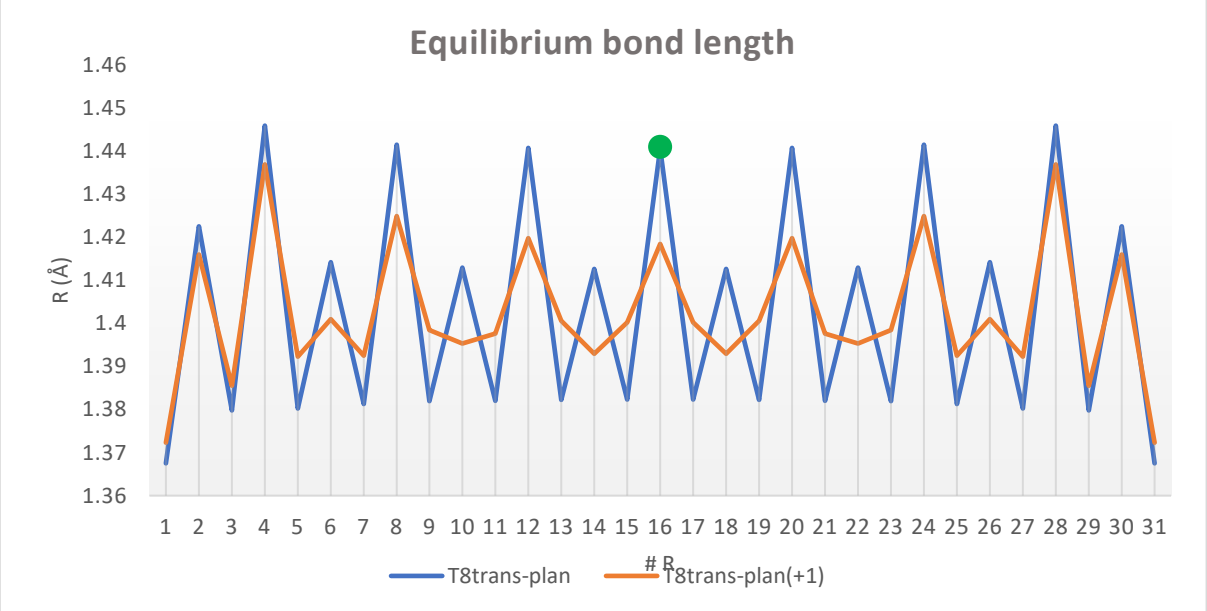

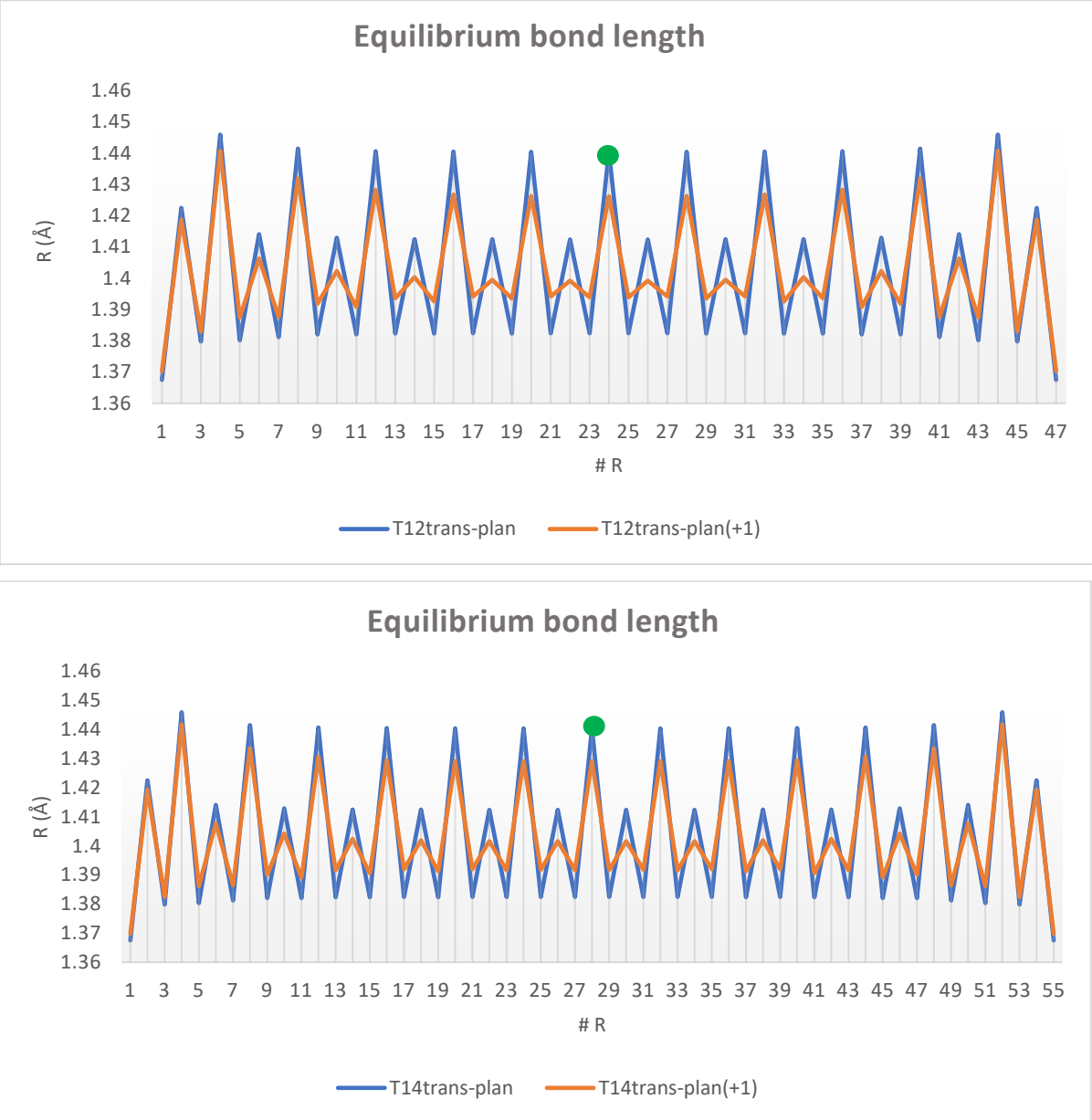

Figure 3.44: equilibrium bond length of neutral and charged oligothiophenes, from T6 to T14; on the horizontal axis # R indicates the number of C-C single or double bond constituting the backbone of the oligothiophene.

From Figure 3.44 it is possible to notice that the oligothiophenes undergo a structural relaxation upon charging. This phenomenon occurs in the central region of the oligomer, where the charge self-localizes; the peripheral thiophene units are unperturbed, in fact the difference between the length value of the CC bond of the neutral oligothiophene and the one of the corresponding charged specie is practically negligible. In general, the main consequence of doping on the geometry of the

oligothiophenes is that the quasi-single CC bonds shorten, and the quasi-double CC bonds stretch. In order to be more quantitative in the description of the spatial extent of the induced charged defect, i.e. the so-called polaron, it is possible to compute the bond length difference for each CC bond between the one of the charged oligothiophene and the one of the corresponding neutral specie. The values are graphically reported in Figure 3.45, the region where the polaron self-localizes, that we arbitrarily decide to individuate from the first CC bond for which the absolute value of the bond length difference is greater than 0,01 Å, is indicated by a light-blue panel.

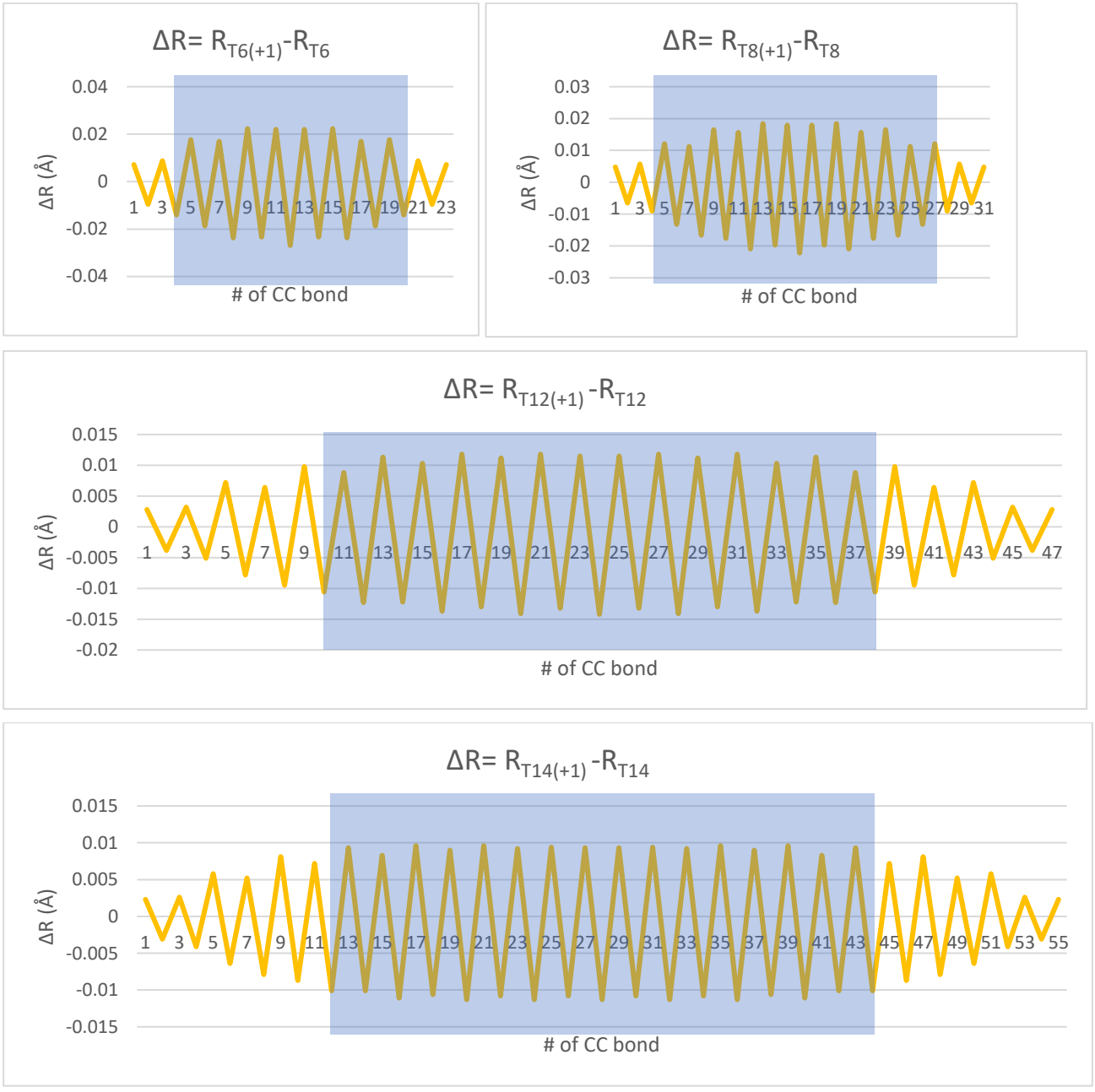

Figure 3.45: the bond length difference for each CC bond between the one of the charged oligothiophene and the one of the corresponding neutral specie.

The values of the spatial extent of the polaron, obtained by the analysis of the geometry relaxation that occurs in oligothiophenes upon doping, are reported in Table 3.10; in square brackets the corresponding results predicted by the Raman local parameters are recalled.

Table 3.10: spatial extent of the polaron predicted by the geometry relaxation for oligothiophenes with increasing chain length. The values deduced considering the Raman local parameters (from Table 3.9) are reported in squared brackets to ease the comparison.

Oligothiophene	Number of CC bond from geometry relaxation	Corresponding thiophene unit from which large ΔR occurs	Polaron spatial extent
T6-T6(+1)	4 [5]	2 [2]	4 thiophene units + the external inter-ring bonds [4]
T8-T8(+1)	5 [8]	2 [3]	6 thiophene units [4 + the external inter-ring bonds]
T12-T12(+1)	10 [12]	3 [4]	7 thiophene units [6 + the external inter-ring bonds]
T14-T14(+1)	12 [12]	4 [4]	8 thiophene units + the external inter-ring bonds [8 + the external inter-ring bonds]

The results obtained with the two methods show similar trends, even if the comparison cannot be excessively stressed, since the polaron delocalization length obtained by the geometry analysis strictly depends on the arbitrary chosen critical value of ΔR=0,01 Å. The results shown in Tables 3.9 and 3.10 are coherent and relevant because they underline the major issue concerning the use of B3LYP functional in DFT simulations, that is the so-called delocalization and self-interaction errors: hybrid functionals tend

to over-delocalize, therefore the longer is the chain length of the oligothiophene the larger is the delocalization of the charged species.

Notably, the slightly more than eight thiophene units' delocalization length of the polaron in the T14(+1) model is very similar to the one reported in literature of 8,7 thiophene units, obtained by pulse radiolysis in chloroform of poly(3-decylthiophene) (P3DT) **[8]**.

As a last analysis, it is valuable to discuss if the difference about the geometry relaxation of the perturbed region of the oligothiophenes upon doping predicted by the local Raman parameters and the one obtained by the analysis of the equilibrium CC bonds length. To reach this goal it is useful to plot in Figure 3.46 the Bond Length Alternation (BLA) parameter for all the neutral and charged oligothiophenes, from T6 to T14; BLA is calculated with the following equation:

$$BLA = R_{k\,C-C} - R_{(k-1)\,C=C} \qquad \text{(eq. 3.10)}$$

where R_{kC-C} is the equilibrium bond length of the k-th quasi-single CC bond and $R_{(k-1)\,C=C}$ is the equilibrium bond length of the (k-1)-th quasi-double CC bond.

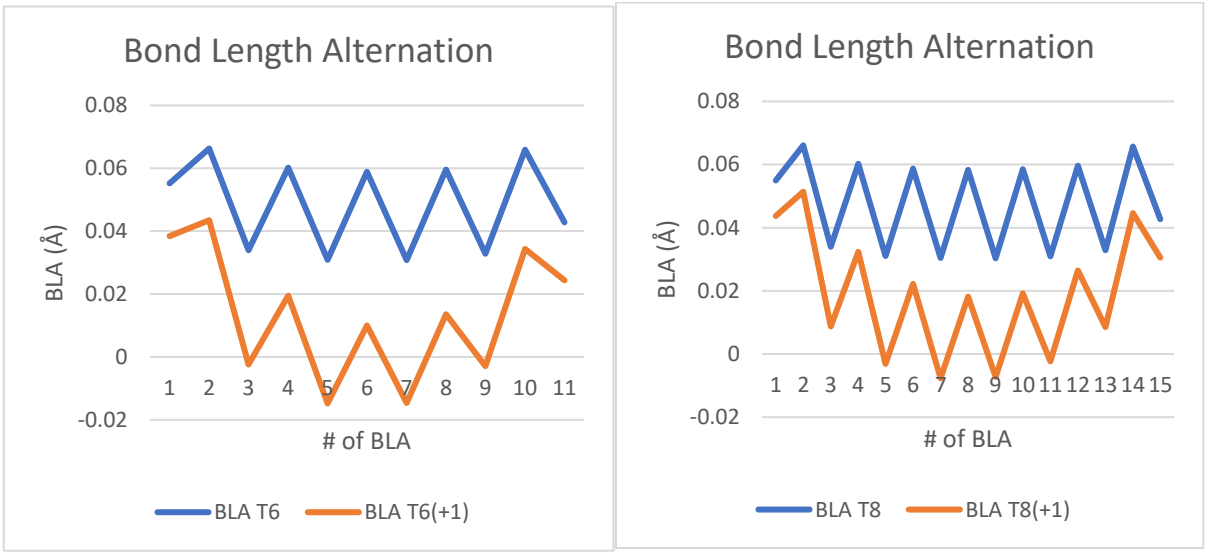

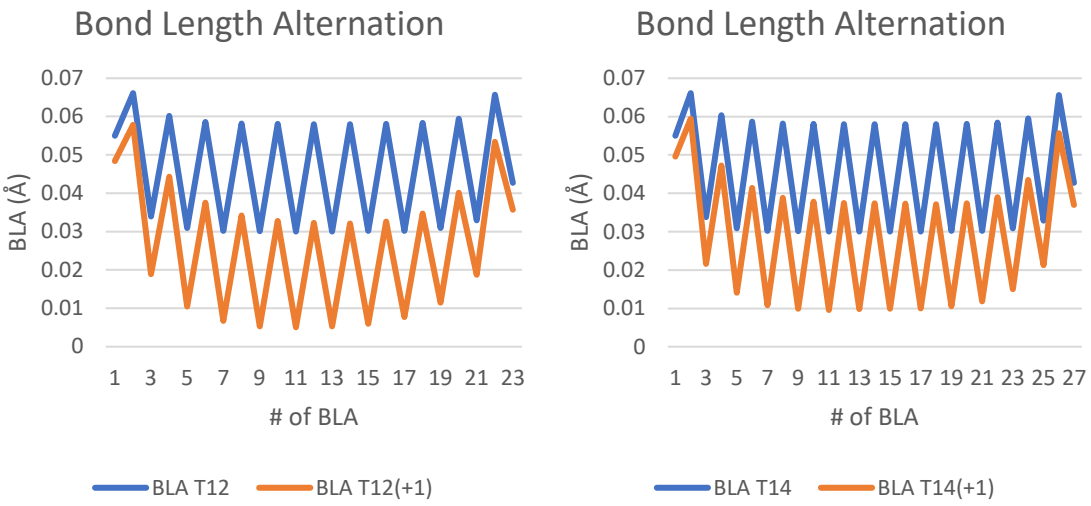

Figure 3.46: BLA of neutral and charged oligothiophenes, from the T6 to the T14 model.

Firstly, it is important to notice that BLA of neutral oligothiophenes is always positive and sufficiently large to assume that the molecular backbone is described by a sequence of alternated quasi-double and quasi-single CC bonds.

In this respect, we observe that the Raman local parameters predict that the polaron exhibits a quinoid structure (see Section 3.2.2), while the BLA parameter allows to obtain different results:

- A common feature to all the models of charged oligothiophenes is that the BLA at the extremities of the oligomer is similar to the one of neutral molecules, thus confirming the fact that the peripheral thiophene units are practically unperturbed.
- For the T6(+1) model, the BLA of the central region of the molecule, that is the perturbed one upon the charge injection, reaches negative values, thus meaning that the central CC bonds invert their character of quasi-single and quasi-double bonds. In this case, the BLA parameter confirms the quinoid structure of the polaron, predicted by the $\partial\alpha/\partial R$ parameters.
- For the T8(+1) model, the BLA still reaches negative values but in this case they are practically vanishing: the polaron exhibits the equalization of the quasi-single and quasi-double CC bonds.
- For the T12(+1) and T14(+1) models, the BLA parameter of the central perturbed region of the oligomers is positive, but very small; also in this case the polaron exhibits the equalization of the quasi-single and quasi-double CC bonds.

The equalization of the quasi-single and quasi-double CC bonds as a consequence of the doping process is an expected phenomenon, for example it is registered even in other classes of polyconjugated materials like polyenes **[30].**

From the previous considerations, two relevant results can be stated.

1. The T6 model is too short to properly describe the polaron, because the characteristic dimension of the charge defect, i.e. its delocalization length, and the chain length are comparable.
2. The calculated local Raman parameters are not reliable because they predict a quinoid structure of the polaron for all the considered oligomers, even for the longer ones. For this reason, it is reasonable to think that the calculated intensity of the Raman spectrum of charged oligothiophenes, that is directly affected by the $\partial\alpha/\partial R$ parameters, could be not properly described and typically overestimated. We will further analyse and discuss this very relevant aspect also in Chapter 5, when we will compare the results obtained with DFT quantum-chemical simulations and the ones obtained experimentally.

3.3. The effect of the range-separated CAM-B3LYP functional on the geometry and on the spectroscopic features of oligothiophenes.

In this Section we analyse the effect of a different DFT functional with respect to B3LYP, on the geometry and on the vibrational IR and Raman spectra of neutral and charged oligothiophenes. The functional we adopt here is CAM-B3LYP, thus meaning Coulomb-Attenuating Method applied to the B3LYP functional, which is classified as a range-separated functional.

As it is discussed in the previous Sections, the main issues concerning the use of B3LYP functional are related with the self-interaction energy problem, the delocalization error and the treatment of static-electron correlation (especially for cases in which degenerate states may play a role): for example the spatial extent of the polaronic charge defect, introduced into the oligomer upon the doping process and described by the molecular geometry relaxation, increases with the increasing chain length of the oligothiophene and so with its conjugation length, without reaching a plateau value.

The range-separated DFT functionals aims at reducing the problem of the self-interaction and delocalization error by introducing a damping function to the HF exchange part of the functional, however still adopting the B3LYP XC approach **[47]**

The main consequence deriving from the use of range-separated functionals, like CAM-B3LYP, is generally a better description of the electronic structure of the excited

states (especially those characterised by a charge-transfer nature) and charged states, where sometimes static correlation contribution might play a crucial role.

For the study case here considered, we expect that CAM-B3LYP can mitigate the over-delocalization of the charged state better describing the self-localization of the polaron species by increasing the number of thiophene units, namely when the oligomer passes from short to long. Indeed, it was demonstrated that range-separated functionals lead to reasonable polaron localization lengths and reorganization energies, as extrapolated to the polymer limit, for various organic conjugated polymers, in contrast to hybrid DFT functionals (e.g., B3LYP) which instead provide unphysical values.

Dealing with a different XC functional, we expect that the CAM-B3LYP will impact the IR and Raman spectra too of both neutral and charged oligothiophenes, and especially on the IR and Raman peaks corresponding to the ECC-like normal modes, which are highly sensitive to the conjugation length.

In this Section we will compare the results between B3LYP and CAM-B3LYP, for what concerns the computed vibrational spectra, the IR and Raman local parameters and the geometry, mainly the equilibrium C-C bond length and the Bond Length Alternation (BLA) parameter, of neutral and charged oligothiophenes. The models we will consider are the neutral/pristine T6, T8 and T12 and the corresponding charged/doped T6(+1), T8(+1) and T12(+1).

For all quantum-chemical simulations performed with CAM-B3LYP, the basis set is kept the same as before, namely 6-31G**; neutral species (0) were computed in the restricted (closed-shell) configuration, while charged species (i.e., radical cation, +1) were treated in the unrestricted configuration (as doublet).

3.3.1. Geometry and vibrational spectra of neutral and charged oligothiophenes: results from CAM-B3LYP functional.

Geometry relaxation upon doping. We start the discussion about the CAM-B3LYP functional comparing in Figure 3.47 the values of bond length difference between the equilibrium length of each CC bond of the charged oligothiophenes and the one of the corresponding neutral specie, ΔR measured in Å. In each panel we compare values obtained using B3LYP (green) and CAM-B3LYP functionals (yellow).

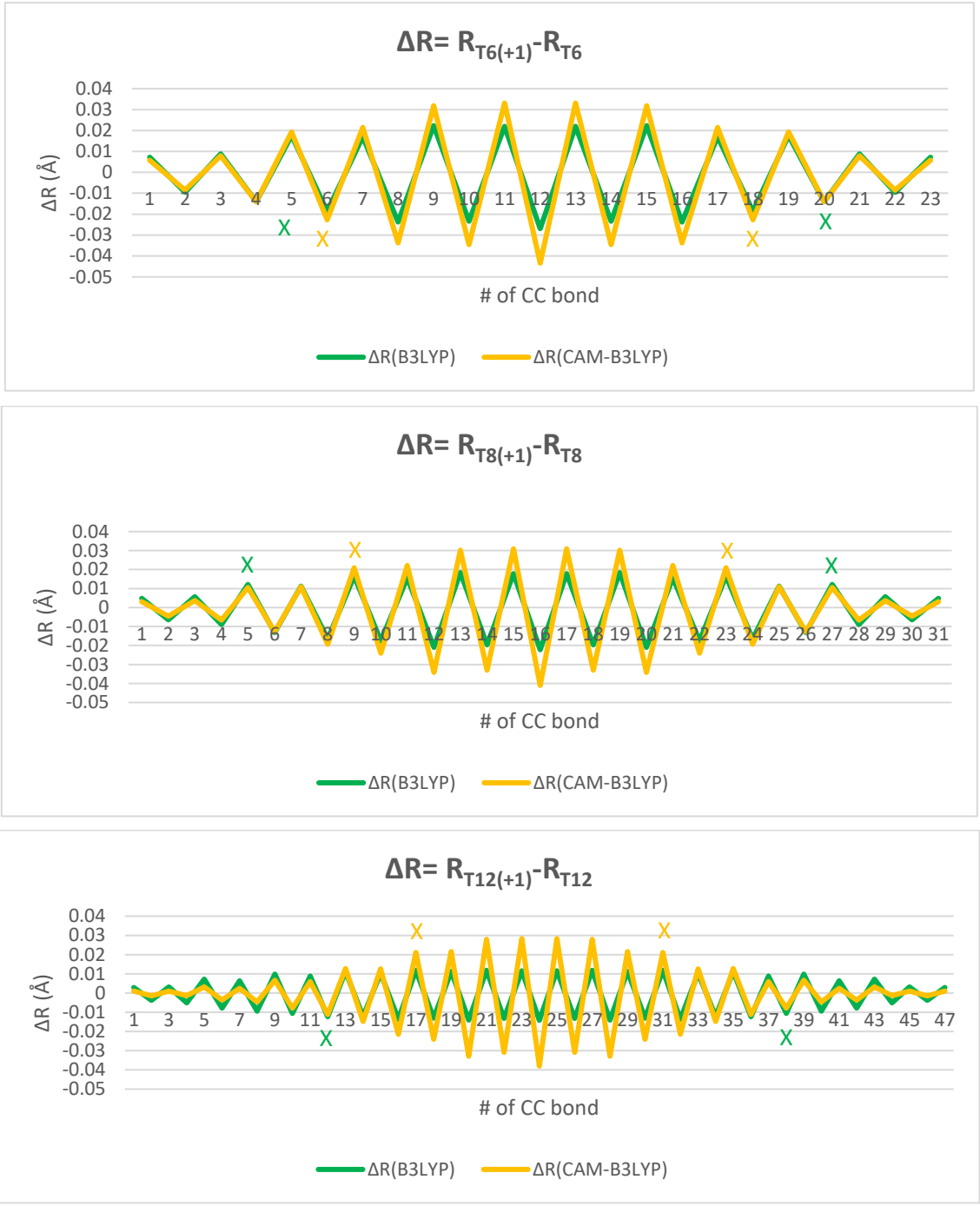

Figure 3.47: bond length difference between the CC bonds of the charged oligothiophenes and the corresponding one of the neutral species.

Figure 3.47 confirms the spatial localization of the charge as introduced by CAM-B3LYP which confines the structural relaxation of the charged state in the central part of the oligomer chain. This is markedly in contrast with respect to B3LYP, which delocalizes the charge defect over the entire chain regardless the oligomer length. To take consciousness of this aspect, we set the threshold value of ΔR equal to 50% of the maximum value of ΔR to individuate the perturbed region: in the case of B3LYP the

threshold value for ΔR is 0,01 Å, while in the case of CAM-B3LYP is 0,02 Å. In Figure 3.47 we use the symbol X (green for the B3LYP case and yellow for the CAM-B3LYP case) to indicate the first and last CC bond, whose ΔR value reaches the threshold. The results for what concerns the polaron delocalization length predicted by the CAM-B3LYP functional are reported in Table 3.11; in square brackets we recall also the corresponding values obtained with B3LYP functional.

Table 3.11: spatial extent of the polaron predicted by the geometry relaxation for oligothiophenes with increasing chain length and obtained with CAM-B3LYP functional; in square brackets the corresponding B3LYP results are recalled.

Oligothiophene	**Number of non-modified CC bond before geometry relaxation** (starting from one end**)**	**Number of non-perturbed thiophene unit before geometry relaxation**	**Polaron spatial extent**
T6-T6(+1)	6 [4]	2 [2]	3 thiophene units [4 + the external inter-ring bonds]
T8-T8(+1)	9 [5]	3 [2]	4 thiophene units [6]
T12-T12(+1)	17 [10]	5 [3]	4 thiophene units [7]

Table 3.11 numerically demonstrates that the delocalization length of the polaron (three or four thiophene units) resulting from the geometry optimization performed with CAM-B3LYP, after T8(+1), does not depend on the chain length of the oligothiophene, as it occurs by using B3LYP.

Interestingly, CAM-B3LYP provides a different description of the kind of geometry relaxation of the central region perturbed by the charge injection through the doping process with respect to the one offered by the B3LYP functional, reported in Section 3.2.1

In Figure 3.48 we report for the three neutral and charged oligothiophenes the Bond Length Alternation (BLA) parameter, computed as the difference between the equilibrium length of a quasi-double CC bond and the one of the adjacent quasi-single CC bond (eq. 3.10). Quasi single and quasi double bond notation is referred to the geometry of the neutral molecule, in fact they correspond to even and odd positions respectively, along the backbone.

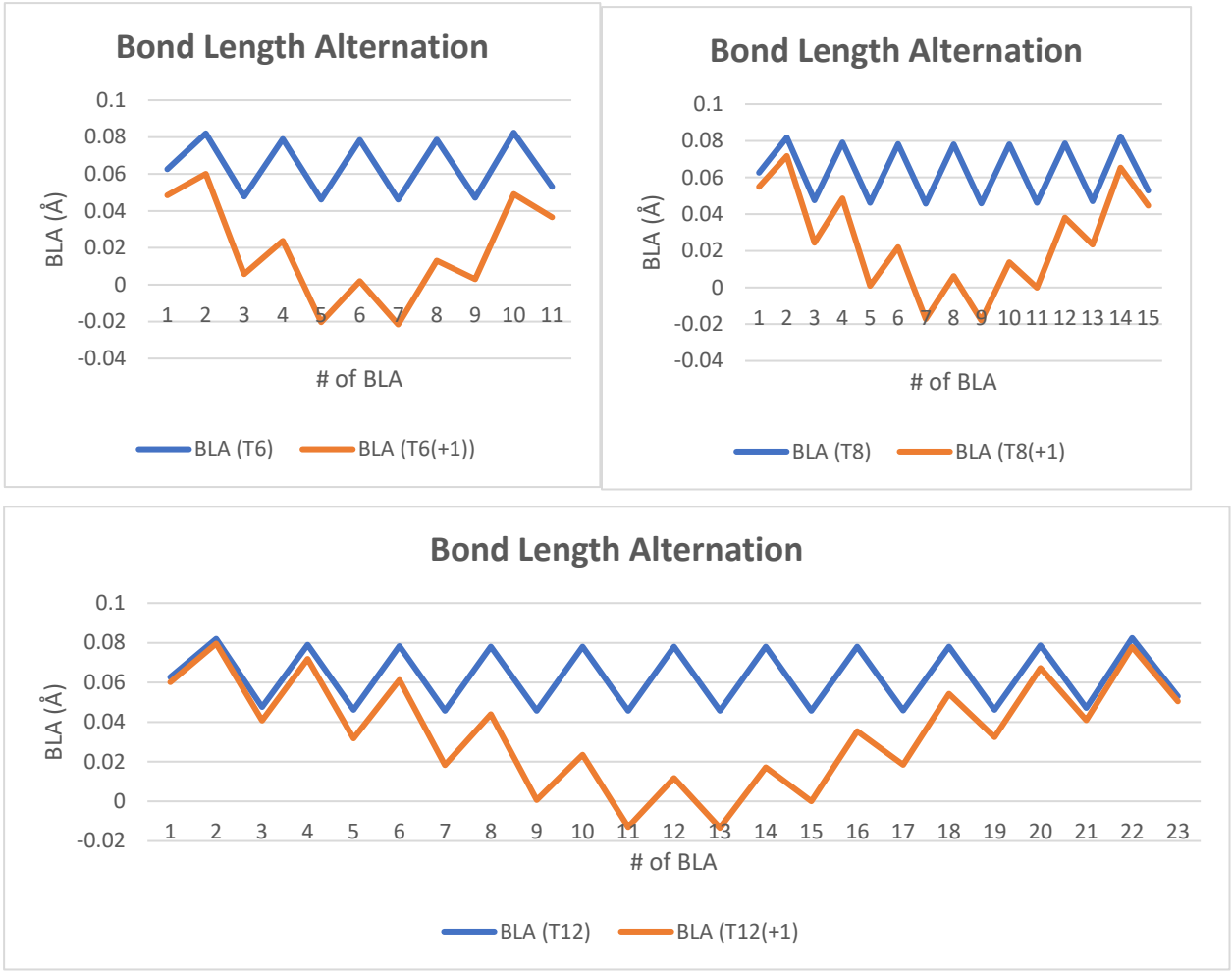

Figure 3.48: Bond Length Alternation (BLA) of neutral and charged oligothiophenes, calculated with CAM-B3LYP. The numerical label of BLA indicates the location of the pair of single/double bonds from the left to the right end of the molecule.

From Figure 3.48 it is possible to obtain valuable considerations:

- BLA of neutral T6, T8 and T12 is positive and quite large: the pristine oligothiophenes are conjugated materials, constituted by alternated quasi-single and quasi-double CC bonds.
- BLA of the neutral oligomers and the one of the corresponding charged species is very similar for the CC bonds near to the ends, thus confirming that the polaron self-localizes in the central region of the molecule, while the peripheral thiophene units remain unaltered after the doping process.
- For what concerns the central region of the molecule, the BLA calculated with CAM-B3LYP functional exhibit small but negative values both in short and long oligomers, thus meaning that the most perturbed CC bonds by the charge invert

their character of quasi-single and quasi-double bonds: according to the description offered by CAM-B3LYP, the region perturbed by the charge exhibits a quinoid structure. This is the main difference with the prediction of the geometry obtained with the use of the B3LYP, according to which the polaron shows a quinoid structure only for the short T6 model, while equalized quasi-single and quasi-double CC bonds in the longer models (see Section 3.2).

Vibrational spectra and local parameters. In Figure 3.49 we report the IR (first panel) and Raman spectra (second panel) of neutral oligothiophenes, from T6 to T12, in the wavenumber region between 1400 and 1650 cm^{-1}, where the most intense IR and Raman peak appears.

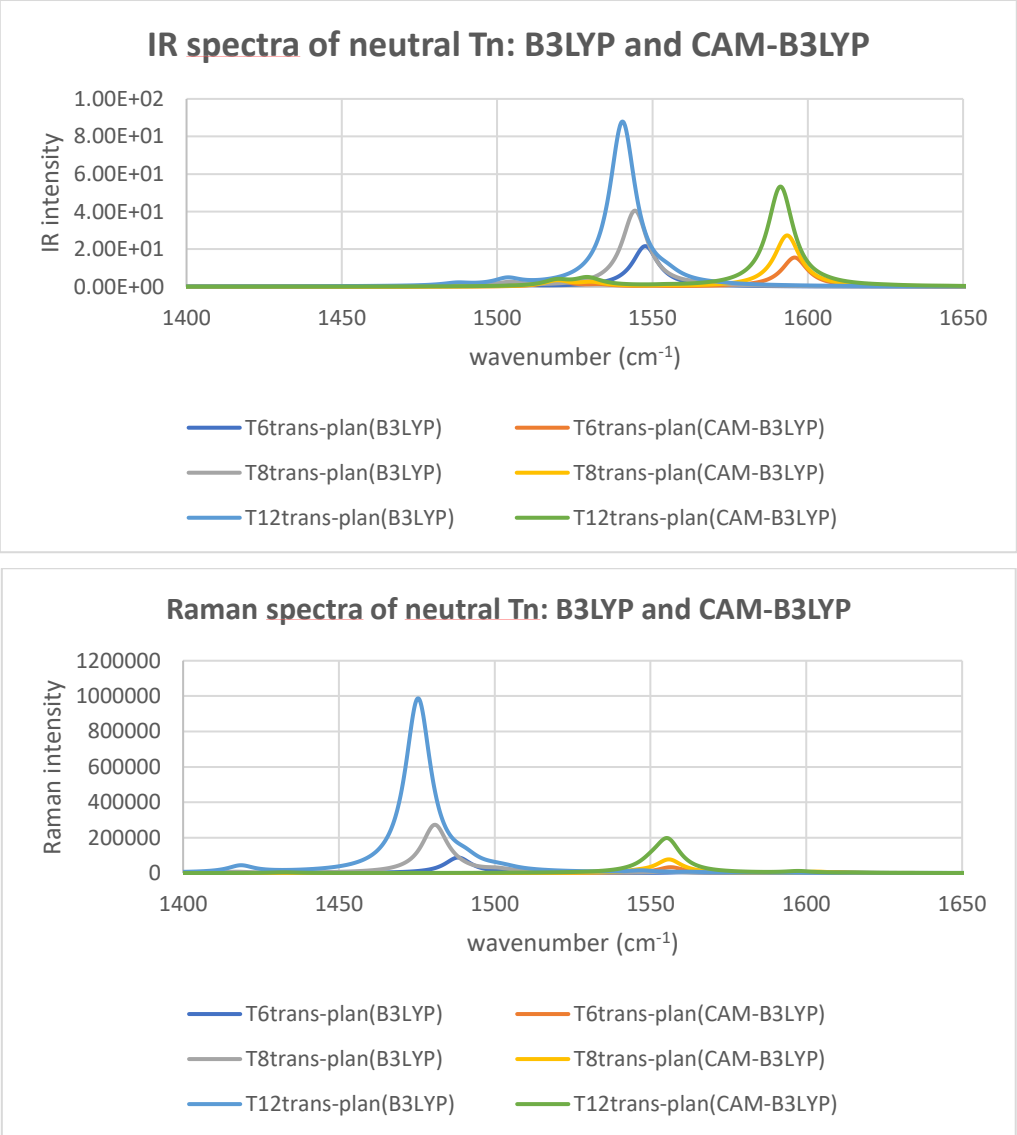

Figure 3.49: IR and Raman spectra of neutral oligothiophenes, from T6 to T12, calculated with B3LYP and CAM-B3LYP functional.

From Figure 3.49, we can obtain two important considerations about the effect of the CAM-B3LYP functional on the vibrational spectra:

1. Because CAM-B3LYP limits the delocalization, thus implying a lower conjugation length, the frequency of the most intense IR and Raman vibrations is characterised by a higher wavenumber (blue-shift of the frequency) with respect the one computed using B3LYP; this is particularly true for what concerns the collective Raman ECC normal mode, which is extremely sensitive to the delocalization length.
2. The IR and Raman intensity of the most relevant peaks of the vibrational spectra calculated with CAM-B3LYP is lower than the one obtained with the B3LYP functional, especially for what concerns the strongest Raman peak: this is probably due to a reduced electrons-phonon coupling as a consequence of a lower conjugation length estimated by CAM-B3LYP than B3LYP.

In order to be more quantitative, we report in Table 3.12 for each considered oligothiophene the frequency difference and the intensity ratio in Table 3.13, for both the IR and Raman case, between the results calculated with the CAM-B3LYP and the B3LYP functional.

Table 3.12: IR and Raman frequency difference between the results calculated with the CAM-B3LYP and the B3LYP functional.

Tn	$\Delta\boldsymbol{\nu}^{\boldsymbol{IR}} = \boldsymbol{\nu}^{\boldsymbol{IR}}{}_{\boldsymbol{CAM-B3LYP}} - \boldsymbol{\nu}^{\boldsymbol{IR}}{}_{\boldsymbol{B3LYP}}$	$\Delta\boldsymbol{\nu}^{\boldsymbol{Raman}} = \boldsymbol{\nu}^{\boldsymbol{Raman}}{}_{\boldsymbol{CAM-B3LYP}} - \boldsymbol{\nu}^{\boldsymbol{Raman}}{}_{\boldsymbol{B3LYP}}$
T6	$1596 - 1548 = 48\ cm^{-1}$	$1556 - 1489 = 67\ cm^{-1}$
T8	$1593 - 1544 = 49\ cm^{-1}$	$1556 - 1481 = 75 cm^{-1}$
T12	$1591 - 1540 = 51\ cm^{-1}$	$1555 - 1475 = 80\ cm^{-1}$

Table 3.13: IR and Raman intensity ratio difference between the results calculated with the CAM-B3LYP and the B3LYP functional.

Tn	$\frac{I^{IR}{}_{CAM-B3LYP}}{I^{IR}{}_{B3LYP}}$	$\frac{I^{Raman}{}_{CAM-B3LYP}}{I^{Raman}{}_{B3LYP}}$
T6	$\frac{244}{339} = 0{,}72$	$\frac{157112}{322745} = 0{,}49$
T8	$\frac{428}{635} = 0{,}67$	$\frac{361527}{1218482} = 0{,}30$
T12	$\frac{837}{1375} = 0{,}61$	$\frac{858833}{4426514} = 0{,}19$

We now focus our attention on the effects of the CAM-B3LYP functional on the vibrational spectra of charged T6(+1), T8(+1) and T12(+1); in Figure 3.50 we report the IR (top panel) and Raman spectra (bottom panel) in the wavenumber region between 500 and 1600 cm^{-1} calculated with both CAM-B3LYP and B3LYP functionals.

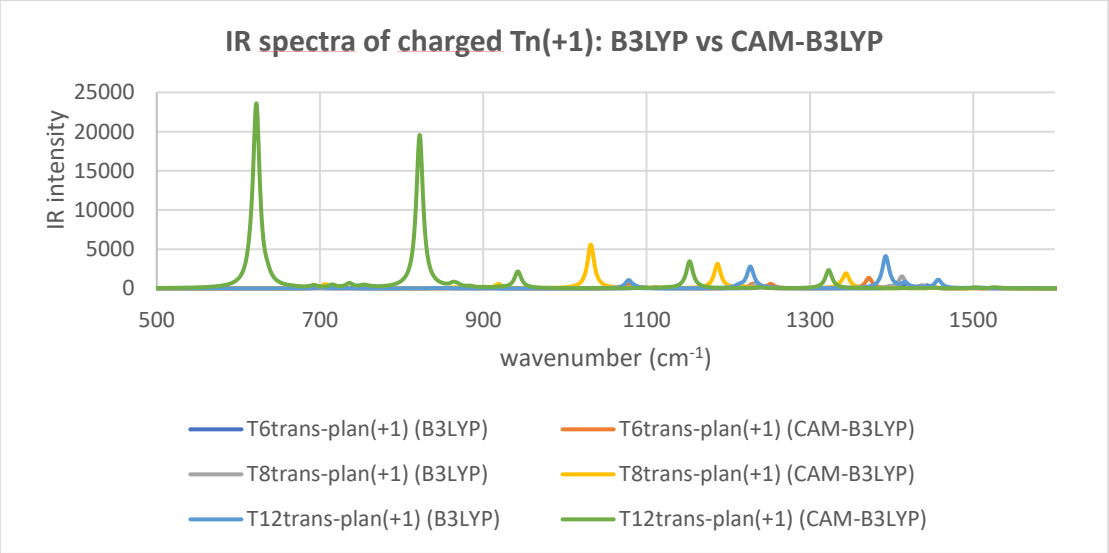

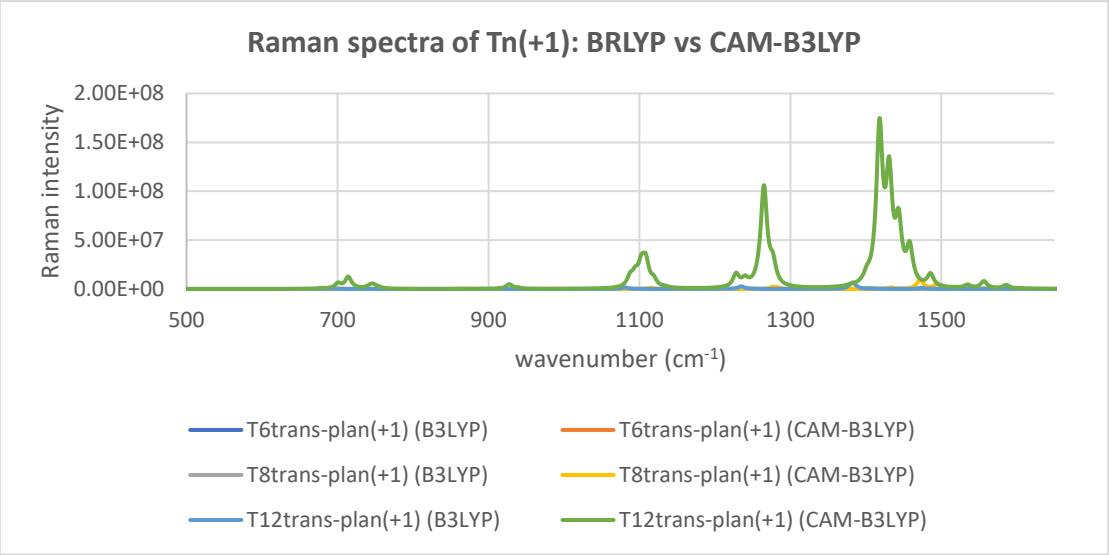

Figure 3.50: IR and Raman spectra of charged oligothiophenes, from T6(+1) to T12(+1), calculated with CAM-B3LYP and B3LYP functionals.

From Figure 3.50 it is possible to notice the tremendous effects of the range-separated functional on the vibrational spectra when the oligothiophenes pass from the neutral to the charged state:

- for the IR spectrum, the most relevant aspect is the anomalous frequency red-shift the peaks associated to the most intense IRAVs are subjected to; this is valid for all the three considered oligothiophenes, but it is particularly evident in the T12(+1) model, in which the strongest IRAVs peaks have frequencies of 622 and 822 cm^{-1}. Another phenomenon is the magnification of the IR intensity of the IRAVs peaks, especially visible in long oligomers. As it will be clarified in the following, the IR intensity of the strongest peak associated to the most important IRAV obtained from the use of CAM-B3LYP tends to largely increase with the number of thiophene units constituting the oligomer backbone, without reaching a plateau value.
- For the Raman spectrum, the four RAVs peaks pattern obtained with B3LYP (see Section 3.2) is predicted also by CAM-B3LYP, however at higher frequencies: this phenomenon is expected because of the reduced extension of the self-trapped charge. The main difference regards the Raman activity of the RAVs peaks, which is dramatically higher in the case of the CAM-B3LYP with respect to the one obtained using B3LYP. Also in the case of the Raman activity of charged oligothiophenes, we will show that it increases with the chain length, without reaching a plateau value.

We now report in Table 3.14 the numerical results of the CAM-B3LYP calculated IR and Raman frequency, IR intensity and Raman activity of the most intense peak of the two vibrational spectra, for both neutral and charged oligothiophenes; in square brackets we recall the corresponding data calculated with the B3LYP functional.

Table 3.14: CAM-B3LYP calculated IR and Raman frequency, IR intensity and Raman activity of the most intense peak of the two vibrational spectra; in square brackets the corresponding data calculated with the B3LYP functional are recalled.

oligothiophene	ν_{IR} (cm^{-1})	I_{IR} (km/mol)	ν_{Raman} (cm^{-1})	I_{Raman} (A^4/amu)
T6	1596 [1548]	$2{,}44 \times 10^2$ [$3{,}39 \times 10^2$]	1556 [1489]	$1{,}57 \times 10^5$ [$3{,}23 \times 10^5$]
T8	1593 [1544]	$4{,}28 \times 10^2$ [$6{,}35 \times 10^2$]	1556 [1481]	$3{,}62 \times 10^5$ [$1{,}22 \times 10^6$]
T12	1591 [1540]	$8{,}37 \times 10^2$ [$1{,}38 \times 10^3$]	1555 [1475]	$8{,}59 \times 10^5$ [$4{,}43 \times 10^6$]
T6(+1)	1372 [1414]	$2{,}12 \times 10^4$ [$7{,}18 \times 10^3$]	1523 [1449]	$2{,}60 \times 10^6$ [$4{,}07 \times 10^5$]
T8(+1)	1032 [1413]	$8{,}76 \times 10^4$ [$2{,}37 \times 10^4$]	1471 [1406]	$2{,}89 \times 10^7$ [$3{,}23 \times 10^6$]
T12(+1)	622 [1393]	$3{,}64 \times 10^5$ [$5{,}31 \times 10^4$]	1418 [1383]	$6{,}81 \times 10^8$ [$2{,}06 \times 10^7$]

The previous data regarding the frequency and intensity, represented in semi-logarithmic scale, of the most intense IR peak are graphically reported in Figure 3.51 and 3.52 respectively: the left panel of each figure shows the CAM-B3LYP calculated results, while the right panel the B3LYP calculated ones.

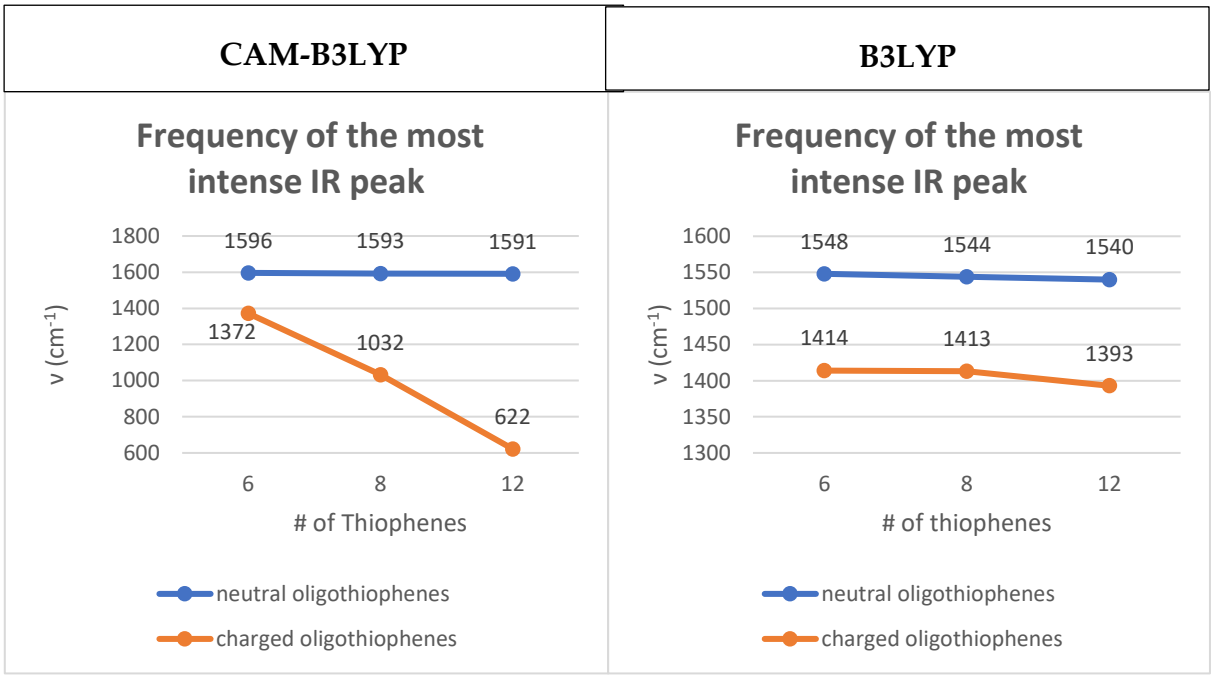

Figure 3.51: frequency of the most intense IR peak calculated with CAM-B3LYP (left panel) and B3LYP (right panel).

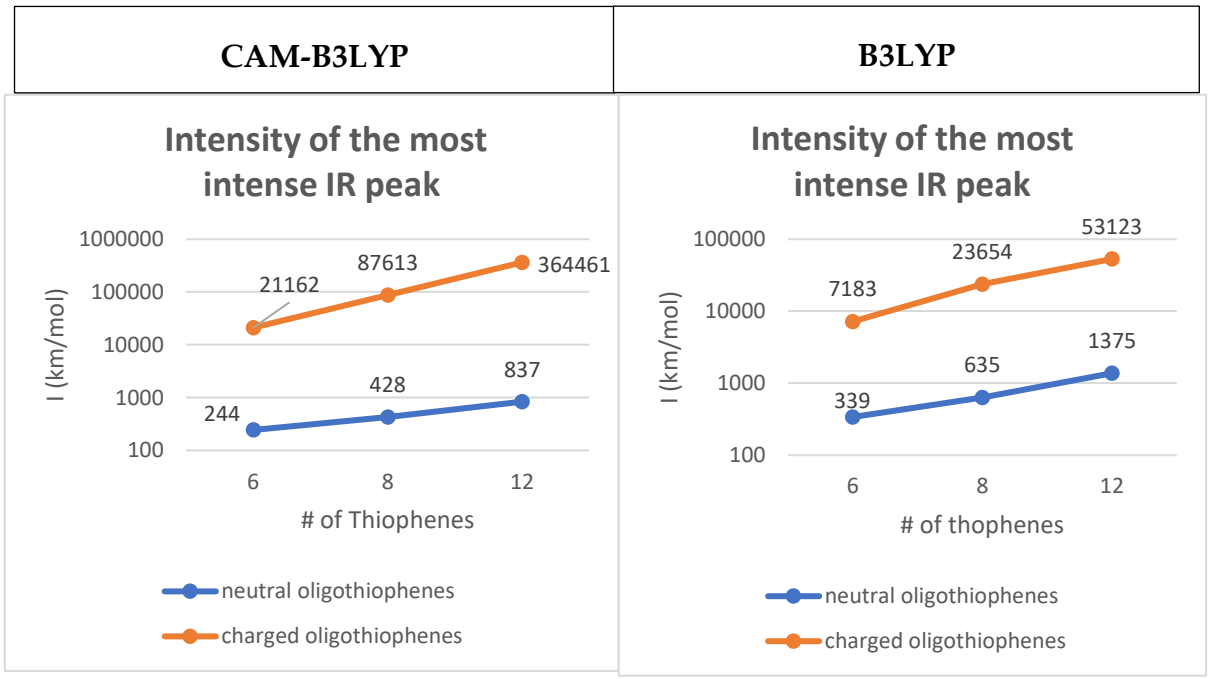

Figure 3.52: intensity of the most intense IR peak calculated with CAM-B3LYP (left panel) and B3LYP (right panel).

The data regarding the frequency and intensity, represented in semi-logarithmic scale, of the most intense Raman peak are graphically reported in Figure 3.53 and 3.54

respectively: the left panel of each figure shows the CAM-B3LYP calculated results, while the right panel the B3LYP calculated ones.

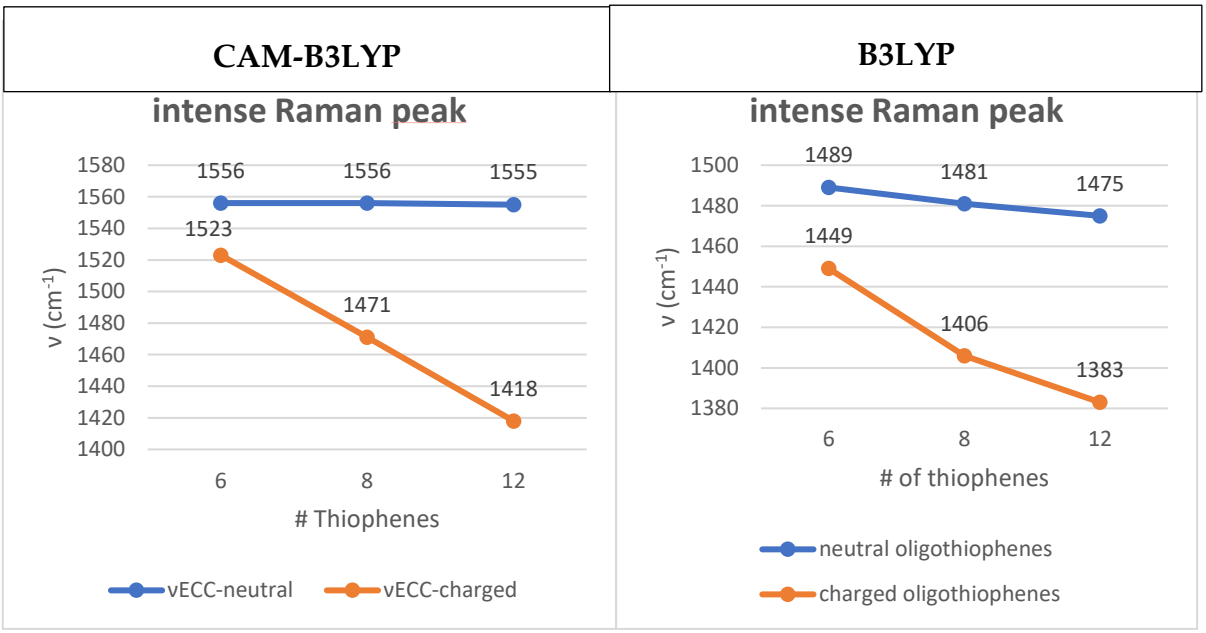

Figure 3.53: frequency of the most intense Raman peak calculated with CAM-B3LYP (left panel) and B3LYP (right panel).

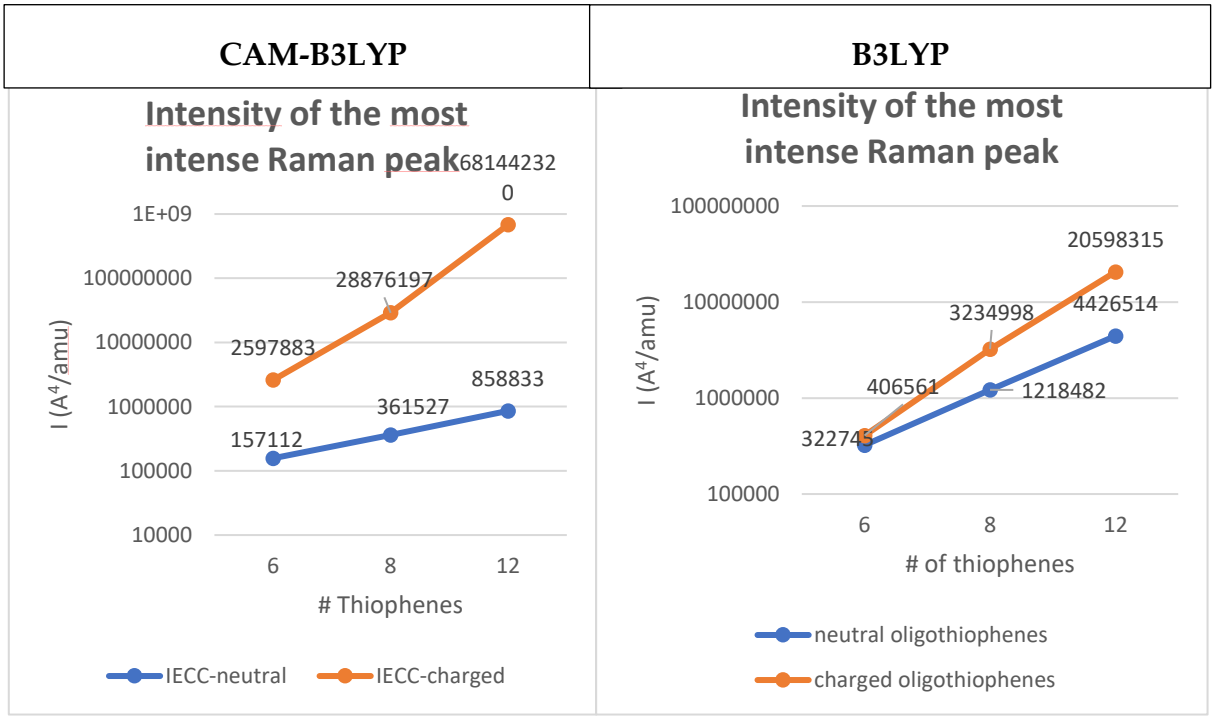

Figure 3.54: intensity of the most intense Raman peak calculated with CAM-B3LYP (left panel) and B3LYP (right panel).

Table 3.14 and Figures 3.51-3.54 confirm that CAM-B3LYP presents important issues in properly predicting the vibrational frequency of both the most intense IRAV and RAV of the charged oligothiophenes, that undergo a dramatic red-shift: they linearly decrease with the number of thiophene unit of the oligomer without reaching a plateau value, at difference of what is obtained using B3LYP. It seems that, for charged species, CAM-B3LYP behaves in the opposite way than for the neutral species, showing a softening of the frequencies and an increase of the intensities, as usually happens when the effect of the conjugation of the π electrons is overestimated. The comparison among shorter and longer molecules confirms this tendency of CAM-B3LYP in the case of the charged oligomers.

In order to rationalize the unphysical and enormous red-shift of the frequency of the most intense IRAV in the IR spectrum of charged oligothiophenes according to CAM-B3LYP calculations, we tried to detect any anomalies in the diagonal (and also the main out-of-diagonal) force constants of the **F** matrix (refer to Chapter 2) obtained with the CAM-B3LYP functional with respect to the ones resulted from the B3LYP calculations. We implemented this analysis for the T12(+1) model because it is the one for which the frequency red-shift of the most intense IRAVs is more pronounced; the comparison between the force constants values obtained with CAM-B3LYP and B3LYP, reported in Figure 3.55, shows no important differences to explain such remarkable decreasing of the IRAV frequency.

On the other hand, looking to the vibrational eigenvectors, we can confirm that the stronger IRAV predicted with CAM-B3LYP functional is a collective ECC mode, showing very similar features as the corresponding eigenvector of the strongest IRAV, according to B3LYP functional. The sketch of these eigenvectors of the most intense IRAV obtained with CAM-B3LYP (left panel) and B3LYP (right panel) is reported in Figure 3.56.

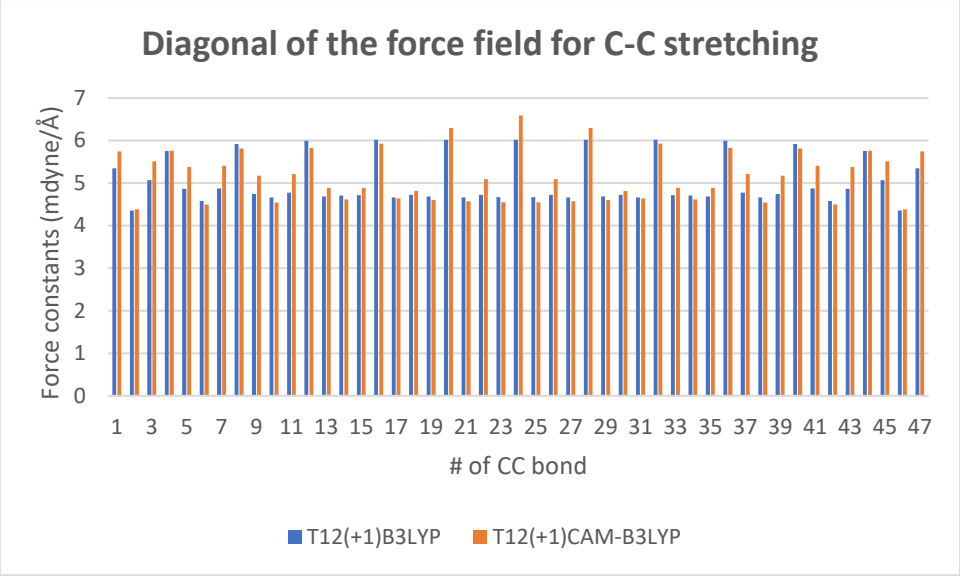

Figure 3.55: diagonal force constants for C-C stretching of T12(+1) model calculated with CAM-B3LYP and B3LYP functionals.

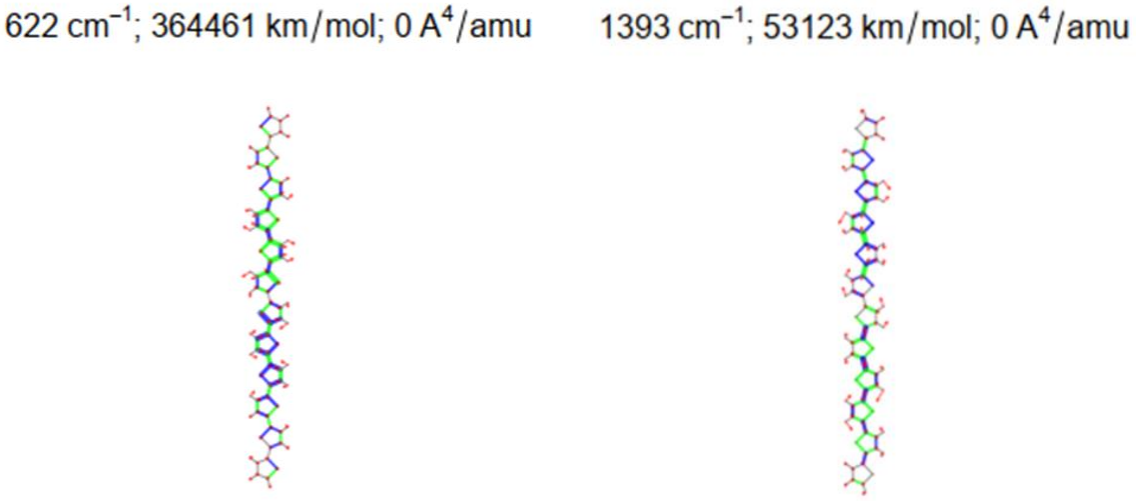

Figure 3.56: sketch of the most intense IRAV of T12(+1) obtained with CAM-B3LYP (left panel) and with B3LYP (right panel).

We also analysed the Electrostatic Potential (ESP) and the IR partial charges with hydrogen charges summed into heavy atoms (C and S) of the atoms of the T12 and T12(+1) models calculated with CAM-B3LYP and B3LYP functionals and we do not find evidence of some anomalous behaviour of the CAM-B3LYP calculation. For sake of brevity, we report here in Table 3.15 only the sum of the all ESP and IR partial charges in a central region composed by four thiophene rings of T12(+1): the greater value calculated with CAM-B3LYP than the one obtained with B3LYP is ascribed to the higher localization of the polaron, but it definitely does not explain the anomalies in the CAM-B3LYP IR and Raman spectra.

Table 3.15: sum of all ESP and IR partial charges of heavy atoms in the four inner thiophene rings of T12(+1) calculated with the CAM-B3LYP and B3LYP functionals.

CAM-B3LYP		**B3LYP**	
Total ESP charge in the perturbed region	Total IR charge in the perturbed region	Total ESP charge in the perturbed region	Total IR charge in the perturbed region
0,524862 e	0,581856 e	0,353886 e	0,364244 e

The extremely high IR intensity and Raman activity of the CAM-B3LYP calculated spectra with respect to the corresponding B3LYP calculated ones can be rationalised by means of the very large values of the ∂My/∂R and ∂α/∂R parameters; their values for the three neutral and charged oligothiophenes are reported in Figure 3.57 and Figure 3.58 respectively, in which the left panel shows the results obtained with CAM-B3LYP, while the right panel the ones obtained with B3LYP.

CAM-B3LYP	**B3LYP**

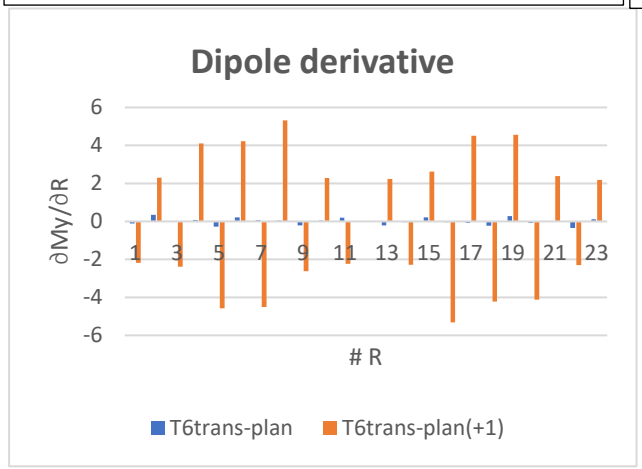

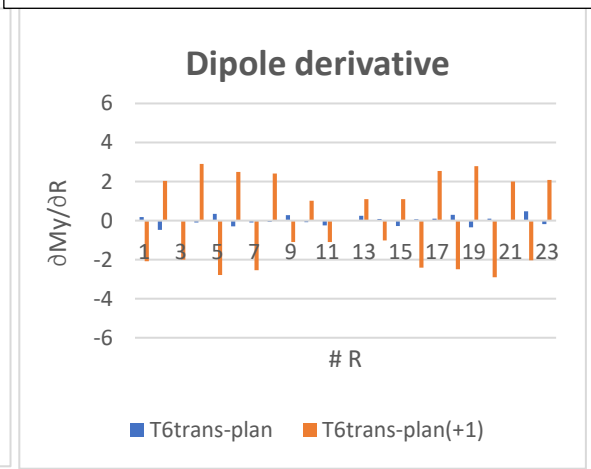

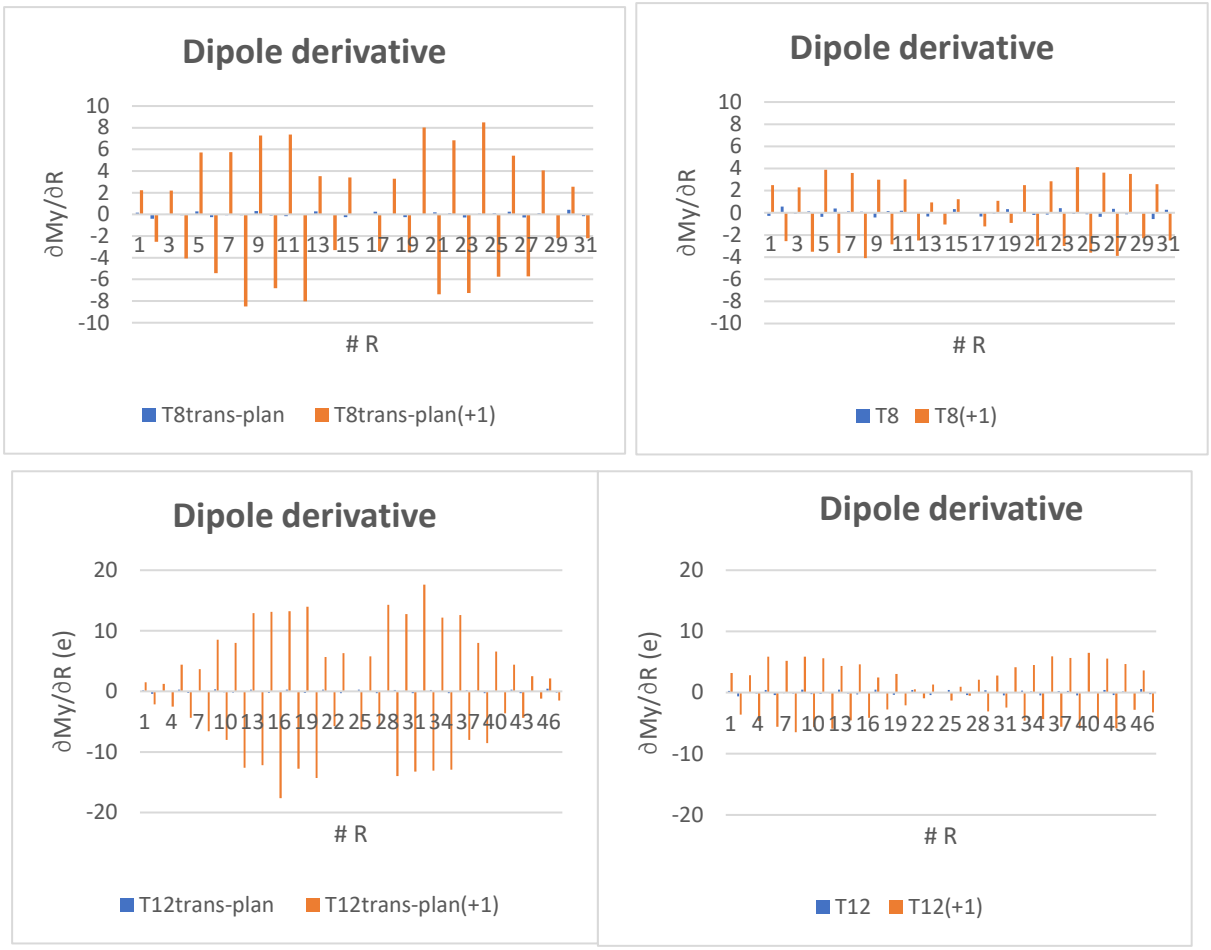

Figure 3.57: ∂My/∂R of neutral and charged oligothiophenes obtained with CAM-B3LYP and B3LYP.

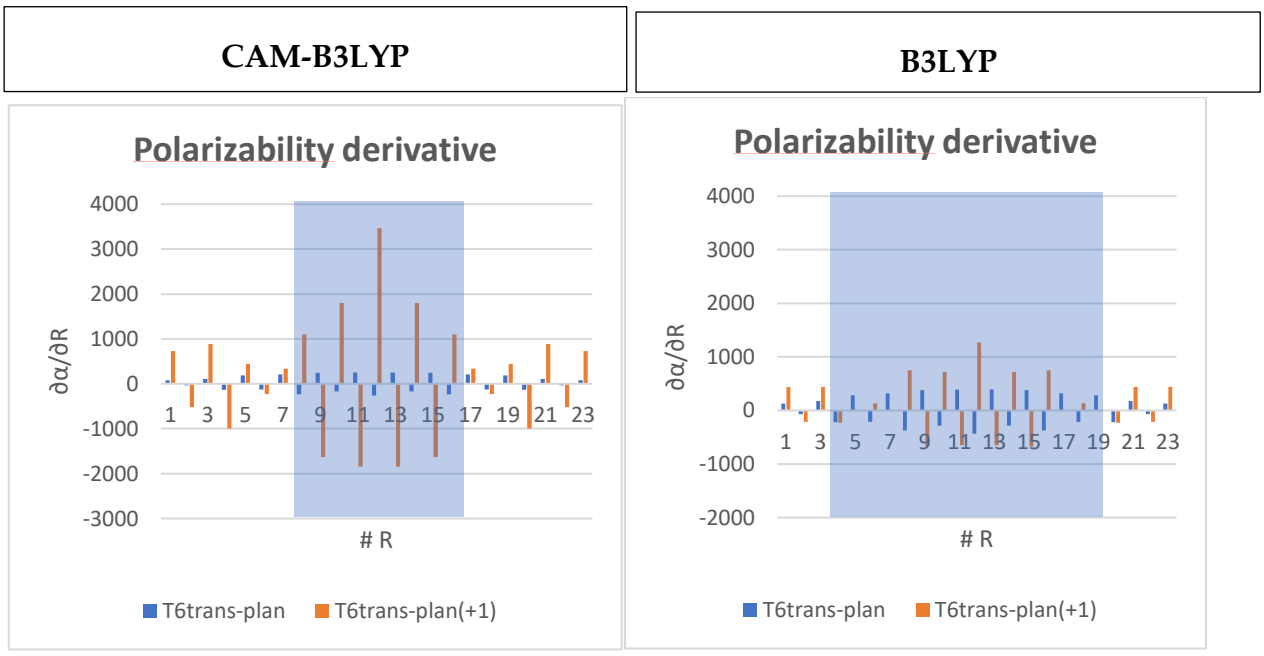

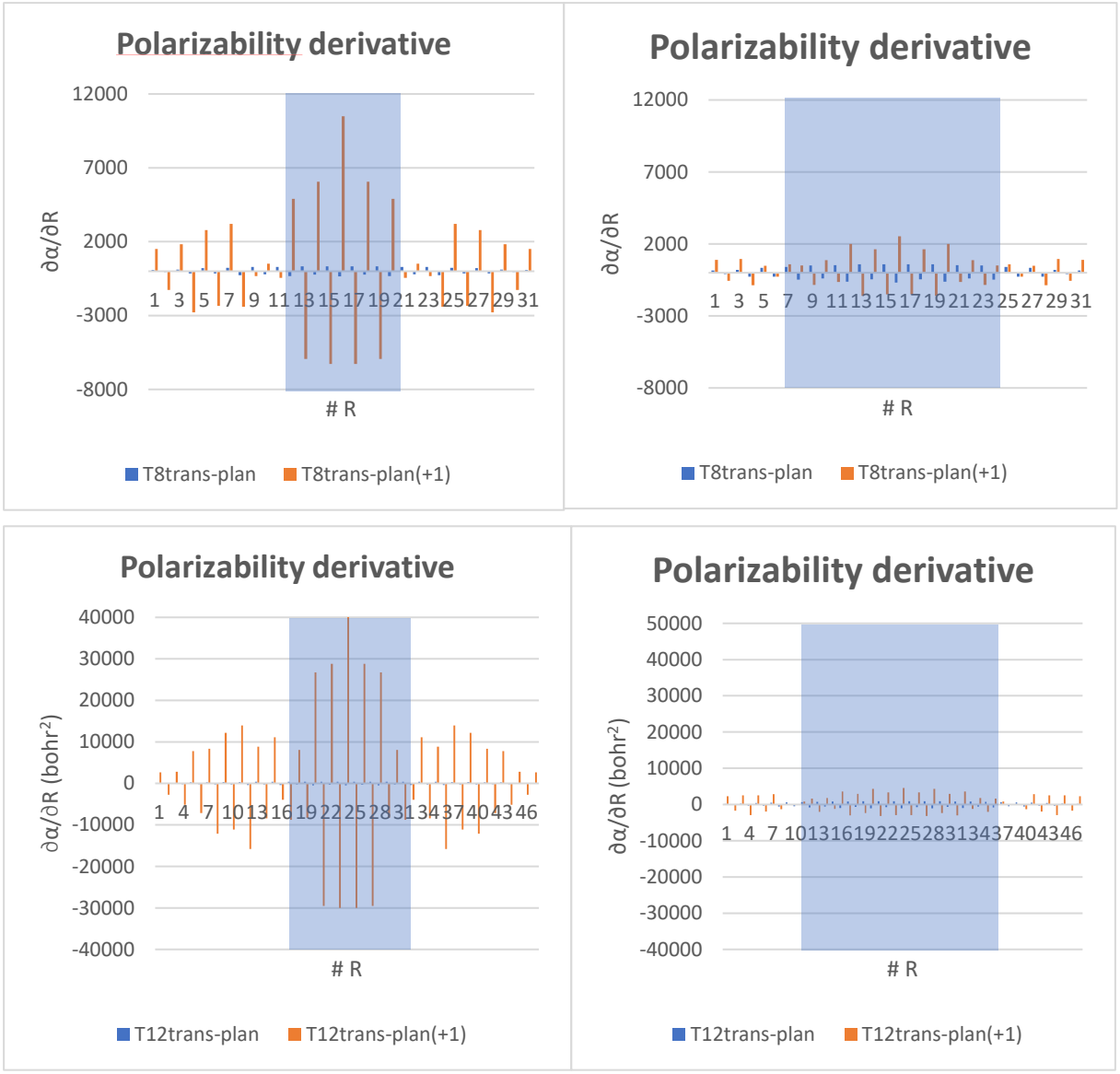

Figure 3.58: ∂α/∂R of neutral and charged oligothiophenes obtained with CAM-B3LYP and B3LYP.

The light-blue panels in Figure 3.58 indicate the oligomer region where the ∂α/∂R parameters invert their sign with respect to the neutral species, individuating the quinoid structure predicted by the local Raman parameters: it is clear that the polaron spatial extent is smaller if calculated with the CAM-B3LYP functional than if calculated with B3LYP. The numerical results concerning the CAM-B3LYP functional are reported in Table 3.15; in square brakets we recall the data resulting from the B3LYP calculations.

Table 3.16: polaron spatial extent predicted by the local Raman parameters, resulting from the use of the CAM-B3LYP functional; in square brackets the corresponding B3LYP results are recalled.

Oligothiophene	Number of CC bond starting from which $\partial\alpha/\partial R$ sign inversion occurs	Number of thiophene unit after which $\partial\alpha/\partial R$ sign inversion occurs	Polaron spatial extent
T6-T6(+1)	8 [5]	3 [2]	2 + the external inter-ring bonds [4]
T8-T8(+1)	12 [8]	4 [3]	2 + the external inter-ring bonds [4+the external inter-ring bonds]
T12-T12(+1)	17 [12]	5 [4]	4 [6 + the external inter-ring bonds]

3.3.2. The hybrid approach: geometry derived from CAM-B3LYP and vibrational sepctra computed with B3LYP.

As we underlined in the previous Section, CAM-B3LYP is suitable for the description of the geometry of oligothiophenes, especially for what concerns the delocalization length of the polaron forming upon the doping process, but presents serious problems in predicting both the IR and Raman spectra of charged oligomers, in particular considering the anomalous red-shift of the vibrational frequency of IRAVs.

On the other hand, the B3LYP functional overestimates the delocaliztion length of the charge defect induced by the extraction of one electron from the oligomer to the dopant, but it seems to predict in a more reliable way the vibrational spectra of both neutral and charged oligothiophenes.

We introduced a hybrid approach that combines the positive aspects of the two different functionals and we tested it on the neutral T12 and charged T12(+1) models;

whenever we refer to results calculated with this approach, we will use the term "Hybrid".

It is a two-step method:

1. Firstly, a geometry *optimization* performed with CAM-B3LYP .
2. Second, a frequency and intensity calculation on top of the CAM-B3LYP geometryas performed with B3LYP.

The result of this procedure is a molecule characterized by a CAM-B3LYP optimized geometry and by vibrational spectra obtained with B3LYP; it is important to specify that both steps are performed with the 6-31G** basis set.

Vibrational spectra and local parameters. Figure 3.59 shows the IR spectrum in the wavenumber region between 500 and 1700 cm^{-1}(left panel) and the Raman spectrum in the wavenumber region between 1000 and 170 cm^{-1}(right panel) of neutral T12, calculated with the CAM-B3LYP and the B3LYP functionals and with the hybrid approach.

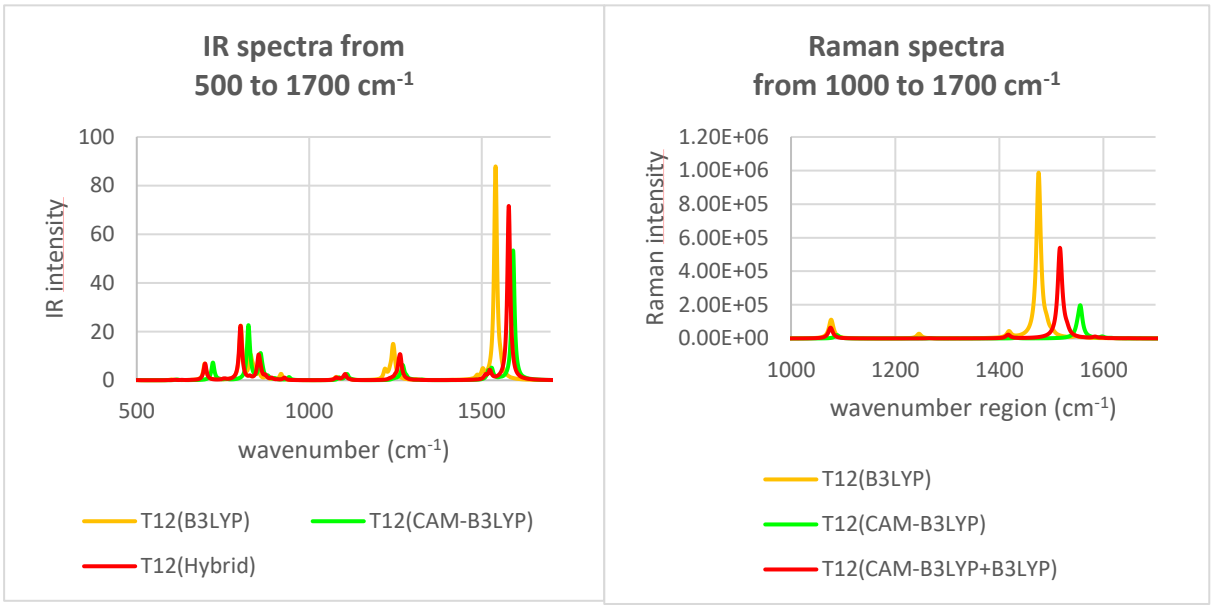

Figure 3.59: IR (left panel) and Raman spectrum (right panel) of neutral T12, calculated with CAM-B3LYP, B3LYP and the hybrid approach.

From Figure 3.59 it is possible to notice how the vibrational spectra calculated with the hybrid approach presents peaks with features in between the ones of pure B3LYP calculated spectra and the ones of the CAM-B3LYP spectra in terms of both frequency and intensity: this is an expected result because the hybrid approach is based on the CAM-B3LYP geometry optimization, which makes larger the BLA of the oligothiophene, thus explaining the frequency blue-shift of the normal modes

involving the stretching of the C-C bonds and this is especially valid for the collective Raman active ECC vibration.

In Figure 3.60 we report the normalized IR spectrum on the most intense peak in the wavenumber region between 500 and 1700 cm^{-1}(top panel) and the normalized Raman spectrum on the most intense peak in the wavenumber region between 1000 and 1700 cm^{-1} (bottom panel) of the charged T12(+1), both calculated with the CAM-B3LYP and the B3LYP functionals and with the hybrid approach. The normalization procedure is needed to make the three spectra comparable due to the out-of-scale IR intensity and Raman activity obtained with the CAM-B3LYP functional.

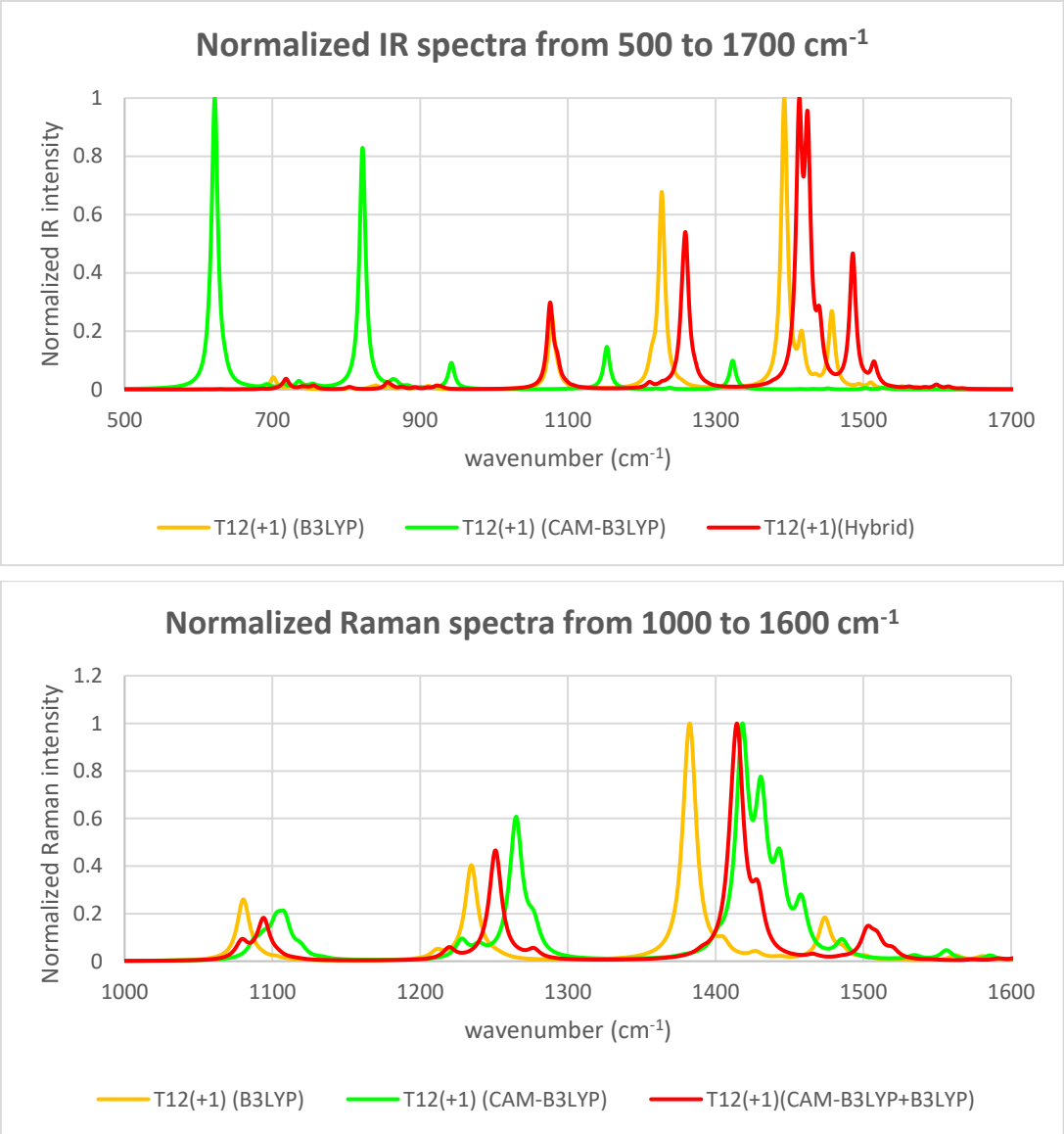

Figure 3.60: normalized IR (above panel) and Raman spectra (below panel) of charged T12(+1), calculated with CAM-B3LYP, B3LYP and the hybrid approach.

From Figure 3.60 it is possible to notice that the hybrid approach is able to correct the enormous red-shift of the frequency of the IRAVs and the extremly high intensity of the spectra observed using the CAM-B3LYP functional: the IR and Raman spectra calculated with the hybrid approach resemble the ones obtained with B3LYP . The reason of the higher frequency of the ECC-like IRAVs and RAVs with respect to the ones calculated by the B3LYP functional is the more "rigid" geometry derived from the initial use of CAM-B3LYP.

Since the IR and Raman spectra from the hybrid approach are similar to the ones resulting from the use of B3LYP , we expect also the corresponding local parameters to present similar values and patterns. To confirm this aspect, we report in Figure 3.61 the ∂My/∂R parameters (top panel) and the ∂α/∂R parameters (bottom panel) of the charged T12(+1), calculated with B3LYP and the hybrid approach.

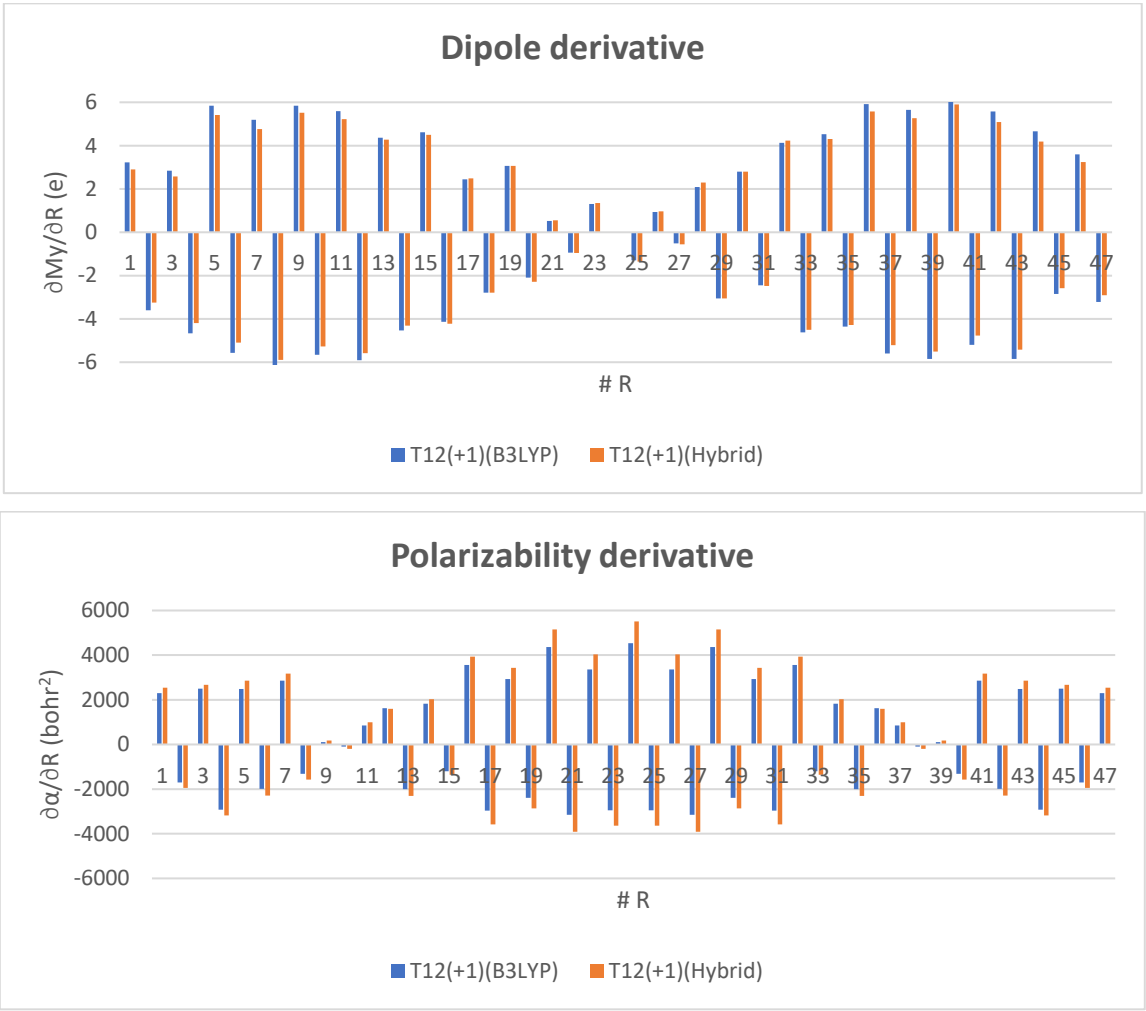

Figure 3.61: ∂My/∂R (above panel) and ∂α/∂R (below panel) of T12(+1), calculated with B3LYP and the hybrid approach.

The very similar IR and Raman parameters (see Figure 3.61) calculated with B3LYP and with the hybrid approach allow to rationalize the similar intensity of the IR and Raman spectra calculated with the two methods.

Interestingly, the $\partial\alpha/\partial R$ parameters show no changes in the sign pattern passing from the B3LYP calculated ones to the hybrid approach calculated ones. This means that the quinoidization of the central perturbed region of the oligothiophene upon the doping process occurs starting from the same CC bond in both cases: according to the Raman local parameters and in spite of the different geometry, the polaron delocalization length is the same if obtained with the B3LYP functional or with the hybrid approach.

Analysis of the geometry. We conclude the comparison between the results obtained with the B3LYP functional and the ones obtained with the hybrid approach analysing the equilibrium bond length values and the Bond Length Alternation (BLA) parameters for the T12(+1) model. It should be noticed that the geometry calculated with the hybrid approach coincides with that obtained with the CAM-B3LYP functional, by definition. The aim of the comparison is to better illustrate how differently the two methods describe the structural relaxation which occurs in the oligothiopohene when the electron is withdrawn from the oligomer to the dopant by the doping process. We report in Figure 3.62 the equilibrium bond length values (top panel) and the BLA parameter (bottom panel) of the T12(+1) model.

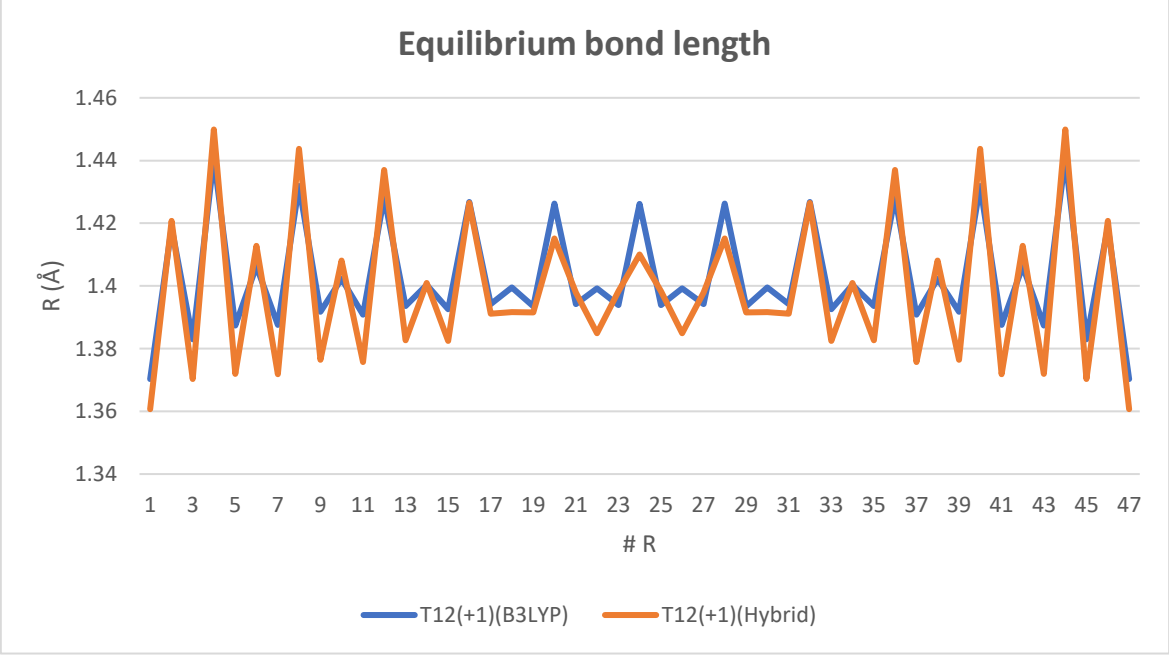

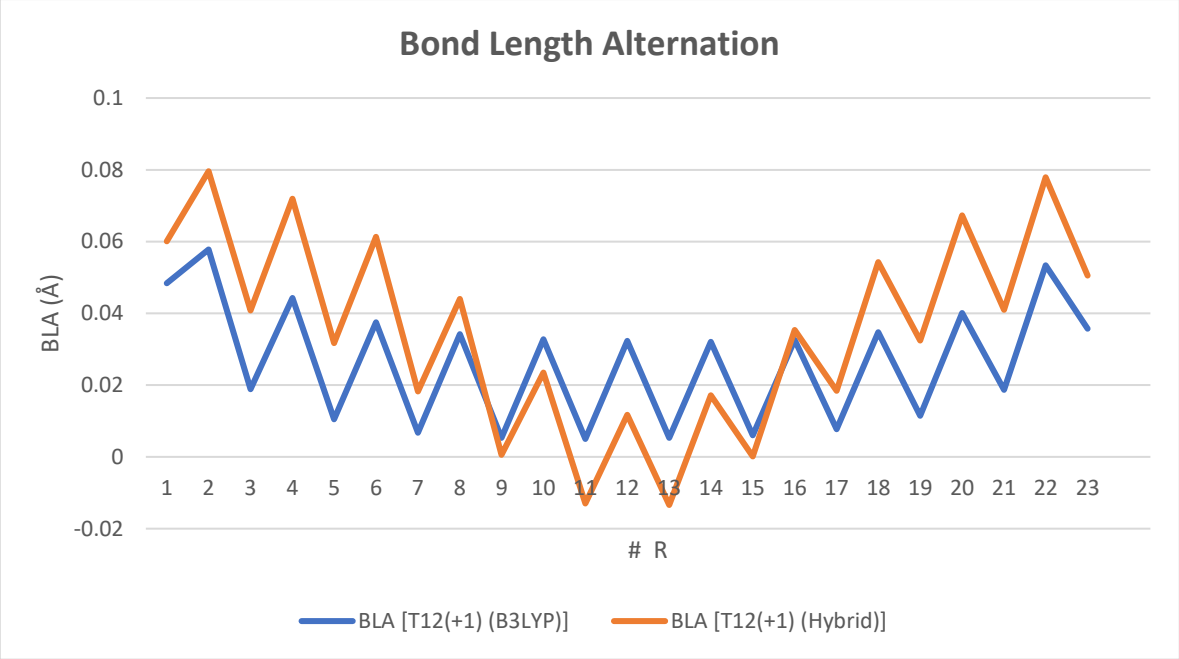

Figure 3.62: equilibrium bond length (top panel) and BLA parameter (bottom panel) of T12(+1), calculated with B3LYP functional and the hybrid approach.

From Figure 3.62 it is possible to notice that the two methods describe differently the structural relaxation in the central perturbed region of the oligothiophene upon the doping process. In particular, the B3LYP functional describes the polaron as an equalized structure, since the BLA parameter is positive and almost vanishing in the central region of the oligomer, while the hybrid approach describes the polaron as a quinoid structure in the most central region, since the BLA values are negative, and as a more aromatic structure in the external part of the perturbed region.

4 Molecular models of alkyl-substituted oligothiophenes.

In this Chapter we discuss the models of unsubstituted oligothiophenes presented in Chapter 3 adding the lateral substituents constituted by alkyl chains in order to more properly mimic the polymer poly(3-hexylthiophene) (P3HT). Figure 4.1 shows the chemical structure of an oligothiophene (in our study we will focus our attention on the octamer) with lateral hexyl alkyl chains, which are attached to the C atom in position 3 of each Thiophene unit.

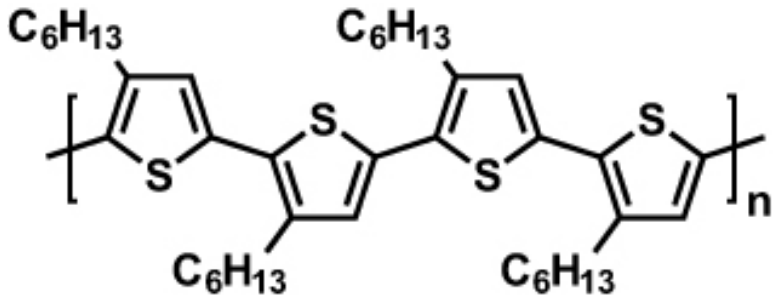

Figure 4.1: chemical structure of an oligothiophene with lateral hexyl chains. In our study n is equal to 8.

Before explaining how Chapter 4 is organized and analysing the results, it is useful to clarify the notation we introduce considering more complex models:

- The label Tn indicates unsubstituted oligothiophenes formed by a sequence of n rings in the neutral state, exactly as in Chapter 3.
- The label 3HT8 indicates the octamer of (3-hexyl thiophene), thus meaning a T8 with lateral hexyl chains -$(CH_2)_7CH_3$ in the neutral state.
- The label 3ET8 indicates the octamer of (3-ethyl thiophene), thus meaning a T8 with lateral ethyl (-CH_2-CH_3) groups in the neutral state.
- All the previous labels followed by the (+1) notation are used to indicate the considered species in the charged state, derived from the extraction of one single electron from the oligomer to the dopant.

All the DFT computations on the models of oligothiophenes with lateral alkyl chains were performed on the guess geometry from ref. **[15]** and reported in Figure 4.2: the alkyl chains assume the *all-trans* conformation and they are tilted by an angle θ=140° with respect to the axis of the backbone, constituted by the thiophene units. The torsional angle involving the C-C bond of the alkyl unit is such that the plane which contains the CC bonds of the hexyl is orthogonal to the plane of the rings and the two subsequent chains, on the right and on the left side respectively with respect to the chain axis, run in the opposite directions with respect to the plane of the rings. The backbone of the oligomers is constrained to be planar along the geometry optimization procedure, for both the neutral and charged state. This because the models we are going to present aim at mimicking the P3HT at solid state, in which the polymeric chains assume a planar conformation.

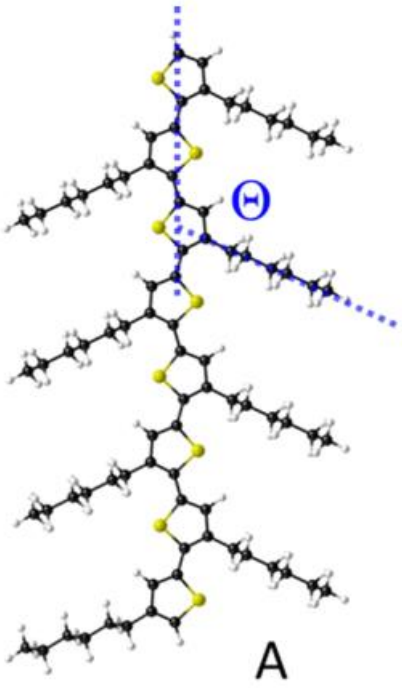

Figure 4.2: molecular model of 3HT8 with geometry close to that of the molecule in the single crystal; the hexyl chains are tilted by θ=140° with respect to the axis of the backbone.

Firstly, we will study how the IR and Raman vibrational spectra and also how the geometry of the considered molecules modifies passing from the unsubstituted models to the alkyl substituent ones, namely by comparing the results obtained for T8 and T8(+1) and those related to 3HT8 and 3HT8(+1).

Then we will focus our attention on the effect of the alkyl chain length on the spectroscopic and geometrical properties by substituting the hexyl chains with ethyl chains and so comparing the 3HT8 and 3ET8 models: this because we need to understand if it is acceptable (from the viewpoint of the prediction of the main

spectroscopic features) to perform less expensive DFT calculations from the view point of the computational resources.

4.1. The effect of the lateral hexyl chains: comparison between the neutral T8 and 3HT8 and between the charged T8(+1) and 3HT8(+1).

In this Section we study the effects of the lateral alkyl chains on the IR and Raman spectra and on the geometry of the oligothiophenes: we will compare the results regarding the fully hydrogenated T8 model with the hexyl substituted octamer indicated as 3HT8, both in the neutral and charged state.

All the quantum-chemical calculations presented in this Section are performed with the B3LYP functional and the 6-31G** basis set and in the unrestricted configuration for what concerns the charged species.

4.1.1. Comparison between T8 and 3HT8.

In Figure 4.3 we report the IR spectrum of the T8 and 3HT8 in the wavenumber region between 500 and 3500 cm^{-1}.

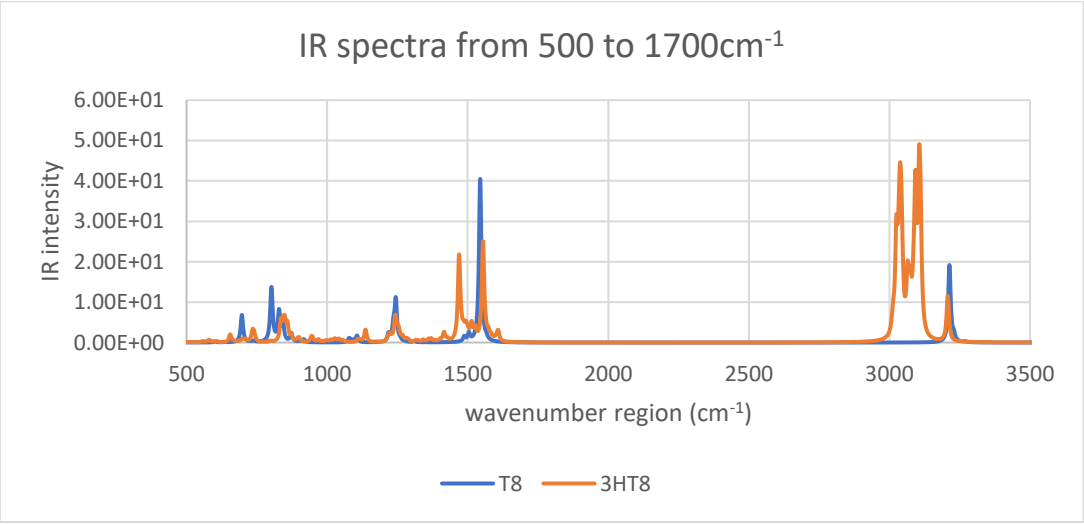

Figure 4.3: IR spectrum of neutral T8 and 3HT8 in the wavenumber region between 500 and 3500 cm^{-1}.

Figure 4.4 shows the same IR spectra of Figure 4.3, focusing on selected spectral regions, in order to better underline the differences between spectra: the top panel shows the spectra in the wave number region between 500 and 1700 cm^{-1}, while the

bottom panel shows the spectra in the wavenumber region between 2900 and 3300 cm^{-1}.

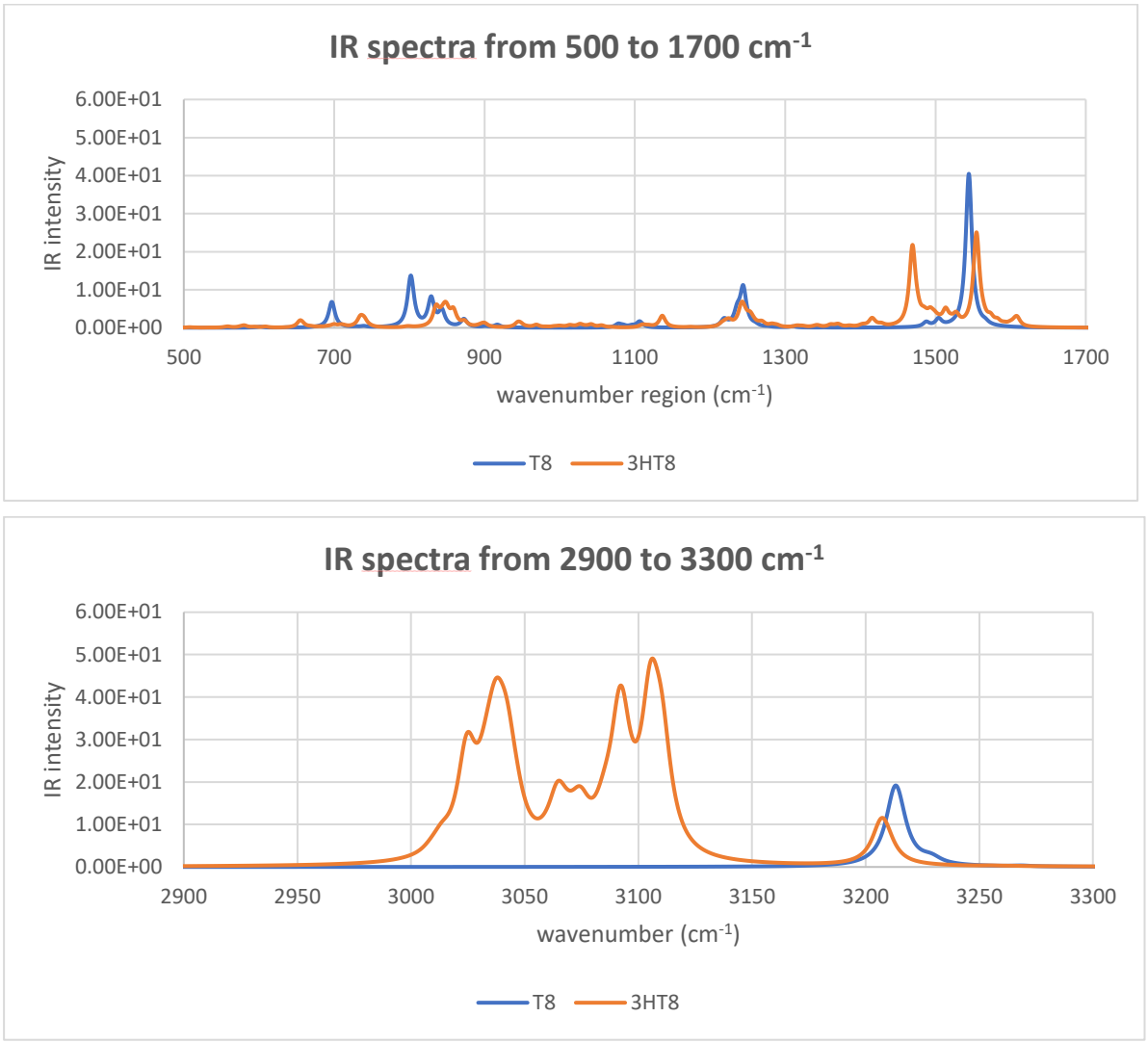

Figure 4.4: IR spectrum of neutral T8 and 3HT8 in the 500-1700 cm-1 wavenumber region (top panel) and in the 2900-3300 cm^{-1} wavenumber region (bottom panel).

From Figures 4.3 and 4.4, it is possible to notice that the IR spectrum of neutral T8 and 3HT8 are similar, but the one of the oligothiophene with the hexyl chains presents a more structured pattern and, as expected, strong C-H stretching bands associated to the modes involving CH_2 and CH_3 units. Focusing on the IR spectrum of neutral 3HT8, we can individuate four main peaks in the wavenumber region between 500 and 1700 cm^{-1} and a complex, structured band in the 3000-3150 cm^{-1} wavenumber region and a peak at about 3200 cm^{-1}. The peaks with frequency around 800, at 1242, 1554 and 3207 cm^{-1} show a correspondence with the IR spectrum of the neutral T8, also for what concerns the associated normal modes, while the peaks at 1469 cm^{-1} and the structured

bands in the wavenumber region between 3000 and 3150 cm^{-1} are peculiar of the IR spectrum of 3HT8:

1) The normal mode associated to the peak with frequency at 1469 cm^{-1} shows some ECC-like character, mostly localized in the central region of the oligomer: the inter-ring CC bonds shrink in phase and the quasi-double CC bonds vibrate out-of-phase with respect to the previous bonds, while the quasi-single CC bonds belonging to each thiophene unit are practically not involved in the vibration. The coupling of the hexyl chains with the backbone occurs through the vibration of the first CC bond connecting a thiophene with the alkyl chain: all these CC bonds stretch in-phase, and they are in-phase with the inter-ring collective CC stretching. The sketch of the eigenvector is reported in Figure 4.5.

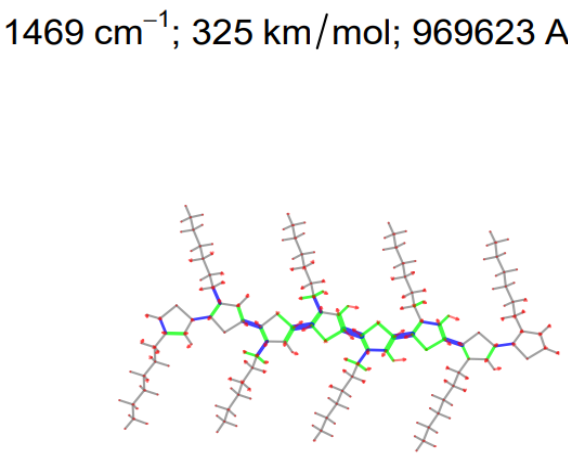

Figure 4.5: sketch of the eigenvector associated to the IR intense peak with frequency at 1469 cm^{-1}.

It is important to underline the fact that the previously described normal mode is IR active, but also Raman active, as it can be deduced from the high value of the Raman activity reported in Figure 4.5. This phenomenon is induced by the lower symmetry of the 3HT8 molecule, which, at difference of the T8 molecule, does not belong to the C_{2h} symmetry point group and so the IR/Raman activity mutual exclusion principle is no more valid.

2) As already mentioned, in the wavenumber region between 3000 and 3300 cm^{-1} of the IR spectrum of 3HT8, the structured band on the lower frequencies side is determined by the (sp^3 C)-H stretching transitions; the peak with frequency 3207 cm^{-1} is determined by the (sp^2 C)-H stretching and so the vibration involves the C-H bonds linked to the thiophene rings.

We now analyse the Raman spectrum of T8 and 3HT8, which is reported in Figure 4.6 in the wavenumber region between 1300 and 1600 cm^{-1}, where the most intense peaks appear.

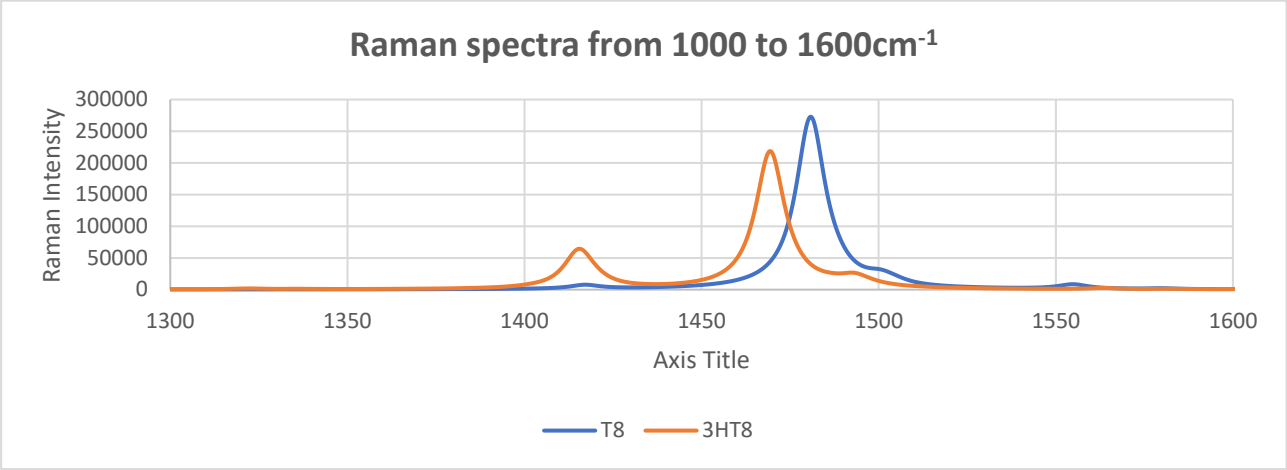

Figure 4.6: Raman spectrum of neutral T8 and 3HT8 in the 1300-1600 cm^{-1} wavenumber region.

The Raman spectrum of 3HT8 is constituted by two main peaks:

1) The peak with frequency at 1415 cm^{-1} is peculiar of the Raman spectrum of 3HT8 and it is not present in the T8 model. This because the associated normal mode, sketched in Figure 4.7, is mainly determined by the in-phase stretching of the all quasi-single CC bonds of the Tn sequence, thus showing some ECC-like character, while in each ring, the two quasi-double CC bonds participate to the normal mode to a different extent. This kind of vibration is coupled with the stretching of the CC bonds of each lateral hexyl chain, mainly with opposite phase with respect to the single CC bonds of the Tn backbone.

$$1415\ cm^{-1};\ 13\ km/mol;\ 150084\ A^4/amu$$

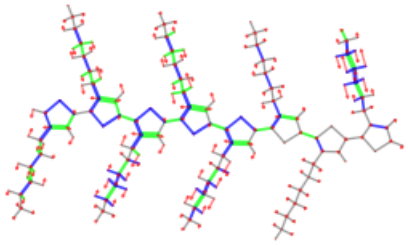

Figure 4.7: sketch of the eigenvector associated to the strong Raman peak with frequency at 1415 cm^{-1}.

2) The most intense Raman peak has frequency at 1469 cm^{-1} and it goes in par with the principal peak in the Raman spectrum of T8; the description of the associated normal mode has been already presented when we analysed the IR spectrum (Figure 4.5). It is interesting to notice that, while the most intense Raman normal mode of T8 corresponds to the collective Я vibration, the one of 3HT8 exhibits only a partial ECC-like character, due to the dynamic coupling of the backbone with the first CC bond of the alkyl chain. In fact, the frequency of the most intense ECC-like Raman mode of 3HT8 undergoes a redshift with respect to the one of T8, because the first CC bond of the alkyl chains is involved in the conjugated system, contributing to increase the π-electrons delocalization: this corresponds to a softening of the normal modes with ECC-like character.

The similarities of the IR and Raman spectrum of T8 and the one of 3HT8 can be rationalized by means of the dipole derivative parameters and the polarizability derivative parameters respectively, both with respect the internal C-C stretching coordinate. The $\partial M^y/\partial R$, where y indicates the direction of the molecular axis. and the $\partial\alpha/\partial R$ parameters of T8 and 3HT8 are reported in the top panel and in the bottom panel of Figure 4.8 respectively. The reported values refer to the CC bonds belonging to the Tn backbone.

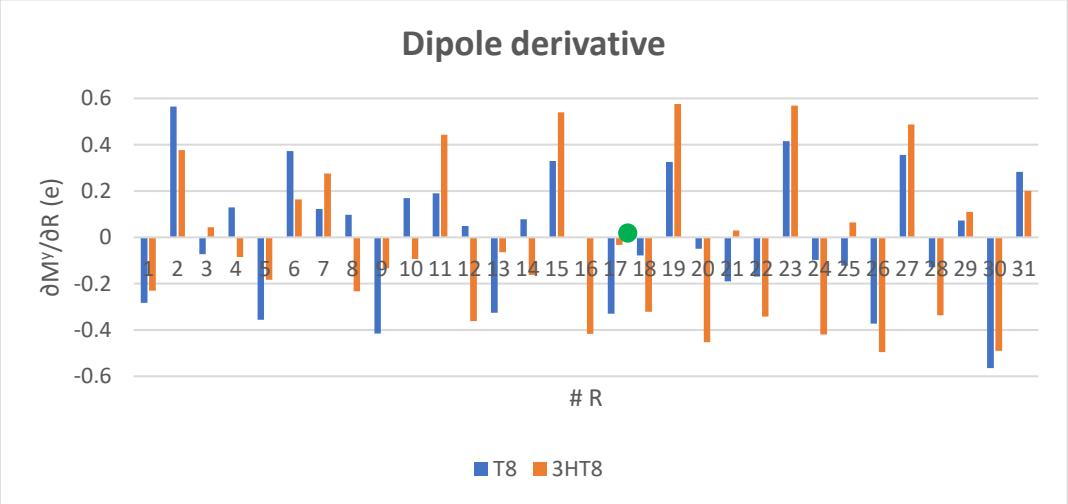

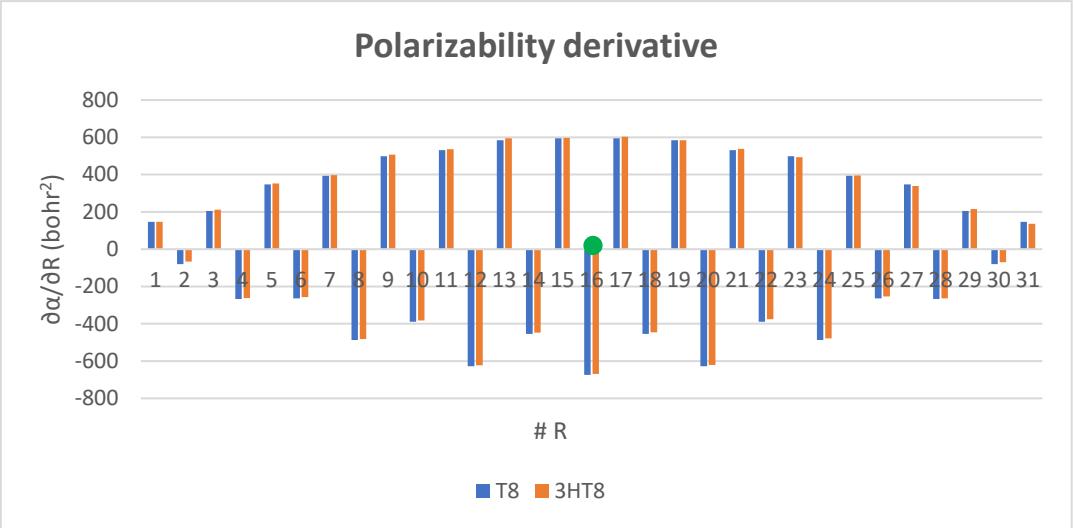

Figure 4.8: IR (top panel) and Raman local parameters (bottom panel) of neutral T8 and 3HT8.

For what concerns the IR local parameters, the $\partial M^y/\partial R$ values of 3HT8 generally respect the sign pattern observable in the case of T8, except for some CC bonds; the central CC bond, indicated in Figure 4.8 with a green dot, exhibits a null $\partial M^y/\partial R$ value for T8 and a negative one for 3HT8. Another important difference is the asymmetry of the IR local parameters pattern of 3HT8 with respect the central CC bond: this is because 3HT8 does not belong to any symmetry point group, due to the presence of the lateral alkyl chains.

For what concerns the Raman local parameters, 3HT8 and T8 exhibit very similar values, thus explaining why the intensities of the main Raman bands of the two considered molecules are very similar. Moreover the $\partial\alpha/\partial R$ parameters have the same pattern for both the models: also in the case of the neutral 3HT8, the Raman local parameters indicate that the backbone of the oligomer is constituted by a rigorous alternation of quasi-single and quasi-double CC bonds, whose stretching vibration has the opposite effect (opposite sign) on the modulation of the polarizability.

We now focus on the analysis of the geometry and in particular of the equilibrium bond length of the CC bonds constituting the backbone of neutral T8 and 3HT8, whose values are shown in Figure 4.9.

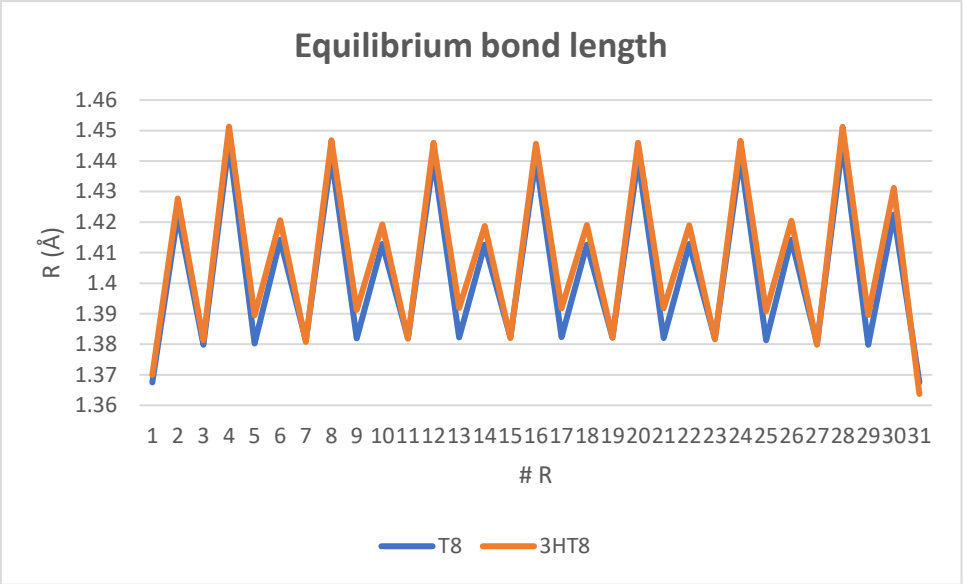

Figure 4.9: equilibrium bond length values of the CC bonds in the backbone of T8 and 3HT8.

The only relevant difference between the calculated values of the equilibrium length of the CC bonds of T8 and 3HT8 is the fact that the quasi-double CC bond and the quasi-single CC bond of (almost) every thiophene unit connecting the C atom the hexyl chain is attached to are longer with respect to the corresponding ones in the T8 model: this because the first CC bond of each alkyl chain is involved in the π-conjugated system; the conjugation of this CC bond is confirmed also by the analysis of the geometrical parameters.

4.1.2. Comparison between T8(+1) and 3HT8(+1).

In this Section we will analyse how the vibrational spectra change and how the geometry of the oligothiophene with lateral hexyl chains relaxes upon the doping process; the results regarding the charged 3HT8(+1) model will be systematically compared with the ones of the T8(+1) model.

Also in the case of charged species, the geometry optimization is performed such that the molecules are planar: for the T8(+1) species it is sufficient to make the DFT computation to recognize the C_{2h} symmetry, while for the 3HT8(+1) species we had to impose that all the dihedral angles of the backbone are fixed at 180°. This procedure is needed because the molecule naturally tends to distort if no constrains are imposed. For sake of completeness, we specify that we performed the quantum-chemical calculations both in a free and constrained geometry optimization configuration: as it will be shown in Figure 4.10, the differences concerning the vibrational spectra of flat and distorted 3HT8(+1) are minimal. The frequency of the ECC-like most intense IRAV and RAV of the flat molecule is slightly lower than the one of the distorted molecules

because of the grater conjugation length. Since the differences between the constrained flat and freely optimized 3HT8(+1) are substantially negligible for what concerns the vibrational spectra and also the IR and Raman local parameters and the equilibrium length of the CC bonds in the backbone, from now on we will report here only the result obtained with the constrained geometry.

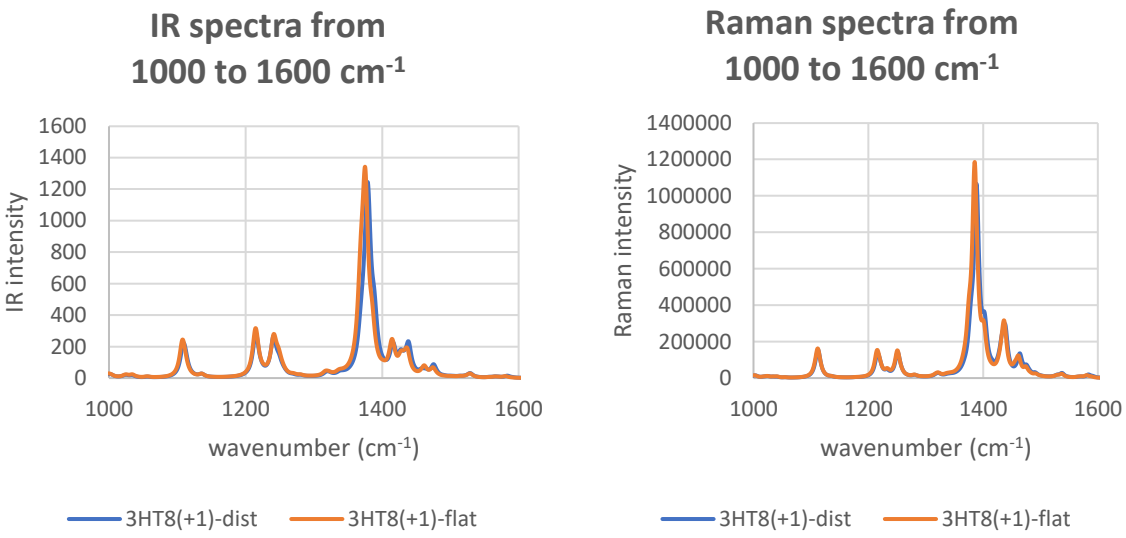

Figure 4.10: IR (left panel) and Raman spectrum (right panel) of flat and distorted 3HT8(+1).

IR spectra and dipole derivative parameters. We start the discussion presenting in Figure 4.11 the IR spectrum in the 1000-1600 cm^{-1} wavenumebr region of the neutral 3HT8 and the charged 3HT8(+1).

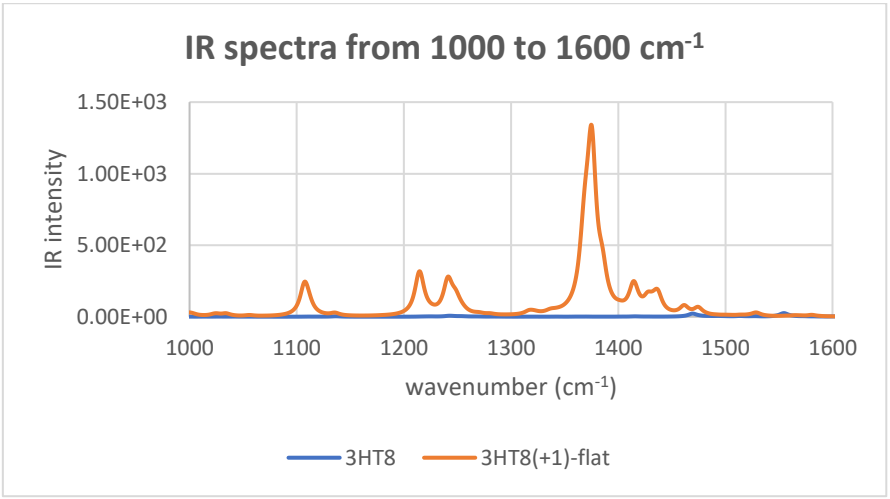

Figure 4.11: IR spectrum of neutral 3HT8 and charged 3HT8(+1) in the 1000-1600 cm^{-1} wavenumber region.

From Figure 4.11 it is possible to notice that the IR spectrum of the charged 3HT8(+1) is constituted by six intense peaks, whose associated normal modes are silent or almost silent in the IR when the molecule is in the neutral/pristine state. For this reason they represent the IRAVs of the octamer of (3-hexyl thiophene), which arise from the doping procees. We now compare in Figure 4.12 the IR spectrum of T8(+1) and 3HT8(+1).

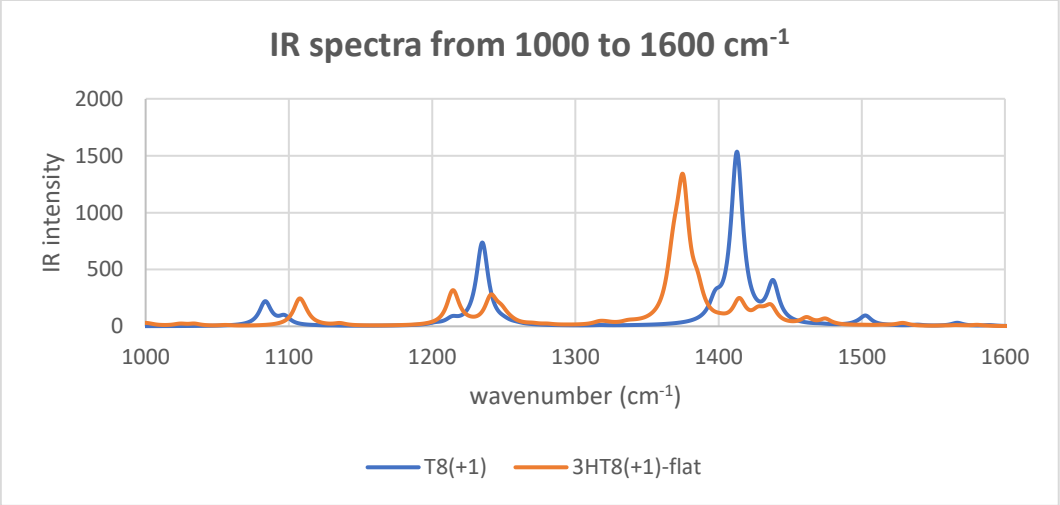

Figure 4.12: IR spectrum of the charged T8(+1) and the 3HT8(+1) in the 1000-1600 cm^{-1} wavenumber region.

Figure 4.12 shows that the IR spectrum of T8(+1) and 3HT8(+1) present similar features, with the activation of normal modes rather close in frequncy. We now analyse all the six IRAVs peaks of 3HT8(+1), comparing their eigenvectors with the ones of the IRAVs of T8(+1) showing similar frequency:

1) The first peak has frequency 1107 cm^{-1}, whose corresponding peak in the T8(+1) model has frequency 1084 cm^{-1}. The associated eingenvectors are reported in the left panel and in the right panel of Figure 4.13 respectively.

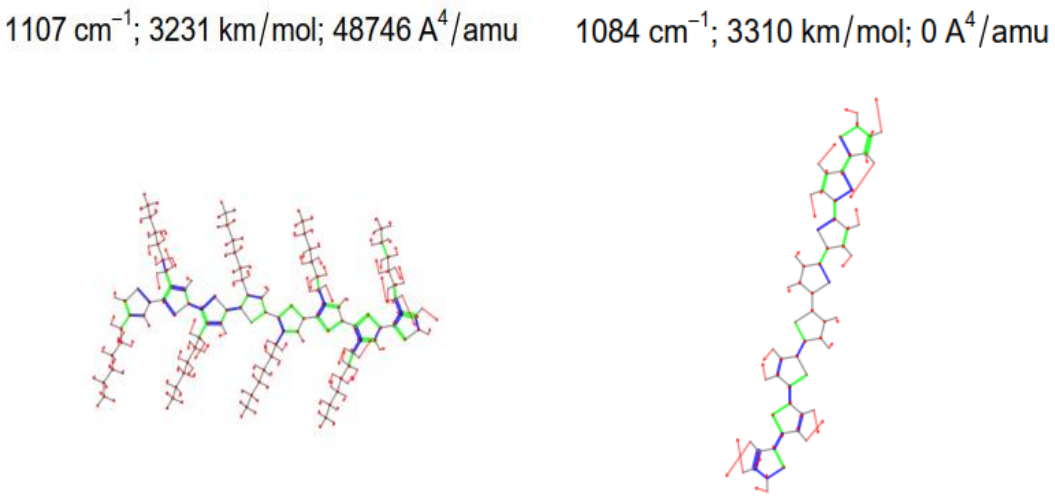

Figure 4.13: sketch of the eigenvector of normal mode having frequency 1107 cm^{-1} for 3HT8(+1) (left panel) and 1084 cm-1 for T8(+1) (right panel).

Both the normal modes present a node in the centre of the molecule, and both show some ECC-like character because of the in-phase stretching of all the quasi-single CC bonds, while the main difference regards the quasi-double CC bonds, which surely are more involved in the 3HT8(+1) model. The hexyl chains of 3HT8(+1) are coupled with the vibration of the backbone through the CC bond connecting the lateral chain to the thiophene ring: it vibrates out-of-phase with respect to the quasi-single CC bond within the thiophene unit.

2) The second and third peaks have frequency 1214 and 1241 cm^{-1} respectively, whose corresponding peak in the T8(+1) model has frequency 1235 cm^{-1}. The eigenvectors of the two normal modes for 3HT8(+1) are sketched in the left panels of Figure 4.14, while the one for T8(+1) in the right panel.

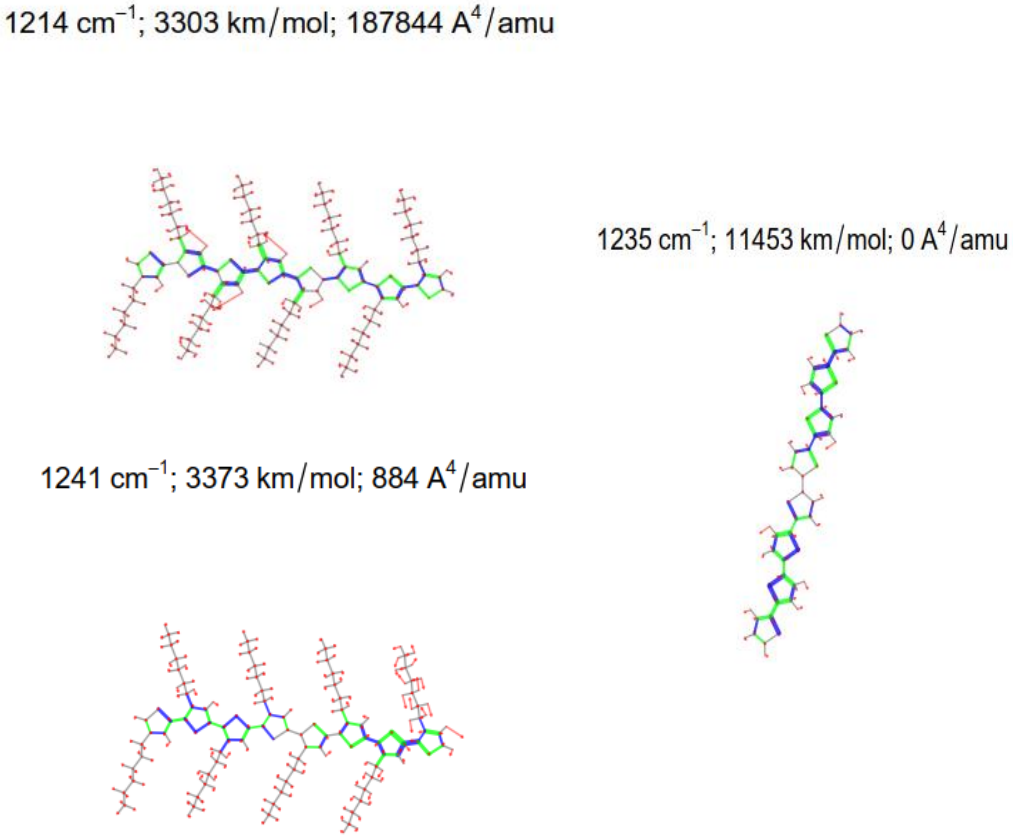

Figure 4.14: sketch of the eigenvector of normal modes having frequency 1214 and 1241 cm^{-1} for 3HT8(+1) (left panels) and 1235 cm^{-1} for T8(+1) (right panel).

The analysis of the eigenvectors allows to determine that 1241 cm^{-1} normal mode of 3HT8(+1) is the same of the 1235 cm^{-1} normal mode of T8(+1): in both cases the vibration, with a central node, exhibits an ECC-like character because the bonds belonging to each thiophene vibrate with the correct sign according to the Я pattern, while the inter-ring bonds do not. The first CC bond of the hexyl chains stretches (or shrinks) in phase with respect to the quasi-single CC bond of each thiophene unit.

The normal mode associated to the 1214 cm^{-1} peak, which shows a quite collective ECC-like character, is a peculiar IRAV of 3HT8(+1) and silent in the IR considering the T8(+1) model: in fact a quite important contribution to the vibration arises from the first CC bond of the lateral alkyl chains, vibrating out-of-phase with respect to the quasi-single CC bond of each thiophene ring.

3) The most intense IRAV has frequency 1375 and 1413 cm^{-1} for 3HT8(+1) and for T8(+1) respectively, whose eigenvectors are sketched in Figure 4.15. The lower frequency registered for 3HT8(+1) is ascribed to the higher π-electrons delocalization, induced by the conjugation of the first CC bond of the alkyl

chains, as already explained for the most intense ECC-like Raman normal mode of neutral 3HT8.

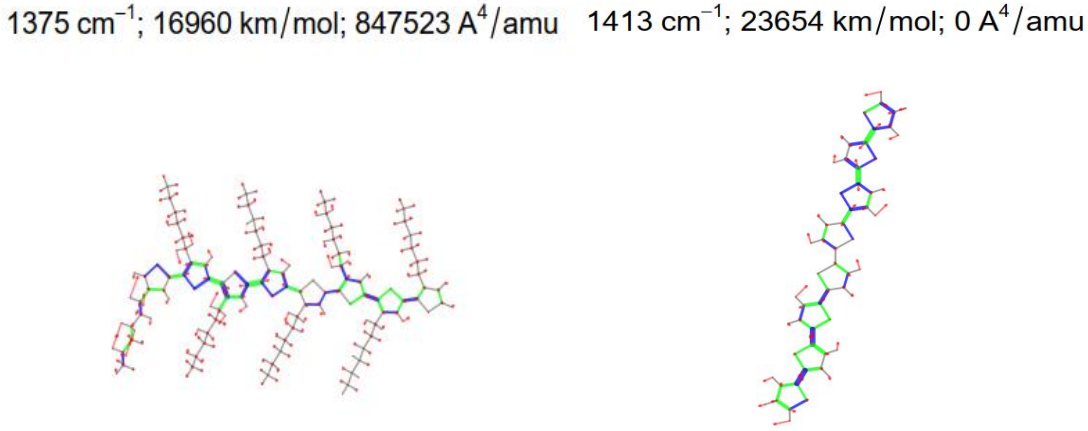

Figure 4.15: sketch of the eigenvector of the most intense IRAV, having frequency 1375 cm^{-1} for 3HT8(+1) (left panel) and 1413 cm^{-1} for T8(+1) (right panel).

In both cases the vibration associated to the most intense IRAV is an ECC-like normal mode with a node in the centre of the molecule. Focusing on the 3HT8(+1), almost all the hexyl chains are not involved in the vibration.

4) The peak with frequency 1414 cm^{-1} is peculiar of the IR spectrum of 3HT8(+1) and is absent in the one of T8(+1): the reason is that the eigenvector of the associated normal mode, sketched in Figure 4.16, shows some ECC-like character, but an important contribution to the vibration is given by the alternated stretching and shrinking of the CC bonds that constitute the lateral hexyl chain, not present in the T8(+1) model.

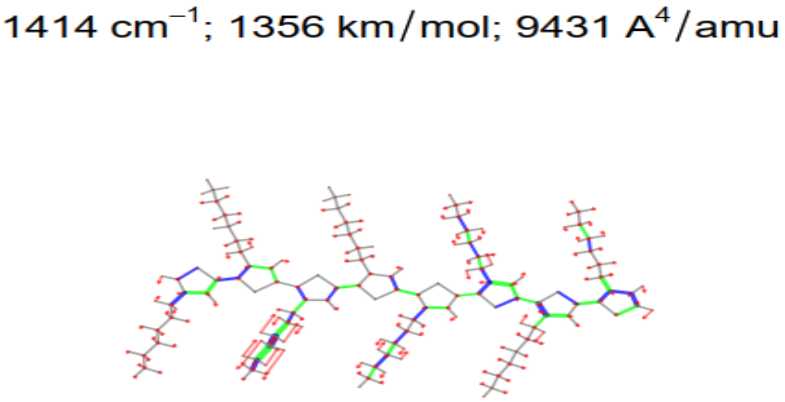

Figure 4.16: sketch of the eigenvector of the peculiar IR normal mode having frequency 1414 cm^{-1} of 3HT8(+1).

5) The last peak has frequency 1437 cm^{-1}, whose corresponding peak in the T8(+1) model has frequency 1438 cm^{-1}. The associated eingenvectors are reported in the left panel and in the right panel of Figure 4.17 respectively.

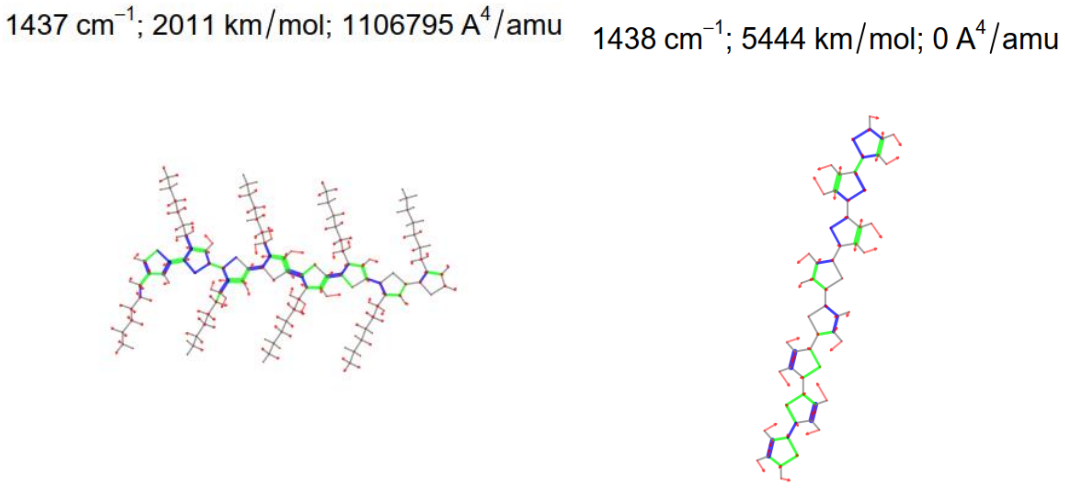

Figure 4.17: sketch of the eigenvector of normal mode having frequency 1107 cm^{-1} for 3HT8(+1) (left panel) and 1084 cm^{-1} for T8(+1) (right panel).

In this case the definition of the normal mode of the 3HT8(+1) is more complicated, even though it seems to resemble the one of T8(+1) because each quasi-single CC bond of each thiophene unit vibrates in phase, showing some ECC-like character, and because the inter-ring bonds vibrate with the wrong phase according to the Я pattern, except for the first three left-side thiophenes which exibit a proper ECC- like character.

From the analysis of the eigenvectors of the intense IRAVs peaks, it is possible to observe that the IR spectrum of 3HT8(+1) presents a more structured pattern with six IRAVs instead of the four intense peaks of the IR spectrum of T8(+1). Moreover, all the IR active normal modes of 3HT8(+1) are also Raman active (the Raman activity values which are reported in A^4/amu in the various sketches, are non zero), while this does not occur in the T8(+1) specie. The reason for these two relevant differences has to be ascribed to the lower symmetry of 3HT8(+1) with respet to the C_{2h} symmetry of the T8(+1) molecule due to the presence of the hexyl chains.

Apart from these aspects, the IR spectrum of the charged oligothiophene with and without the lateral alkyl chains presents a similar pattern: the main common feature is the activation in the IR of normal modes that are silent or barely silent in the IR if the molecule is in the neutral state, constituting the IRAVs and so the IR spectroscopic fingerprint of the doped material.

As we largely discussed in Chapter 3, the full rationalization of the onset of IRAVs and their large intesity compared to the IR peaks of the molecules in the pristine state can be obtained analysing the IR local parameters, namely the dipole derivatives with respect to the internal CC bond stretching coordinate. In Figure 4.18 we compare its component in the direction of the molecular axis of 3HT8(+1) and T8(+1), indicated as $\partial M_y/\partial R$.

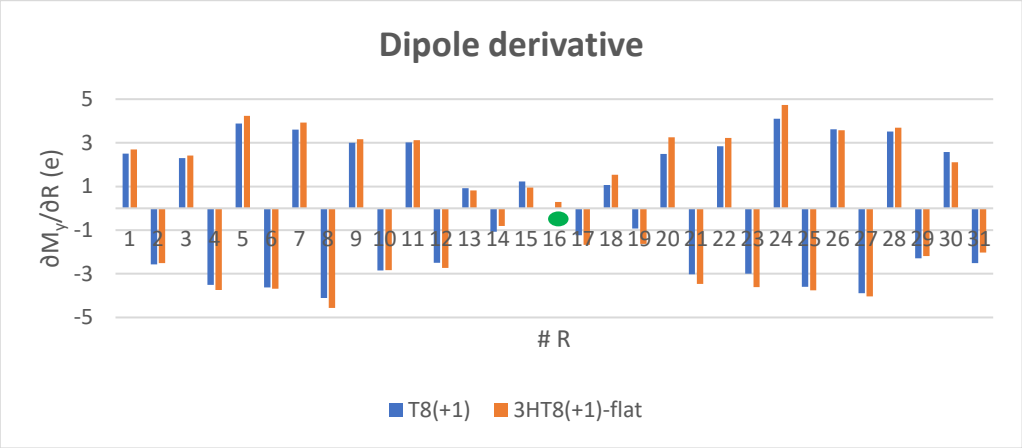

Figure 4.18: dipole derivative with respect to the internal CC stretching coordinate parameters of 3HT8(+1) and T8(+1).

From Figure 4.18 it is clear that the $\partial M_y/\partial R$ parameters of 3HT8(+1) and T8(+1) have similar values and an identical pattern which shows a systematic alternation of positive and negative values, which is the fundamental aspect needed to rationalize the high intensity of the IRAVs. Since there are no appreciable differences in $\partial M_y/\partial R$ parameters of the two considered molecules, we can reasonably assume that the activation mechanism of the IRAVs remain unaltered considering oligothiophenes with or without lateral alkyl chains.

Raman spectra and polarizability derivative parameters. In Figure 4.19 we report the Raman spectrum of 3HT8(+1) and T8(+1) in the wavenumber region between 1000 and 1600 cm^{-1}.

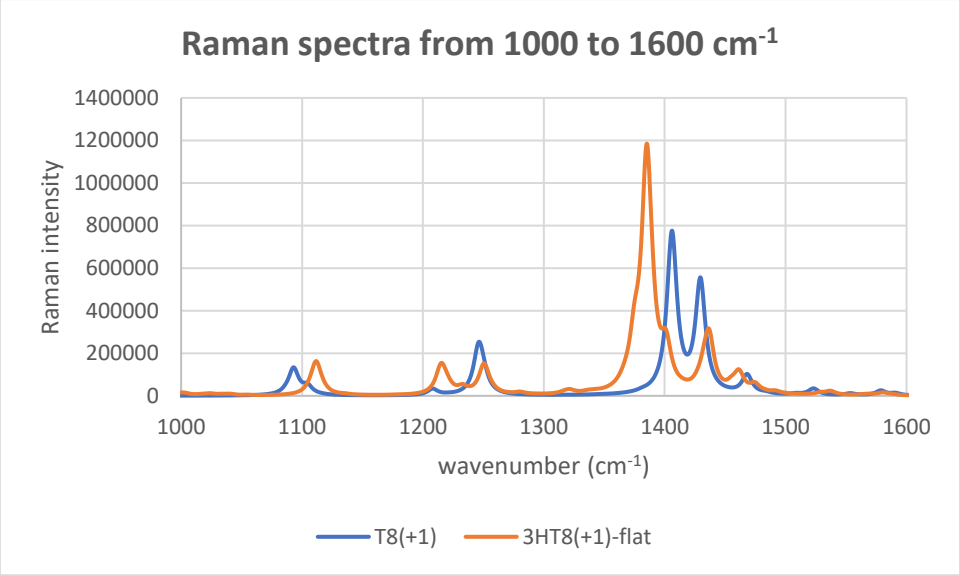

Figure 4.19: Raman spectrum of 3HT8(+1) and T8(+1) in the 1000-1600 cm^{-1} wavenumber region.

Except for the first of the two peaks with frequency around 1200 cm^{-1}, the Raman spectrum of 3HT8(+1) exhibits peaks with a correspondence one to one with the relevant peaks of the Raman spectrum of T8(+1), as it will be demonstrated by the following analysis of the eigenvectors of the associated normal modes:

1) The first peak has frequency 1112 cm^{-1}, whose corresponding peak in the T8(+1) model has frequncy 1093 cm^{-1}. The associated eingenvectors are reported in the left panel and in the right panel of Figure 4.20 respectively.

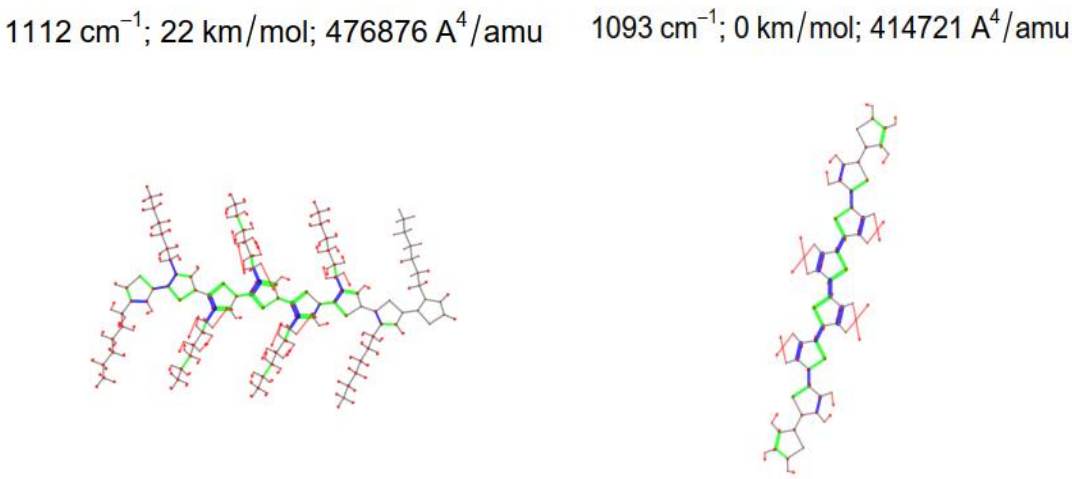

Figure 4.20: sketch of the eigenvector of normal mode having frequency 1112 cm^{-1} for 3HT8(+1) (left panel) and 1093 cm^{-1} for T8(+1) (right panel).

Both the normal modes show the same ECC-like character, even if more localized in the 3HT8(+1) model, because the quasi-single CC bonds of the backbone stretch or shrink in phase and the quasi-double CC bonds. The first CC bond of the hexyl chains vibrates out-of-phase with respect to the quasi-single bonds of the backbone.

2) The 1216 cm^{-1} peak is the only peculiar Raman peak of 3HT8(+1) that is absent in the Raman spectrum of T8(+1), whose eigenvector is reported in Figure 4.21.

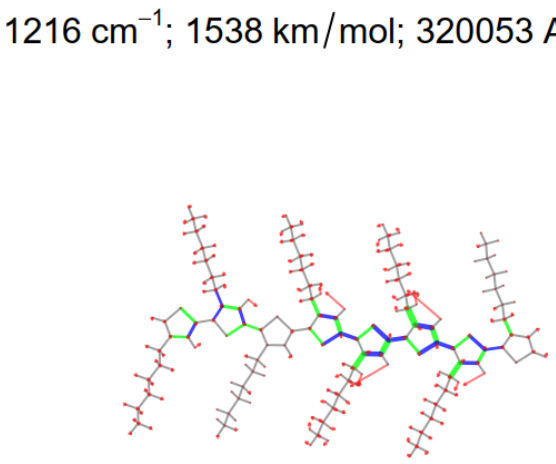

Figure 4.21: sketch of the eigenvector of the peculiar Raman normal mode having frequency 1216 cm^{-1} of 3HT8(+1).

The vibration shows some ECC-like character, determined by the in-phase stretching of the quasi-single CC bonds of the backbone, mostly localized on the right side of the molecule. The hexyl chains are coupled with the backbone vibration through the stretching with opposite sign of their first CC bond.

3) The third peak has frequency 1250 cm^{-1}, whose corresponding peak in the T8(+1) model has frequncy 1246 cm^{-1}. The associated eingenvectors are reported in the left panel and in the right panel of Figure 4.22 respectively.

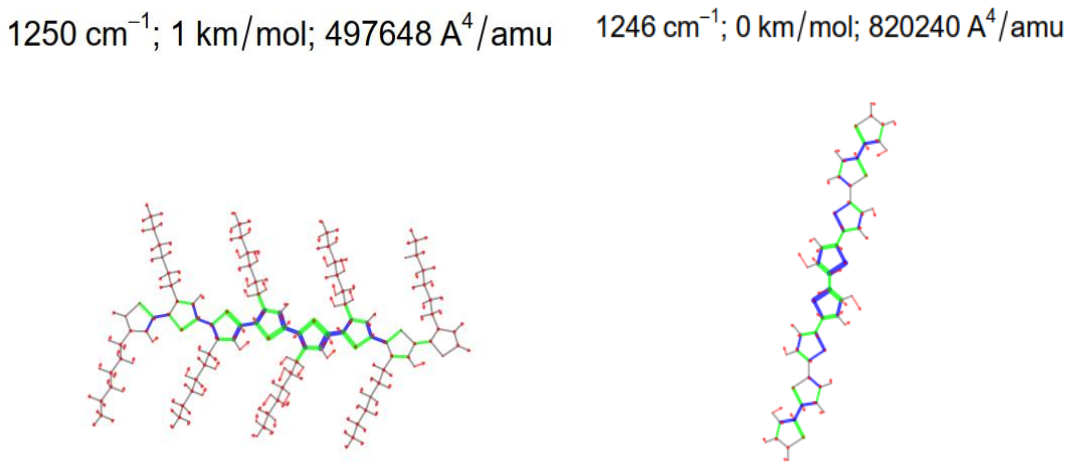

Figure 4.22: sketch of the eigenvector of normal mode having frequency 1250 cm^{-1} for 3HT8(+1) (left panel) and 1246 cm^{-1} for T8(+1) (right panel).

In both the eigenvectors, the ECC-like character is determined by vibration of the bonds belonging to the thiophene rings with the correct sign according to the Я pattern and by vibration with the wrong phase of the inter-ring bonds.

4) The most intense RAV has frequency 1385 and 1406 cm^{-1} for 3HT8(+1) and for T8(+1) respectively, whose eigenvectors are sketched in Figure 4.23. The frequency redshift occurring in 3HT8(+1) with respect to T8(+1) is rationalized in the same way of the most intense IRAV: the normal modes with an important projection along the ECC are subjected to a softening, since the higher conjugation of the system, induced by the first CC bond of the hexyl chains.

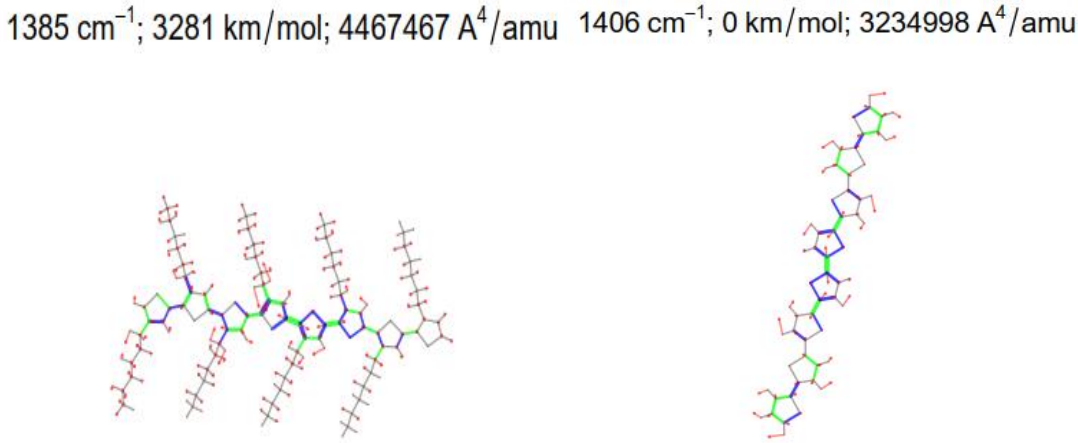

Figure 4.23: sketch of the eigenvector of the most intense RAV, having frequency 1385 cm^{-1} for 3HT8(+1) (left panel) and 1406 cm^{-1} for T8(+1) (right panel).

In both cases, the normal mode associated to the most intense RAV is an ECC-like vibration, mostly localized in the central region of the oligothiophene, even if in the 3HT8(+1) model the lower symmetry of the system makes the Я mode not involving the last two left-side thiophene units and makes the presence of the two nodes in the RAV eigenvector of T8(+1) more difficult to detect.

5) The fifth relevant peak has frequency 1437 cm^{-1} and its corresponding peak in the Raman spectrum of T8(+1) has frequency 1430 cm^{-1}. The associated eingenvectors are reported in the left panel and in the right panel of Figure 4.24 respectively.

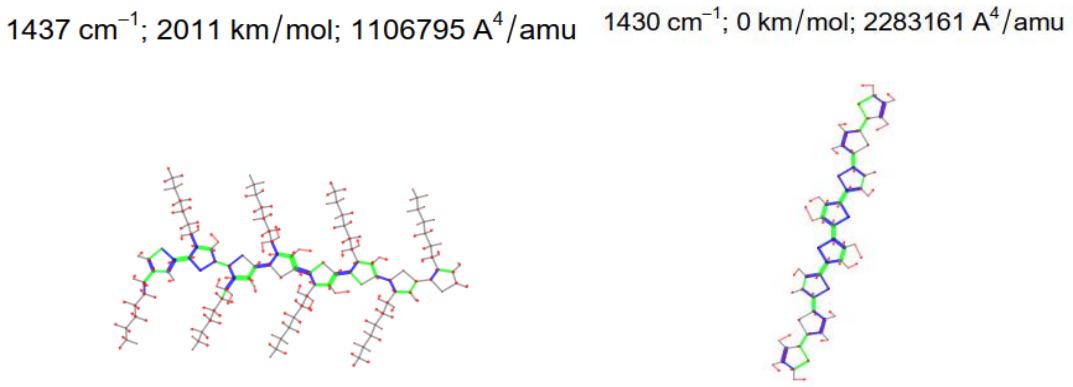

Figure 4.24: sketch of the eigenvector of normal mode having frequency 1437 cm^{-1} for 3HT8(+1) (left panel) and 1430 cm^{-1} for T8(+1) (right panel).

Although the two peaks in the Raman spectrum of 3HT8(+1) and T8(+1), their associated normal modes cannot be classified as the same vibration: in the case of T8(+1) the ECC-like character is perfectly defined in the central region, but in the case of 3HT8(+1) it is defined in the two first left-side thiophene rings, while in the central region of the oligothiophene the quasi-single CC bonds vibrate out-of-phase, generating a mode with a only partial Я character.

6) The last important peak of the Raman spectrum of 3HT8(+1) has frequency 1461 cm^{-1}, whose corresponding peak in the T8(+1) model has frequncy 1468 cm^{-1}. The associated eingenvectors are reported in the left panel and in the right panel of Figure 4.25 respectively.

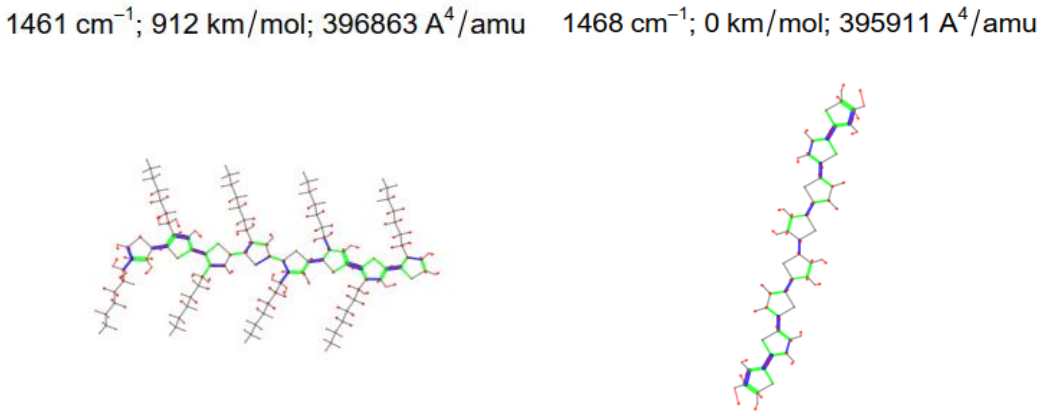

Figure 4.25: sketch of the eigenvector of normal mode having frequency 1461 cm^{-1} for 3HT8(+1) (left panel) and 1468 cm^{-1} for T8(+1) (right panel).

Both the normal modes present an ECC-like character with two nodes located three thiophene units from the end of the oligomer. The lateral hexyl chains substantially are not involved in the vibration.

The analysis of the eigenvectors of the most intense Raman modes allows to observe that the most relevant peaks of the Raman spectrum of T8(+1) find correspondence also in the Raman spectrum of 3HT8(+1). The most important common feature is the activation in the Raman of normal modes, which are silent or almost silent if the oligothiophene is in the pristine state, constituting the RAVs and so the Raman spectroscopic fingerprint of the doped material.

It is possible to rationalize the mechanism from which the RAVs arise by means of the polarizability derivative with respect the internal CC bonds stretching coordinate, whose values (trace of the polarizability tensor) for T8(+1) and 3HT8(+1) are compared in Figure 4.26.

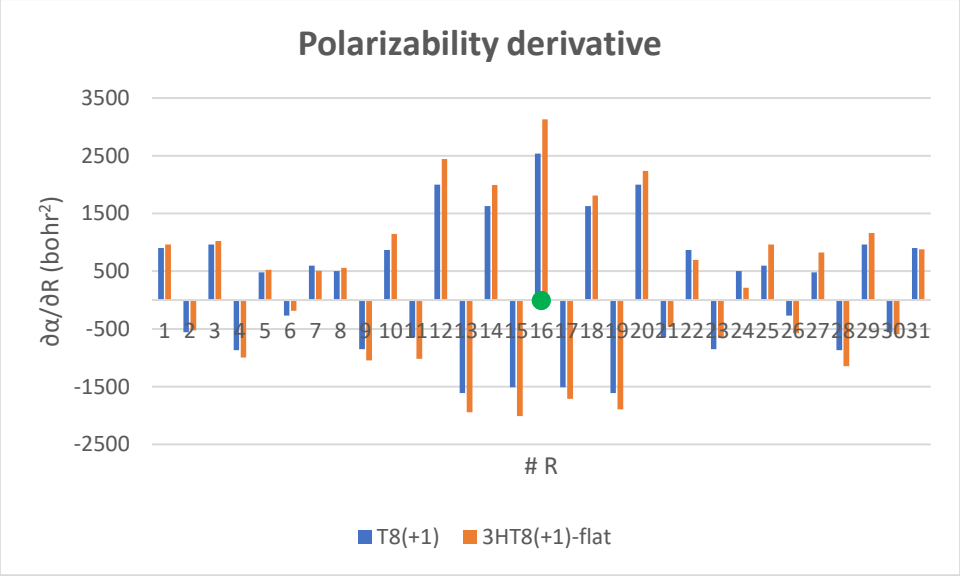

Figure 4.26: polarizability derivative with respect to the internal CC stretching coordinate parameters of T8(+1) and 3HT8(+1).

From Figure 4.26 it is clear that the ∂α/∂R parameters of 3HT8(+1) and T8(+1) show similar values and an identical pattern in terms of positive and negative values, which is the fundamental aspect needed to rationalize the high intensity of the RAVs. Since there are no appreciable differences in ∂α/∂R parameters of the two considered molecules, we can reasonably assume that the activation mechanism of the IRAVs remains unaltered considering oligothiophenes with or without lateral alkyl chains. Also the considerations regarding the polaron delocalization length predicted by sign inversion of the local Raman parameters with respect to the ones of the neutral molecule, presented in Chapter 3 for unsubstituted oligothiophenes, are still valid in the case of oligothiophenes with lateral alkyl chains.

Geometry relaxation upon doping. In Figure 4.27 we report the equilibrium bond length (top panel) and the BLA parameter (bottom panel) of the CC bonds constituting the backbone of the T8(+1) and the 3HT8(+1) molecules.

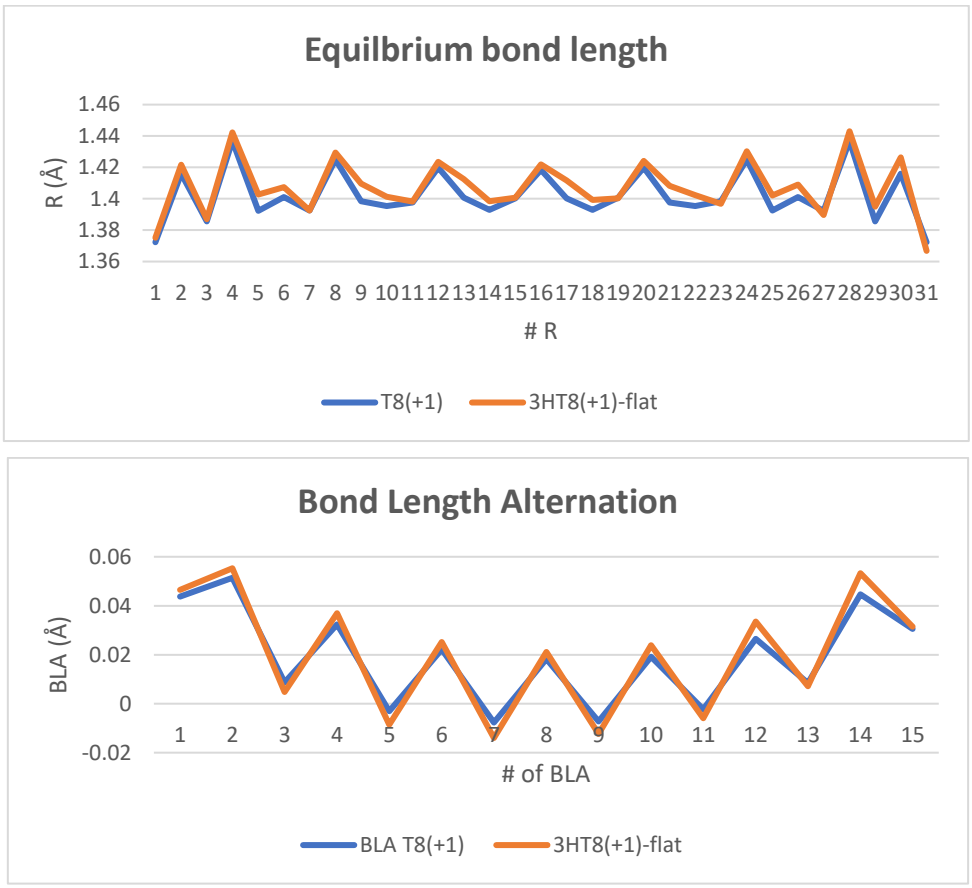

Figure 4.27: equilibrium bond length values (top panel) and BLA parameter (bottom panel) of the CC bonds constituting the oligothiophene backbone for T8(+1) and 3HT8(+1).

From the top panel of Figure 4.27, it is possible to notice that the geometry relaxation of the CC bonds of the oligomer backbone, that occurs as a consequence of the extraction of the electron from the oligothiophene to the dopant, produces very similar results for the oligothiophene with and without hexyl chains. The main difference regards the quasi-double and quasi-single CC bond connecting the C atom the lateral alkyl chains are attached to: both appear longer than the corresponding bonds in the T8(+1) model. Anyway, these differences produce modest effects in the BLA parameter of 3HT8(+1), which in fact resembles well the one of T8(+1), as it is clear from the bottom panel of Figure 4.26: the main effect is that the BLA of 3HT8(+1) reaches more negative values than the BLA of T8(+1) in the central perturbed region, even if they are still very small (slightly above 0,01 Å) and so we can safely assume that also in the case of 3HT8(+1) the polaron presents equalized quasi-single and quasi-double CC bonds, as discussed for T8(+1).

4.2. The effect of the length of the lateral alkyl chains: comparison between neutral and charged 3HT8 and 3ET8.

In the previous Section we presented the results regarding the neutral 3HT8 and charged 3HT8(+1). In order to properly understand the effect of the doping process on the lateral alkyl chains and not only on the backbone, but we also analysed how the IR and Raman local parameters and the equilibrium bond length of the CC bonds constituting the hexyl chains change upon doping. In particular, we collected the intensity local parameters and geometrical parameters of the CC bonds of a central alkyl chain such that it is attached to a thiophene ring belonging to the central region mostly perturbed by the polaronic charge induced defect. In Figure 4.28 we report the $\partial M_x/\partial R$, the $\partial\alpha/\partial R$ parameters and the values of the equilibrium bond length for the CC bonds of the considered hexyl chain of the neutral 3HT8 and the charged 3HT8(+1).

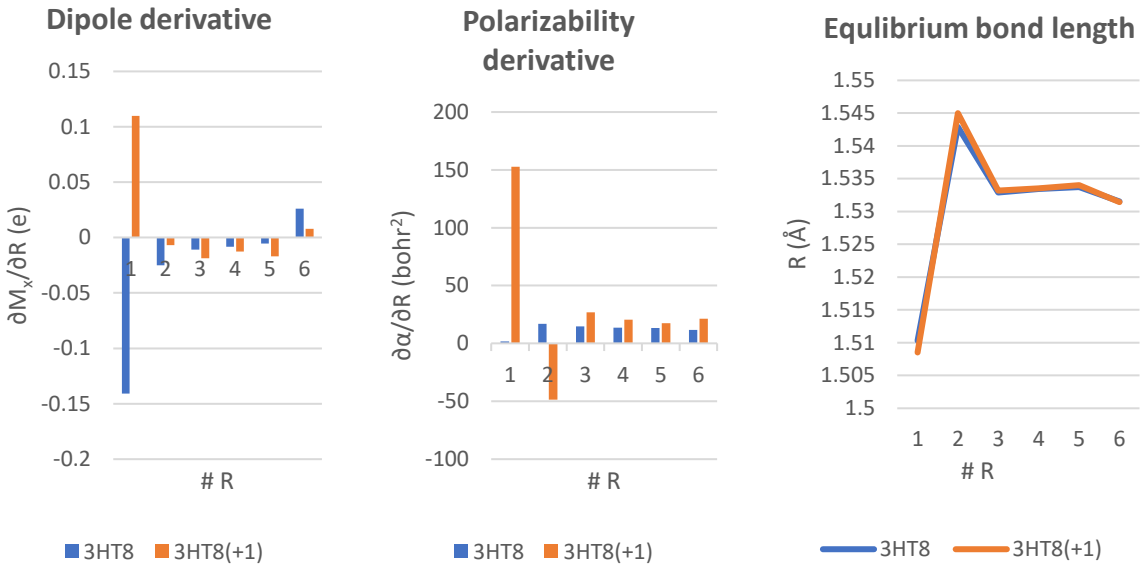

Figure 4.28: IR and Raman local parameters and values of equilibrium bond length of CC bonds of a central hexyl chain of the neutral 3HT8 and the charged 3HT8(+1).

Before commenting the results, it useful to specify that the CC bond labelled as 1 is the bond that connects the alkyl chain with the thiophene ring, while the other five CC bonds are the ones belonging to the hexyl chain.

From Figure 4.28 it is clear that only the first CC bond is subjected to significant variations in terms of intensity and geometric parameters when the 3HT8 passes from the neutral to the charged state (3HT8(+1)). For this reason, it is reasonable to expect that substituting the hexyl chains with a shorter one constituted by only two CC bonds, i.e. the ethyl chain (-CH_2-CH_3), does not induce dramatic variations in the vibrational spectra – at least concerning the main bands which involve vibrations of the π-conjugated backbone - and from the geometrical point of view. This would be important because it would allow to save computational resources if we are interested in calculations on alkyl substituted oligomers with a larger number of thiophene units of the backbone, as it has been done for the fully hydrogenated series (from T6 to T14) presented in Chapter 3.

In this Section we will compare the vibrational spectra and the geometrical parameters of the neutral 3HT8 and 3ET8 and the charged 3HT8(+) and 3ET8(+1), where the label 3ET8 indicates the octamer of (3-ethyl thiophene). All the DFT computations are performed with B3LYP functional and 6-31G** basis set and with the unrestricted configuration for the charged species. In Figure 4.29 we report:

- In the top left panel, the IR spectrum of the neutral 3HT8 and 3ET8 in the wavenumber region between 500 and 1700 cm^{-1}.
- In the top right panel, the IR spectrum of the charged 3HT8(+1) and 3ET8(+1) in the wavenumber region between 1000 and 1600 cm^{-1}.
- In the bottom left panel, the Raman spectrum of the neutral 3HT8 and 3ET8 in the wavenumber region between 1300 and 1600 cm^{-1}.
- In the bottom right panel, the Raman spectrum of the charged 3HT8(+1) and 3ET8(+1) in the wavenumber region between 1000 and 1600 cm^{-1}.

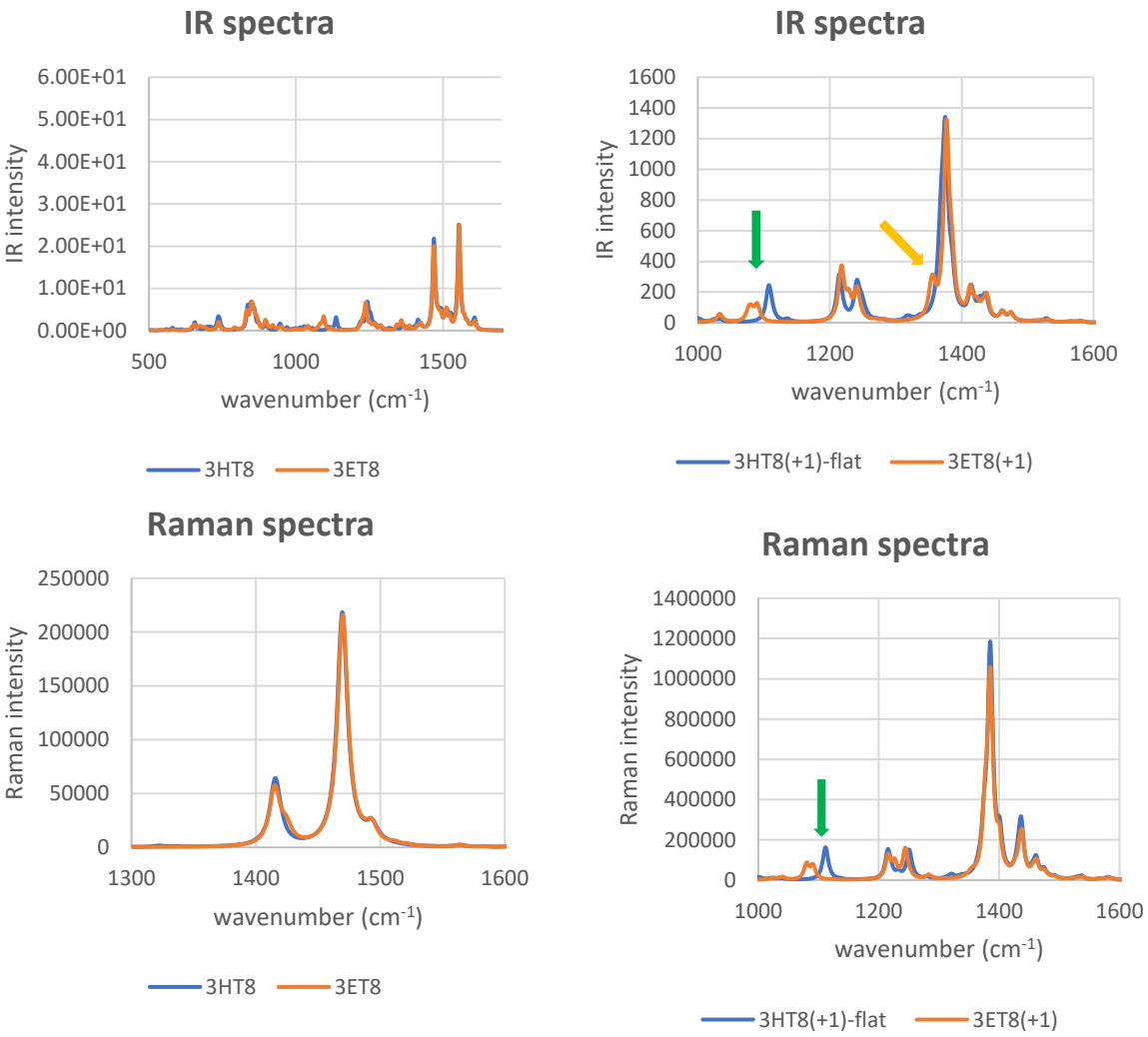

Figure 4.29: IR and Raman spectra of the neutral 3HT8 and 3ET8 (left panels) and of the charged 3HT8(+1) and 3ET8(+1) (right panels).

As it can be noticed from the left panels of Figure 4.29, the IR spectrum in the considered wavenumber region and the Raman spectrum of the neutral 3HT8 and 3ET8 substantially overlap, presenting no appreciable differences in terms of both frequency and intensity, if one neglects the rather weak bands mainly involving bending modes of the CH_2 sequence of the hexyl chains. For what concerns the charged species, the only important difference between the IR and Raman spectrum of 3HT8(+1) and 3ET8(+1) refers to the frequency redshift of the peak around 1100 cm^{-1}, indicated with a green arrow in the right panels of Figure 4.29. It is interesting to notice the small peak, indicated with a yellow arrow in Figure 4.29, in the IR spectrum of 3ET8(+1) with frequency slightly below the one of the most intense IR peak, absent in the IR spectrum of 3HT8(+1).

As expected, the major difference regarding the vibrational spectra of the octamer with hexyl and the one with ethyl chains can be appreciated in the C-H stretching wavenumber region of the IR spectrum of the two neutral species, as reported in Figure 4.30.

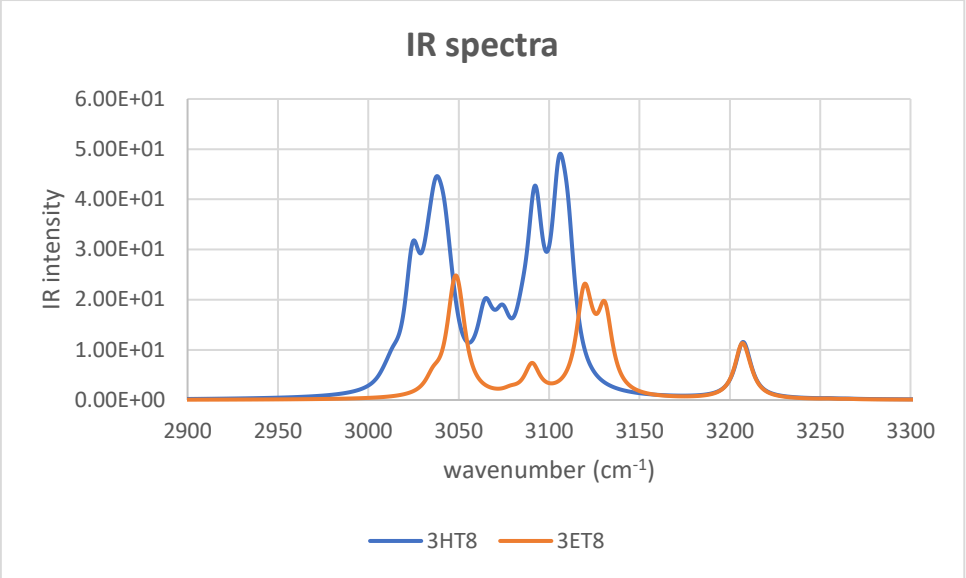

Figure 4.30: IR spectrum of neutral 3HT8 and 3ET8 in the 2900-3300 cm^{-1} wavenumber region.

The peak with frequency above 3200 cm^{-1} coincides in the two IR spectra, since the associated normal mode is the C-H stretching of the C-H bonds present in the backbone of the oligomer, which remains the same passing from 3HT8 to 3ET8. On the contrary, the spectral region between 3000 and 3150 cm^{-1} of 3HT8, determined by the stretching of the C-H bonds of the alkyl chains, presents more structured and more intense bands than the one of 3ET8, since the total CH stretching intensity increases linearly with the number of C-H bonds that can participate to the vibration.

The very similar vibrational spectra of neutral and charged 3HT8 and 3ET8 in the region affected by CC stretching vibrations can be rationalised by means of the IR and Raman local parameters.

In Figure 4.31 we report:

- In the top left panel, the $\partial M_y/\partial R$ parameters of the neutral 3HT8 and 3ET8.
- In the top right panel, the $\partial M_y/\partial R$ parameters of the charged 3HT8(+1) and 3ET8(+1).

In Figure 4.32 we report:

- In the bottom left panel, the ∂α/∂R parameters of the neutral 3HT8 and 3ET8.
- In the bottom right panel, the ∂α/∂R parameters of the charged 3HT8(+1) and 3ET8(+1).

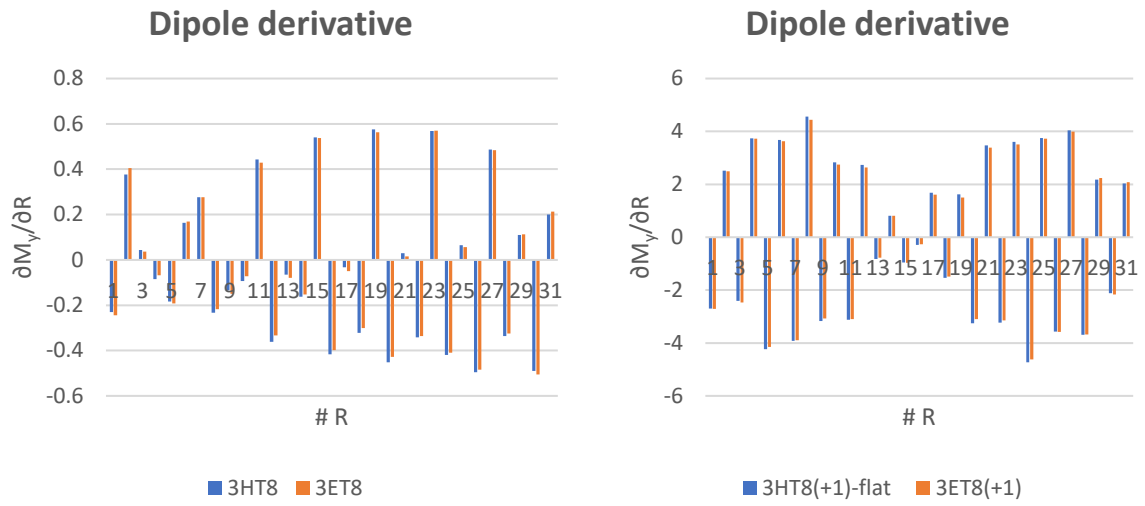

Figure 4.31: IR local parameters of the neutral 3HT8 and 3ET8 (left panel) and of the charged 3HT8(+1) and 3ET8(+1) (right panel).

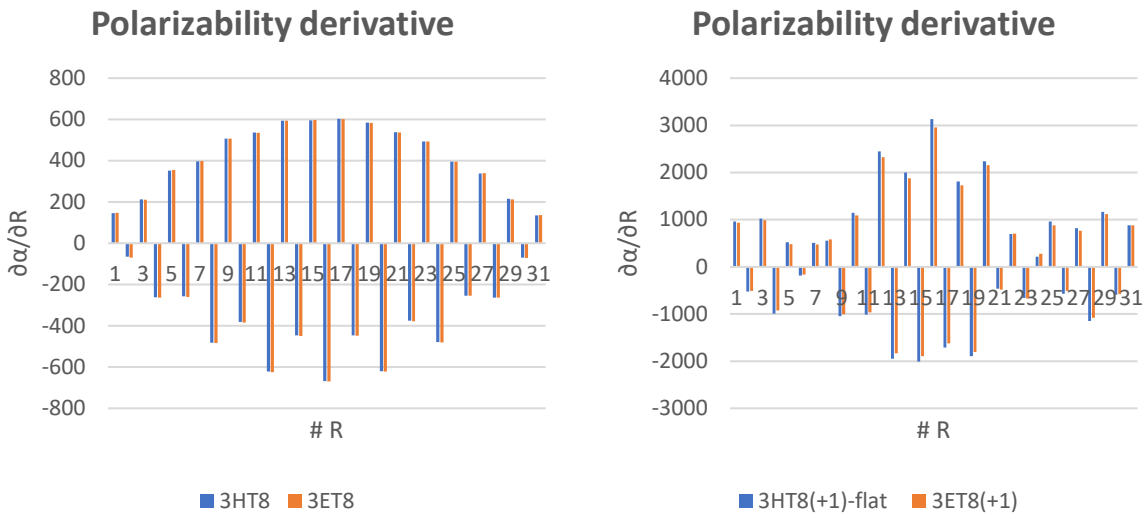

Figure 4.32: Raman local parameters of the neutral 3HT8 and 3ET8 (left panels) and of the charged 3HT8(+1) and 3ET8(+1) (right panels).

From Figure 4.31 and 4.32 it is evident that IR and Raman local parameters present very similar values and an identical sign pattern, thus explaining why the IR and

Raman spectra of the octamer of (3-hexyl thiophene) do not undergo significant modifications when the lateral hexyl chains are substituted with the shorter ethyl chains.

From the analysis of the vibrational spectra of the neutral and charged octamer with lateral hexyl and ethyl chains, we have demonstrated that the most important spectroscopic features are independent on the length of the alkyl chains. In particular, the six IRAV and RAV peaks structure of the IR and Raman spectra can be appreciated in both the 3HT8(+1) and 3ET8(+1) models. This result is very important because it confirms that:

1) the relevant spectroscopic fingerprints of the oligothiophenes in the neutral and charged state are practically independent on the presence and the type of the alkyl chains.
2) Since they are essentially determined by vibrations involving the stretching and shrinking of the CC bonds, the activation mechanisms of IRAVs and RAVs in charged oligothiophenes do not vary passing from unsubstituted models to the ones with alkyl chains of any length.
3) For what concerns the geometry relaxation occurring upon the doping process, the electron extraction from the oligomer to the dopant induces primary effects on the CC bonds of the backbone of the oligothiophenes, while the lateral alkyl chains have insignificant effects on this process. This is shown in Figure 4.33, which reports the equilibrium bond length values for the CC bonds of the backbone of 3HT8(+1) and 3ET8(+1), and the two plots appear coincident.

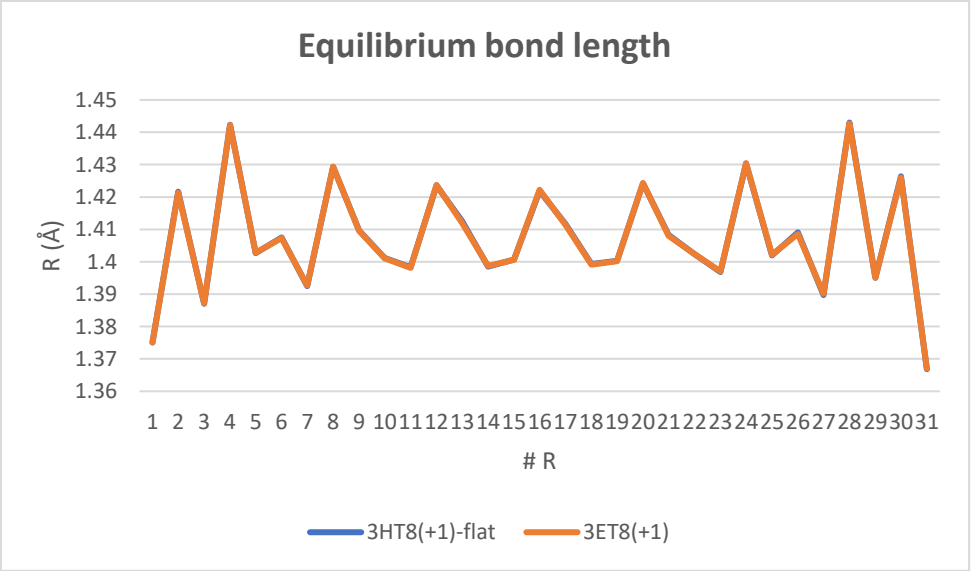

Figure 4.33: equilibrium bond length values for the CC bonds of the backbone of 3HT8(+1) and 3ET8(+1).

5 Comparison with the experimental data.

In this Chapter we will provide a comparison between the DFT calculated and the experimental IR and Raman spectra; in particular, we will focus our attention on the vibrational spectra of charged species. All the spectra are visualized with the Omnic software and a scaling factor of 0,9742 is applied to the computed frequencies to fit the experimental data. This value is obtained such that the second most intense peak of the B3LYP-calculated Raman spectrum of neutral 3HT8 coincides in frequency with the one of the experimental spectrum of P3HT.

Before going into the details of the Chapter, it is useful to specify the notation used to label the calculated vibrational spectra visualized with Omnic; the scheme is the following:

Type of spectrum_oligothiophene _functional_scaling factor

where:

- *Type of spectrum* indicates if the plot deals with an IR or a Raman spectrum.
- *Oligothiophene* indicates the oligomer to which the spectrum is referred, with indication of the charge in the case of cations.
- *Functional* indicates the level of theory used in the DFT calculation and it can be B3LYP and Hybrid (geometry optimization with CAM-B3LYP and the vibrational frequencies with B3LYP).
- *Scaling factor* indicates the applied scaling factor: if the unscaled version of the spectrum is considered, the label is *unscal*, otherwise *0,9742scal* to specify that a 0,9742-scaling factor is used.

Scientific literature **[9, 15, 16, 29, 49, 52-57]** reports numerous works regarding vibrational spectroscopy of pristine and doped P3HT at solid-state as powders, films, nanofibres and also in solution. Regio-regular P3HT is a semi-cristalline material and its crystalline structure has been characterized since longtime. In this study we will limit to consider only doped P3HT at the solid state. We aim at mimiking the charged defect, i.e. the polaron, which should be accomodated in the crystalline domains of the material, thus giving rise to a new doped phase, characterized by a ordered morphology. This is important to specify becaue if the molecular environment changes, the vibrational spectra can undergo relevant modifications. This happens

even without considering doped P3HT: the IR and Raman spectrum of P3HT in pristine state show remarkable differences if the material is in the melt phase, is higlhly crystalline or contains a high degree of disorder, as for instance when the material presents a large amount of amorphous phase. Indeed both intra-molecular disorder, e.g. conformational defects along the bakbone, and different inter-molecular interactions, e.g. more or less effective packing of the polymer chains, correspond to a perturbation of the dynamics of the whole system and for this reason vibrational spectroscpy is used as structural probe to investigate the phases of the polymer **[15]**. For the above observations, it is reasonable to think that the doping induced charged defect self-localizes into the polymeric chain differently if the material is crystalline or if it involves amorphous phases or if the material is in solution.

Furthermore, all the quantum-chemical simulations presented in the previous Chapters are carried out *in vacuo*, thus meaning that the molecule is considered isolated: intermolecular interactions of any kind are not taken into account in our models. In particular, we do not consider the interaction of each polymeric chains with the other molecules in the semicrystalline phase, that in real P3HT are instead present. In this framework, also the simulated doping process is far from the reality: in our models we simulated only the singly charged cation of an oligothiophene, neglecting the dopant counterion and their possible Coulomb interactions.

For the reasons listed above, the DFT calculations we performed necessarily provides an approximated description of real doped P3HT.

The aim of this Section is to compare the experimental IR and Raman spectra of doped P3HT with the ones of a molecular model which can mimic sufficiently well the polymer, although all the limitations we explained before. In other words, the purpose of this Chapter is to check the correspondence, in terms of spectroscopic pattern – namely IRAVs and RAV - between the theoretical predictions and the experimental results. This allows using our models (and the physical quantities obtained with our DFT investigation) in order to interpret the vibrational characteristics of doping induced charge defect, namely of the polaron.

5.1. IR spectra

In Figure 5.1 we report the experimental IR spectrum of a deposited film of P3HT, doped from a chloroform solution with dissolved I_2, (blue spectrum) and of doped 3HT8 in the wavenumber region between 700 and 1600 cm^{-1}; the main peaks are labelled with numbers from one to nine.

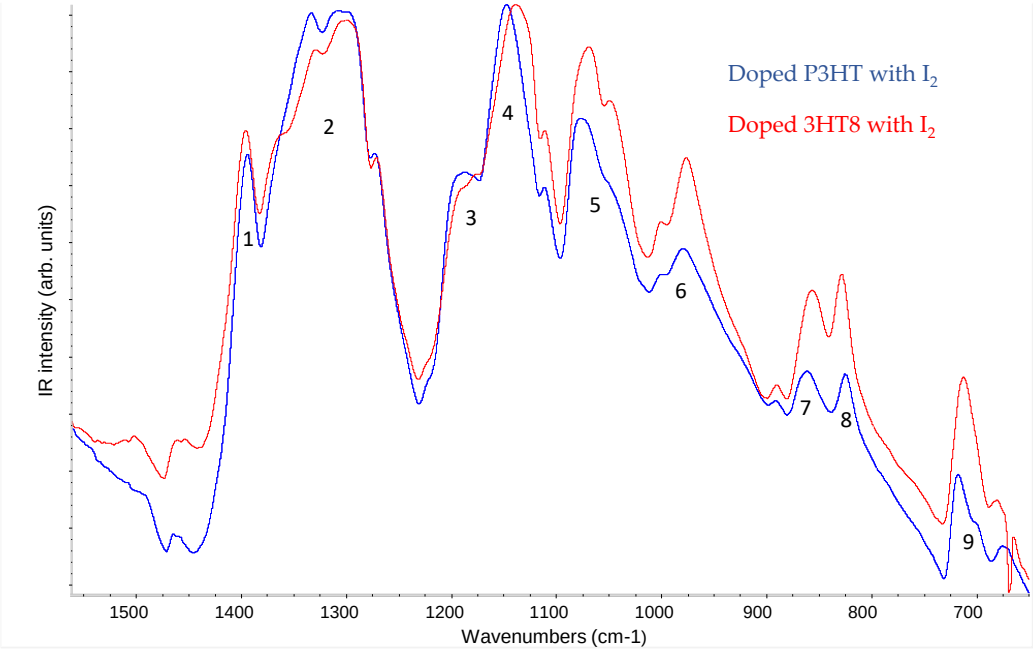

Figure 5.1: experimental IR spectrum of P3HT and 3HT8.

As it can be noticed from Figure 5.1, the IR spectrum of doped P3HT and its octamer are very similar with a pattern constituted by nine sometimes structured, intense peaks, in the considered wavenumber region between 1500 and 650 cm^{-1}. The experiments show that the octamer of (3-hexyl thiophene) is a sufficiently long oligomer that its spectrum properly mimics that of the polymer. This means the polaronic charged defect induced within the polymeric chain by the doping process can be fully described, at list from the point of view of the IR spectrum, by 3HT8.

This datum is partially in agreement with the results obtained from the DFT simulations, since in Chapter 3 the IR spectrum, and in particular the IRAVs pattern, of the charged unsubstituted oligothiophene with eight thiophene rings (T8(+1)) and with a higher number of units (T12(+1), T14(+1)) are similar.

On the other hand, for the comparison with the experimental spectra, the models of oligothiophenes with lateral alkyl chains, should be more suitable. In Chapter 4 we discussed the results for the octamer of (3-alkyl thiophene) and we showed that the IR spectrum of 3HT8(+1) and 3ET8(+1) present negligible differences. Moreover, we analysed also the vibrational spectra of longer alkyl-substituted oligomers and in particular of the 3ET12 model, whose calculation was performed with both B3LYP and CAM-B3LYP. All these models will be considered in the following comparison with the experimental data.

In Figure 5.2 we report the IR spectrum of 3ET12(+1) and 3ET8(+1), both studied with the B3LYP functional, to show that also in the case of alkyl-substituted oligothiophenes the IRAVs pattern changes passing from short to longer oligomers, but not in a dramatic way.

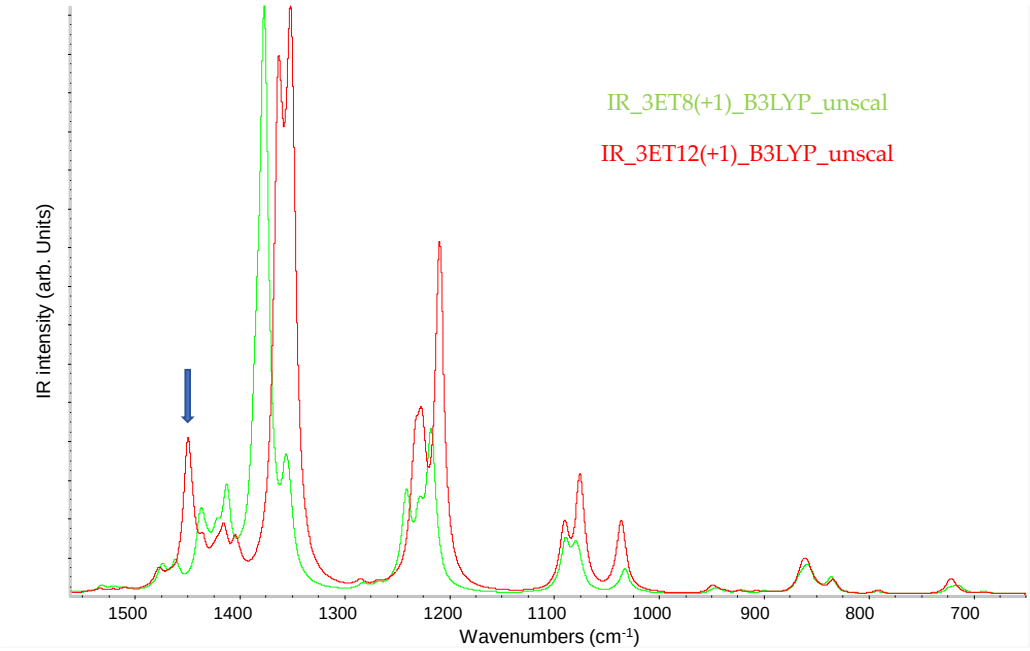

Figure 5.2: IR spectrum in the 700-1500 cm^{-1} wavenumber region of 3ET8(+1) and 3ET12(+1).

Only the higher frequency IRAVs of 3ET12(+1), namely the two intense IRAVs around 1350 cm^{-1} and the doublet having frequency around 1200 cm^{-1}, present a shift at lower wavenumbers with respect to the ones of the shorter model. The main difference between the IR spectrum of 3ET8(+1) and 3ET12(+1) is the peak with frequency around 1450 cm^{-1}, indicated in Figure 5.2 by the blue arrow, which is present in the IR spectrum of the long oligomer, while the spectrum of ET8(+1) shows several rather weak bands in the same spectral region. Apart from these differences, the two IR spectra show a similar in the IRAVs pattern, thus confirming that the effect of the backbone chain length does not affect very much the IRAVs and so that the doped octamer of (3-alkyl thiophene) shares common spectroscopic properties of longer doped chains and doped P3HT.

Since the IR spectrum of the same molecule, 3HT8, has been obtained both from DFT simulations and from experiments, in Figure 5.3 we are going to compare the vibrational spectrum of I_2 doped 3HT8 (experiment) and the B3LYP-calculated one of 3HT8(+1).

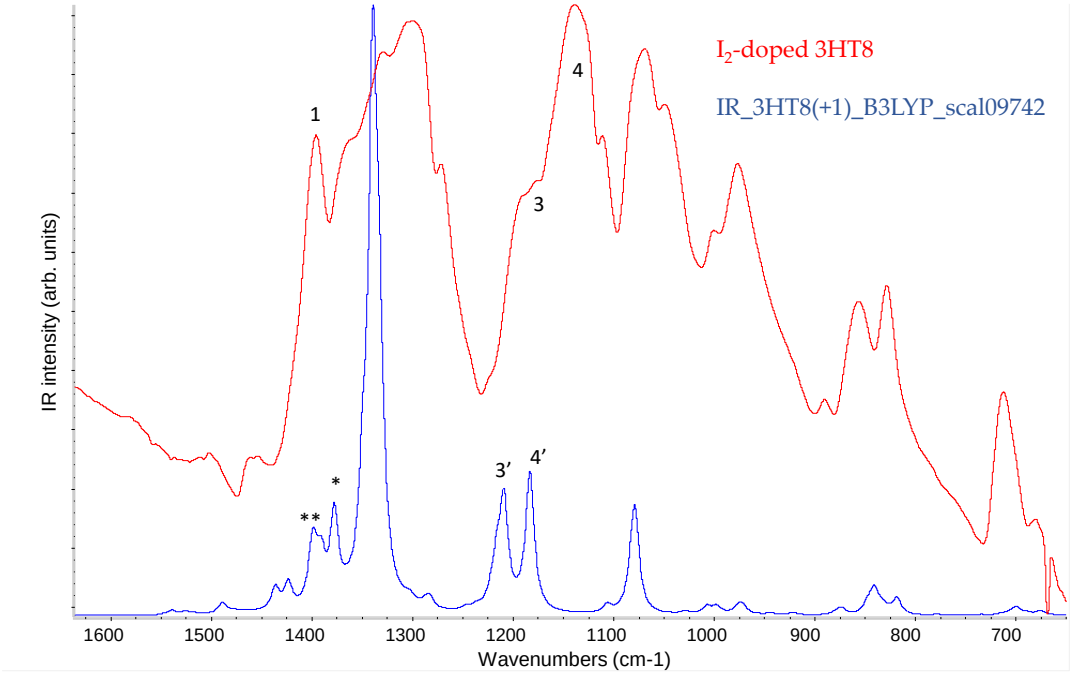

Figure 5.3: B3LYP-calculated IR spectrum of 3HT8(+1) and experimental IR spectrum of I2-doped 3HT8.

Figure 5.3 shows that the DFT simulated IR spectrum of 3HT8(+1) presents the same peaks pattern of the IR spectrum of I_2-doped 3HT8 registered experimentally. This result is of crucial importance because it demonstrates that the model we obtained from quantum-chemical calculations is in good agreement with the experimental results. Some observations are needed:

1) The peak with frequency around 700 cm^{-1}, the doublet with frequency slightly above 800 cm^{-1} and the slightly below 1000 cm^{-1} peak of the calculated spectrum appear to have a too small intensity with the respect the corresponding peaks, maybe because the IR intensity of the most intense IRAV peaks is overestimated by the computation.
2) The doublet with frequency around 1200 cm^{-1}, labelled as 3 and 4 respectively presents a quite large frequency blueshift with respect the corresponding peaks in the experimental spectrum, labelled as 3′ and 4′; in particular:
   - $\Delta\nu = \nu_{3'} - \nu_3 = 1210 - 1193 = 17$ cm^{-1}
   - $\Delta\nu = \nu_{4'} - \nu_4 = 1183 - 1140 = 43$ cm^{-1}
3) The calculated most intense IRAV peak appears very sharp with respect to the one obtained experimentally, that is broader and structured: this is partially due to the small band width (FWHM =10 cm-1) arbitrarily selected for the theoretical spectra. It is possible to tune properly this parameter in order to make the spectrum to better resemble the experimental one, but we prefer to

adopt the usual procedure, with a common fixed FWHM value for all the IR bands. Interestingly, if one considers in detail the DFT predicted IR transition one finds that the strong peak hides other components very close in frequency, which could be related to the presence of shoulders on the profile of the experimental band.

4) The peak with frequency around 1400 cm^{-1} of the experimental IR spectrum of 3HT8, labelled with 1, could be tentatively assigned to the one of the simulated spectrum labelled with **, at least because they coincide in frequency. This analysis needs further confirmation for two relevant reasons:
   - The structure of the peak: in the experimental spectrum, the peak is sharp and intense, moreover it presents the same features in all the analysed samples: for instance, look the IR spectrum of 3HT8 and P3HT reported in Figure 5.1. In the case of the simulated spectrum of 3HT8(+1), the peak is much less intense, moreover longer model molecules show an evolution of the pattern in the region of the experimental band #1 (see discussion below).
   - If we increase the band width parameter of the calculated spectrum, it is reasonable to think that the two peaks labelled as * and ** would be incorporated in the most intense IRAV peak to make it more structured, such that it would resemble the experimental structured broad band.

   For these reasons, the assignment of a precise peak of the simulated spectrum to the experimental peak with frequency 1396 cm^{-1} (peak 1) is not clear from the comparison with the B3LYP-calculated spectrum of 3HT8(+1).

To solve this problem, we consider the B3LYP-calculated spectrum of 3ET12(+1), already presented in Figure 5.2, because we know it has a sharp peak with higher frequency than the one of the most intense IRAV; in Figure 5.4 we compare it with the reference experimental spectrum of I_2-doped 3HT8.

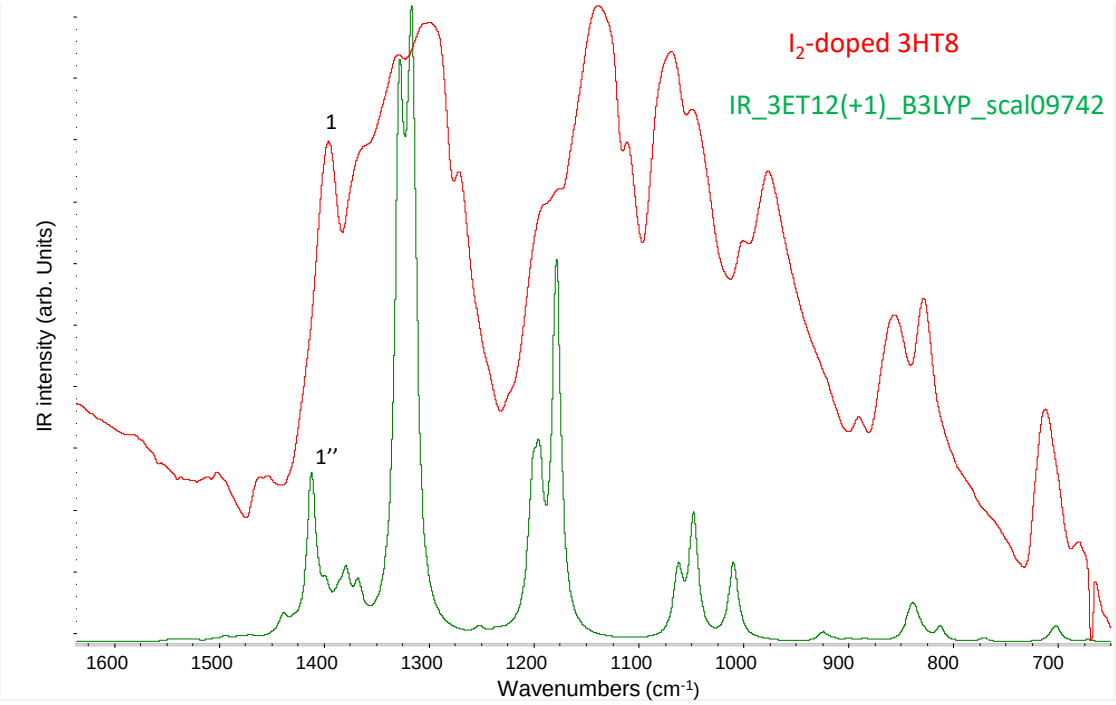

Figure 5.4: B3LYP-calculated IR spectrum of 3ET12(+1) and experimental IR spectrum of I2-doped 3HT8.

Applying the 0,9742-scaling factor to the calculated peaks frequencies of 3ET12(+1), we notice that the peak with frequency slightly higher than 1400 cm^{-1} has a very similar wavenumber value of the one of the experimental 1 peak: we can safely associate the peak 1 of the experimental spectrum of doped 3HT8 and the 1'' peak of the simulated IR spectrum of 3ET12(+1). The eigenvector of the 1412 cm^{-1} normal mode associated to the 1'' peak, whose unscaled frequency is 1450 cm^{-1}, is reported in Figure 5.5.

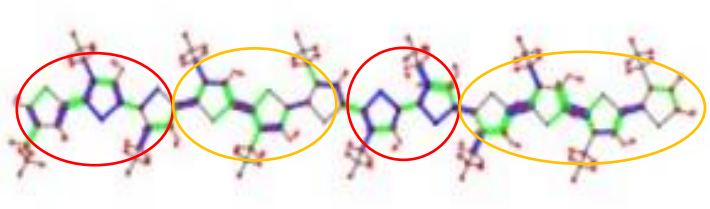

Figure 5.5: sketch of the eigenvector of the normal mode associated to the 1412 cm-1 (unscaled 1450) peak of the B3LYP-calculated IR spectrum of 3ET12(+1).

The normal mode can be ascribed as an ECC-like vibration with three nodes: the phase changes sign four times, as indicated by the coloured circles in Figure 5.6. The major contribution to the vibration comes from the more peripheral thiophene units, thus from the less perturbed regions of the molecule upon doping, as depicted by the presence of thicker blue and green segments for the CC bonds. The peripheral character of the considered ECC-like normal mode can be the explanation of the fact that the sharp intense 1 peak is observed in the experimental spectrum of doped 3HT8 but not in the spectrum of the model of the same molecule. In particular, this aspect confirms the over-delocalization of the polaronic defect induced by the DFT calculation run with B3LYP: the charged defect results to be spread all over almost the whole octamer, while in the dodecamer a larger unperturbed region affects - with a non-negligible contribution - the dynamics of the system, thus explaining why its IR spectrum does present the sharp intense 1'' peak.

The three nodes of the considered ECC-like normal mode can be better understood by analysing the analogous model of the unsubstituted oligothiophene (T12(+1)), due to the higher symmetry of the molecule, belonging to C_{2h} point group: in fact, a similar peak (□ peak) can be observed even in the IR spectrum of T12(+1) close in frequency to the 1450 cm^{-1} peak of the 3ET12(+1) model. In Figure 5.6 we compare the B3LYP-calculated IR spectrum of T12(+1) and of 3ET12(+1) (first panel) and we report also the eigenvector of the normal mode of T12(+1) we are analysing (second panel).

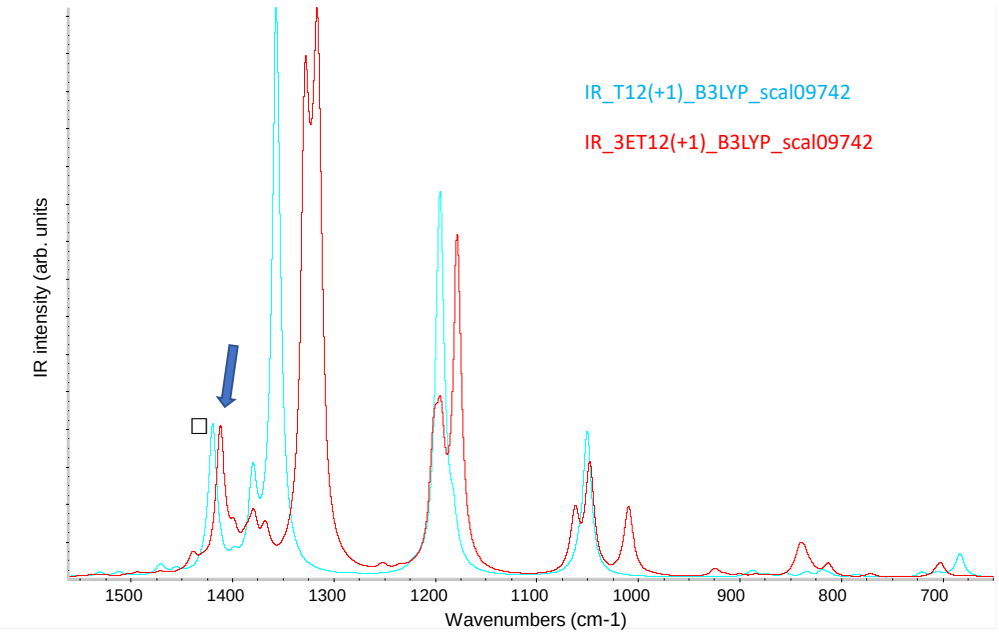

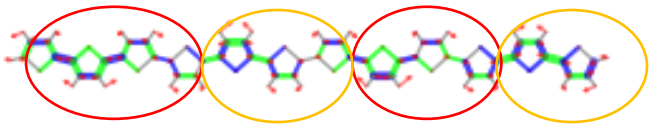

Figure 5.6: top panel: B3LYP-calculated IR spectrum of T12(+1) and 3ET12(+1). Bottom panel: sketch of the eigenvector of the normal mode associated to the 1'' peak.

In Figure 5.7 we report the experimental IR spectrum of doped 3HT8 with the two B3LYP-calculated spectra of 3HT8(+1) and 3ET12(+1), in which the nine most relevant peaks are numbered according to the following notation:

- Numbers (without apex) for the experimental result.
- Numbers with a prime for the IR peaks of 3HT8(+1).
- Numbers with two primes for the IR peaks of 3ET12(+1).

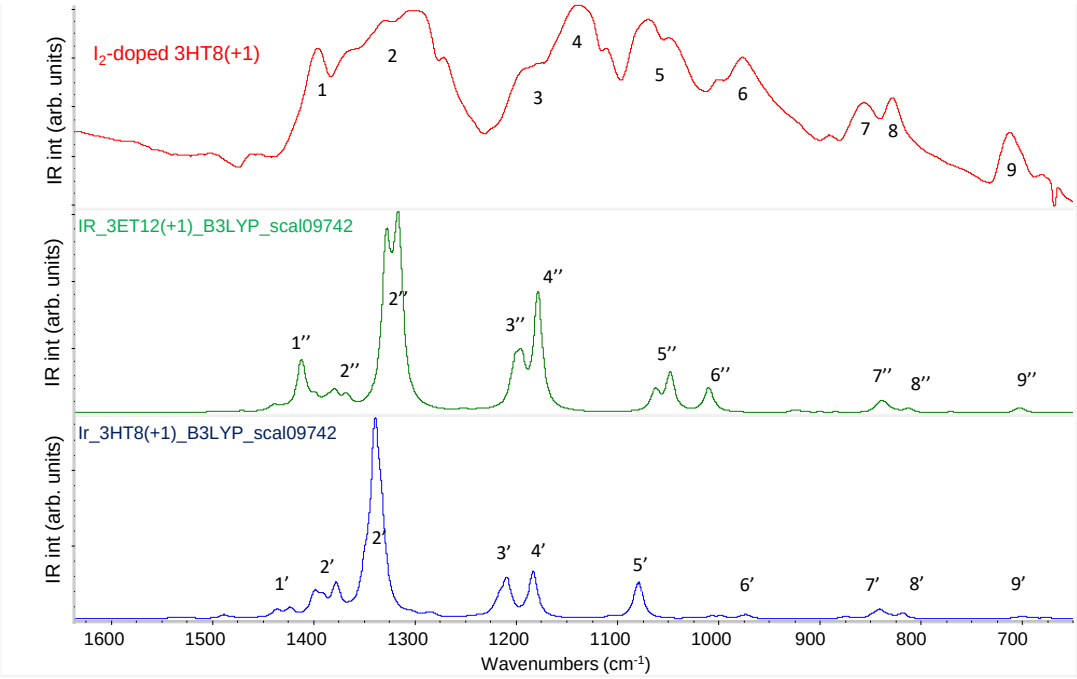

Figure 5.7: from the top to the bottom: experimental IR spectrum of I2-doped 3HT8; B3LYP-calculated IR spectrum of 3ET12(+1); B3LYP-calculated IR spectrum of 3HT8(+1).

Focusing on the 3HT8(+1) model, we are sure to assign number 1' to the 1424 cm^{-1} peak, whose unscaled frequency is 1461 cm^{-1}, because the eigenvector of its associated normal mode resembles the one of peak 1'' of the 3ET12(+1) model, as it is shown in Figure 5.8.

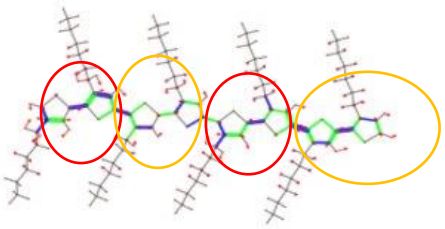

Figure 5.8: sketch of the eigenvector of the normal mode associated to the 1'' peak in the IR spectrum of 3HT8(+1).

From Figure 5.8 it is clear that the eigenvector shows a less well-defined ECC-like character than the eigenvector of the corresponding normal mode in the 3ET12(+1) model, thus explaining why the 1' peak in the IR spectrum of 3HT8(+1) is so weak in intensity.

Knowing that the main contribution to the normal mode generating the peak 1 comes from the more peripheral thiophene units, we tried to develop a model of 3HT8(+1) able to better describe the unperturbed peripheral regions, such that the IR spectrum correctly predicts the sharp intense peak 1 without increasing the number of thiophene units. To achieve this goal, the model 3HT8(+1) was implemented with the so-called hybrid approach: the geometry optimization is performed with CAM-B3LYP, which is known to predict more localized charge defect (see Section 3.3), while the B3LYP is used for the simulation of the spectroscopic features. The spectrum is reported in Figure 5.9, together with the IR experimental spectrum and the one of 3HT8(+1) obtained with B3LYP.

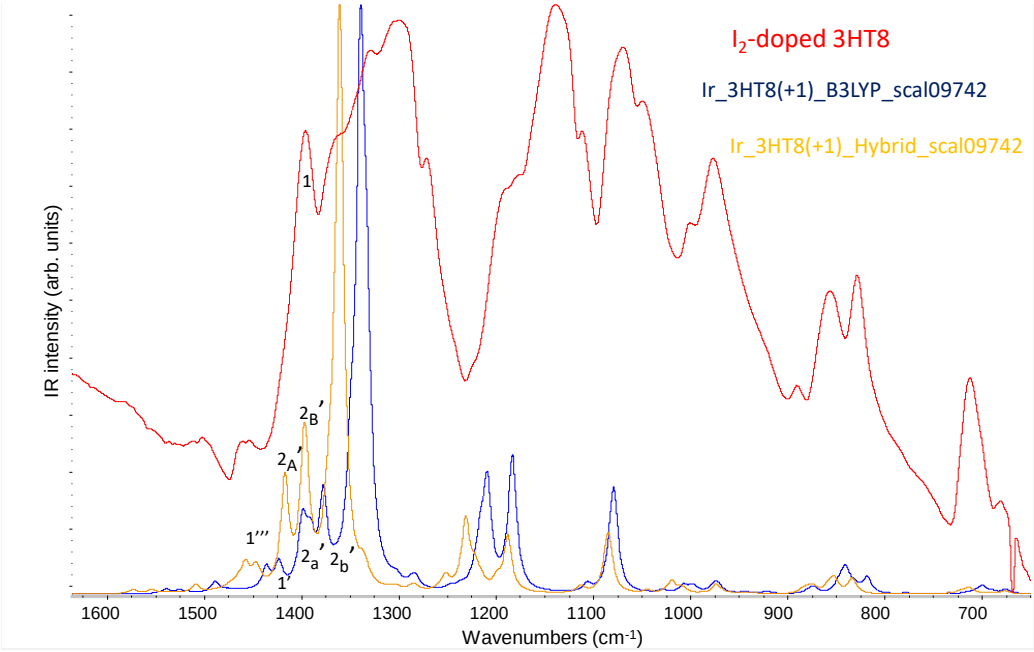

Figure 5.9: experimental IR spectrum of doped 3HT8 and simulated IR spectrum of 3HT8(+1) with B3LYP and hybrid approach.

The effect of the hybrid approach is to induce a blue-shift of the frequency of the main ECC-like IRAVs peaks because of a less delocalization of the π electrons, and of the polaron along the backbone due to the use of CAM-B3LYP range-separated functional for the geometry optimization procedure. However, the correction in terms of geometry induced by CAM-B3LYP is not sufficient to correct the IR spectrum of 3HT8(+1): the sharp and intense 1 peak of the experimental spectrum of doped 3HT8 does not find in the calculated spectrum a correspondent peak with the same features, thus confirming that the model of the octamer of (3-hexyl thiophene) is not sufficiently long to properly describe the contribution of the unperturbed peripheral regions of the backbone to the dynamics of the system. This conclusion is confirmed by the comparison of the eigenvectors of peaks labelled as 1′, 2_a′ and 2_b′ and as 1‴, 2_A′ and 2_B′ in the B3LYP-3HT8(+1) and in the hybrid-3HT8(+1) models respectively: 1′ and 1‴ peaks have very similar normal modes, as well as 2_a′ and 2_A′, and 2_b′ and 2_B′. From this we can deduce that the 1 peak in the experimental spectrum corresponds to the peak labelled as 1‴ in the IR spectrum of the hybrid model of 3HT8(+1), which shows the same normal mode of 1′ peak in the B3LYP model (already assigned to the 1 peak): the description offered by the B3LYP corrected with CAM-B3LYP from the geometrical point of view does not improve the one obtained by B3LYP, used for both the geometry optimization and the frequencies calculation. In Figure 5.10 we report the sketch of the eigenvector of the normal modes associated to the 1‴, 2_A′ and 2_B′ peaks (left panels) and to the 1′, 2_a′ and 2_b′ peaks (right panels).

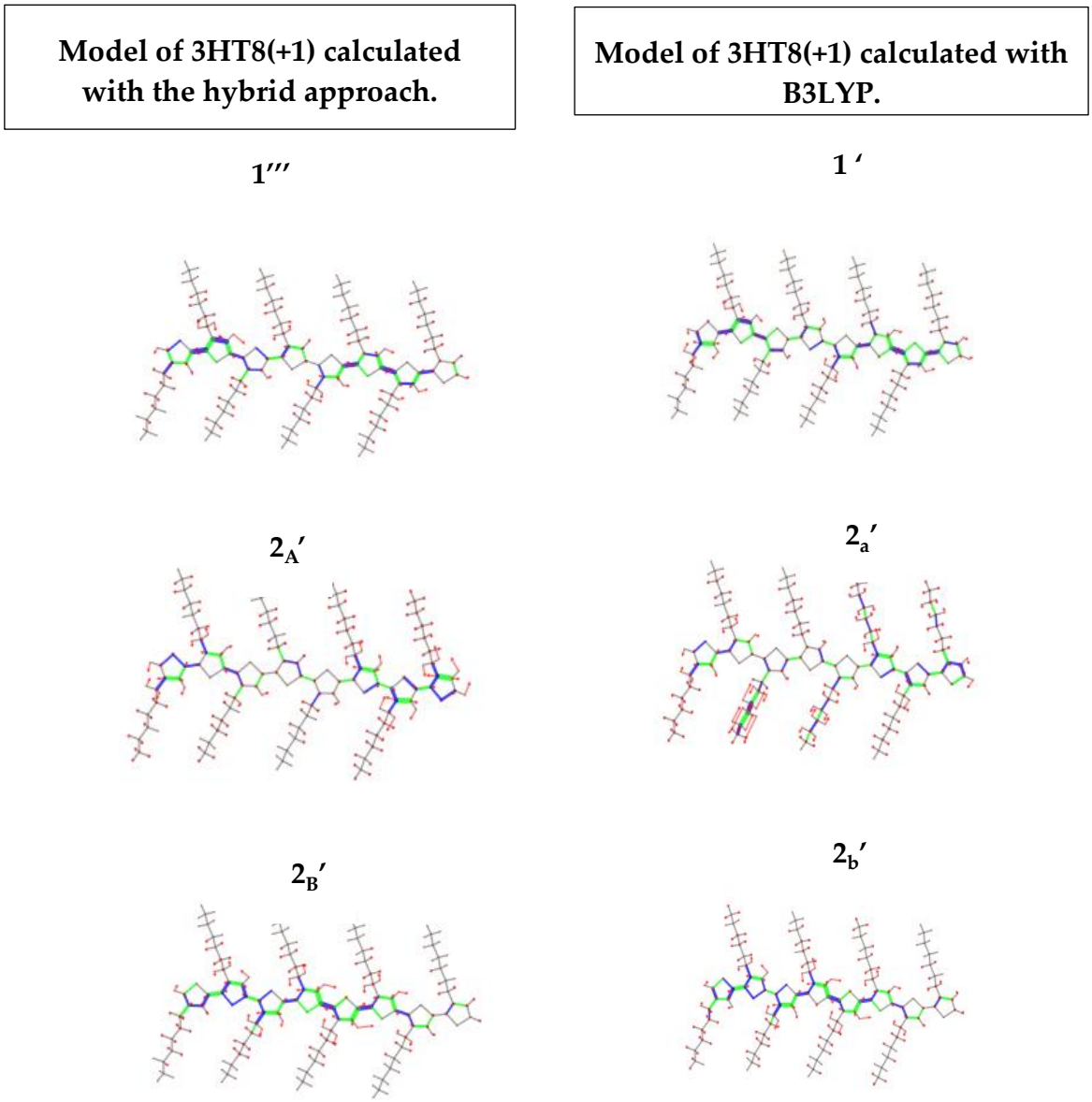

Figure 5.10: sketch of the eigenvector of the normal modes associated to1''', 2A' and 2B' peaks of the IR spectrum of 3HT8(+1) obtained with the hybrid approach (left panels) and to 1', 2a' and 2b' peaks of the IR spectrum of 3HT8(+1) obtained with B3LYP (right panels)

We conclude this Section presenting in Figure 5.11 the comparison between the experimental IR spectrum of I_2-doped P3HT and the spectrum of all the models of alkyl-substituted oligothiophenes we obtained by quantum-chemical simulation, exploiting different oligomer chain length, different alkyl substituents chain length and different functionals. We consider only the IRAVs spectral region from 1000 to 1500 cm^{-1}.

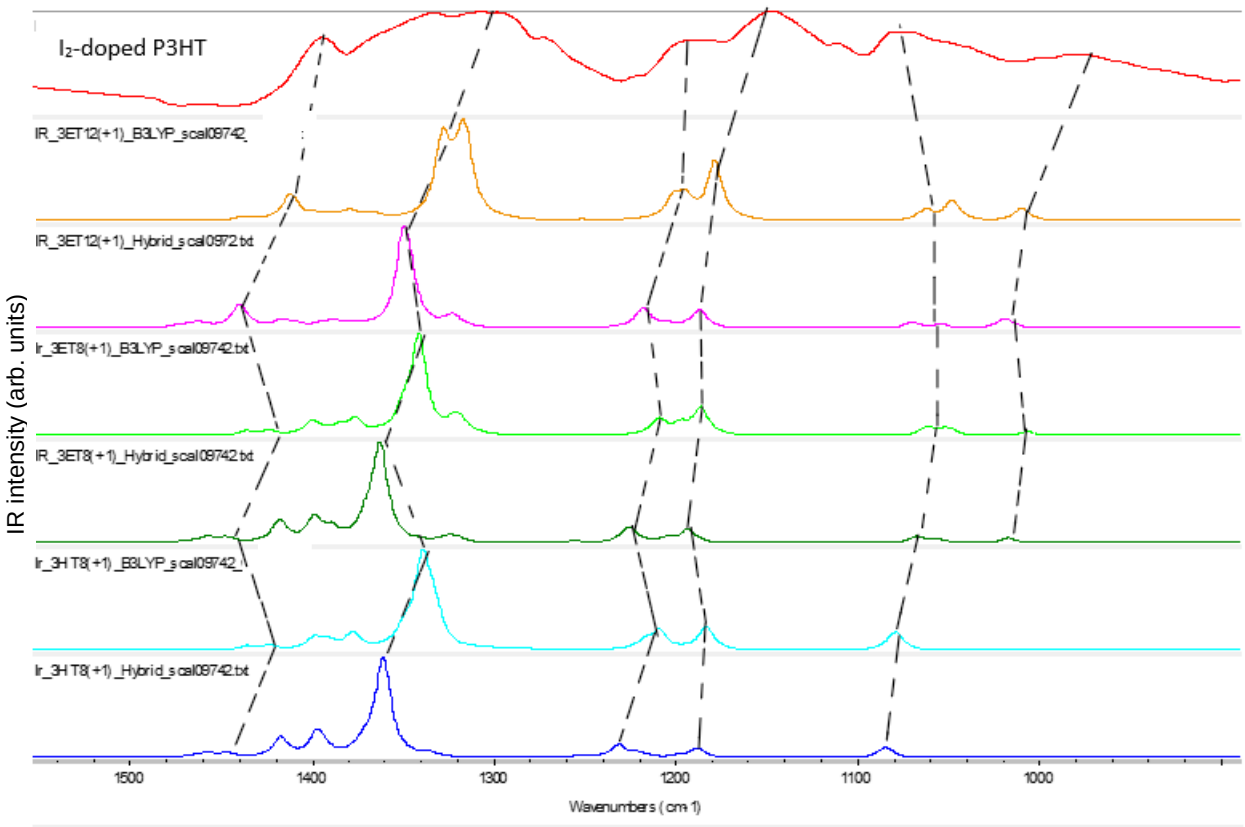

Figure 5.11: IR spectrum of I2-doped P3HT and simulated IR spectrum of alkyl-substituted oligothiophenes.

Two foundamental observations can be obtained from Figure 5.11:

1) The long model of the dodecamer of (3-ethyl thiophene) (yellow and pink spectra) is the model which better mimic P3HT from the IR spectroscopic point of view: its IR spectrum precisely reproduces in terms of frequency and intensity all the most intense peaks of the experimental spectrum of the I_2-doped polymer.
2) The IR spectra of all the alkyl-substituted oligothiophenes obtained by quantum-chemical simulations are characterized by the same most relevant peaks observable in the experimental spectrum. Indeed, we have demonstrated that the bands we observe in the IR spectrum are exactly the IR spectroscopic fingerprints, i.e. the IRAVs, of P3HT after being subjected to the doping process. We have also shown that IRAVs and their activation mechanism are indipendent on the model molecule we choose for the DFT simulations: this means that they are not an artifact of the calculation, but they constitute the IR spectroscopic markers of the polaron formed into P3HT upon doping.

5.2. Raman spectra

In Figure 5.12 we compare the experimental Raman spectrum of I_2-doped P3HT with the Raman spectrum of the charged species obtained by DFT simulations, namely the B3LYP-calculated 3HT8(+1).

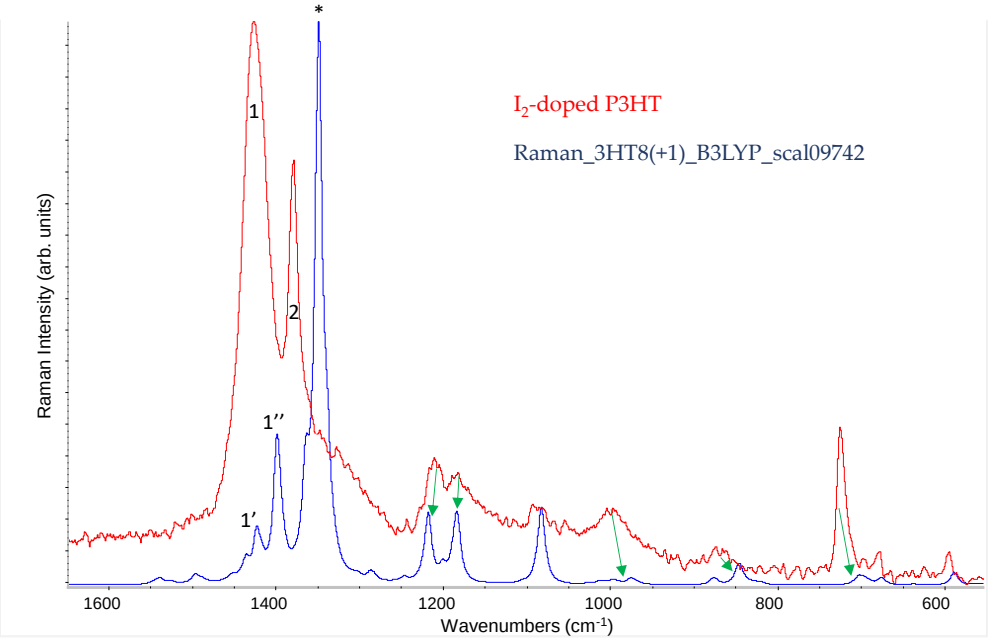

Figure 5.12: experimental Raman spectrum of I2-doped P3HT and B3LYP-calculated Raman spectrum of 3HT8(+1).

A first observation from Figure 5.12 is that the bands of the experimental spectrum in the wavenumber region between 600 and 1200 cm^{-1} are correctly predicted by the calculated spectrum of 3HT8(+1): the one-to-one correspondence is indicated in Figure 5.12 by green arrows.

The important differences between the experimental and simulated Raman spectra regard the high-wavenumber spectral region, from 1300 to 1500 cm^{-1}. In this region, the experimental Raman spectrum of I_2-doped P3HT presents two main bands, labelled as 1 and 2 with frequency 1427 cm^{-1} and 1380 cm^{-1} respectively; band 1 is constituted by at least two components. The calculated spectrum of 3HT8(+1) exhibits three main bands: the first two, with frequency 1423 cm^{-1} (unscaled frequency: 1461 cm^{-1}) and 1399 cm^{-1} (unscaled frequency: 1437 cm^{-1}), labelled as 1' and 1'', the third one, labelled with *, has frequency 1349 cm^{-1} (unscaled frequency: 1385 cm^{-1}) and it is the most intense peak of the spectrum. For our discussion, it is useful to recall in Figure 5.13 the sketch of the eigenvectors of the normal modes associated to peaks 1',1'' and *.

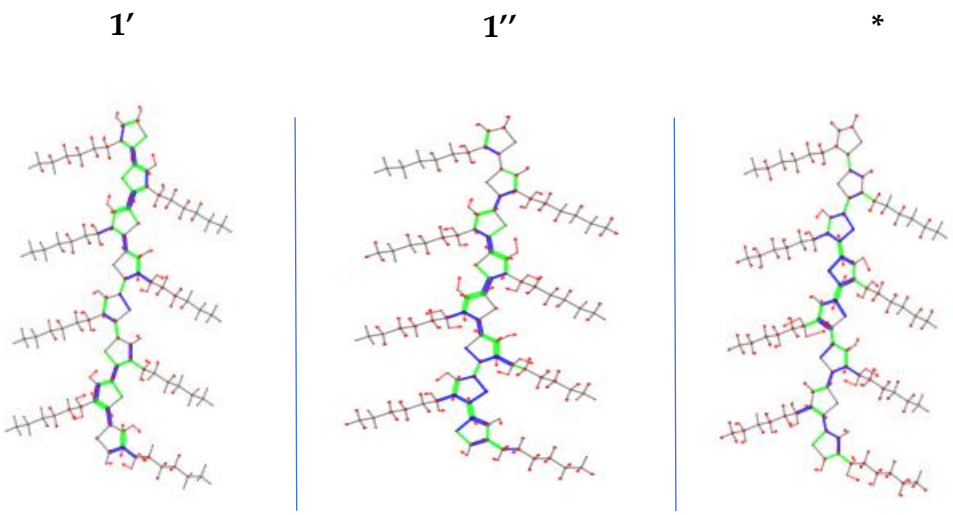

Figure 5.13: sketch of the eigenvector of the normal mode associated to the 1′, 1′′ and * peaks in the B3LYP-calculated Raman spectrum of 3HT8(+1).

The three normal modes are all ECC-like vibrations with two nodes, but with a fundamental difference: the normal mode of the most intense Raman peak (the * peak) is more localized in the central perturbed region of the charged oligomer and the peripheral thiophene units are parctically not involved in the vibration; on the contrary, the greatest contribution to the normal modes asssociated to peaks 1′ and 1′′ comes from the unperturbed thiophene rings (especially the one associated to peak 1′) or at least it comes from similar contributions from the peripheral units and the central region of the molecule (peak 1′′). In other words, the most intense Raman normal mode of 3HT8(+1) mainly describes the ECC vibration of the most perturbed rings belonging to the polaron, which self-localizes in the central region of the alkyl-substituted oligothiophene, while the normal modes associated to peaks 1′ and 1′′ mainly describe the ECC oscillation of the less perturped peripheral thiophene units, that are affected in some ways by the presence of the charged defect in the adjacent rings. In this regard, it is useful to recall that the trend of the local Raman parameters provide a clear indication of the presence of three differently perturbed regions in the molecule, showing a systematic reversal of the sign of the $\frac{\partial \alpha}{\partial R}$ parameters at the boundary between a more aromatic-like structure of the peripheral rings and a more quinoidal strucure in the inner region.

In Figure 5.14 we report the experimental Raman spectrum of pristine P3HT and of the doped polymer.

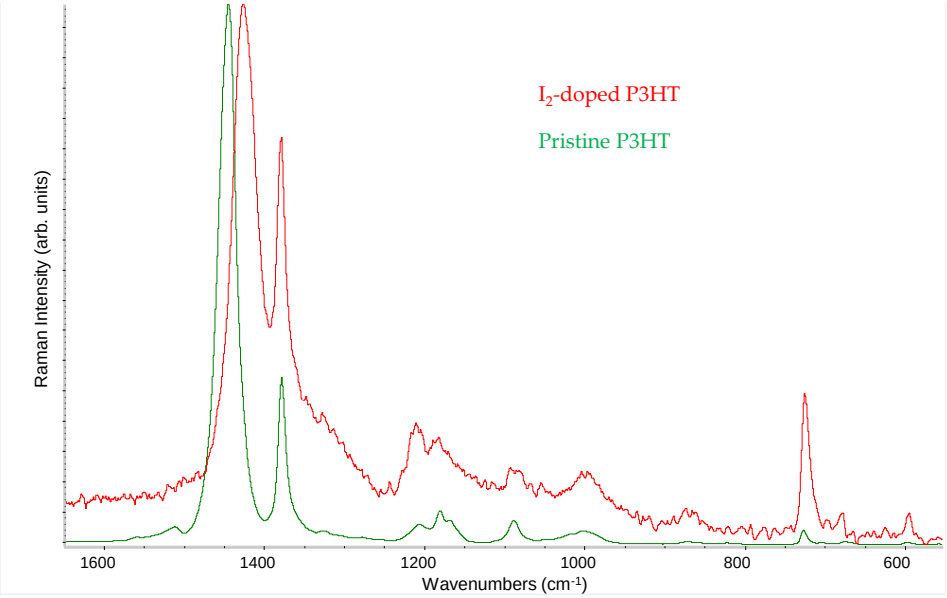

Figure 5.14: experimental Raman spectrum of pristine and doped P3HT.

From Figure 5.14 it is possible to notice that the Raman spectrum of pristine and doped P3HT presents the same patterns with two most relevant peaks, which are the ones labelled as 1 and 2 in Figure 5.12. When P3HT passes from the pristine to the doped state, the peak 1 undergoes a red-shift in frequency and broadens, while the band 2 remains stable and with constant frequency. Moreover, a large, rather weak component arises on the lower wavenumber side of band 2. This clarifies that the Raman spectrum of doped P3HT only slightly changes with respect to the one of the pristine polymer, at difference from the DFT prediction.

To assign a peak of the calculated spectrum of 3HT8(+1) to peak 2 of the experimental spectrum, it is possible to analyse the eigenvector of the corresponding peak of the Raman spectrum of neutral 3HT8 and then find in the calculated spectrum of 3HT8(+1) the normal mode having a very similar eigenvector. Moreover, if the assumption according to which the frequency of peak 2 practically does not change upon doping, as it is clear from Figure 5.14, is valid also for the simulated spectra, the peak we are looking for in the spectrum of 3HT8(+1) should exhibit the same wavenumber of the second intense peak in the spectrum of the neutral 3HT8 molecule. To complete the peaks assignment, we report in Figure 5.15 the experimental Raman spectra of neutral and pristine P3HT and the B3LYP-simulated spectra of 3HT8 and 3HT8(+1) in the wavenumber region of interest (1200-1600 cm^{-1}).

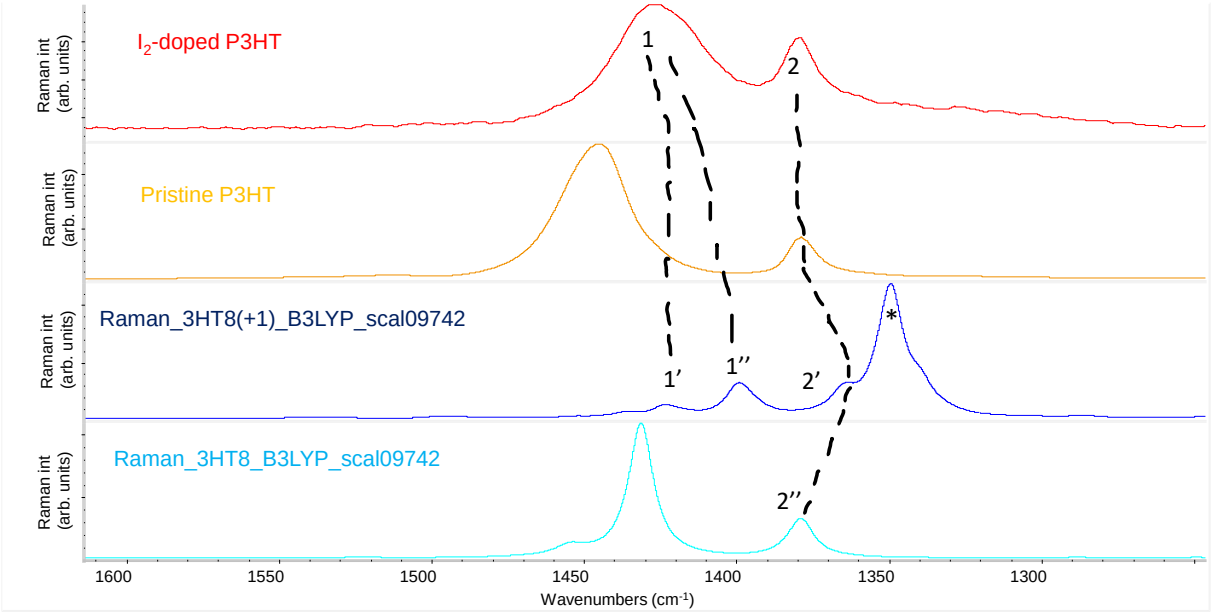

Figure 5.15: experimental Raman spectra of pristine and doped P3HT and B3LYP-calculated Raman spectra of 3HT8 and 3HT8(+1).

According to Figure 5.15, the peak in the simulated Raman spectrum of 3HT8(+1) with the most similar frequency to peak 2 in the experimental spectrum of doped P3HT is the one labelled as 2′. To verify that peak 2′ corresponds to peak 2, we need to check that eigenvector of its associated normal mode is the same or at least highly related to the one associated to peak 2′′ in the calculated spectrum of 3HT8. The sketch of the eigenvector of the normal mode associated to peaks 2′ and 2′′ are reported in Figure 5.16 on the left and right panels respectively.

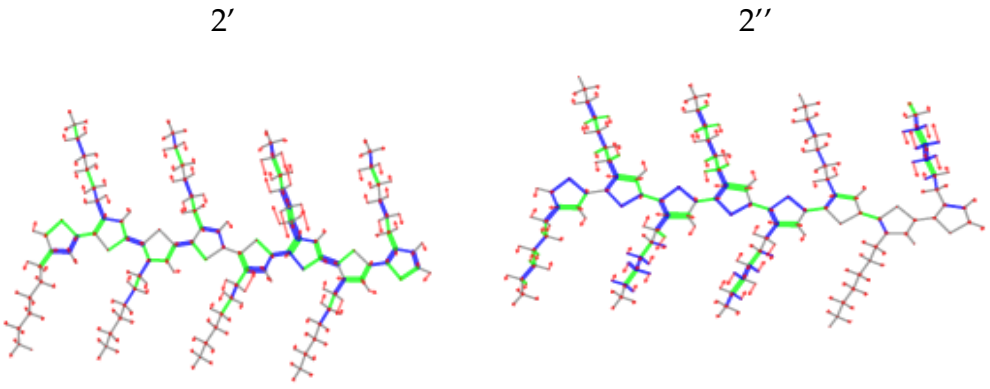

Figure 5.16: sketch of the eigenvector of the normal mode associated to peaks 2′ and 2′′.

The two eigenvectors show several analogies: in both cases, the inter-ring CC bonds vibrate almost in phase and with most of the quasi-single CC bonds of the thiophene rings; moreover, the lateral hexyl chains, which provide a large contribution to the vibration, are coupled with

the backbone through the first CC bond, that typically vibrates out-of-phase with respect to the quasi-single CC bonds of the rings.

The eigenvectors analysis allows to correctly assign peak 2 of the experimental Raman spectrum of doped P3HT to peak 2' in the simulated spectrum of 3HT8(+1). The consequence of this choice is that we can safely individuate peaks 1' and 1'' as the two components that constitute the broad, structured band 1 in the experimental spectrum.

We now focus on the most intense peak of the calculated Raman spectrum of 3HT8(+1), labelled with *, which does not find any correspondence in terms of either frequency or intensity with the experimental spectrum of doped P3HT. In fact, the B3LYP calculation predicts its frequency to very low wavenumbers with respect the most intense peaks of the experimental spectrum, which are already assigned to the calculated peaks 1', 1'' and 2'. For what concerns the strong peak *, it could be tentatively assigned to the broad feature in the experimental spectrum, marked with the arrow in figure 5.14. However, the DFT simulation of 3HT8(+1) dramatically overestimates its Raman intensity: indeed, it is the strongest band of the spectrum, with Raman activity of $4{,}47 \cdot 10^6$ A^4/amu, while the activity of the peaks 1', 1'' and 2' are $3{,}97 \cdot 10^5$ A^4/amu, $1{,}11 \cdot 10^6$ A^4/amu and $4{,}18 \cdot 10^5$ A^4/amu respectively. From these considerations, we can deduct that the peak *, which describes an ECC-like vibration mainly localized on the central highly perturbed region of the oligothiophene, is an artifact of the quantum-chemical calculation and so not observable (or observable with a totally different intensity) in the experimental spectrum of doped P3HT. Thanks to:

A) the eigenvector analysis and the assignment of the structured experimental peak 1 to peaks 1' and 1'', whose normal modes are vibrations involving peripheral thiophene units,
B) The stability in frequency of peaks 2 when P3HT passes from the pristine to the doped state,
C) The correspondence of the Raman spectra of neutral and doped P3HT, except for the frequency red-shift of peak 1,

we can conclude that Raman experiment essentially detects the ECC-like vibrations of the slightly perturbed thiophene units, namely of the rings adjacent to the highly perturbed thiophene units in the inner region of the polaron, while the vibration of the central thiophene rings has much less relevance in the experimental spectrum. The mechanism of the activation of the most intense predicted Raman band, which has not a similar counterpart in the experimental spectrum of doped P3HT, is rationalized by means of the Raman local parameters $\partial\alpha/\partial R$: they show a signs pattern coherent with the phase inversion of the ECC-like vibration of the normal mode associated to the peak *, as it is shown in Figure 5.17. Moreover, the highest values of the $\partial\alpha/\partial R$ parameters are the ones dealing with the CC bonds of the central region, where the geometry distortion of the polaron mainly self-localizes upon the doping process, thus

explaining the extremely high intensity of the normal mode associated to the peak *. This analysis suggests that Raman spectroscopy is extremely sensitive to local variations induced by the doping process: in particular, it is possible that the discrepancies between theory and experiment come from the fact that the quantum-chemical simulations over-estimate the Raman local parameters of the inner most perturbed region of the charged alkyl-substituted oligothiophene. In this regard we can notice that the $\partial\alpha/\partial R$ parameters describe the central thiophene rings as a quinoid structure, while the calculated geometry presents more equalized quasi-single and quasi-double CC bonds, without reaching a "sign reversal" of the BLA.

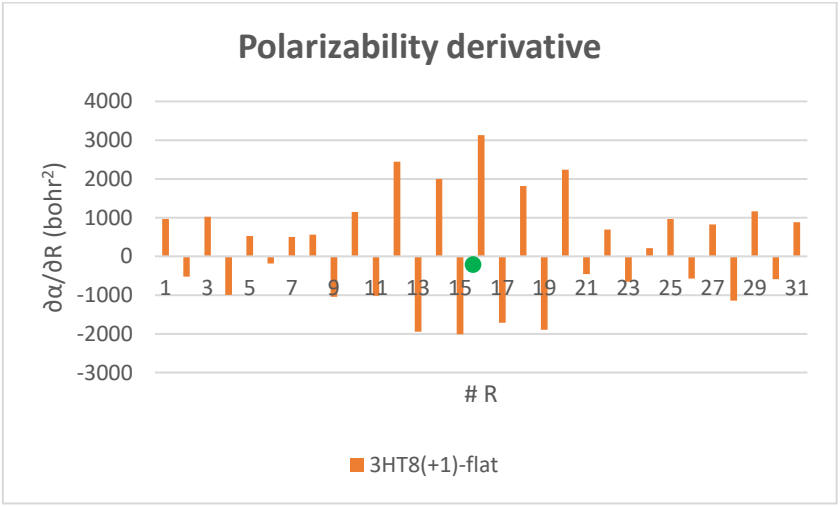

Figure 5.17: comparison between the eigenvector associate to the most intense Raman peak of 3HT8(+1) and the local Raman parameters of 3HT8(+1).

To try amending the discrepancy between the B3LYP-calculated Raman spectrum of 3HT8(+1) and the experimental one of I_2-doped P3HT, we have considered also different molecular models and functionals in order to increase the contribution of the unperturbed regions of the backbone; in particular, we considered the dodecamer of (3-ethyl thiophene) to increase the chain length, and thus increasing the number of the

peripheral less perturbed rings, computed with B3LYP and the hybrid approach (geometry optimization with CAM-B3LYP and frequencies calculation with B3LYP) to reduce the polaron over-delocalization, typical of B3LYP. In addition, the octamer of (3-hexyl thiophene) and of (3-ethyl thiophene) have been studied with the hybrid approach. In Figure 5.18 we report the reference experimental Raman spectrum, the B3LYP-calculated spectrum of 3HT8(+1) and the Raman spectra we obtained for all the different models in the wavenumber region between 1000 and 1700 cm^{-1}.

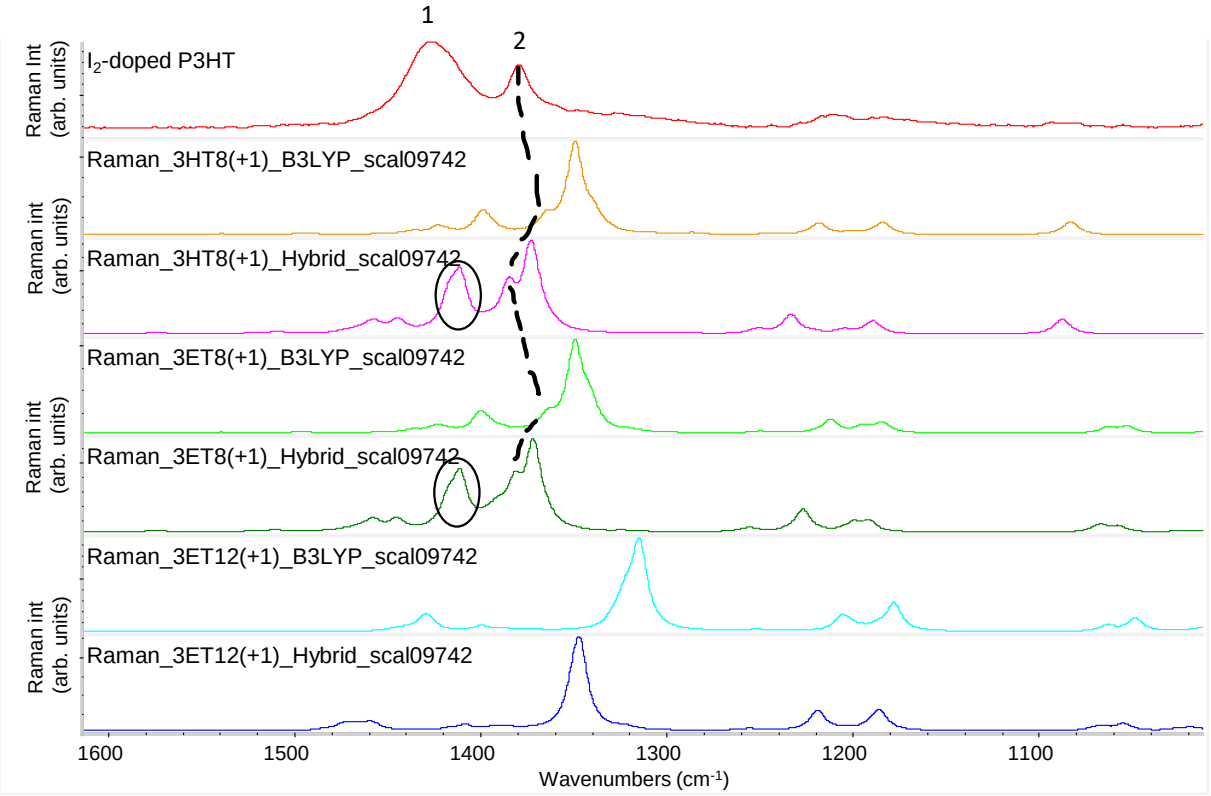

Figure 5.18: Raman spectrum of I2-doped P3HT and simulated Raman spectrum of alkyl-substituted oligothiophenes.

From Figure 5.18, we can notice that all the DFT models present similar RAVs peaks pattern, with the most intense Raman normal mode, whose eigenvector is the ECC-like vibration mostly localized in the central perturbed region of the alkyl-substituted oligothiophene: this confirms the main problem previously presented, which is not solved either using a range-separated functional like CAM-B3LYP to limit the polaron delocalization length or increasing the number of thiophene units of the backbone. Actually, in longer models (3ET12(+1)) the result is even worse, since we register a higher frequency red-shift of the most intense peak, probably caused by an excessive over-delocalization of the charged defect, partially mitigated by the hybrid approach. This conclusion confirms that the most intense peak of the simulated Raman spectra is an artifact of quantum-chemical calculations and not detectable by the experimental

Raman spectroscopy. Even though the RAVs pattern is similar for all the studied models, some important differences can be noticed:

1) The corresponding band of peak 1 of the experimental spectrum, according to the Hybrid models of 3HT8(+1) and 3ET8(+1) presents a high intensity and a more structured nature, (the band is indicated by a black circle in Figure 5.18), thus better mimicking the experimental datum. This aspect, however, cannot be observed in dodecamer models (see blue and light-blue spectra), probably because of the so high intensity of the peak * that the ECC-like normal modes mostly localized on the peripheral units appear negligible.
2) The peak 2 in the experimental spectrum, which is stable when the polymer passes from the pristine to doped state, find correspondence in the calculated Raman spectra of the octamers models, but it seems to vanish (or at least to lose some relevance) in the spectrum of the longer oligomer.

These results show that the DFT simulation of the Raman spectrum of charged species is very complicated and that it is necessary to tune all the parameters of the quantum-chemical calculations in an extremely fine way to fit the experimental data. From the results obtained by all the DFT simulations we exploited, we can state that the calculation of Raman spectrum of charged oligothiophenes remains an open problem, which has to be further investigated with more refined models, that are able to take into account at least phenomena like the interaction of the oligothiophene with the dopant counter-ion. In addition, the Raman resonance effect and the intermolecular interactions with the other polymeric chains that are present in the real material should be considered.

5.3. A possible solution to the problems regarding the calculated Raman spectra: DFT simulation with the dopant counterion.

In order to solve the problems related to the simulation of the Raman spectrum of charged species, we tried to develop a molecular model which takes into account the interaction between the oligothiophene and the dopant counterion. The very preliminary molecular model we developed is constituted by an octamer of (3-ethyl thiophene), indicated as 3ET8(+1), interacting with a Cl_3^- anion. It is important to underline that the one we present here is a preliminary study of the effect of the counterion on the vibrational spectra, thus the suitability of this kind of calculations should be quite low for several reasons:

1) We used the Cl_3^- anion, while the doping process of P3HT is performed with Iodine.
2) We located the counterion over the central CC bond of the oligomer at an approximate distance of 4Å, without checking if the effect of the anion changes if its position varies.
3) No constraints on the chain conformation were imposed during the geometry optimization procedure, thus the oligothiophene is subjected to an important distortion, while the molecular models previously presented were characterized by a constrained flat geometry.

We decide to compare the same molecular model, 3ET8(+1), without and with the counterion and in both cases the hybrid approach was exploited, thus meaning that the geometry optimization is performed at CAM-B3LYP level, while the frequencies calculation at the B3LYP level. The same scaling factor of 0,9742 is applied for the spectra of both models.

In Figure 5.19 we report the simulated Raman spectrum of the isolated 3ET8(+1) and the one of the 3ET8(+1)/Cl_3^- anion dimer.

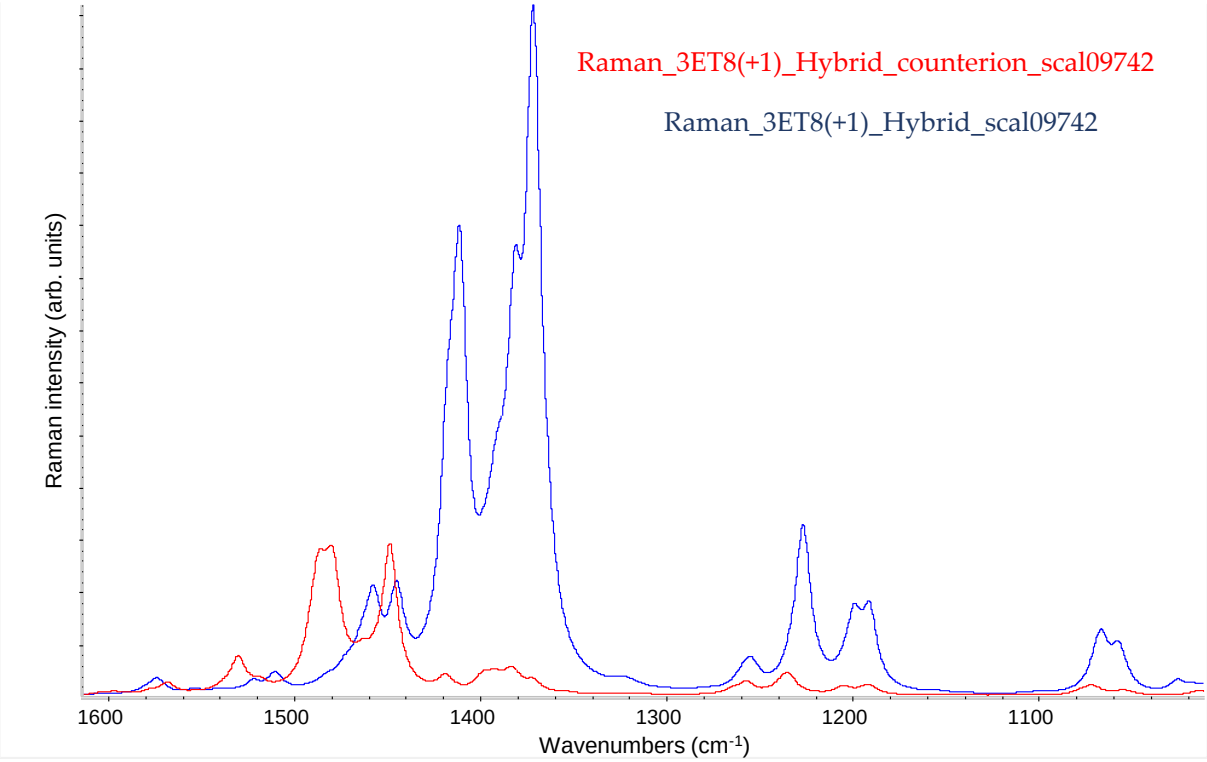

Figure 5.19: experimental Raman spectrum of I2-doped P3HT and calculated Raman spectrum of 3ET8(+1) with and without counterion.

1) The calculation with counterion induces a frequency blue-shift of the most intense peaks with respect to the ones estimated by the computation of the isolated molecule.
2) The Raman intensity of the most relevant peaks is strongly decreased.

Both effects are positive because they seem to solve the main problem concerning the simulation of the Raman spectrum of charged oligothiophene, related to the appearance of a band characterized by low frequency and extremely high intensity, which does not find any correspondence with the experimental Raman spectrum of I_2-doped P3HT. In order to verify the better agreement of the simulated Raman spectrum of 3ET8(+1) with the counterion with respect to the corresponding model of the isolated molecule with the experimental result, the analysis of the eigenvectors of the normal modes associated to the most intense Raman peaks is needed: their sketches are reported in Figure 5.20, from the one associated to the 1449 cm^{-1} peak (1487 cm^{-1} in the unscaled version of the spectrum) to the ones associated to the 1481 and 1486 cm^{-1} peaks (around 1520 cm^{-1} in the unscaled version of the spectrum).

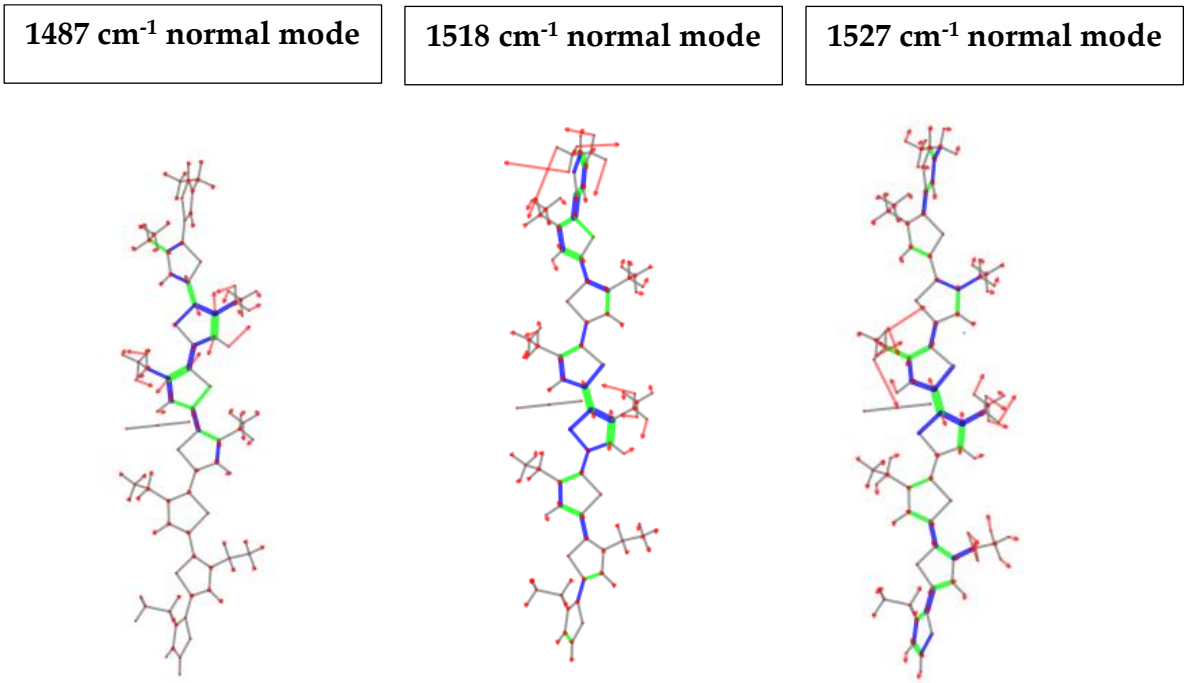

Figure 5.20: sketch of the eigenvectors of the normal modes associated to the most intense peaks of the Raman spectrum of 3ET8(+) with the counterion.

As it can be noticed from Figure 5.20, the eigenvectors of the most intense Raman normal modes show partial ECC- like character, but they are very localized on small regions of the oligothiophene, probably due to the presence of the counterion and especially to the distorted geometry, which does not allow collective vibrations. For

this reason, the eigenvector analysis is complicated, thus confirming the limits of the 3ET8(+1)/counterion dimer molecular model. Even though the proper assignment of the calculated peaks to the experimental ones cannot be obtained by this kind of computations, it is important to remark that the insertion of the dopant counterion into the DFT simulation represents a promising approach to solve the anomalies observed in the calculation of the Raman spectrum of charged species: in fact the extremely high intensity and low frequency Raman peak predicted by all the models of isolated oligothiophenes does not appear in the Raman spectrum of 3ET8(+1) with the counterion.

The better description of the Raman spectrum of 3ET8(+1) with the counterion with respect to the one provided by the molecular model of isolated oligothiophenes is rationalized considering the local Raman parameters, which are reported in Figure 5.21. As it will be shown by the figure, the $\partial\alpha/\partial R$ parameters present smaller values in the case with counterion and this is especially true for the central CC bonds: this explains why the very intense normal mode describing the ECC-like vibration of the central perturbed region, corresponding to the dominant Raman feature of isolated 3ET8(+1), does not appear or at least appears with a much more modest intensity in the Raman spectrum of 3ET8(+1) with the dopant counterion.

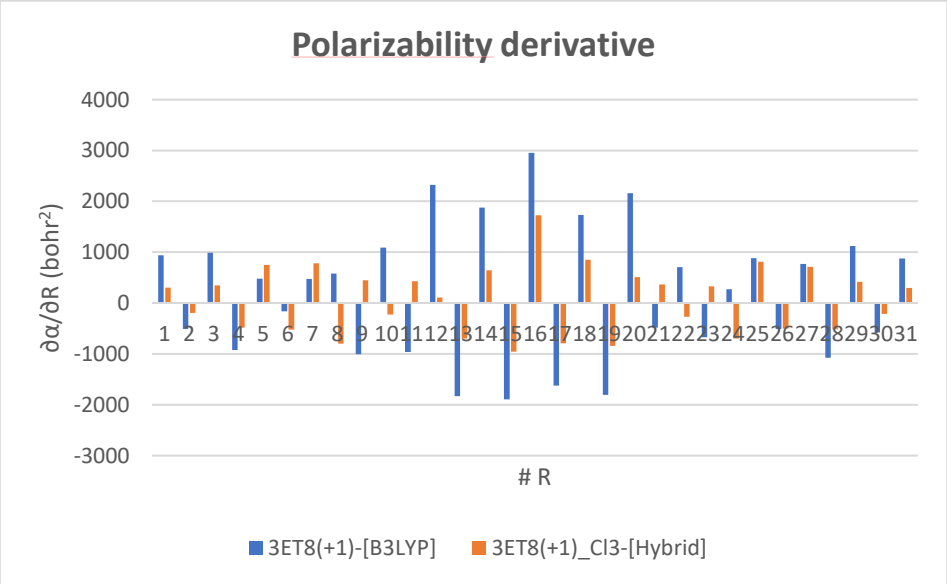

Figure 5.21: Raman local parameters of 3ET8(+1) with and without counterion

Moreover, the molecular model with the presence of the counterion seems to be a promising approach for the resolution of the relevant problems related to the use of CAM-B3LYP for the prediction of the IRAVs of charged oligothiophenes, that it predicts IR spectra characterised by an extremely high intensity and a very large and

unphysical frequency red-shift of the main ECC band (recall Section 3.3). In Figure 5.22 we report the CAM-B3LYP- simulated spectrum of 3ET8(+1) in the molecular model with and without the counterion.

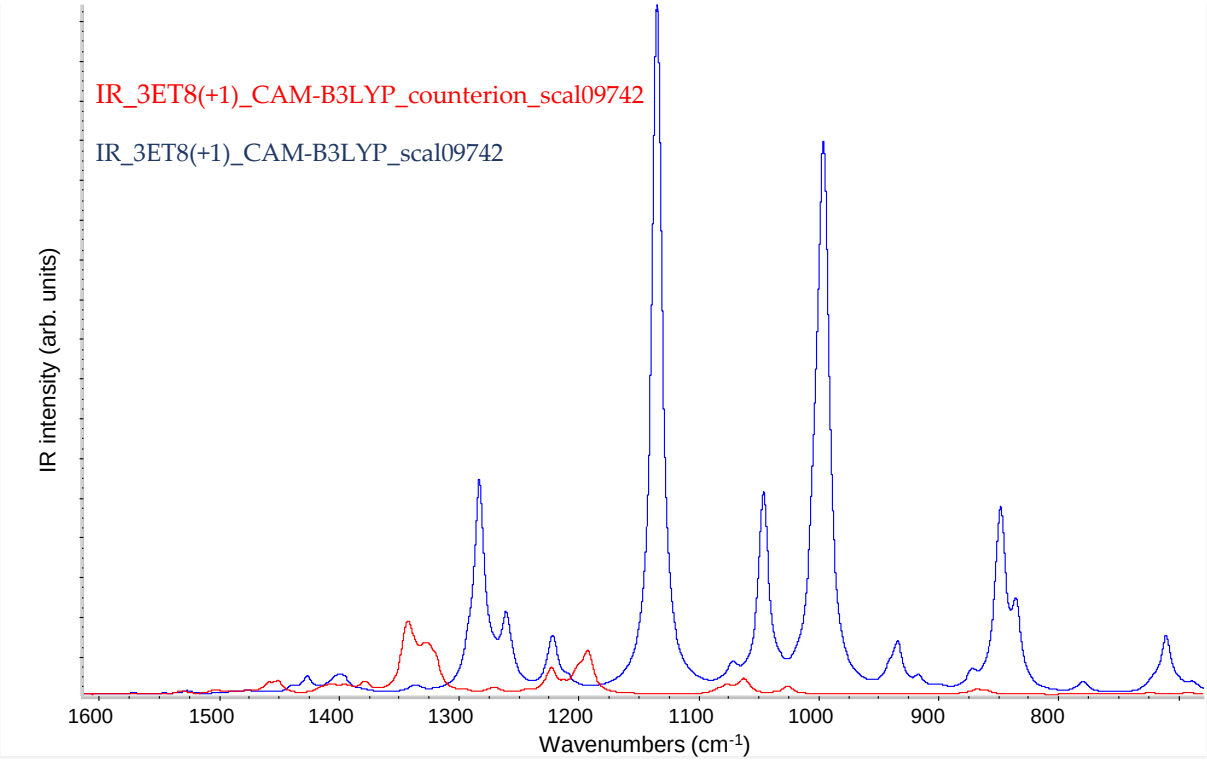

Figure 5.22: CAM-B3LYP-calculated IR spectrum of 3ET8(+1) with and without counterion.

Figure 5.22 suggests that the hybrid approach (geometry optimization at CAM-B3LYP level and frequencies calculation at B3LYP level), introduced to solve the issues of the CAM-B3LYP functional, could be unnecessary if a proper molecular model constituted by the charged oligothiophene and the dopant counterion is used in the quantum-chemical calculation.

6 Conclusion and future developments

This Thesis deals with the application of Density Functional Theory (DFT) for the quantum-chemical prediction and for the analysis of the vibrational spectroscopic response of poly(3-hexyl thiophene) (P3HT), when it undergoes a chemical doping process. DFT simulations are used to interpret the IR and Raman spectra of doped P3HT, by means of the modelling of isolated molecules (oligomers) mimicking the structure and the properties of the polymer.

Firstly, an analysis of the spectroscopic features of unsubstituted oligothiophenes of different chain lengths, in their neutral and charged (radical cation) electronic state is presented.

Quantum-chemical calculations nicely reproduce the well-known vibrational spectra of neutral (pristine) oligothiophenes and polymer: the Raman spectrum is dominated by a very intense peak, whose associated normal mode can be ascribed to the collective ECC (Effective Conjugation Coordinate) vibration, while the IR spectrum does not present a similar feature. Indeed, in the case of unsubstituted planar oligothiophenes the ECC mode is silent in the IR spectrum, according to the mutual exclusion principle of IR and Raman activity of a normal mode for molecules characterized by an inversion centre.

DFT calculations were then performed to study the vibrational spectra of charged unsubstituted oligothiophenes after the extraction of a single electron from the oligomer, mimicking the charged defect, i.e., the so-called polaron. The main results obtained by the analysis of the quantum-chemical calculations of charged oligothiophenes can be summarized as follows:

1) All molecular models present an IR spectrum characterized by the same pattern, that is constituted by four intense bands. These IR bands are however silent or barely silent in the IR spectrum of oligothiophenes in their neutral state. The computed intense IR bands refer to the so-called IRAVs, thus meaning Infrared Activated Vibrations. IRAVs are the IR spectroscopic fingerprints of the polaron.
2) The Raman spectrum of charged oligothiophenes present intense peaks which are inactive in the Raman spectrum when the oligomer is in the neutral state and for this reason, they can be considered the Raman spectroscopic evidence of the polaron formation within the oligomeric chain upon doping. These new

strong Raman bands are defined as RAVs, meaning Raman Activated Vibrations.

3) The analysis of the IR local parameters, namely the dipole derivative with respect to the internal CC bond stretching coordinate $\left(\frac{\partial M}{\partial R}\right)$, and of the eigenvectors of the IRAVs allows the full rationalization of the activation mechanisms and of the very high intensity of the IRAVs upon charging. IR local parameters of charged species exhibit a systematic alternation of positive and negative values with respect to those of the corresponding neutral species: this explains the onset of IRAVs upon doping, because the charged electronic state shows large IR activity for the alternating stretching and shrinking of the CC bonds, namely for ECC-like modes. IRAVs are indeed ECC-like normal modes with CC bond stretching and shrinking that is coherent with the sign pattern as shown by the $\frac{\partial M}{\partial R}$ parameters. Moreover, the absolute values of the IR local parameters for charged oligothiophenes are higher than those of neutral oligomers, thus explaining the large IR intensity of IRAVs.
4) Same considerations of point 3) are valid for the simulated RAVs, which are fully rationalized by means of the Raman local parameters, namely the polarizability derivative with respect to the internal CC bond stretching coordinate $\left(\frac{\partial \alpha}{\partial R}\right)$ parameters, leading to high intensities.
5) The Raman local parameters also allow the characterization of the molecular structure of the polaron, giving information on its delocalization length in terms of thiophene units and on its structure, predicted as quinoid. This result is then compared with the variation of the BLA (Bond Length Alternation), defined as the bond length difference between two adjacent CC bonds, induced by charging the structure, highlighting that the central perturbed region of the oligothiophene backbone presents equalized quasi-single and quasi-double CC bonds. This result suggests that the Raman local parameters related to the defected central region are over-estimated by the quantum-chemical calculations and that the quinoid structure of the polaron is excessively emphasized.

Besides the assignment and full rationalization of the IR and Raman spectra of pristine and doped oligothiophenes, DFT simulations revealed also the effect of the oligomeric chain length, considering oligothiophenes with increasing number of thiophene rings, from six to fourteen.

DFT simulations demonstrate the sensitivity of the ECC normal modes to the conjugation length: the higher the π electrons delocalization the lower is the vibrational frequency of the ECC mode, thus supporting the rationalization offered by the ECC theory. Furthermore, a high conjugation length means also a more effective

electron-phonon coupling, thus explaining the increasing IR and Raman intensity passing from short to long oligomers.

Focusing on the most intense IRAV, it was demonstrated that its frequency dispersion and intensity increasing with the oligomer length approach plateau values starting from the molecular model of the oligothiophene consisting of twelve rings. This result is in contrast with the experimental evidences, which show unchanged IR pattern already for a doped octamer. This aspect proves the intrinsic limits of the quantum-chemical calculations, related in this case to the over-delocalization effects induced by the DFT method.

The effect of different functionals on the vibrational spectra and on the geometrical parameters of the charged oligothiophenes was analysed. The exploited functionals are the hybrid B3LYP and the range-separated CAM-B3LYP, highlighting advantages and disadvantages:

a) B3LYP correctly predicts the IR and Raman spectra of charged oligothiophenes, although it induces an excessive over-delocalization of the charged defect: the spatial extent of the polaron, in fact, continuously increases by increasing the number of thiophene units.
b) CAM-B3LYP limits the polaron over-delocalization (namely the self-interaction error), however the IRAVs result to be extremely high in intensity and characterized by an unphysical red-shifted frequency towards very low wavenumbers. Also the RAVs are predicted with a very large Raman activity.

CAM-B3LYP resulted to be not suitable for the simulation of the IR and Raman spectra of charged oligothiophenes. A solution to this problem was proposed by adopting the so-called hybrid approach for the DFT simulations, which combines the positive aspects of both functionals: the geometry optimization procedure is performed at CAM-B3LYP level, while the IR and Raman frequencies/intensities at B3LYP level.

The second part of this Thesis is dedicated to the quantum-chemical calculations of molecular models of neutral and charged alkyl-substituted oligothiophenes.

A comparison between the IR and Raman spectra of unsubstituted oligothiophenes and of the corresponding hexyl-substituted oligomers is presented. Focusing on the charged species, the main result is that IRAVs and RAVs patterns are only barely affected by the presence of the lateral alkyl chains, even though they are characterized by a higher number of active vibrations due to the dynamic coupling of the alkyl chains with the molecular backbone.

Importantly, the IRAVs and RAVs activation mechanisms is the same described for the unsubstituted oligothiophenes, namely the occurrence of these features does not depend on the symmetry of the system but only on the charged state of the system.

The same conclusion can be obtained even by changing the lateral alkyl chains from hexyl to ethyl substituents. The discussed results demonstrate that the IRAVs and RAVs constitute the IR and Raman spectroscopic fingerprints of the polaron, regardless the molecular model adopted.

Finally, a comparison between the DFT calculated IR and Raman spectra of hexyl-substituted oligothiophenes and the experimentally doped P3HT is presented.

The simulated IR spectrum of the octamer of (3-hexyl thiophene) shows good a agreement with the experimental results. The IRAVs pattern is properly predicted: the interpretation of the IR spectrum of doped P3HT as the signature of the polaron is corroborated by the results of DFT calculations.

On the contrary, the simulated Raman spectra predict the most intense RAV peak with a very high intensity and low frequency, such that it does not find correspondence with the main peaks of the experimental Raman spectrum of doped P3HT.

These results show that a good DFT simulation of the Raman spectrum of charged species is a difficult task and either empirical procedure or high level of theory should be considered in order to reproduce the experimental data. A preliminary study pointing in this direction is proposed, namely considering molecular models constituted by the charged oligothiophene in the presence of a dopant counterion: promising results were obtained, and the calculated IR and Raman spectra better resemble the experimental data.

Future developments.

The main purpose of this Thesis, thus the rationalization of the onset of IRAVs and RAVs of P3HT and the molecular characterization of the polaron through its vibration, is achieved. However, further work has still to be done to obtain a complete knowledge of the vibrational and structural properties of doped polythiophenes, and to resolve the open problem of DFT simulation of the Raman spectrum of charged species.

Two main development lines can be followed:

1) Refinement of the DFT calculations for the study of the polaronic states, such that they can take into account the intermolecular interactions occurring in real systems. The main strategies are:
    - Development of a molecular model of the dimer constituted by the charged oligothiophene and the dopant counterion in order to mimic the electrostatic interaction between them. The proper selection of the counterion, the control of its position and the imposition of a constrained flat geometry to the oligothiophene backbone are the fundamental parameters to take into account.
    - Development of a periodic 1-D model of the (doped) polymer chain, in order to avoid effects of the ends and size confinement typical of the

oligomers. In addition, calculations on a suitably modelled 3D crystal structure could include the interaction between neighbour polymeric chains of the crystalline domains of P3HT. DFT calculations at solid state, namely including the periodic boundary conditions, will be executed with the code Crystal17.

- Use of quantum-chemical approaches (like Time-Dependent-DFT approaches) able to simulate the resonance Raman effect in the calculation of the Raman spectra of charged oligothiophenes.

2) Study of the structural, electronic and vibrational properties of different charged defects, e. g. with reference to the bipolaronic state, which occurs when two charges are injected (or extracted) into the polymer. Doubly charged species can exist as singlet or in the triplet state: DFT calculations must take into account these aspects and for this reason they will deserve a deep quantum-chemical investigation.

The above presented future perspectives are the main, but not unique, possibilities. New challenges in the application of novel quantum chemistry approaches to doped π-conjugated materials will arise in the future and they will require the development of new computational tools.

Bibliography

[1] Skotheim, T. A., (ed.). Handbook of Conducting Polymers, (Dekker, New York), 1986.

[2] Brédas, J. L.; Silbey, R, (eds.). Conjugated Polymers: The Novel Science and Technology of Highly Conducting and Nonlinear Optically Active Materials, (Springer Netherlands), 1991.

[3] Zhao, X.; Zhan, X. Electron Transporting Semiconducting Polymers in Organic Electronics. Chem. Soc. Rev. 2011, 40, 3728–3743.

[4] Wood, S.; Hollis, J.R.; Kim, J-S. Raman spectroscopy as an advanced structural nanoprobe for conjugated molecular semiconductors. J. Phys. D: Appl. Phys. 2017, 50, 073001.

[5] Denti, I.; Cimò, S.; Brambilla, L.; Milani, A.; Bertarelli, C.; Tommasini, M.; Castiglioni, C. Polaron Confinement in n-Doped P(NDI2OD-T2) Unveiled by Vibrational Spectroscopy. Chem. Mater. 2019, 31, 6726-6739.

[6] Zhao, W.; Ding, J.; Zou, Y.; Di, C.A.; Zhu, D. Chemical Doping of Organic Semiconductors for Thermoelectric Applications. Chem. Soc. Rev. 2020, 49, 7210–7228.

[7] Lüssem, B.; Keum, C.M.; Kasemann, D.; Naab, B.; Bao, Z.; Leo, K. Doped Organic Transistors. Chem. Rev. 2016, 116, 13714–13751.

[8] Takeda, N.; Miller, J.R. Poly(3-decylthiophene) Radical Anions and Cations in Solution: Single and Multiple Polarons and Their Delocalization Lengths in Conjugated Polymers. J. Phys. Chem. B 2012, 116, 14715-14723

[9] Louarn, G.; Trznadel, M.; Buisson, J.P.; Laska, J.; Pron, A.; Lapkowski, M.; Lefrant, S. Raman Spectroscopic Studies of Regioregular Poly(3-alkylthiophenes). *J. Phys. Chem.* 1996, *100*, 12532-12539.

[10] Kaloni, T.P.; Giesbrecht, P.K.; Schreckenbach, G.; Freund, M.S. Polythiophene: From Fundamental Perspectives to Applications. Chem. Mater. 2017, 29, 10248–10283

[11] Harrison, M.G.; Friend, R.H., (Eds: K. Müllen, G. Wegner). Electronic Materials: The Oligomer Approach, Vol. 198, (Wiley-VCH, Weinheim, Germany 515).

[12] Perepichka, I.F., (Eds. J. F. Perepichka, D. F. Perepichka). Handbook of Thiophene Based Materials: Applications in Organic Electronics and Photonics, (John Wiley & Sons Ltd. Chichester, U.K.), 2009.

[13] Zerbi, G.; Gussoni, M.; Castiglioni, C. Vibrational Spectroscopy of Polyconjugated Aromatic Materials with Electrical Non-Linear Properties. In Conjugated Polymers: The Novel Science and Technology of Highly Conducting and Nonlinear Optically Active Materials (Eds. Brédas, J.L., Silbey, R.). (Springer: Dordrecht, The Netherlands), 1991; p. 435; Hernandez, V. ; Castiglioni, C. ; Del Zoppo, M.; Zerbi, G. Confinement potential and π-electron delocalization in polyconjugated organic materials, Phys. Rev. B 1994, 9815.

[14] Tashiro, K.; Kobayashi, M.; Kawai, T.; Yoshino, K. Crystal Structural Change in Poly(3-Alkyl Thiophene)s Induced by Iodine Doping as Studied by an Organized Combination of X-Ray Diffraction, Infrared/Raman Spectroscopy and Computer Simulation Techniques. Polymer (Guildf) 1997, 38, 2867–2879.

[15] Brambilla, L.; Tommasini, M.; Botiz, I.; Rahimi, K.; Agumba, J.O.; Stingelin, N.; Zerbi, G. Regio-Regular Oligo and Poly(3-HexylThiophene): Precise Structural Markers from the Vibrational Spectra of Oligomer Single Crystals. Macromolecules 2014, 47, 6730–6739.

[16] Brambilla, L.; Capel Ferrón, C.; Tommasini, M.; Hong, K.; López Navarrete, J.T.; Hernández, V.; Zerbi, G. Infrared and Multi-Wavelength Raman Spectroscopy of Regio-Regular P3HT and Its Deutero Derivatives. J. Raman Spectrosc. 2018, 49, 569–580.

[17] Buono, A.; Sun,N.H.; Raos, G.; Gila, L.; Cominetti, A.; Catellani, M.; Meille, S.V. Form II Poly(3-butylthiophene): Crystal Structure and Preferred Orientation in Spherulitic Thin Films. Macromolecules 2010, 43(16), 6772.

[18] Bolognesi, A.; Porzio, W.; Provasoli A.; Comotti, A.; Sozzani, P.; Simonutti, R. Structural and thermal behavior of poly-(3-octylthiophene): A DSC, 13C MAS

NMR, XRD, photoluminescence, and Raman scattering study. Macromol. Chem. Phys. 2001, 202(12), 2586.

[19] Baggioli, A.; Meille, S.V.; Raos, G.; Po, R.; Brinkmann, M.; Famulari, A. Intramolecular CH/π interactions in alkylaromatics: Monomer conformations for poly(3-alkylthiophene) atomistic models. Int. J. Quantum Chem. 2013, 113(18), 2154.

[20] Gussoni, M.; Castiglioni, C.; Zerbi, G. Vibrational spectroscopy of polyconjugated materials: polyacetylene and polyenes. In Clark R J J, Hester R E (eds.), Spectroscopy of advanced materials, (Wiley, New York) 1991, Ch 5, 251-353.

[21] Castiglioni, C.; Tommasini, M.; Zerbi, G. Raman Spectroscopy of Polyconjugated Molecules and Materials: Confinement Effect in One and Two Dimensions, Philos Trans R Soc A 2004, 362, 2425–2459.

[22] Castiglioni, C.; Navarrete, J.T.L.; Zerbi, G.; Gussoni, M. A simple interpretation of the vibrational spectra of undoped, doped and photoexcited polyacetylene: Amplitude mode theory in the GF formalism. Solid State Commun 1988, 65, 625-630.

[23] Mele, E.J.; Rice, M.J. Vibrational excitations of charged solitons in polyacetylene. Phys Rev Lett 1980, 45, 926–929.

[24] Etemad, S.; Pron, A.; Heeger, A.J.; MacDiarmid, A.G.; Mele, E.J.; Rice, M.J. Infrared-active vibrational modes of charged solitons in (CH)x and (CD)x. Phys Rev B 1981, 23, 5137–5141.

[25] Anderson, M.; Ramanan, C.; Fontanesi, C.; Frick, A.; Surana, S.; Cheyns, D.; Furno, M.; Keller, T.; Allard, S.; Scherf, U.; Beljonne, D.; D'Avino, G.; von Hauff, E.; Da Como, E. Displacement of polarons by vibrational modes in doped conjugated polymers, Phys Rev Materials 2017, 1, 055604.

[26] Ehrenfreund, E.; Vardeny, Z.; Brafman, O.; Horovitz, B. Amplitude and phase modes in trans polyacetylene resonant Raman- scattering and induced infrared activity, Phys Rev B 1987, 36, 1535–1553.

[27] Vardeny, Z.; Ehrenfreund, E.; Brafman, O.; Horovitz, B. Resonant Raman Scattering from Amplitude Modes in trans-(CH)x and -(CD)x, Phys Rev Lett, 51(1983)2326-2329.

[28] Painelli, A.; Girlando, A.; Del Freo, L.; Soos, Z.G. Infrared intensity and local vibrations of charged solitons. Phys Rev B 1997, 56, 15100–15108.

[29] Yin, J.; Wang, Z.; Fazzi, D.; Shen, Z.; Soci, C. First-Principles Study of the Nuclear Dynamics of doped conjugated Polymers. J. Phys. Chem. C 2016, 120, 1994-2001.

[30] Castiglioni, C.; Tommasini, M. Infrared Active Vibrations in Doped π-Conjugated Materials: The Mechanism of Activation of Raman Modes. Asian J. Phys. 2022, 31, 14221–1776.

[31] Lopez Navarrete, J.T.; Zerbi, G. Lattice Dynamics and Vibrational Spectra of Polythiophene. I. Oligomers and Polymer. J. Chem. Phys. 1998, 94, 957–964.

[32] Lopez Navarrete, J.T.; Zerbi, G. Lattice Dynamics and Vibrational Spectra of Polythiophene. II. Effective Coordinate Theory, Doping Induced, and Photoexcited Spectra. J. Chem. Phys. 1998, 94, 965–970.

[33] Agosti, E.; Rivola, M.; Hernandez, V.; Del Zoppo, M.; Zerbi, G. Electronic and Dynamical Effects from the Unusual Features of the Raman Spectra of Oligo and Polythiophenes. Synth. Met. 1999, 100, 101–112.

[34] Louarn, G.; Mevellec, J.Y.; Buisson, J.P.; Lefrant, S. Comparison of the Vibrational Properties of Polythiophene and Polyalkylthiophenes. Synth. Met. 1993, 55, 587–592.

[35] Akimoto, M.; Furukawa, Y.; Takeuchi, H.; Harada, I.; Soma, Y.; Soma, M. Correlation between Vibrational Spectra and Electrical Conductivity of Polythiophene. Synth. Met. 1986, 15, 353–360.

[36] Wilson, E.B.; Decius, C.; Cross, P.C. Molecular Vibrations: The Theory of Infrared and Raman Vibrational Spectra, (McGraw-Hill, New York), 1955.

[37] Califano, S. Vibrational States, (Wiley), 1976.

[38] Long, D.A. Raman Spectroscopy, (McGraw-Hill, London), 1980.

[39] Keresztury, G. Raman Spectroscopy: Theory and Instrumentation in Introduction to the Theory and Practice of Vibrational Spectroscopy, Handbook of Vibrational Spectroscopy, (John Wiley & Sons Ltd), 2002.

[40] Born, M; Oppenheimer, J.R. *"Zur Quantentheorie der Molekeln"* [On the Quantum Theory of Molecules]. Annalen der Physik 1927, 389 (20), 457–484.

[41] Szabo, A.; Ostlund, N.S. (Ed. Dover Pubblications, INC) Modern quantum chemistry. Introduction to Advanced Electronic Structure Theory, (Mineola, New York), 1996.

[42] Parr, R.G.; Yang, W. DFT of Atoms and Molecules, Oxford Univ. Press, 1989.

[43] Burke, K. The ABC of DFT, (Irvine), 2007.

[44] Stephens, P.J.; Devlin, F.J.; Chabalowski, C.F.; Frisch, M.J. Ab Initio Calculation of Vibrational Absorption and Circular Dichroism Spectra Using Density Functional Force Fields.

[45] Lee, C.; Yang, W.; Parr, R.G. Development of the Colle-Salvetti Correlation-energy formula into a functional of the electron density. Phys. Rev. B, 1988, 37, 785. The Journal of

Physical Chemistry 1994, 98, 11623.

[46] Vosko, S.H.; Wilk, L.; Nusair, M. Accurate spin-dependent electron liquid correlation energies for local spin density calculations: a critical analysis. Canadian Journal of Physics 1980, 58, 1200.

[47] Yanai, T.; Tew, D.P.; Handy, N.C. A new hybrid exchange–correlation functional using the

Coulomb-attenuating method (CAM-B3LYP). Chemical Physics Letters 2004, 393, 51–57.

[48] Baer, R.; Livshits, E.; Salzner, U. Tuned Range-Separated Hybrids in Density Functional Theory. Annu. Rev. Phys. Chem. 2010, 61, 85–109.

[49] Arrigoni, A.; Brambilla, L.; Castiglioni, C.; Bertarelli, C. Conducting Electrospun Nanofibres: Monitoring of Iodine Doping of P3HT through Infrared (IRAV) and Raman (RaAV) Polaron Spectroscopic Features. Nanomaterials 2022, 12(23), 4308.

[50] Frisch,M.J.; Trucks, G.W.; Schlegel, H.B.; Scuseria, G.E.; Robb, M.A.; Cheeseman, J.R.; Scalmani, G.; Barone, V.; Mennucci, B.; Petersson, G.; Nakatsuji, H.; Caricato, M.; Li, X.; Hratchian, H.P.; Izmaylov, A.F.; Bloino, J.; Zheng, G.; Sonnenberg, J.L.; Hada, M.; Ehara, M.; Toyota, K.; Fukuda, R.; Hasegawa, J.; Ishida, M.; Nakajima, T.; Honda, Y.; Kitao, O.; Nakai, H.; Vreven, T.; Montgomery, J.A.; Peralta, J.E.; Ogliaro, F.; Bearpark, M.; Heyd, J.J.; Brothers, E.; Kudin, K.N.; Staroverov, V.N.; Kobayashi, R.; Normand, J.; Raghavachari,K.; Rendell, A.; Burant, J.C.; Iyengar, S.S.; Tomasi, J.; Cossi, M.; Rega, N.; Millam, J.M.; Klene, M.; Knox, J.E.; Cross, J.B.; Bakken, V.; Adamo, C.; Jaramillo, J.; Gomperts, R.; Stratmann, R.E.; Yazyev, O.; Austin, A.J.; Cammi, R.; Pomelli, C.; Ochterski, J.W.; Martin, R.L.; Morokuma, K.; Zakrzewski, V.G.; Voth, G.A.; Salvador, P.; Dannenberg, J.J.; Dapprich, S.; Daniels, A.D.; Farkas, Ö.; Foresman, J.B.; Ortiz, J.V.; Cioslowski,;J.; Fox, D.J. Gaussian 09, Revision D.01, Gaussian Inc., Wallingford CT 2009.

[51] Zbinden, Infrared Spectroscopy of High Polymers. (Accademic Press, New York), 1964.

[52] Enengl, C.; Enengl, S.; Pluczyk, S.; Havlicek, M.; Lapkowski, M.; Neugebauer, H.; Ehrenfreund, E. Doping-Induced Absorption Bands in P3HT: Polarons and Bipolarons. ChemPhysChem 2016, 17, 3836 – 3844

[53] Brambilla, L.; Kim, J.-S.; Kim, B.J.; Hernandez, V.; Lopez Navarrete, J.T.; Zerbi, G. Poly(3-hexylthiophene-2.5-diyl): Evidence of different polymer chain

conformations in the solid state from a combined study of regioregularity control and Raman spectroscopy. J. Mol. Struct. 2020, 1221, 128882.

[54] Stanfield, D.A.; Wu, Y.; Tolbert, S.H.; Schwartz, B.J. Controlling the Formation of Charge Transfer Complexes in Chemically Doped Semiconducting Polymers. Chem. Mater. 2021, 33, 2343−2356

[55] Yamamoto, J.; Furukawa, Y. Electronic and Vibrational Spectra of Positive Polarons and Bipolarons in Regioregular Poly(3-hexylthiophene) Doped with Ferric Chloride. J. Phys. Chem. B 2015, 119, 4788−4794

[56] Stanfield, D.A.; Mehmedovic, Z.; Schwart, B.J. Vibrational Stark Effect Mapping of Polaron Delocalization in Chemically Doped Conjugated Polymers. *Chem. Mater. 2021, 33, 8489−8500*

[57] Mansour, A.E.; Valencia, A.M.; Lungwitz, D.; Wegner, B.; Tanaka, N.; Shoji, Y.; Fukushima, T.; Opitz, A.; Cocchi, C.; Koch, N. Understanding the evolution of the Raman spectra of molecularly p-doped poly(3-hexylthiophene-2,5-diyl): signatures of polarons and bipolarons. Phys. Chem. Chem. Phys. 2022, 24, 3109.

List of Figures

List of Tables

Acknowledgments

Il traguardo della laurea in Ingegneria dei materiali e delle nanotecnologie è per me motivo di vero orgoglio e di felicità, perché posso dire di avercela fatta, nonostante le numerose difficoltà che ho incontrato durante il percorso universitario: le persone che citerò possono confermare! Molte sono le persone da ringraziare, senza le quali sarebbe stato certamente più complicato superare tutti i momenti di sconforto.

La prima persona che voglio ringraziare è la Prof. Chiara Castiglioni, senza la quale questo lavoro di tesi non sarebbe stato possibile. Ringrazio Chiara per avermi ricordato il valore della gentilezza e della disponibilità all'aiuto, per avermi illuminato sulla bellezza della spettroscopia vibrazionale, per la sua presenza e guida costanti, per avermi insegnato molto… insomma per essere stata un esempio, sia umano sia professionale.

Ringrazio anche il mio Correlatore, il Prof. Daniele Fazzi, per avermi fatto scoprire le innumerevoli ed affascinanti sfaccettature del mondo computazione e per essere stato sempre disponibile, con consigli tecnici e discussioni stimolanti, nonostante i tanti impegni per i quali è incaricato.

Ringrazio tutto il gruppo di ricerca FunMat e in particolare il Dr. Luigi Brambilla, per aver condiviso gli spettri sperimentali, e il Prof. Matteo Tommasini, per la sua disponibilità ad aiutarmi con i problemi tecnici.

Ringrazio i miei genitori, Anna ed Enrico, a cui questo lavoro di tesi è dedicato: da sempre sono e sempre saranno un punto di riferimento fondamentale nella mia vita. A loro l'ingrato compito in questi anni di università di sopportarmi ma soprattutto di criticarmi: in questo, hanno dimostrato tutto il loro amore perché per loro sarebbe stato sicuramente più semplice voltarsi dall'altra parte nei momenti di incomprensione. Ringrazio anche mio fratello Giovanni, che mi ha insegnato che a volte è giusto prendere la vita con leggerezza, e per il bene che mi dimostra continuamente. Spero che la mia famiglia, Klaus compreso, sia orgogliosa di questo mio risultato, almeno tanto quanto lo sono io.

Ringrazio i miei amici, di tutta la vita e quelli più recenti, Giorgia, Sara, Rudi, Asia, Michele, Stefano, Andrea e Alessandra per le gran risate che ci siamo fatti e per tutti i momenti passati assieme, che hanno alleggerito questi anni.

Ringrazio gli amici del mondo del tennistavolo, che sono davvero numerosi e che quindi non posso citare tutti. A titolo di rappresentanza il mio allenatore Mauro, i miei compagni di squadra Matteo, Silvio e Lorenzo, Samuele, il nostro prete Andrea, Marco

e Gloria, Giacomo, Simonetta e Filippo… ma l'elenco da fare sarebbe molto più lungo, mi scuso in anticipo con tutti coloro che non ho nominato. La passione per il ping-pong che ci lega ha permesso che nascesse una profonda amicizia anche al di fuori delle palestre e che spero persisterà negli anni avvenire.

Ringrazio anche i miei ex-compagni e Prof del liceo, presenti alle serate da Paola, che hanno creduto in me più di quanto non l'abbia fatto io, e i miei compagni di università, con cui ho condiviso le gioie e i dolori che il Polimi sa regalare; fra essi un ringraziamento speciale va a Marco, per l'infinita pazienza e l'aiuto notevole che mi ha dato negli anni di studio.

Infine, un augurio a me stesso: sulle ali dell'euforia per la tanto desiderata e sofferta Laurea magistrale raggiunta, mi auguro di non perdere mai la curiosità e di poter vivere seguendo le mie passioni e i miei sogni. Ad maiora!

Carlo